APPROACHES FOR PID CONTROLLER DESIGN WITH APPLICATIONS AND EXPERIMENTAL VALIDATION

Ph.D. THESIS

by

HANWATE SANDEEP DEVRAO

DEPARTMENT OF ELECTRICAL ENGINEERING
INDIAN INSTITUTE OF TECHNOLOGY ROORKEE
ROORKEE - 247667 (INDIA)
JULY, 2018

APPROACHES FOR PID CONTROLLER DESIGN WITH APPLICATIONS AND EXPERIMENTAL VALIDATION

A THESIS

Submitted in partial fulfilment of the
requirements for the award of the degree

of

DOCTOR OF PHILOSOPHY

in

ELECTRICAL ENGINEERING

by

HANWATE SANDEEP DEVRAO

DEPARTMENT OF ELECTRICAL ENGINEERING
INDIAN INSTITUTE OF TECHNOLOGY ROORKEE
ROORKEE - 247667 (INDIA)
JULY, 2018

INDIAN INSTITUTE OF TECHNOLOGY ROORKEE
ROORKEE

CANDIDATE'S DECLARATION

I hereby certify that the work which is being presented in the thesis entitled **"APPROACHES FOR PID CONTROLLER DESIGN WITH APPLICATIONS AND EXPERIMENTAL VALIDATION"** in partial fulfilment of the requirements for award of the Degree of Doctor of Philosophy and submitted in the Department of Electrical Engineering of the Indian Institute of Technology Roorkee, Roorkee is an authentic record of my own work carried out during a period from July, 2013 to July, 2018 under the supervision of Dr. Yogesh Vijay Hote, Associate Professor, Department of Electrical Engineering, Indian Institute of Technology Roorkee, Roorkee.

The matter presented in this thesis has not been submitted by me for the award of any other degree of this or any other Institution.

Hanwate Sandeep Devrao

This is to certify that the above statement made by the candidate is correct to the best of my knowledge.

Yogesh Vijay Hote

(Supervisor)

The Ph.D. Viva-Voce Examination of Hanwate Sandeep Devrao, Research Scholar, has been held on .....

Chairman SRC **Signature of External Examiner**

This is to certify that the student has made all the corrections in the thesis.

Signature of Supervisor **Head of the Department**

Dated:_____

What we are is the result of what we have thought, is built by our thoughts, is made up of our thoughts. If one speaks or acts with a pure thought, happiness follows one, like a shadow that never leaves.

Dhammapada Ch.–1(Yamaka-vaggo). ver.–2

Abstract

Control systems are ubiquitous in everyday life. A control system is a mathematical law that enables the achievement of desired characteristics. Among many such laws, one of the most popular ones is a PID controller. It is a fundamental control algorithm that that is widely used for the control in industry due to its simplicity and flexibility. There exist innumerable techniques in the control literature for tuning a PID controller, however no such technique has been developed that can suffice for all types of situations. This calls for further research and challenges in tuning of PID controllers.

Most of the conventional techniques of tuning a PID controller like Ziegler Nichols, Chiens-Hrones-Reswick (C-H-R), Cohen-Coon are simple but are applicable to only a certain class of systems. Hence, there is a need to develop techniques that are not only applicable to a more general class of systems but simultaneously avoid the computational complexity which is exhibited in many soft computing techniques. Further, the techniques must be easily implementable on a hardware system as well. It is observed that the major drawback of the optimal control techniques is that they cannot be implemented on a hardware. Hence, a new approach known as the QRAWCP is developed which transforms an optimal LQR controller into a classical PID controller. This technique is also accompanied by the augmentation of an additional pole to the closed loop system consisting of a LQR controller. In this thesis, a well-structured manner of selecting the additional pole is proposed. Further, it is entirely possible, that all the states of the system are not measurable. To ameliorate this limitation, a LQG based PID controller is designed that comprises of a Kalman filter which acts as an observer and the LQR controller that can be utilized for optimal tuning of the resulting system. Further, both the schemes elucidated above are validated via hardware simulations. The hardware setups used in this thesis for validation of the proposed techniques are QUBE DC servo system, Cart inverted pendulum system and the rotary inverted pendulum (RIPS) system.

There are numerous techniques of tuning a PID controller, and each one has its own advantages and limitations. The adaptive control scheme, first proposed in this thesis, uses multiple candidate controllers, each of which is tuned via different control approaches and the resultant output of the

system follows the best of these multiple approaches via the assignment of appropriate weights for each control scheme. It is observed that the proposed adaptive strategy outperforms the individual control techniques. The proposed scheme, in its current form is then modified via the addition of a median filter and an epsilon term to get rid of the problem in which the derivative term becomes zero. To validate the effectiveness and strength of the modified scheme, it is then tested on a hardware setup of a Cart Inverted pendulum system.

Next, all the approaches developed above are tested primarily on two setup, i.e., DC servo system and Cart Inverted Pendulum system (CIPS). Various illustrative examples are provided to compare the proposed technique with the existing techniques in the literature. To investigate the robustness of the proposed technique, the effect of input disturbances, measurement noise, addition of input gains, are also taken into consideration. The simulation examples are compared via time response plots and performance indices. An interactive and animated graphical user interface is also developed for analysis, design and validation of controllers for cart inverted pendulum system (CIPS).

Finally, the problem of load frequency control of a power system is presented. Both the QRAWCP and the adaptive scheme developed above are applied to different models of the power system. The effect of non-linearities such as governor dead-band and generation rate constraint is also explored for different studies. To investigate the strength of the proposed technique for a more realistic power system model in the presence of non-linearities, a 10 machine New England system, having a topology similar to IEEE 39 bus system is also considered. The effect of parametric uncertainty is ascertained by the perturbation of parameters by $\pm$ 50%. To analyze the effectiveness of the proposed controller design techniques, a comprehensive comparative study with respect to the performance indices and time response is also undertaken. The simulation studies are a testimony to the effectiveness and efficiency of the proposed technique.

Overall, in this thesis, an attempt has been made by the author to develop simple and reliable control schemes to design a controller to obtain an improved time response and better disturbance rejection behaviour. Through illustrated examples and hardware validation, it is evident that the schemes are practically useful in the analysis and design of the control system.

Acknowledgements

Undertaking this Ph.D. has been a truly life-changing experience for me and it would not have been possible to do without the support and guidance that I received from many people. First and foremost, I would like to express my sincere gratitude to my supervisor Dr. Yogesh Vijay Hote for the continuous support during my Ph.D. study and research, for his patience, motivation, enthusiasm, and immense knowledge. I am also extremely grateful to Sir for his positive attitude to solve all kind of problems that I faced during my stay at IITR. A person with an amicable and positive disposition, Sir has always made himself available to clarify my doubts despite his busy schedule and I consider it as a great opportunity to do my doctoral programme under his guidance and to learn from his research expertise. His guidance helped me in all the time of research throughout the journey of Ph.D. work. I could not have imagined having a better supervisor and mentor for my Ph.D. study. Thank you Sir, for all your help and support.

I am also thankful to the members of my student research committee: Dr. Indra Gupta, Associate Professor, Department of Electrical Engineering, Dr. P. M. Pathak, Associate Professor, Department of Mechanical and Industrial Engineering, Dr. B. Tyagi, Associate Professor, Department of Electrical Engineering, for their encouragement, insightful comments, suggestions and hard questions in various presentation during my research work tenure. I am grateful to the reviewers whose constructive suggestions and invaluable advices improved the quality of my publication derived from this work. I would also like to acknowledge Dr. B. Das, Head of the Department of Electrical Engineering, for his help on various occasions. I am thankful to Mr. Anil Agarwal, Mr. Jakir Hussain, and Sandeep Kumar, Lab Assistants of Control and Robotics Laboratory for delivering all type of help in conducting experiment during my research work. I am highly obliged to owe my sincere thanks to the technical and administrative staff of electrical engineering department, especially to Mr. Mohan Singh and Mr. Rishabh, who helped me in all possible ways during the work.

I thank my fellow labmates, Siddharth, Pushkar, Arvind, Sudarshan, Jitendra, Mahendra for the stimulating discussions, for the sleepless nights we were working together during some period, and for all the fun we have had in the last five years. I am lucky to have my friends Santosh Rajgade (Asst. Professor, Govt. College of Engineering, Chandrapur), Mr. Govind Waghmare

(Project Manager,Lagos, Nigeria), Dr. Sahaj Saxena (Assistant Professor, Thapar University, Patiala), Dr. Swati (Assistant Professor, Thapar University, Patiala), and Dr. Nishant (Assistant Professor, JUIT, Wagnaghat), Akshit Budhraja (Research Scholar, Duke Univeristy, USA), Dr. K. Raju (Assistant Professor Saraswati Education, Tirupati), Dr. Charu Sharma (Research Associate, Norway) for supporting me in every walk of research life. My sincere thanks to the family of my supervisor (Mrs. Swapnaja, Mrudula and Mayank) with whom I enjoyed homely treatment, birthday functions and memorable trips. I like to thank Shivam Jain, Soumyadeep Bose who helped me in all the stages of writing the thesis.

I owe a debt of gratitude to my father Mr. Devrao R. Hanwate, mother Mrs. Yashoda D. Hanwate, who always encourages and let me to pursue what I like. Special thanks to my parents-in-law (Waghmare family), sisters (Kranti, Sarika and Rohini) and brother in laws (P.M. Bhadre, A.G. Kadam and K.G. Bhalerao). My heartfelt thanks to my maternal uncle late Mr. S.G. Gaikawad and his family (Mrs.Gaikwad, Jitu, Raju, Mahendra) for his prayer and well wishes to attain this task. Lovely thank to my all nephews (Shubham, Jeevan and Sahil) and niece (Mansi, Roshni and Sara) for enthusiastic knowledgeable interactions, and also to my lovely daughter Swara who introducing a new spirit of joy and energy during my research work. Last but not the least, I would like to thank my wife Pallavi, for her unfailing support and patience towards completion of this thesis, who sacrifices a lot so that I can focus on my research.

Last, but not the least, I would like thank to all the teaching and non-teaching staff of Department of Electrical Engineering, IIT Roorkee, those who directly and indirectly supported me during my research work. Finally, I would like to thank the Ministry of Human Resource and Development, Government of India, for providing fellowship to pursue the doctoral degree at Indian Institute of Technology Roorkee, India.

(HANWATE SANDEEP DEVRAO)

Contents

List of Figures

List of Tables

List of Symbols

$\mathbb{R}$	Set of real numbers
$\mathbb{R}^+$	Set of real positive numbers
α	Learning rate constant
Q	Real positive semi definite matrix
R	Real positive definite matrix
P	Solution of Riccati equation
$\mathbb{N}$	Set of natural numbers
$H(x,u,t)$	Hamiltonian operator
$\mathbf{x}$	Vector x
$\mathbf{x}^\intercal$	Transpose of vector x
$y'(t)$	Derivative of signal $y(t)$
$\int x(t)dt$	Integral of signal $x(t)$
$Y(s)$	Laplace transform of $y(t)$
$\mathcal{O}(W)$	Order of transfer function $W(s)$
$\sigma(Z)$	Degree of polynomial $Z(s)$
$\mathscr{D}f$	Derivative of f with respect to t
L_2	Time domain Lebesgue space
θ	Angle
$\Re$	Real part of complex number
x	Position
$(t+1)$	Next time interval
j	Unit imaginary number

Abbreviations

CHR	**C**hiens **H**rones **R**eswick
CIPS	**C**art **I**nverted **P**endulum **S**ystem
IAE	**I**ntegral **A**bsolute **E**rror
IMC	**I**nternal **M**odel **C**ontrol
ISE	**I**ntegral **S**quare **E**rror
ITAE	**I**ntegral **T**ime **A**bsolute **E**rror
LFC	**L**oad **F**requency **C**ontrol
LTI	**L**inear **T**ime **I**nvariant
LQG	**L**inear **Q**uadratic **G**aussian
LQR	**L**inear **Q**uadratic **R**egulator
MIMO	**M**ulti **I**nput **M**ulti **O**utput
PID	**P**roportional **I**ntegral **D**erivative
QRAWCP	**Q**uadratic **R**egulator **A**pproach **W**ith **C**ompensating **P**ole
RIPS	**R**otary **I**nverted **P**endulum **s**ystem
SBL	**S**tability **B**oundary **L**ocus
SISO	**S**ingle **I**nput **S**ingle **O**utput
SIMO	**S**ingle **I**nput **M**ulti **O**utput
ZN	**Z**iegler **N**ichols

Chapter 1

Introduction

Control systems are ubiquitous in everyday life. They are present everywhere. The behaviour of such systems is determined by a set of elementary propositions that can be comprehended by anyone. Even, fundamental thoughts and relations can be translated into mathematical forms. Mathematical modelling allows us to describe and predict the expected response of a wide variety of systems. Systems can simply be defined as those parts of the real world that have determined or virtual or even flexible boundaries. These boundaries delineate the system from its environment.

Looking around us, we can observe control systems everywhere. From the regulator of the fan to the switch of our tube-light, control systems are widely scattered around us [3]. Fridges, dishwashers, electric boilers, vacuum cleaners, washing machines etc. are all controlled systems. They could be simply on-off systems like the switch of the tube-lights, discrete control system such as the regulator in the fan or continuous control system like the DC servo motor. The first two examples are the open loop systems, whereas the last example describes a closed loop feedback system.

Feedback control systems are a fundamental part of numerous physical, electrical, chemical, metallurgical, biological and other engineering systems [4]. Addition of feedback loop(s) to an open loop system generally increases the speed of response of the system and minimizes the effect of random disturbances, process noise, parametric uncertainty, etc. Over the last few decades, remarkable innovation has been witnessed in the theory of control systems and in their applications

to innumerable real-life systems. PID controller [5] is one of the most important control system, which serves as the backbone of more than 90% of the modern control industries [6]. The fundamental features of the PID controllers and various tuning techniques [7] that satisfy multifarious design requirements are discussed in the upcoming sections of the thesis.

1.1 Overview of PID

PID is an acronym for **P**roportional **I**ntegral **D**erivative controller [5, 8], which is a feedback mechanism that has become ubiquitous in the modern control industry. Over the past few decades, there has been a rapid advancement in the theory of control systems, yet the PID controller remains a perennial workhorse in the modern industry [9]. The universal prevalence and popularity of the PID controller can be ascribed to its simplicity, flexibility and ability to function in a wide range of operating conditions [6]. As its name suggests, PID comprises of three modes [10], i.e, proportional(P), integral(I) and derivative(D), which can act individually or in tandem with each other [11]. The individual P, I and D blocks in a PID controller can be rearranged and put up at different places in a closed loop system [12], leading to new structures like PI-PD, PI-D, I-PD controllers [13, 14], etc. Numerous techniques of tuning a PID controller are delineated in literature, making it a fascinating algorithm to implement in real world scenarios [15]. The applications of such a control scheme are not limited merely to electrical engineering, but have been extended to multifarious problems spread across widespread disciplines like aerospace, process control[16], bio-medical [17] electronics and telecommunication [4], robotics [18, 19] management[20], psychology[21], etc.

The controller synthesis schemes of a PID controller can be broadly classified into conventional control methods[22], IMC control schemes[23], soft computing methods[24], optimal control techniques[1, 18] and robust control approaches[25]. Ziegler-Nichols(ZN) [26], Cohen Coon and CHR (Chiens Hrones Reswick)[27], named after their respective discoverers are the widely popular conventional approaches which depend on the open loop response of the plant[28]. Internal model control is a highly rated control scheme that is based on the concept of Q parameterization and it is characterized by an internal model consisting of the model of the plant and a

controller[29]. On the other hand, soft computing schemes [30] belong to the Computational intelligence family and comprise of a large number of heuristic search techniques like Genetic algorithm (GA), particle swarm optimization (PSO), firefly algorithm (FFA), etc. Optimal control techniques like linear quadratic regulator (LQR)[31], linear quadratic gaussian (LQG) deal with the maximization or minimization of a single or multiple performance criterion and then use to obtain a control law. Finally, robust control approaches [25, 32] such as H_∞ based schemes, Lyapunov theory, explicitly deal with uncertainty and aim to achieve optimal performance in the presence of uncertain environment, modelling errors, etc.

1.2 Motivation

All the techniques mentioned in the previous section encounter certain limitations in their implementation. The conventional control techniques like ZN and CHR are intended for a Type 0 plant having only real poles and zeros [5, 33] and fail to give appreciable results for a system of Type 1 and a system having complex conjugate poles and zeros [34]. On the other hand, the soft computing techniques [35] involve numerous random parameters and require a large computation time in software[36, 37]. In the internal model control scheme, the model of the system must be highly accurate and resemble the actual plant as close as possible, else this approach may lead to misleading and inaccurate results[29, 38]. Further, the choice of the filter time constant (λ), is random [39] and there do not exist explicit rules for its selection[40]. One can even design a controller by using a simple Ackermann's formula but the selection of desired poles needs expert selection and is a random process[41].

To ameliorate the drawbacks of the Ackermann's formula, an advanced state space optimal approach known as Linear Quadratic regulator (LQR) was formulated. In LQR technique, the feedback gain K is chosen optimally via minimization of a quadratic cost function[42]. For the physical realization of the LQR controller, one needs to transform it into the form of a PID controller[1, 43]. It is pertinent to mention here that, application of LQR controller to a system does not increment the order of the system transfer function [44], whereas the addition of a PID controller, having a non-zero value of the integral gain will increase the order of the system by 1. Hence, there arises a

need to augment an additional pole to the characteristic equation of the closed loop LQR system. Thus, despite the superiority of the proposed LQR scheme, few limitations are still present.

- Till the present date, the additional pole was randomly chosen to be certain number of times the real part of the dominant pole in the system. Also, the nature of the system for the application of LQR-PID was unspecified.
- Further, the implementation of the LQR on a real time system is difficult, since all the states of a system are not measurable, but for practical realization, all the states of the system must be measurable.

All the control schemes elucidated in the preceding paragraphs have certain advantages and certain limitations[45]. It is difficult to satisfy all the desired performance specifications with a single controller [46]. A solitary design technique would not be able to meet multiple desired requirements in the presence of noise, input disturbance, parametric uncertainties, modelling errors, etc. Thus, there exist a few research gaps, which are given below.

- There is no single control strategy that can incorporate multiple controllers designed via different control schemes. The output of such a control scheme should be able to subsume the best points of each design technique.
- Such a control scheme should be physically realisable.

To address the above issues, a clear and more logical framework is required for conventional LQR controller and its modified version in PID [1, 47] form which is simple to understand and realistic for implementation while posing a sound fundamental basis.

1.3 Contribution of the thesis

The aforementioned discussion is the motivation to carry out research work. The work is mainly concerned with the design of a PID controller via QRAWCP approach and adaptive control scheme.

In the thesis, an attempt has been made to keep the mathematics at a reasonably simple level, and emphasis has been given to the results that enhance insight and intuition. The simulation studies of all the examples and case studies have been done with the help of MATLAB® and Simulink software [48]. The major contributions of the thesis can be viewed in the following objectives.

- **Design and validation of QRAWCP based PID controller for SISO and SIMO systems using optimal control theory**

  In this objective, the concept of optimal LQR [1, 43, 49] and LQG is used to derive the PID controller via QRAWCP [50] for a general class of SISO and SIMO systems. The proposed methodology has been demonstrated through illustrative examples of a second and fourth order system with repeated poles. Apart from these, the proposed technique has been applied to the illustrative examples by considering the model of a PMS motor and manutec robot system via simulation. Further, a comprehensive analysis of the proposed QRAWCP approach has been performed for a solar tracker system. The results, hence obtained are compared with recent techniques from the literature. Furthermore, the impact of input disturbances, output noise and parametric uncertainties has also been investigated for the proposed approach. To validate the performance of the proposed scheme for real time systems, it is also tested on the hardware setup of a QUBE servo for position and velocity control and also for balancing the rotary inverted pendulum system. The results signify the efficacy and superiority of the proposed technique.

- **Adaptive control policy**

  In this objective, a generalized adaptive control scheme is proposed for linear time invariant (LTI) systems. The proposed strategy is elucidated via two illustrative examples of different models[51]. A two candidate controller is designed for the position control of the model of a flexible robotic arm system, wherein the individual controllers are tuned via PID-LQR and SBL-PID, respectively. Next, three candidate controllers are derived for the position control of a DC servo system model and the individual controllers here are tuned via LQR [1], SBL [52] and ZN techniques, respectively. For each of the above cases, the results obtained via the proposed approach are compared with the design approaches of the individual controllers. It is observed that the proposed adaptive strategy outperforms the

individual control techniques. The proposed scheme, in its current form is then modified via the addition of a median filter and an epsilon(ε) term to get rid of the problem in which the derivative term becomes zero. To validate the effectiveness and strength of the modified scheme, it is then verified via illustrative examples and also implemented on hardware setup of a Cart Inverted pendulum system.

- **Application to Cart Inverted Pendulum system**

  The primary objective of this work is the design and implementation of different control strategies that have been developed [53] in the preceding chapters to a cart inverted pendulum system (CIPS)[54, 55]. First, a simplified model of the CIPS is derived. Then, the QRAWCP approach, is used to design a PID controller for the obtained model. To tackle the problem of parametric uncertainties, a combination of Kharitonov's theorem [56] and SBL technique [57] is applied to tune the PID controller. Further, an adaptive control policy[2], comprising of two candidate PID controllers that are tuned via SBL and LQR respectively is applied to the given system and the effects of input disturbance, variation in input gain and input time delay are also explored. To investigate the effectiveness of the adaptive scheme to real life situations, it is also implemented on the hardware setup of CIPS system [53]. Further, a modified adaptive control policy is also used to tune a PID controller. Finally, an interactive and animated graphical user interface is developed for analysis, designing and validation of controllers for cart inverted pendulum system (CIPS).

- **Application to Load frequency control**

  This objective focuses on the application of different techniques discussed in the preceding chapters to the problem of load frequency control [58], which is a system to regulate the power flow between different areas while holding the frequency to a constant value[59, 60]. First, QRAWCP approach is applied to a single area and two area power system comprising of reheated and non-reheated turbine. To investigate the robustness of the proposed controller, the LFC parameters are perturbed by $\pm 50\%$. Further, the effect of non-linearities such as governor dead-band (GDB) and generation rate constraint(GRC) [38, 61] is explored for the different cases given above. To investigate the strength of the proposed technique for a more realistic power system model in the presence of non-linearities, a New England

system, having a topology similar to IEEE 39 bus system is also considered. Then, the adaptive control scheme is applied on a single area and two area power system comprising of a non-reheated turbine. The effect of parametric uncertainty is ascertained by the perturbation of parameters by $\pm 50\%$. To analyze the effectiveness of the proposed aforementioned controller design techniques, a comprehensive comparative study with respect to the performance indices and time response is also undertaken. The simulation studies are a testimony to the effectiveness and efficiency of the proposed technique.

1.4 Organization of thesis

The work done in this thesis for PID control strategies has been presented in seven different chapters. The description of each research objective is included in the introduction section of each chapter.

Chapter 1 describes the background of PID controller, optimal controller and adaptive controller along with their salient features and advantages. Some of the research gaps and issues pertaining to different controller design schemes are discussed in the motivation section. The contribution of the thesis work is provided. Finally, the organization of the thesis work is presented.

Chapter 2 gives a brief description of classical PID tuning techniques such as Ziegler Nichols, Cohen Coon, and C-H-R approaches. Next, the mathematical formulae and the theory of internal model control (IMC) and stability boundary locus (SBL) are discussed. Finally, the different performance indices, used for the evaluation of the system performance are examined.

Chapter 3 finds the use of optimal control approaches such as LQR and LQG to formulate the QRAWCP-PID controller for a general class of SISO and SIMO systems. Illustrative examples of different order systems are analyzed. The proposed scheme is also applied on the model of the solar tracking system and an exhaustive comparative analysis with respect to time response, parametric uncertainties and robustness is performed. Finally, the proposed scheme is implemented on the hardware setup of a QUBE servo for position and velocity control and also for balancing the rotary inverted pendulum system.

Chapter 4 introduces a new adaptive control policy for linear time invariant systems. Two case studies for position control of the model of a flexible robotic arm system and DC servo system are discussed. It is observed that, in both the cases, the proposed adaptive strategy outperforms the individual control techniques. The proposed scheme, in its current form is then modified via the addition of a median filter and a epsilon(ε) term and the modified scheme is tested on the hardware setup of a cart inverted pendulum system.

Chapter 5 deals with the application of the control schemes discussed in the preceding chapters, i.e., QRAWCP, adaptive policy and modified adaptive scheme to the problem of cart inverted pendulum system (CIPS). The effect of parametric uncertainties is dealt with by combining the Kharitonov's theorem with the stability boundary locus (SBL) approach of tuning PID controllers. To investigate the effectiveness of the adaptive scheme to real life situations, it is also implemented on the hardware setup of CIPS system. Finally, an interactive and animated graphical user interface is developed for analysis, design and validation of controllers for CIPS.

Chapter 6 explores the application of the control schemes discussed in the preceding chapters, i.e., QRAWCP and adaptive control policy to the problem of load frequency control. The aforementioned schemes are applied for different case studies of single and multi-area power systems comprising of non-reheated and reheated turbine. To investigate the strength of the proposed technique for a more realistic power system model in the presence of non-linearities, a New England system, having a topology similar to IEEE 39 bus system is also considered. The effect of parametric uncertainties is ascertained by the perturbation of parameters by $\pm 50\%$. Further, a comprehensive comparative study with respect to the performance indices and time response is also undertaken.

Chapter 7 compiles the salient conclusions of the present study regarding the use of QRAWCP scheme and adaptive control policy for different systems with numerical illustrations, practical applications and hardware validations. The recommended direction for future investigations is also discussed.

Chapter 2

PID tuning techniques

This chapter is dedicated to the study of different structures of PID based control schemes. It begins with a brief introduction to PID controllers. Next, three PID forms, i.e., ideal PID, series PID and parallel PID are elaborated. Numerous control techniques are available in literature, and it is almost impossible to enlist all of them, thus only five popular control techniques, are singled out and discussed in detail. Those five techniques are the conventional methods like Ziegler Nichols, Cohen coon, CHR as well as techniques like Stability boundary locus and the internal model control scheme, which will be extensively used in the upcoming chapters of the thesis.

2.1 Overview of PID controller

PID Stands for : **P** (Proportional) **I** (Integral) and **D** (Derivative). So, it also called three term control. These controllers exhibit certain advantages, such as

- Simple in design [62].
- Good record of past success [9].
- PID controllers are used in more than 90% of the industrial applications [6].
- Flexibility to design [10].

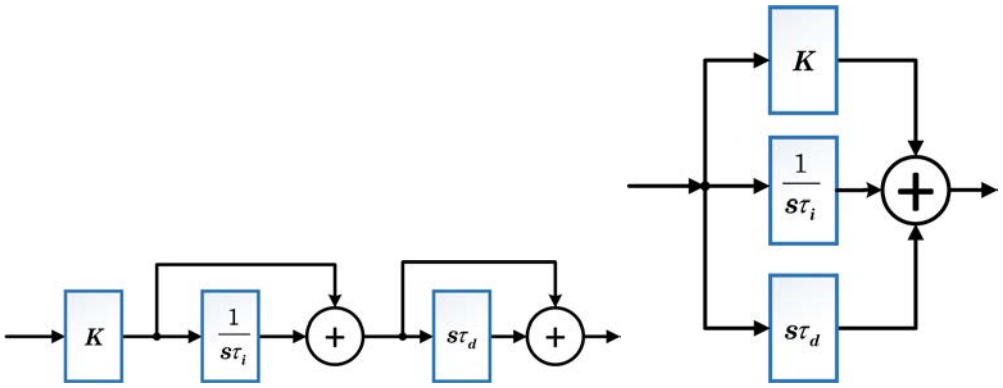

Figure 2.1: Control structures of PID controllers

- It is a "Trikal jnana" controller, i.e., it has information about past(Integral), present(Proportional) and future(Derivative) [9, 63].

PID has been used in a wide range of application areas such as Aerospace [64], Marine [65], Biomedical [66], Power system [67], Electronics, Tele-communication [68] and so on. During the 1930s, three mode controllers with proportional(P), integral(I), and derivative(D) (PID) actions became commercially viable and gained widespread industrial acceptance [5, 69]. These types of controllers are still the most widely used controllers in process industries. As discussed above, their success is a result of innumerable good features because of simplicity, robustness and wide applicability.

There exist three major variations in the structure of PID controller [5], they are, ideal PID, series PID and parallel PID controller. Fig. 2.1(a) and 2.1(b) depicts the structures of series and parallel PID controller, respectively. The primary distinction among these forms is the effect of setting coefficients on the controller's behaviour. Each of these three forms are described below.

(i) Ideal PID: In this, the adjustment of the proportional gain affects the proportional, integral and derivative terms. Thus, a simple readjustment of one parameter affects all the three actions. The controller output of an ideal PID is given below.

$$c(t) = K_p \left(e(t) + \frac{a}{\tau_i} \int e dt + \tau_d \frac{de}{dt} \right) \tag{2.1}$$

The main feature of such type of controller is that the gain term K_p is distributed to all the terms in the parenthesis and all the portions of the PID controller are influenced by the gain. But the integral and the derivative time constants (τ_i, τ_d) can act independently.

(ii) ***Series PID:*** Such a structure finds usage in the peculiarities of pneumatic controller mechanism and in the analog circuits [6]. The controller output of series PID is given as,

$$c(t) = K_p \left(\left(\frac{\tau_d}{\tau_i} + 1 \right) e(t) + \frac{a}{\tau_i} \int e(t)dt + \tau_d \frac{de}{dt} \right) \tag{2.2}$$

Here, too, gain term K_p is distributed to all the terms in the parenthesis. The distinctive or the characteristic feature is that the integral and the derivative terms have an effect on the proportional term also. In other words, readjusting τ_i or τ_d influences the proportional term as well.

(iii) ***Parallel PID:*** It is the simplest form of the PID controller and widely used in the literature among the control practitioners [41]. Each of the three actions occurs in different terms and the combined action is simply the sum of the three individual actions. It is given by

$$c(t) = K_p e(t) + \frac{1}{\tau_i} \int e(t)dt + \tau_d \frac{de(t)}{dt} \tag{2.3}$$

On first look, it may appear that this structure is the best as each term controls each action separately. But in many of the applications, it is better than only one term affects all the three control actions.

Various tuning methods have been proposed from 1942 [26] until the present time for obtaining better and more acceptable system response based on our desired control objectives such as percent of overshoot (M_p), integral error-based performance indices, settling time (t_s), manipulated variable behaviour, etc. Some of these tuning methods have considered only one of these objectives as a criteria for their tuning while others have developed their algorithm by considering an appropriate weighted combination of the multiple control objectives.

2.2 Ziegler Nichols tuning

Ziegler Nichols tuning [26] approach is a heuristic approach for setting the parameters of a PID controller based on the transient response of the plant. These tuning rules give an educated estimation of the parameter values, and can be used to provide initial settings for further refinement. The Ziegler-Nichols (ZN) tuning approaches can be broadly categorised into two parts [3], that are explained below.

(a) Method 1: It is used, when the model of the plant is unknown. For the applicability of this method, the open loop step response curve should be *S* shaped. One can obtain such step response curves experimentally or by dynamic simulation. Such a *S* shaped curve is characterised by two constants, known as the delay time (L) and time constant (T). For a system, having this curve, the transfer function of plant can be approximated by

$$\frac{Y(s)}{U(s)} = \frac{Ke^{-Ls}}{Ts+1} \tag{2.4}$$

Table 2.1 gives the tuning rules of a PID controller by Ziegler Nichols approach.

The transfer function of a PID controller is given by

$$C(s) = K_p + \frac{K_i}{s} + K_d s \tag{2.5}$$

Substituting the values of K_p. K_i and K_d from Table 2.1, we get

$$C(s) = 1.2\frac{T}{L}\left(1 + \frac{1}{2Ls} + 0.5Ls\right) \tag{2.6}$$

Simplifying further, we finally obtain

$$C(s) = 0.6T\frac{\left(s+\frac{1}{L}\right)^2}{s} \tag{2.7}$$

Table 2.1: Ziegler Nichols parameters for method 1

Control Type	K_p	T_i	T_d
P	$\frac{T}{L}$	∞	0
PI	$0.9\frac{T}{L}$	$\frac{L}{0.3}$	0
PID	$1.2\frac{T}{L}$	$2L$	$0.5L$

(b) Method 2: This technique is based on varying of the proportional gain from 0 to a critical gain K_c, at which sustained oscillations are obtained.

1. Initially, turn the proportional gain (K_p) of the system to zero.
2. Now, gradually increase K_p while continuously observing the output.
3. Continue the above step until the output of the controller begins to exhibit sustained oscillations.
4. The gain at which the system exhibits these sustained oscillations is known as the critical gain.
5. Note down the critical gain (K_c) and the time period (T_c) of sustained oscillations.
6. Calculate the K_p, T_i and T_d, using the formulas given in Table 2.2.

Table 2.2: Ziegler Nichols parameters for method 2

Control Type	K_p	T_i	T_d
P	$0.5K_c$	-	-
PI	$0.45K_c$	$0.85T_c$	-
PID	$0.6K_c$	$0.5T_c$	$0.13T_c$

2.3 Cohen Coon method

Cohen Coon approach [70] is a conventional PID design technique, that is applicable to more number of processes as compared to Ziegler Nichols approach. It is a versatile control strategy that can work even if dead time is less than two times the length of the time constant in contrast to the Ziegler Nichols tuning technique which gives appreciable results only when dead time is less

than half the length of the time constant. Both the ZN and Cohen Coon schemes are applicable for a quarter-amplitude damping response. The Cohen-Coon tuning method is generally used for self-regulating processes. Most control loops, e.g., flow, temperature, pressure, speed, and composition, contain self-regulating processes. The most common exception is a level control loop, which contains an integrating process. The main drawbacks of the Cohen Coon method [71] are that it gives oscillatory response and may lead to instability, if there are perturbations in gain of the system. For example, if the rule provides for a controller gain of 2, it is recommended to use only 1. Such an adjustment will provide an admissible stability margin and will prevent oscillations.

Cohen Coon approach makes use of three system parameters, i.e., process gain (G_p), dead time (τ_d) and time constant of the system (τ), that are obtained using the open loop response curve of the system. A set of Cohen Coon tuning rules are given in Table 2.3.

Table 2.3: Cohen Coon tuning parameters

Control Type	K_p	T_i	T_d
P	$\frac{1.03}{G_p}\left(\frac{\tau}{\tau_d}+0.34\right)$	-	-
PI	$\frac{0.9}{G_p}\left(\frac{\tau}{\tau_d}+0.092\right)$	$3.33\tau_d\frac{\tau+0.092\tau_d}{\tau+2.2\tau_d}$	-
PD	$\frac{1.24}{G_p}\left(\frac{\tau}{\tau_d}+0.129\right)$	-	$0.27\tau_d\frac{\tau-0.324\tau_d}{\tau+0.129\tau_d}$
PID	$\frac{1.35}{G_p}\left(\frac{\tau}{\tau_d}+0.185\right)$	$2.5\tau_d\frac{\tau+0.185\tau_d}{\tau+0.611\tau_d}$	$0.37\tau_d\frac{\tau}{\tau+0.185\tau_d}$

2.4 C-H-R Method

This approach is a modification of the ZN tuning technique and was propounded by Chiens, Hrones and Reswick in 1952 [27, 72]. It is concerned with the regulation of set point and rejection of disturbance. The design criteria used in this technique is "quickest response without overshoot" and "quickest response with 20% overshoot". The process model, used in CHR is the same as the one we assumed in ZN approach. It is given as

$$G(s)=\frac{Ke^{-Ls}}{Ts+1} \tag{2.8}$$

Here L represents the delay and T is the time constant of the first order system with delay.

Once, a and T are determined, one can compute the P/PI/PID parameters using the procedure given in Table 2.4, and Table 2.5 respectively.

Table 2.4: PID parameters for zero overshoot using CHR set point response method

Control Type	K_p	T_i	T_d
P	0.3/a	-	-
PI	0.35/a	1.2T	-
PID	$0.6K_c$/a	T	0.5L

Table 2.5: PID parameters for 20% overshoot using CHR set point response method

Control Type	K_p	T_i	T_d
P	0.7/a	-	-
PI	0.6/a	T	-
PID	$0.9K_c$/a	1.4T	0.47L

2.5 Drawbacks of classical techniques

The principal drawback of ZN, Cohen Coon and CHR control methods is that they are intended for Type 0 plant having real poles and zeroes. These techniques fail for Type 1 plant and those plants with complex poles and zeros. To ameliorate such drawbacks, we need new techniques which can work for a general plant [6, 73, 74]. In the section below, we discuss two of these techniques, i.e., Internal model control scheme and Stability boundary locus approach.

2.6 IMC

Morari et.al developed a new control system strategy that is known as Internal model control (IMC). It is a well laid out mechanism for controller design based on Q parameterization principle and has been developed for integer order (IO) as well as fractional order (FO), SISO and MIMO continuous time and discrete time systems. It provides a good trade-off between a robust controller and an optimal controller. An extensive literature survey of the IMC technique is presented in

[75]. IMC has also been used in a number of application areas like Microwave oven, induction motor, boiler, evaluation of artificial pancreas, etc.

The IMC approach has two distinct advantages [76]: (1) It explicitly takes into account the model uncertainty. (2) It allows the designer to trade-off control system performance with system robustness to process changes and modelling errors.

The block diagram of the IMC control scheme is shown in Fig. 2.2. In this diagram, G_p denotes the transfer function of the process and G_m is the transfer function of the process model. Also, G_{cl} is the IMC controller transfer function.

For the sake of convenience and simplicity, the IMC model in Fig. 2.2 can be simplified and transformed into a system in classical feedback form, which is illustrated in Fig. 2.3.

The steps of IMC scheme for a second order plant are given below. For a higher order plant, one can use model order diminution techniques to apply the given approach.

Consider a plant, which can be represented by a general second transfer function given as

$$G(s) = \frac{a_0 s + a_1}{b_0 s^2 + b_1 s + b_2} \tag{2.9}$$

Upon taking the factor of a_0 outside as a gain term, equation (2.9) can be re-written in the following form

$$G(s) = \frac{a_1(1 + a_2 s)}{b_0 s^2 + b_1 s + b_2} \tag{2.10}$$

where, $a_2 = \frac{a_0}{a_1}$

In this chapter, we will consider the case of $a_2 < 0$. If $a_2 > 0$, an almost identical approach can be applied except the additional lag term.

- Factorise the plant model into minimum phase and non-minimum phase part, respectively. This can be mathematically given as

$$G(s) = G_m(s) G_{nm}(s) \tag{2.11}$$

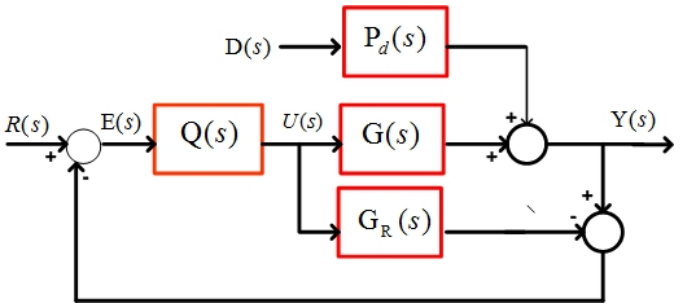

Figure 2.2: IMC control scheme

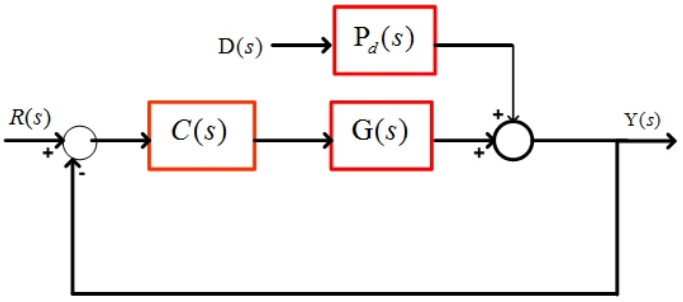

Figure 2.3: IMC control scheme in classical feedback form

Herein, $G(s)$ denotes the plant transfer function and $G_m(s)$ and $G_{nm}(s)$ represent the minimum and non-minimum phase parts, respectively.

Thus,

$$G_m(s) = \frac{a_1}{b_0 s^2 + b_1 s + b_2} \tag{2.12}$$

$$G_{nm}(s) = 1 + a_2 s \tag{2.13}$$

- In this step, we can chose a filter given in the form below,

$$F(s) = \frac{1}{(1+\lambda s)^r} \tag{2.14}$$

Here, r is a parameter, which can be selected in such a manner that the transfer function in (2.15) becomes proper or is at-least semi-proper. λ is a tuning parameter, which is inversely proportional to the speed of the closed loop system.

- The transfer function of the IMC controller $Q(s)$ can be derived as follows

$$Q(s) = \frac{F(s)}{G_m(s)} \tag{2.15}$$

On substituting the above transfer functions from Equation (2.12) and (2.14), we get

$$Q(s) = \frac{b_0 s^2 + b_1 s + b_2}{a_1(1+\lambda_s)} \tag{2.16}$$

- It is possible to convert the IMC controller $Q(s)$ into the classical feedback form via the formula given as

$$C(s) = \frac{Q(s)}{1 - G(s)Q(s)} \tag{2.17}$$

On replacing (2.9) and (2.16) in (2.17), we get,

$$C(s) = \frac{b_1}{a_1\lambda - a_0} + \frac{b_1}{a_1\lambda - a_0}\frac{1}{s} + \frac{b_0}{a_1\lambda - a_0}s \tag{2.18}$$

The transfer function of a PID controller can be stated as

$$C(s) = K_p + \frac{K_i}{s} + K_d s \tag{2.19}$$

- Thus, finally comparing equations (2.18) and (2.19) we get,

$$\begin{aligned} K_p &= \frac{b_1}{a_1\lambda - a_0} \\ K_i &= \frac{b_1}{a_1\lambda - a_0} \\ K_d &= \frac{b_0}{a_1\lambda - a_0} \end{aligned} \tag{2.20}$$

2.7 Stability Boundary Locus (SBL)

There exist various techniques of designing a PID controller. A graphical method to compute the stable values of PID from stability region, known as stability boundary locus(SBL) was formulated by N.Tan [57, 77]. This main advantage of this technique is that it is easy to implement and does

not require sweeping over the controller parameters. Further, it does not require an inversion of the plant model as in IMC scheme. A brief explanation of the method is provided below.

Consider a system, having the transfer function of the form

$$G(s) = \frac{N(s)}{D(s)} \tag{2.21}$$

PID controller can be formulated as

$$C(s) = K_p + \frac{K_i}{s} + K_d s \tag{2.22}$$

Replacing $s = j\omega$ in (2.21) we get,

$$G(j\omega) = \frac{N_e\left(-\omega^2\right) + j\omega N_o\left(-\omega^2\right)}{D_e\left(-\omega^2\right) + j\omega D_o\left(-\omega^2\right)} \tag{2.23}$$

The closed-loop characteristic equation $1 + C(s)G(s) = 0$ using (2.22) and (2.23) can be written as,

$$\begin{aligned}\Delta(s) = &\left[\left(-\omega^2\right) D_o\left(-\omega^2\right) + K_d\left(\left(-\omega^2\right) N_e\left(-\omega^2\right)\right)\right. \\ &\left. + K_p\left(\left(-\omega^2\right) N_o\left(-\omega^2\right)\right) + K_i\left(N_e\left(-\omega^2\right)\right)\right] \\ &+ j\left[(\omega) D_e\left(-\omega^2\right) + K_d\left(\left(-\omega^3\right) N_o\left(-\omega^2\right)\right)\right. \\ &\left. + K_p\left((\omega) N_e\left(-\omega^2\right)\right) + K_i(\omega) N_o\left(-\omega^2\right)\right]\end{aligned} \tag{2.24}$$

Separating real and imaginary parts and equating them to zero, we get, the real part as:

$$\begin{aligned}lK_d\left(\left(-\omega^2\right) N_e\left(-\omega^2\right)\right) + K_p\left(\left(-\omega^2\right) N_o\left(-\omega^2\right)\right) \\ + K_i\left(N_e\left(-\omega^2\right)\right) = \left(\left(\omega^2\right) D_o\left(-\omega^2\right)\right)\end{aligned} \tag{2.25}$$

and imaginary part as:

$$lK_d\left(\left(-\omega^3\right)N_o\left(-\omega^2\right)\right)+K_p\left((\omega)N_e\left(-\omega^2\right)\right) \\ +K_i\left((\omega)N_o\left(-\omega^2\right)\right)=\left((-\omega)D_e\left(-\omega^2\right)\right) \quad (2.26)$$

Let,

$$\begin{aligned} P(\omega) &= \left(-\omega^2\right)N_o\left(-\omega^2\right) \\ Q(\omega) &= N_e\left(-\omega^2\right) \\ R(\omega) &= \left(-\omega^2\right)N_e\left(-\omega^2\right) \\ S(\omega) &= (\omega)N_e\left(-\omega^2\right) \\ T(\omega) &= (\omega)N_o\left(-\omega^2\right) \\ U(\omega) &= \left(-\omega^3\right)N_o\left(-\omega^2\right) \\ X(\omega) &= \left(\omega^2\right)D_o\left(-\omega^2\right) \\ Y(\omega) &= (-\omega)D_e\left(-\omega^2\right) \end{aligned} \quad (2.27)$$

From (2.26) and (2.27), we get

$$K_p\left(P(\omega)\right)+K_i\left(Q(\omega)\right)+K_d\left(R(\omega)\right)=X(\omega) \quad (2.28)$$

and

$$K_p\left(S(\omega)\right)+K_i\left(T(\omega)\right)+K_d\left(U(\omega)\right)=Y(\omega) \quad (2.29)$$

On selecting using (2.28) and (2.29), we get,

$$K_p=\frac{X(\omega)T(\omega)-Y(\omega)Q(\omega)}{P(\omega)T(\omega)-Q(\omega)S(\omega)} \quad (2.30)$$

$$K_i=\frac{Y(\omega)P(\omega)-X(\omega)S(\omega)}{P(\omega)T(\omega)-Q(\omega)S(\omega)} \quad (2.31)$$

Now, selecting the value of K_d and then using (2.31) and (2.32), plot the graph between K_p and

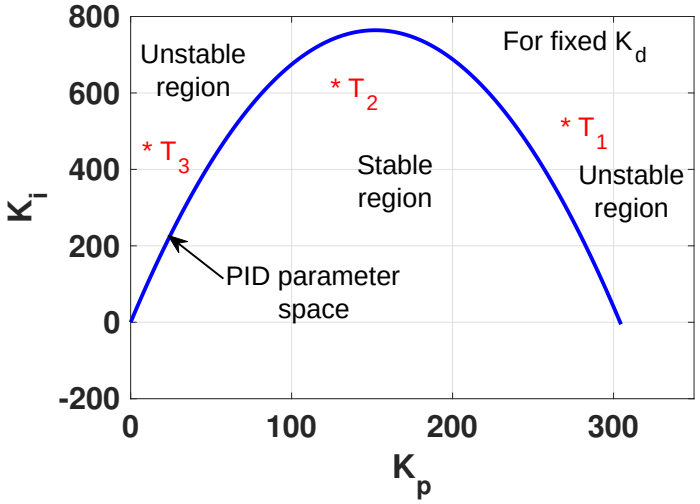

Figure 2.4: Stability Boundary Locus plot

K_i by varying the frequency (ω) from 0 to ∞. The parameter plane ((K_p, K_i) plane) is divided into stable and unstable regions as shown in Fig. 2.4. Choosing a set of test points (T_1, T_2 and T_3) from each region, we are able to segregate stable and unstable boundary of K_p-K_i plane. From the stable region, the parameters K_p and K_i can be determined.

2.8 Performance evaluation

To analyse and test the optimal performance of the control scheme, the performance indices (cost functions) in the form of integral error criterion are selected [45]. They are integrated error (*IE*), integral of the squared error (*ISE*), integral of the absolute error (*IAE*), integral of the time squared error (*ITSE*) and integral of the time weighted absolute error (*ITAE*) defined, respectively, by

$$\begin{aligned} IE = \int_0^\infty e(t)dt,\ ISE = \int_0^\infty e^2(t)dt,\ IAE = \int_0^\infty \left|e(t)\right| dt, \\ ITSE = \int_0^\infty te^2(t)dt,\ ITAE = \int_0^\infty t\left|e(t)\right| dt \end{aligned} \tag{2.32}$$

where, $e(t)$ is the error signal, i.e., the difference between the set-point (desired) input and the actual output. *IE* accumulates the net error and describes the performance of monotonic response [78]. *ISE* index indirectly denotes several characteristics like settling time, overshoot, speed of

response, and all other important features of the transient response. *IAE* index is a measure of disturbance rejection for integral controller. *ITSE* index considers squared long duration error. *ITAE* index accounts for long duration error. Lastly, the control system is optimal if the value of these indices are minimum.

2.9 Concluding remarks

In this chapter, a brief review of five widely cited PID tuning techniques, i.e., Ziegler Nichols approach, Cohen Coon, CHR technique, Internal model control (IMC) scheme and stability boundary locus (SBL) is presented. PID controllers are ubiquitous in industry owing to their simplicity and operability in a wide range of operating conditions. ZN and CHR are the conventional PID tuning techniques, which depend on the open loop response of the plant, whereas IMC scheme is based on Q- parameterization principle and SBL technique is based on the choice of parameters in the stabilising region of the system. There are widely different PID techniques, but the ultimate aim of each of them is the attainment of desired response, in terms of ideal time response specifications, frequency response specifications, lower values of performance indices or a combination of one or more of these factors. The next chapter will focus on a new technique, known as the QRAWCP approach, that makes it possible to practically realise an optimal LQR controller via its transformation into the form of a conventional PID controller.

Chapter 3

Proposed Control Approach–I- An Optimal PID using QRAWCP

In this chapter, a direct formula is propounded for the design of an optimal PID controller for a class of systems via a new technique, known as Quadratic regulator approach with compensating pole (QRAWCP). The beauty of the proposed approach is that the optimal properties of a LQR controller are transferred into a PID controller, and this transformation is accompanied by the augmentation of an additional pole to the characteristic equation of the LQR compensated system. Further, in certain situations, all the states of the system are not observable. In such a case, an additional Kalman filter can be added in series with the LQR controller, which leads to a technique known as Linear Quadratic Gaussian (LQG) method.

Thus, by using this approach, one does not need to go for iterative soft computing techniques which are time consuming [71], computationally inefficient and require a prior knowledge of the search space in which the solution will lie. The superiority of the proposed approach is demonstrated through illustrative examples and via the comparison of the performance indices with the well-known methodologies in literature.

To verify the effectiveness of the proposed approach to real time systems, it is implemented for position control, velocity control of DC servo system and balancing of rotary inverted pendulum. Further, it is also tested on a QUBE servo2 hardware setup [79] for the position control of dc

servo system. Furthermore, during detailed analysis of solar tracker system [35], the proposed approach is compared with the recently applied tuning approaches for sun tracker systems such as particle swarm optimisation (PSO)[80], firefly algorithm (FFA)[81] and cuckoo search algorithm (CSA)[82]. The performance of the existing and proposed approaches is verified in time domain, frequency domain and also via integral performances indices. It is found that the proposed approach exhibits better performance for transient, robustness, and uncertainty aspects in comparison to recently published approaches on soft computing techniques.

3.1 Linear Quadratic Regulator

3.1.1 Introduction

The word LQR is an initialism, that stands for 'Linear Quadratic Regulator'. It belongs to a class of optimal control [83] problems wherein the system dynamics are described by a set of linear differential equations and the performance criteria is delineated by a quadratic weighted function of the states and the control energy. The quadratic cost functional is presented as follows:

$$J = \int_{t_0}^{t_f} \left[x^T(t)Q(t)x(t) + u^T(t)R(t)u(t) \right] dt \tag{3.1}$$

In (3.1), Q and R are the coefficient matrices-Q is positive semi-definite, and R positive definite. The reason behind this choice is that the energy associated with any arbitrary state can only be positive or zero (it is zero at equilibrium point, when the system is initially relaxed). So, according to Sylvester's theorem [41], Q must be positive semi-definite. For R, the case is a bit different. This is because, it is absolutely meaningless to achieve minimum cost function without applying any input. Keeping this in mind, R must always be positive definite. Before delving further into the study of LQR based optimal control, the most obvious question that arises is this, what is the specialty of this technique. The pole-placement technique emerges from the idea of matching time-domain specifications and designing the control law accordingly. However, the pole placement technique is solely based on choice of good poles and does not look into the aspect of control energy minimization. As cost incurred by any engineering problem is a very important issue to

look at, LQR guarantees to achieve a minimum energy cost value using the control law designed using that constraint [84]. It may fail to give the best transient and steady-state characteristics, but when looked at from the economical aspects, it is digestible that although the time-domain characteristics are not up to the mark, the energy cost by the entire process is minimum.

3.1.2 Literature survey

LQR is a popular control technique and is being actively researched upon in the recent past [84]. The work on LQR started off in 1948-1949, with the great work of N. Weiner [85, 86], in automatic control of firing of weapons during World War II. In his work, Wiener designed mean-squared filters by the minimization of the following functional:

$$J = E[e^2(t)] \tag{3.2}$$

This functional is actually the expected value for the mean-squared error function. The generalised performance function that emerged for multi-input multi output (MIMO) systems is as follows:

$$J = \int_0^\infty e^T(t) Q e(t) dt \tag{3.3}$$

where, Q is a positive semi-definite matrix. In a regulation problem, the equilibrium point is always zero. So $e(t) = 0 - x(t)$. Without $u(t)$, (3.1) becomes (3.3) with $e(t) = -x(t)$. This is to reduce the regulation error, and in combination of $u(t)$, as in (3.1), involves the design of an optimal control which guarantees minimum integral squared of tracking error as well as input control energy. This is called the Lagrange's problem of optimization. Following Weiner's work, attempts to solve the Lagrange's problem defined by (3.1) started coming into the picture. In 1957-1965, Bellman worked on the solution of discrete optimal control problems [87–89], where he devised a popular technique of optimization named as 'Dynamic Programming'. The most important landmark in the journey of optimal control was made by Pontryagin (of the former USSR) in the year of 1956 [90]. L. S. Pontryagin, together with his associates presented to the world his famous theory of 'Maximum Principle' in [91]. The detailed analysis and description of this principle is given in [92]. Gramkrelidze, one of Pontryagin's associates, also reported a fascinating article

regarding this field, in [93]. During this period, in 1960, it was R. E. Kalman who gave to the control engineering world the concepts of 'Linear Quadratic Regulator' and 'Linear Quadratic Gaussian', which can be found in [94]. The main intention of Kalman behind these contributions is to provide *optimal feedback control laws*, as feedback control system is the backbone of both classical and modern control theory and applications. Kalman used his concepts of LQR and LQG to develop the theories on optimal filtering and estimation, leading to the birth of the famous 'Kalman Filter', in discrete form [95]. The continuous version of the Kalman filter was developed by Kalman, in association with Bucy [96]. However, the formulation of optimal feedback control proposed by Kalman was heavily dependent on the Riccati Equation. This equation is named after Jacopo Riccati, an Italian mathematician. He had proposed the solutions for some nonlinear differential equations in the year of 1724 [97, 98]. In spite of publishing the base for Kalman's theory, he was completely ignorant of how much important his theory will prove to be, in the field of control literature.

Following the historical background of LQR, in the recent times, theoretical advancements in this field include the works of [99], where the authors have worked on the effect of changing input gains, if LQR is used to design the control. In [100], integral sliding mode control combined with the conventional LQR problem was desired meant for Linear Time-Varying systems, in order to enable LQR to deal with robust control problems. Similar attempt was made in [101], where the robustification was done using the concept of disturbance observer based control. A numerical computation based solution of the algebraic riccati equation (an integral step of the optimal control design using LQR) was proposed in [1, 102, 103]. As PID is very familiar among most of today's industries, J. He *et. al.* proposed an approach to tune PID control parameters with the help of LQR based optimal gain matrix[104]. Moving onward to areas where LQR is still being applied in recent times, lead to the works of [43, 50, 105–108], which imply that the research in this field is still prevalent and going on at steady pace.

3.1.3 Mathematical formulation

For a linear, time-invariant (LTI) system, which is asymptotically stable, the performance index (i.e. the cost function) J is defined as follows:

$$J = \frac{1}{2}\int_0^\infty \left[x^T(t)Qx(t) + u^T(t)Ru(t)\right] dt \tag{3.4}$$

This cost function is subjected to the following system constraint:

$$\dot{x}(t) = Ax(t) + Bu(t) \tag{3.5}$$

The optimal control law is obtained using the Pontryagin Minimum Principle [83]. This is described in the following steps:

- Step 1: Hamiltonian

  The Hamiltonian for this problem is defined as follows:

$$H(x,u,t) = \frac{1}{2}\left[x^T(t)Qx(t) + u^T(t)Ru(t)\right] + \lambda^T\left[Ax + Bu\right] \tag{3.6}$$

- Step 2: Control Law

  Partial differentiation of (3.6) with respect to u gives the optimal control law:

$$u^* = -R^{-1}B^T\lambda \tag{3.7}$$

- Step 3: State and Co-state equations are:

$$\begin{bmatrix}\dot{x}\\ \dot{\lambda}\end{bmatrix} = \begin{bmatrix}A & -BR^{-1}B^T\\ -Q & -A^T\end{bmatrix}\begin{bmatrix}x\\ \lambda\end{bmatrix} \tag{3.8}$$

- Step 4: Formulation of Algebraic Riccati Equation (ARE):

  Using (3.7), (3.8), and $\lambda = Px$, the ARE is formulated as follows:

$$PA + A^T P - PBR^{-1}B^T P = -Q \tag{3.9}$$

Solving (3.9) for P, the optimal control law is obtained as follows:

$$u^* = -R^{-1}B^T Px \tag{3.10}$$

3.1.4 Q and R selection

Bryson's Rule [109]: LQR is a technique which gives an optimal way to design a controller via minimisation of the error in states and control energy. One of the challenges is to select the suitable weighting matrices Q and R for minimising the cost function. This difficulty can be overcome by using Bryson's rule which gives the initial values of the diagonal elements of Q and R matrix as:

$$q_{ii} = \frac{1}{x_{i_{max}}^2}$$

$$r_{jj} = \frac{1}{u_{j_{max}}^2}$$

where, $i, j = 1, 2, 3, ..., n$. Here, n denoted the number of states of the system. Also $x_{i_{max}}$ and $u_{j_{max}}$ are the maximum acceptable values of i^{th} state and j^{th} control input. This causes the maximum value of each term of cost function to be 1 and not more than that. Hence cost function is minimised such that its value is not more than a particular value.

Modified Bryson's Rule: This rule comes with a slight modification in Bryson's rule [110]. According to this,

$$q_{ii} = \frac{\alpha_i^2}{x_{i_{max}}^2}$$

$$r_{jj} = \rho \times \frac{\beta_j^2}{u_{j_{max}}^2}$$

where, α and β are chosen according to the priority given to the individual state and control input. If α_1 is chosen higher then x_1 will settle fast to minimise the cost function and,

$$\Sigma_{i=1}^{n} \alpha_i^2 = 1$$

$$\Sigma_{j=1}^{m} \beta_j^2 = 1$$

ρ is chosen to maintain a balance between the speed of settling of state and the control energy required. If ρ will be higher then control energy will reduce but states will take more time to settle and overshoot will also increase.

3.2 QRAWCP scheme

This section presents the generalised formulation of Quadratic Regulator Approach with Compensating Pole (QRAWCP) scheme for SISO and SIMO systems in a step by step manner.

3.2.1 SISO system

Let the single input single output (SISO) plant model be represented by the following general transfer function of n^{th} order:

$$G(s) = \frac{b_0}{\sum_{l=0}^{n} a_{n-l} s^{n-l}} \tag{3.11}$$

Representing (3.11) in Controllable Canonical Form of state-space representation in the following equation, we get:

$$\begin{bmatrix} \dot{x}_1 \\ \dot{x}_2 \\ \dot{x}_3 \\ \vdots \\ \dot{x}_n \end{bmatrix} = \begin{bmatrix} 0 & 1 & 0 & 0 & \dots & 0 \\ 0 & 0 & 1 & 0 & \dots & 0 \\ 0 & 0 & 0 & 1 & \dots & 0 \\ \vdots & \vdots & \vdots & \vdots & \ddots & \vdots \\ -a_0 & -a_1 & -a_2 & -a_3 & \dots & -a_n \end{bmatrix} \begin{bmatrix} x_1 \\ x_2 \\ x_3 \\ \vdots \\ x_n \end{bmatrix} + \begin{bmatrix} 0 \\ 0 \\ 0 \\ \vdots \\ b_0 \end{bmatrix} u$$
$$y = \begin{bmatrix} 1 & 0 & 0 & \dots & 0 \end{bmatrix} \begin{bmatrix} x_1 \\ x_2 \\ x_3 \\ \vdots \\ x_n \end{bmatrix} \tag{3.12}$$

The state-space matrices are assigned to the following variables as follows:

$$A = \begin{bmatrix} 0 & 1 & 0 & 0 & \dots & 0 \\ 0 & 0 & 1 & 0 & \dots & 0 \\ 0 & 0 & 0 & 1 & \dots & 0 \\ \vdots & \vdots & \vdots & \vdots & \ddots & \vdots \\ -a_0 & -a_1 & -a_2 & -a_3 & \dots & -a_n \end{bmatrix}; B = \begin{bmatrix} 0 \\ 0 \\ 0 \\ \vdots \\ b_0 \end{bmatrix}$$
$$C = \begin{bmatrix} 1 & 0 & 0 & \dots & 0 \end{bmatrix} \tag{3.13}$$

Using (3.9) and (3.10) with P as a real, symmetric positive definite matrix, the LQR based control law is obtained as follows:

$$K = R^{-1} B^T P$$
$$= \frac{1}{r} \begin{bmatrix} 0 & 0 & 0 & \dots & b_0 \end{bmatrix} \begin{bmatrix} P_1 \\ P_2 \\ P_3 \\ \vdots \\ P_n \end{bmatrix} \tag{3.14}$$

where, $P_j = \begin{bmatrix} p_{j1} & p_{j2} & p_{j3} & \dots & p_{jn} \end{bmatrix}$. Note that, since P is symmetric, $p_{jk} = p_{kj} (1 \leq j,k \leq n)$. With this optimal gain matrix, the modified system matrix is $\tilde{A} = A - BK$. The determinant of $(sI - \tilde{A})$ gives the characteristic polynomial of the closed-loop system. Representing the same in factorized form, we get,

$$|sI - A + BK| = 0 \implies \prod_{i=1}^{n} (s + \lambda_i) = 0 \tag{3.15}$$

Multiplying both sides of (3.15) with a compensating pole placed at $s = -\lambda^{'}$, the resultant characteristic equation turns out to be:

$$(s + \lambda^{'}) \prod_{i=1}^{n} (s + \lambda_i) = 0 \implies s^{n+1} + \sum_{i=0}^{n} c_{n-i} s^{n-i} = 0 \tag{3.16}$$

where, $c_0, c_1, \dots, c_n \in \mathbb{R}$. The generalized expression for (3.15) in polynomial form is as follows:

$$|sI - A + BK| = 0 \implies s^n + \sum_{i=1}^{n} (a_{n-i} + b_0 k_{(n+1-i)}) s^{n-i} = 0 \tag{3.17}$$

After adding the compensating pole at $s = -\lambda^{'}$, the resultant characteristic equation is obtained by multiplying $(s + \lambda^{'})$ on both sides of (3.17), which is written in the following manner:

$$\begin{aligned} s^{n+1} + (a_{n-1} + b_0 k_n + \lambda^{'}) s^n + \sum_{i=2}^{n-1} \Big\{ (a_{n-i} + b_0 k_{(n+1-i)} + \\ \lambda^{'} (a_{n-i+1} + b_0 k_{n-i+1}) \Big\} + \lambda^{'} (a_0 + b_0 k_1) = 0 \end{aligned} \tag{3.18}$$

The value of k_i $(i \in [1,n])$ can be obtained as equal to $\frac{b_0}{r} p_{ni}$. If the control of (3.11) is done by a PID controller $G_c(s) = K_p + \frac{K_i}{s} + sK_d$, then the resultant characteristic equation of the closed-loop system is given as follows:

$$\implies (s^{n+1} + a_1 s^n + a_2 s^{n-1} + \dots + a_0 s) + b_0 (k_d s^2 + k_p s + k_i) = 0 \tag{3.19}$$

Comparing (3.19) with (3.16) for the values of k_p, k_i, and k_d in terms of the closed-loop poles, we obtained the following equation:

$$\begin{aligned} k_i &= \frac{1}{b_0}(-1)^n \left\{ \prod_{i=1}^{n} \lambda_i \right\} \\ k_p &= -\frac{1}{b_0} \left\{ (-1)^{2n-1} b_0 k_i \sum_{i=1}^{n} \left(\frac{1}{\lambda_i} \right) - a_0 \right\} \\ k_d &= \frac{1}{b_0} \left\{ (-1)^{2(n-1)} b_0 k_i \sum_{k=2}^{n} \frac{1}{\lambda_k} \left[\sum_{j=1}^{k-1} \frac{1}{\lambda_{k-j}} \right] - a_1 \right\} \end{aligned} \tag{3.20}$$

These formulae will be helpful if all the closed-loop poles positions are known. The generalized formulae for k_p, k_i, k_d, and $\lambda^{'}$ are obtained by comparing (3.18) and (3.19), and are listed as follows:

$$\begin{aligned} \lambda^{'} &= -b_0 k_n \\ k_p &= k_1 + \lambda^{'} \left(\frac{a_1}{b_0} + k_2 \right) \\ k_i &= \lambda^{'} \left(\frac{a_0}{b_0} + k_1 \right) \\ k_d &= k_2 + \lambda^{'} \left(\frac{a_2}{b_0} + k_3 \right) \\ k_j &= \frac{b_0}{r} p_{nj} \ (j \in [1,3]) \end{aligned} \tag{3.21}$$

An extension of this analysis has been carried out for a system with single input and multi outputs.

3.2.2 SIMO system

The method to obtain the values of controllers' gains is described in the following: Let the single input and multi outputs(SIMO) system be defined by the following equations:

$$\dot{x} = Ax + Bu \tag{3.22}$$

$$y = Cx \tag{3.23}$$

where, $A \in \mathbb{R}^{n \times n}, B \in \mathbb{R}^{n \times 1}, C \in \mathbb{R}^{m \times n}$. In order to formulate a simplified methodology for the implementation of the same control technique, (3.22) is converted into controllable canonical

form, using the transformation $x_c = T_c x$. Let the converted system be defined as the following:

$$\dot{x_c} = A_c x_c + B_c u \tag{3.24}$$

$$y = C_c x_c \tag{3.25}$$

As a system may have numerous degrees of freedom, the matrices A_c, B_c, and C_c can be partitioned into Jordan canonical form as follows:

$$\begin{aligned} A_c &= \begin{bmatrix} A_1 & O_2 & O_2 & O_2 & \dots & O_2 \\ O_2 & A_2 & O_2 & O_2 & \dots & O_2 \\ O_2 & O_2 & A_3 & O_2 & \dots & O_2 \\ \vdots & \vdots & \vdots & \vdots & \ddots & \vdots \\ O_2 & O_2 & O_2 & O_2 & \dots & A_k \end{bmatrix}; B_c = \begin{bmatrix} B_1 \\ B_2 \\ B_3 \\ \vdots \\ B_k \end{bmatrix} \\ C_c &= \begin{bmatrix} C_1 & \mathcal{O}_2 & \mathcal{O}_2 & \mathcal{O}_2 & \dots & \mathcal{O}_2 \\ \mathcal{O}_2 & C_2 & \mathcal{O}_2 & \mathcal{O}_2 & \dots & \mathcal{O}_2 \\ \mathcal{O}_2 & \mathcal{O}_2 & C_3 & \mathcal{O}_2 & \dots & \mathcal{O}_2 \\ \vdots & \vdots & \vdots & \vdots & \ddots & \vdots \\ \mathcal{O}_2 & \mathcal{O}_2 & \mathcal{O}_2 & \mathcal{O}_2 & \dots & C_k \end{bmatrix} \end{aligned} \tag{3.26}$$

where,

$$A_k = \begin{bmatrix} 0 & 1 \\ -a_{k0} & -a_{k1} \end{bmatrix}; B_k = \begin{bmatrix} 0 \\ b_k \end{bmatrix}$$

$$C_k = \begin{bmatrix} 1 & 0 \end{bmatrix}; O_2 = \begin{bmatrix} 0 & 0 \\ 0 & 0 \end{bmatrix}$$

$$\mathcal{O}_2 = \begin{bmatrix} 0 & 0 \end{bmatrix}$$

Using the B_c of (3.26), the optimal gain matrix K_o for the system given in (3.22) is obtained from the Algebraic Riccati Equation:

$$K_o = -\frac{1}{r} B_c^T P \tag{3.27}$$

The matrix P is rewritten for each degree-of-freedom as follows:

$$\begin{aligned} P &= \begin{bmatrix} P_1 & P_2 & P_3 & \dots & P_k \end{bmatrix} \\ P_k &= \begin{bmatrix} p_{11} & p_{12} & p_{13} & \dots & p_{1k} \end{bmatrix}^T \end{aligned} \tag{3.28}$$

Using (3.26) and (3.27), the eigen values of $A_c - B_c K_o$ are to be obtained. Let the set Λ represent the set of these values:

$$\Lambda = \left\{ i \in [1,n] | \lambda_i \in \Lambda \right\} \tag{3.29}$$

Using (3.29), $|sI - A_c + B_c K_o| = 0$ is as follows:

$$\prod_{i=1}^{n} (s + \lambda_i) = 0 \tag{3.30}$$

If there are k number of degree-of-freedoms, then k number of PID controllers are to be used. This implies that the number of compensating poles to be added to the system is $k-1$. Let the resulting factored equation be written as follows:

$$\prod_{j=1}^{k-1} (s + \lambda_j^{'}) \prod_{i=1}^{n} (s + \lambda_i) = 0 \tag{3.31}$$

Each transfer function corresponding to the kth $(k \in \mathbb{N})$ degree-of-freedom is of the following form:

$$P_k(s) = \frac{b_k}{s^2 + a_{k1} s + a_{k0}} \tag{3.32}$$

The generalized characteristic equation of the closed-loop system is obtained using (3.32) in the following:

$$\sum_{i=1}^{k} P_i C_i = -1 \tag{3.33}$$

$$\implies \prod_{j=1}^{k} \left(\frac{b_j}{s^2 + a_{j1} s + a_{j0}} \right) \left(\frac{k_{dj} s^2 + k_{pj} s + k_{ij}}{s} \right) = -1 \tag{3.34}$$

For better clarity, (3.33) is rewritten in the following equation:

$$s^{k-1}\prod_{i=1}^{k}D_i(s)+\sum_{i=1}^{k}\left[\left(\prod_{i=1}^{k}D_i\right)\left(b_i\frac{N_{ci}}{D_i}\right)\right]=0 \tag{3.35}$$

In (3.35), $D_i(i\in[1,n])$ From above (3.35) we can say that, the number of controllers is same as the number of degree of freedom (DOF)s, which is one-half of the system's order.

When $k=2$

In (3.33) and (3.35), with $k=2$, the characteristic equation of the closed-loop system is as follows:

$$s\prod_{j=1}^{2}(s^2+a_{j1}s+a_{j0})+\sum_{j=1}^{2}\left[b_1N_{c1}(s)D_2(s)+b_2N_{c2}(s)D_1(s)\right]=0 \tag{3.36}$$

where, $N_{c1}=k_{d1}s^2+k_{p1}s+k_{i1}, N_{c2}=k_{d2}s^2+k_{p2}s+k_{i2}$. Hence, the resultant equation is given below:

$$\begin{aligned}&s\left\{s^4+(a_{11}+a_{21})s^3+(a_{10}+a_{20})s^2+(a_{21}a_{10}+a_{11}a_{20})s+a_{10}a_{20}\right\}+\\&b_1\left[k_{d1}s^4+(k_{d1}a_{21}+k_{p1})s^3+(k_{d1}a_{20}+k_{i1})s^2+(k_{p1}a_{20}+k_{i1}a_{21})s+k_{i1}a_{20}\right]+\\&b_2\left[k_{d2}s^4+(k_{d2}a_{11}+k_{p2})s^3+(k_{d2}a_{10}+k_{i2})s^2+(k_{p2}a_{10}+k_{i2}a_{11})s+k_{i2}a_{10}\right]=0\end{aligned} \tag{3.37}$$

Grouping together the like terms of (3.37) and rewriting (3.36) as follows:

$$\begin{aligned}&s^5+\{a_{11}+a_{21}+b_1k_{d1}+b_2k_{d2}\}s^4+\left\{a_{10}+a_{20}+b_1(k_{d1}a_{21}+k_{p1})\right\}s^3+\\&\left\{a_{21}a_{10}+a_{11}a_{20}+b_1(k_{d1}a_{20}+k_{i1})+b_2(k_{d2}a_{10}+k_{i2})\right\}s^2+\left\{a_{10}a_{20}+b_1(k_{p1}a_{20}\right.\\&\left.+k_{i1}a_{21})+b_2(k_{p2}a_{10}+k_{i2}a_{11})\right\}s+b_1k_{i1}a_{20}+b_2k_{i2}a_{10}=0\end{aligned} \tag{3.38}$$

Following from (3.31), the same equation can be written in generalised polynomial form as follows:

$$1+P_1C_1+P_2C_2=s^5+p_4s^4+p_3s^3+p_2s^2+p_1s+p_0=0 \tag{3.39}$$

Comparison of (3.38) and (3.39) leads to the following set of formulae:

$$\begin{bmatrix} 0 & 0 & b_1 & 0 & 0 & b_2 \\ b_1 & 0 & b_1a_{21} & 0 & 0 & 0 \\ 0 & b_1 & b_1a_{20} & 0 & b_2 & b_2a_{10} \\ b_1a_{20} & b_1a_{21} & 0 & b_2a_{10} & b_2a_{11} & 0 \\ 0 & b_1a_{20} & 0 & 0 & b_2a_{10} & 0 \end{bmatrix} \begin{bmatrix} k_{p1} \\ k_{i1} \\ k_{d1} \\ k_{p2} \\ k_{i2} \\ k_{d2} \end{bmatrix} = \begin{bmatrix} p_4 - a_{11} - a_{21} \\ p_3 - a_{10} - a_{20} \\ p_2 - a_{21}a_{10} - a_{11}a_{20} \\ p_1 - a_{10}a_{20} \\ p_0 \end{bmatrix} \tag{3.40}$$

The values of the coefficients of (3.39) can be obtained from the eigen values of $(A_c - B_cK_o)$ and the added compensating pole, using the following formulae:

$$p_0 = (-1)^5 \left(\lambda_1\lambda_2\lambda_3\lambda_4\lambda^{'}\right) \tag{3.41}$$

$$p_1 = (-1)^4 \left(\lambda_1\lambda_2\lambda_3\lambda_4 + \lambda_1\lambda_2\lambda_3\lambda^{'} + \lambda_1\lambda_2\lambda_4\lambda^{'} + \lambda_1\lambda_3\lambda_4\lambda^{'} + \lambda_2\lambda_3\lambda_4\lambda^{'}\right) \tag{3.42}$$

$$p_2 = (-1)^3 \left(\lambda_1\lambda_2\lambda_3 + \lambda_1\lambda_2\lambda_4 + \lambda_1\lambda_2\lambda^{'} + \lambda_1\lambda_3\lambda_4 + \lambda_1\lambda_3\lambda^{'} + \lambda_1\lambda_4\lambda^{'} + \lambda_2\lambda_3\lambda_4 + \right. \tag{3.43}$$

$$\left. \lambda_2\lambda_3\lambda^{'} + \lambda_2\lambda_4\lambda^{'} + \lambda_3\lambda_4\lambda^{'}\right) \tag{3.44}$$

$$p_3 = (-1)^2 \left(\lambda_1\lambda_2 + \lambda_1\lambda_3 + \lambda_1\lambda_4 + \lambda_1\lambda^{'} + \lambda_2\lambda_3 + \lambda_2\lambda_4 + \lambda_2\lambda^{'} + \lambda_3\lambda_4 + \lambda_3\lambda^{'} + \lambda_4\lambda^{'}\right) \tag{3.45}$$

$$p_4 = (-1)^1 \left(\lambda_1 + \lambda_2 + \lambda_3 + \lambda_4 + \lambda_5\right) \tag{3.46}$$

Having obtained the values of the coefficients, (3.40) is to be used to compute the PID controller parameters.

3.3 Illustrative Examples

This section illustrates the application of the proposed scheme for different classes of linear time invariant systems.

Example 1: Consider a repeated pole second-order system

$$G_1(s) = \frac{1}{(s+1)^2} = \frac{1}{s^2+2s+1} \tag{3.47}$$

Let us consider the generalized system in variable form as, $G_1(s) = \frac{1}{s^2+a_1 s+a_2}$. On simplification of $1 + G_1(s)C(s) = 0$, we get the closed loop characteristic equation as

$$1 + \frac{1}{s^2 + a_1 s + a_2} \times (k_p + \frac{k_i}{s} + k_d s) = 0 \tag{3.48}$$

On further simplification, we get

$$s^3 + (a_1 + k_d b_0)s^2 + (a_2 + b_0 k_p)s + b_0 k_i = 0 \tag{3.49}$$

In the next step, we obtain the state feedback gain matrix K, via LQR approach as $K = R^{-1}B^T P$. The system matrices A, B and positive definite matrix P and R are given as follows:

$$A = \begin{bmatrix} 0 & 1 \\ -a_2 & -a_1 \end{bmatrix}; \quad B = \begin{bmatrix} 0 \\ 1 \end{bmatrix}; \quad P = \begin{bmatrix} p_{11} & p_{12} \\ p_{12} & p_{22} \end{bmatrix}; \quad R = [1] \tag{3.50}$$

Substituting these values to compute K, we get, $K = [p_{12} \quad p_{22}]$, consequently, it's closed loop system equation becomes

$$|sI - (A - BK)| = s^2 + (a_1 + p_{22})s + a_2 + p_{12} = 0 \tag{3.51}$$

Since Equation (3.51) is of second order, whereas the system with PID controller is of third order, so we augment one extra pole λ_3, thus the characteristic equation becomes $(s + \lambda_3)(s^2 + (a_1 + p_{22})s + (a_2 + p_{12}) = 0$. On further simplification, we get,

$$s^3 + (a_1 + p_{22} + \lambda_3)s^2 + (a_1 + p_{22} + \lambda_3(a_1 + p_{22}))s + (a_2 + p_{12}) = 0 \tag{3.52}$$

Since there are two equations and three unknowns, so in equation (3.49), set K_d to desired value, depending on the actuator rate constant. On comparing the coefficients of Laplace variable of order 2, we get

$$\lambda_3 = K_d - p_{22} \tag{3.53}$$

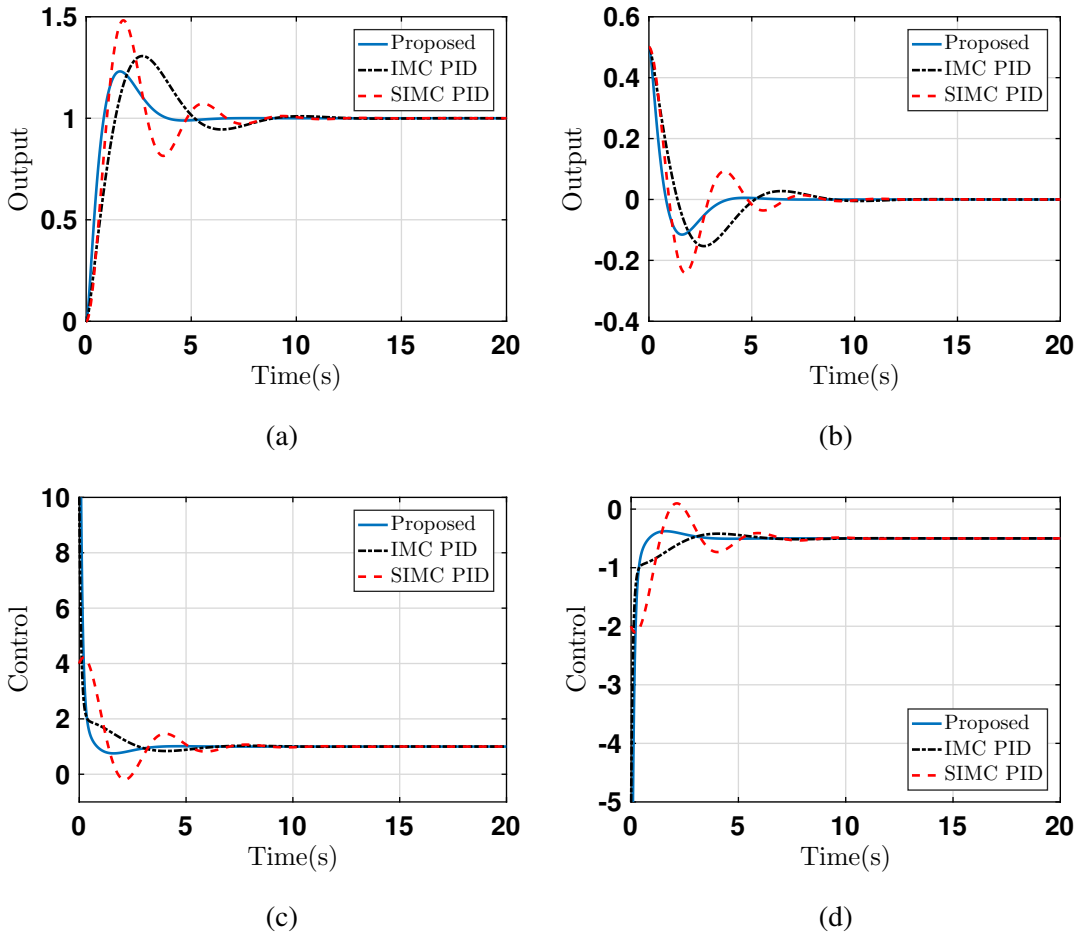

Figure 3.1: Output for step-type (a) set-point, (b) disturbance, and control action for (c) set-point tracking and (d) disturbance rejection of Example 1

On further comparison of (3.49) and (3.52), the other two PID controller gains can be obtained as follows:

$$K_p = p_{12} + \lambda_3(a_1 + p_{12}) \qquad K_i = (a_2 + p_{12})\lambda_3 \tag{3.54}$$

Using the proposed scheme, the PID parameters are $\lambda_3 = -8.5858$ and the controller gain from (3.54) as: $K_p = 21.1421$ $K_i = 20.7279$. We have presumed, $K_d = 10$. For the purpose of comparison and validation of the proposed approach, we consider two techniques from the literature, i.e., IMC PID whose parameter values are given by $K_p = K_i = K_d = 1/\lambda$ in [39] and other is the SIMC approach [111] which, gives $\tau_I = \min(1, 4\lambda)$, $K_p = \tau_I/\lambda$, $\tau_D = 1$.

The comparison of the output response for unit step input is shown in Fig. 3.1(a) wherein, the output obtained by using proposed technique reaches the steady state quickly with minimal overshoot and exhibits smaller oscillations as compared to Skogestad IMC (SIMC)[111]. Also, the response

obtained using second-order filter ($n = 2$) gives less overshoot, but it is sluggish in nature due to the presence of a lag-term. Next, for the observation of disturbance attenuation property, a step disturbance of amplitude of 0.5 units is applied at $t = 0$ seconds. It can be seen in Fig. 3.1(b) that the proposed technique gives faster disturbance attenuation as compared to IMC [39] and SIMC [111]. The control actions for set-point tracking and disturbance rejection performance are depicted in Figs. 3.1(c) and 3.1(d). To test the optimality, different performance indices are given in Table 3.1. It can be seen, that for reference tracking, the proposed technique gives least error among the other methods in the literature. However, for SIMC, *IE* is the least due to oscillatory nature of the response.

***Example 2**:* Now, consider a second order plant which is a model of the PMS set-up[1], designed by Feedback Instruments Limited, England.

From user manual, the transfer function model for angular shaft velocity (ω) versus armature current (i_a) is given as

$$G_2(s) = \frac{1.362 \times 10^8}{s^2 + 1000s + 8.476 \times 10^4} \tag{3.55}$$

This transfer function can be generalized as, $G_1(s) = \frac{b_0}{s^2+a_1 s+a_2}$. Upon simplification of the closed loop characteristic equation, $1 + G_2C(s) = 0$, we get,

$$1 + \frac{b_0}{s^2 + a_1 s + a_2} \times (k_p + \frac{k_i}{s} + k_d s) = 0 \tag{3.56}$$

Rearranging the similar power terms, we get, the final closed loop characteristic equation as

$$s^3 + (a_1 + k_d b_0)s^2 + (a_2 + b_0 k_p)s + b_0 ki = 0 \tag{3.57}$$

In a similar manner as given in example 1, the LQR feedback gain matrix $K = [k_1 \quad k_2]$ is computed, then the matrix $|sI - (A - BK)|$ is obtained and finally the pole λ_3 is augmented to it. Now, the difference between Ghosh LQR-PID [1] and Proposed PID is that, in Ghosh PID, the augmented pole is randomly adjusted as multiple times of real part of the dominant pole of the system. But, there is no well-defined rule on how far we need to select the pole, and the choice

[1]The detailed information is available at http://www.feedback-instruments.com/ products/ education/ control instrumentation/ precision modular control workshop

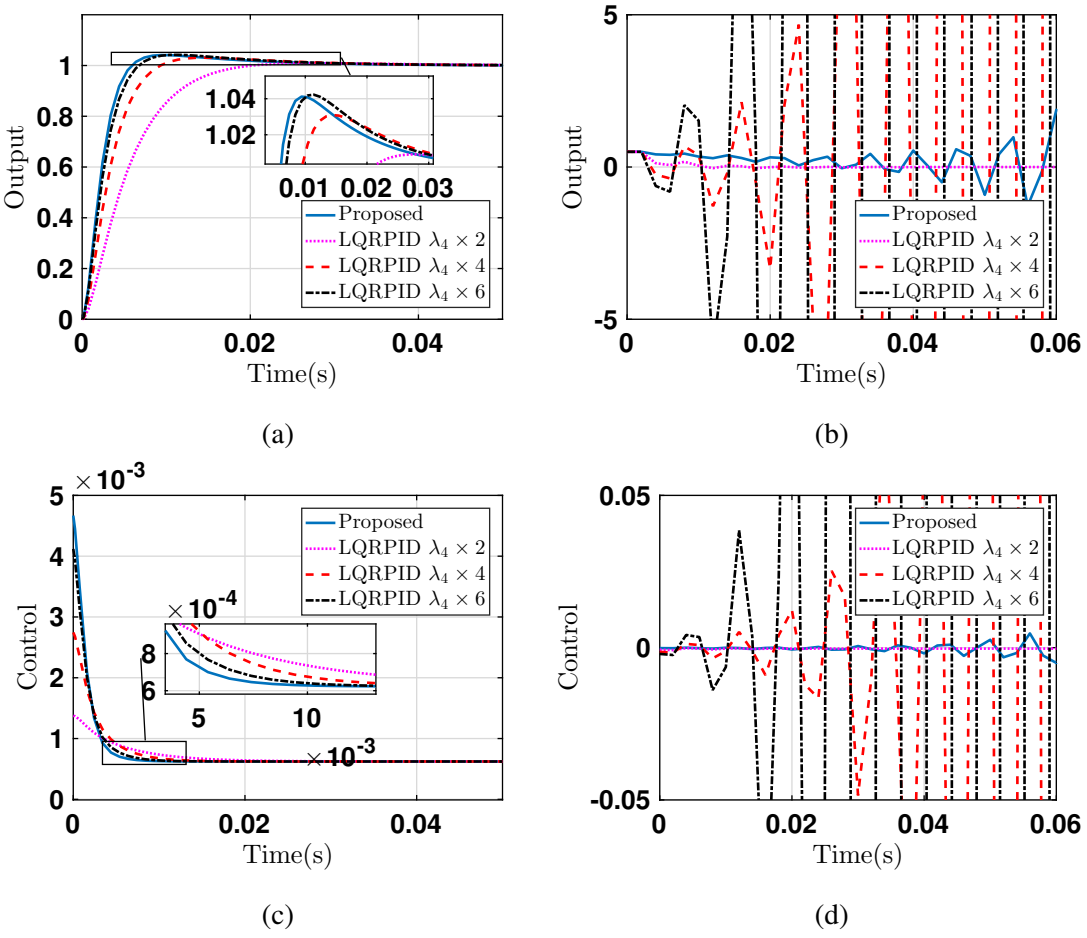

Figure 3.2: Output for step-type (a) set-point, (b) disturbance, and control action for (c) set-point tracking and (d) disturbance rejection of Example 2

of this pole plays a critical role in stabilization of system. But in the proposed PID, a well-structured scheme is recommended for the design of PID controllers. For the present example, we chose $K_d = 4.1191 \times 10^{-6}$ and hence obtain $\lambda_3 = -42.3864$ and other controller gain values as $K_p = 3.1121 \times 10^{-4}$ and $K_i = 0.0264$.

For the comparison and verification of proposed technique with LQR-PID, we have randomly selected the LQR-PID values by adjusting λ_3 as 2, 4, and 6 times of dominant pole of a system, as discussed in [1]. Thus we get, LQR-PID for 2 times multiple: $\lambda_2 \times 2 = -187.0054$, $K_p = 0.0014$, $K_i = 0.1164$, $K_d = 1.3730 \times 10^{-6}$, LQR-PID for 4 times multiple: $\lambda_2 \times 4 = -374.0108$,$K_p = 0.0027$, $K_i = 0.2328$, $K_d = 2.7460 \times 10^{-6}$ and LQR-PID for 6 times multiple: $\lambda_2 \times 4 = -561.0163$,$K_p = 0.0041$, $K_i = 0.3491$, $K_d = 4.1191 \times 10^{-6}$.

The set-point tracking and disturbance rejection capability (along with their control actions) of

the proposed approach and LQR-PID, shown in Fig. 3.2, is the fastest and optimal (see Table 3.1) amongst all.

***Example 3**:* Now, consider the fourth order plant having repeated poles as follows

$$G_3(s) = \frac{1}{(s+1)^4} \tag{3.58}$$

This can be represented by the following fourth order transfer function

$$G_4(s) = \frac{b_0}{s^4 + a_3 s^3 + a_2 s^2 + a_1 s + a_0} \tag{3.59}$$

where, $b_0 = 1$, $a_3 = 4$,$a_2 = 6$, $a_4 = 4$, and $a_0 = 1$.

On further simplification, we get the closed-loop characteristic equation $1 + G_4(s)C(s) = 0$ as

$$s^5 + a_3 s^4 + K_d b_0 s^2 + a_2 s^3 + K_p b_0 s + a_1 s^2 + K_i b_0 + a_0 s = 0 \tag{3.60}$$

Rearranging the terms in (3.60) yields,

$$s^5 + a_3 s^4 + a_2 s^3 + (a_1 + K_d b_0) s^2 + (K_p b_0 + a_0) s + K_i b_0 = 0 \tag{3.61}$$

In a similar manner, as done in example 1, the LQR feedback gain matrix $K = [k_1 \quad k_2 \quad k_3 \quad k_4]$ is calculated, then $|sI - (A - BK)|$ is obtained and finally on augmenting pole $-\lambda_5$, we get the closed-loop characteristic equation as

$$\begin{aligned} s^5 + (a_4 + p_{44} + \lambda_5)\, s^4 + \left(a_2 + p_{34} + (a_4 + p_{44})\, \lambda_5\right) s^3 + \\ \left(a_1 + p_{24} + (a_2 + p_{34})\, \lambda_5\right) s^2 + \left(a_0 + p_{14} + (a_1 + p_{24})\, \lambda_5\right) s + (a_0 + p_{14})\, \lambda_5 \end{aligned} \tag{3.62}$$

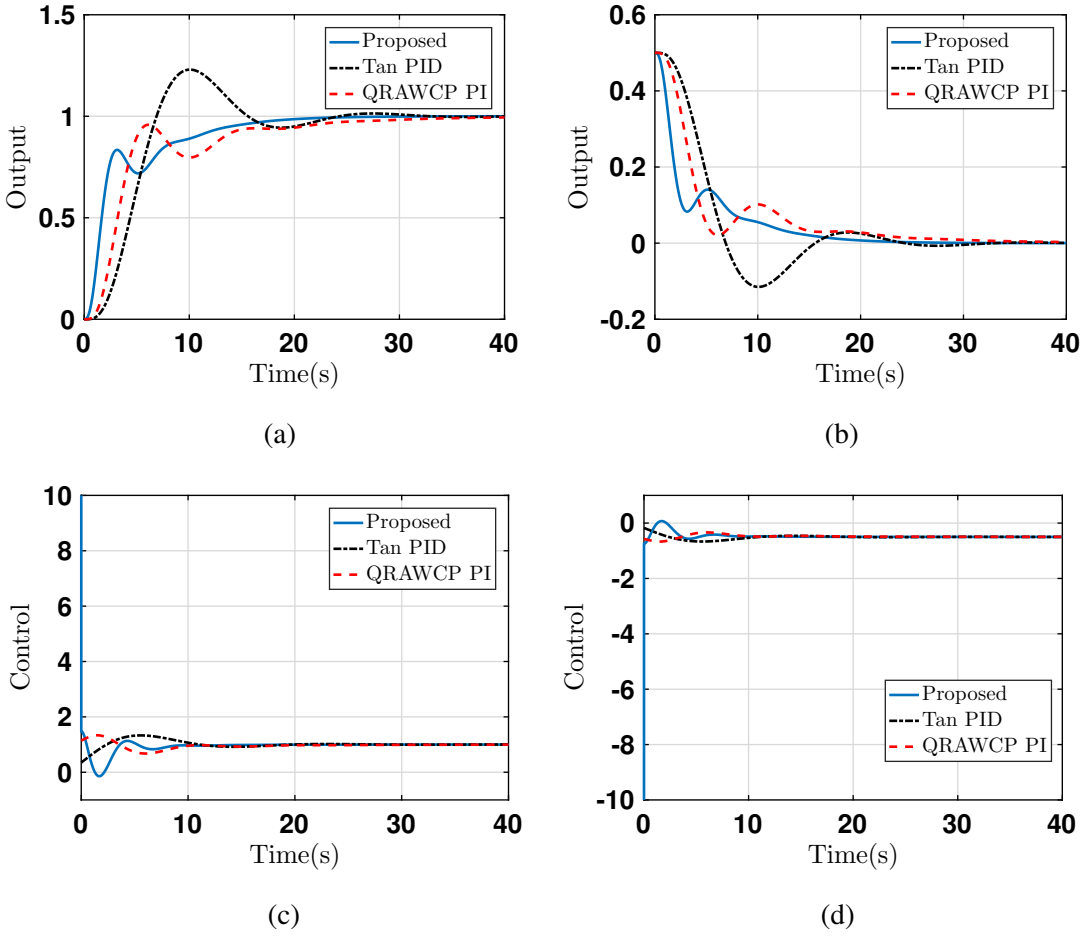

Figure 3.3: Output for step-type (a) set-point, (b) disturbance, and control action for (c) set-point tracking and (d) disturbance rejection of Example 3

Comparing (3.61) and (3.62), the values of augmented pole obtained are are, $\lambda_5 = -\frac{p_{34}}{a_4+p_{44}}$ and PID gains become

$$\begin{aligned} K_p &= \frac{a_1\lambda_5 + p_{24}\lambda_5 + p_{14}}{b_0} \\ K_i &= \frac{(a_0 + p_{14})\lambda_5}{b_0} \\ K_d &= \frac{a_2\lambda_5 + p_{34}\lambda_5 + p_{24}}{b_0} \end{aligned} \tag{3.63}$$

Thus we obtain $\lambda_5 = -0.1945$ and other controller gain values as $K_p = 1.374$, $K_i = 0.2025$ and $K_d = 2.23$. We have also designed a PI controller using proposed approach, thus we obtain QRAWCP-PI controller as, $\lambda_5 = -0.1359$, $K_p = 1.0841$, $K_i = 0.1921$. From [57], the SBL-PI controller values are $K_p = 0.35$, $K_i = 0.3$. The respective results are shown in the Fig. 3.3. The set-point tracking and disturbance responses (along with their control actions) of the proposed approach and LQR-PID, are shown in Fig. 3.3, and it can be concluded that the step response

obtained via the proposed approach is the fastest and optimal among all others. (See Table 3.1, Example 3)

Example 4: Now consider, the transfer function model of Manutec robot [57] of fourth order as

$$G_5(s) = \frac{10}{s(s+2)(s+40)(s+45)} \tag{3.64}$$

This can be represented in the generalized form as

$$G_5(s) = \frac{b_0}{s^4 + a_3 s^3 + a_2 s^2 + a_1 s + a_0} \tag{3.65}$$

where, $b_0 = 10$, $a_3 = 87$,$a_2 = 1970$, $a_1 = 4$, and $a_0 = 1$. On substituting the values of $C(s)$ and $G_5(s)$, we obtain the closed loop characteristic equation as

$$s^5 + a_3 s^4 + K_d b_0 s^2 + a_2 s^3 + K_p b_0 s + a_1 s^2 + K_i b_0 + a_0 s \tag{3.66}$$

Rearranging (3.66) the terms, we obtain

$$s^5 + a_3 s^4 + a_2 s^3 + (a_1 + K_d b_0) s^2 + (K_p b_0 + a_0) s + K_i b_0 = 0 \tag{3.67}$$

Similar to example 1, the LQR feedback gain matrix $K = [k_1 \quad k_2 \quad k_3 \quad k_4]$ is evaluated and then $|sI - (A - BK)|$ is obtained and finally, additional pole, i.e., λ_5 is augmented to the characteristic equation. The final closed loop characteristic equation is given as,

$$\begin{aligned} s^5 + (a_4 + p_{44} + \lambda_5) s^4 + \left(a_2 + p_{34} + (a_4 + p_{44}) \lambda_5\right) s^3 + \left(a_1 + p_{24} + (a_2 + p_{34}) \lambda_5\right) s^2 \\ + \left(a_0 + p_{14} + (a_1 + p_{24}) \lambda_5\right) s + (a_0 + p_{14}) \lambda_5 = 0 \end{aligned} \tag{3.68}$$

Comparing (3.67) and (3.68), the values of augmented pole obtained as $\lambda_5 = -\frac{p_{34}}{a_4 + p_{44}}$ and PID gains becomes, $K_p = \frac{a_1 \lambda_5 + p_{24} \lambda_5 + p_{14}}{b_0}$, $K_i = \frac{(a_0 + p_{14}) \lambda_5}{b_0}$ and $K_d = \frac{a_2 \lambda_5 + p_{34} \lambda_5 + p_{24}}{b_0}$. Thus we obtain $\lambda_5 = -14.2586$ and other controller gain values as $K_p = 6.5379 \times 10^3$, $K_i = 4.5628 \times 10^2$ and $K_d = 3.0040 \times 10^3$. For the verification and validation of the proposed approach, it is compared with SBL-PI controller designed in [57]. We also design a PI controller using proposed approach and get QRAWCP-PI controller as $\lambda_5 = -0.0025624$, $K_p = 1.0143e2$, $K_i = 0.025929$. According

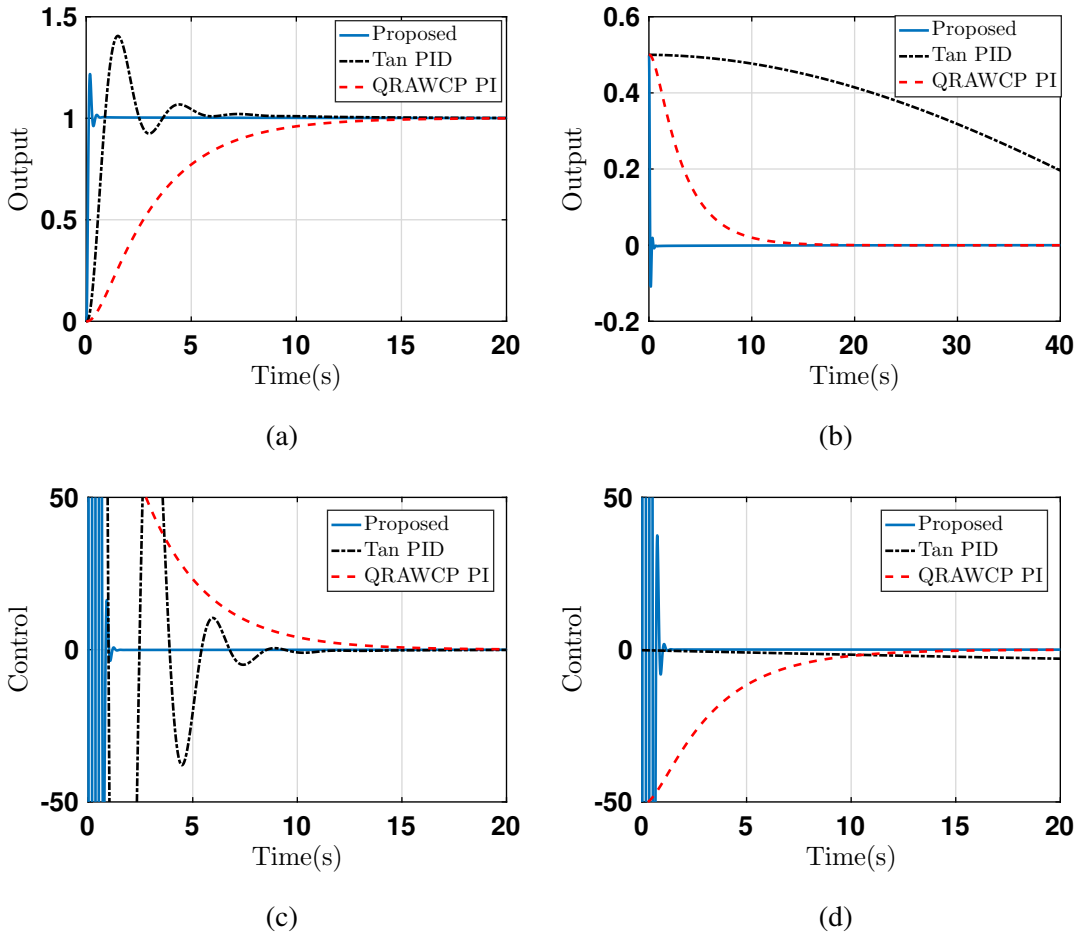

Figure 3.4: Output for step-type (a) set-point, (b) disturbance, and control action for (c) set-point tracking and (d) disturbance rejection of Example 4

to SBL-PI [57] controller gain $K_p = 1000$, $K_i = 187.16$. The respective results are shown in the Fig. 3.4. The set-point tracking and disturbance responses (along with their control actions) of the proposed approach and SBL-PI[57], shown in Fig. 3.4, are the fastest and optimal amongst all others (See Table 3.1, Example 4).

Table 3.1: Comparison of performance indices for illustrative examples

Examples	Method	Reference tracking				Disturbance rejection			
		ISE	IAE	ITSE	ITAE	ISE	IAE	ITSE	ITAE
Example1	Proposed	3.361×10^{-1}	7.806×10^{-1}	1.648×10^{-1}	9.040×10^{-1}	8.403×10^{-2}	3.903×10^{-1}	4.121×10^{-2}	4.520×10^{-1}
	IMCPID	6.319×10^{-1}	1.512×10^{0}	6.471×10^{-1}	3.460×10^{0}	1.580×10^{-1}	7.561×10^{-1}	1.618×10^{-1}	1.730×10^{0}
	SIMC	6.976×10^{-1}	1.515×10^{0}	6.656×10^{-1}	3.036×10^{0}	1.744×10^{-1}	7.573×10^{-1}	1.664×10^{-1}	1.518×10^{0}
Example2	Proposed	1.415×10^{-2}	2.411×10^{-2}	1.650×10^{-4}	4.569×10^{-4}	3.549×10^{0}	2.927×10^{-1}	3.281×10^{-1}	2.442×10^{-2}
	LQR-PIDx2	3.338×10^{-3}	5.766×10^{-3}	8.617×10^{-6}	3.147×10^{-5}	1.115×10^{-3}	3.290×10^{-3}	1.892×10^{-6}	1.761×10^{-5}
	LQR-PIDx4	2.067×10^{-3}	3.790×10^{-3}	3.256×10^{-6}	2.039×10^{-5}	5.573×10^{6}	2.921×10^{2}	5.225×10^{5}	2.638×10^{1}
	LQR-PIDx6	1.615×10^{-3}	3.178×10^{-3}	2.059×10^{-6}	1.823×10^{-5}	2.673×10^{17}	4.565×10^{7}	2.586×10^{16}	4.340×10^{6}
Example3	Proposed	1.612×10^{0}	3.636×10^{0}	3.021×10^{0}	1.791×10^{1}	4.029×10^{-1}	1.818×10^{0}	7.553×10^{-1}	8.957×10^{0}
	SBLPI	2.742×10^{0}	5.151×10^{0}	6.147×10^{0}	3.462×10^{1}	9.203×10^{-1}	2.950×10^{0}	2.323×10^{0}	1.581×10^{1}
	QRAWCP-PI	2.742×10^{0}	5.151×10^{0}	6.147×10^{0}	3.462×10^{1}	6.855×10^{-1}	2.575×10^{0}	1.537×10^{0}	1.731×10^{1}
Example4	Proposed	6.399×10^{-2}	1.448×10^{-1}	3.399×10^{-3}	3.448×10^{-1}	1.600×10^{-2}	7.755×10^{-2}	8.893×10^{-4}	3.143×10^{-1}
	SBLPI	5.573×10^{-1}	1.187×10^{0}	3.419×10^{-1}	2.422×10^{0}	6.489×10^{0}	1.568×10^{1}	9.867×10^{1}	2.722×10^{2}
	QRAWCP-PI	2.051×10^{0}	3.533×10^{0}	3.280×10^{0}	1.041×10^{1}	5.128×10^{-1}	1.774×10^{0}	8.202×10^{-1}	5.437×10^{0}

3.4 Comprehensive analysis for solar tracker system

In this section, a third order real time plant model of solar tracker system is considered. The solar tracker system with DC servo motor and PID controller is shown in Fig. 3.5. To obtain maximum efficiency from solar panel, minimum two axes of sun tracker are required, i.e., one is azimuth angle (θ) that measures the angle of incoming sunlight to the surface of PV cell and other is tilted angle (α) which measures the inclination angle of sunlight. As sun tracker is a non-interacting system, controller designed for single axis will be the replica for another axis also. Therefore, the analysis has been carried out on a single axis sun tracker system as shown in Fig. 3.6. Mathematical model of sun tracker is determined using basic laws of physics. For the major hardware parts such as DC servo motor, it's speed transfer function G_1 is given in (3.69) and G_2 is for position control in (3.70). A gear ratio (N) and other parameters with values are listed in Table 3.2. Now, we

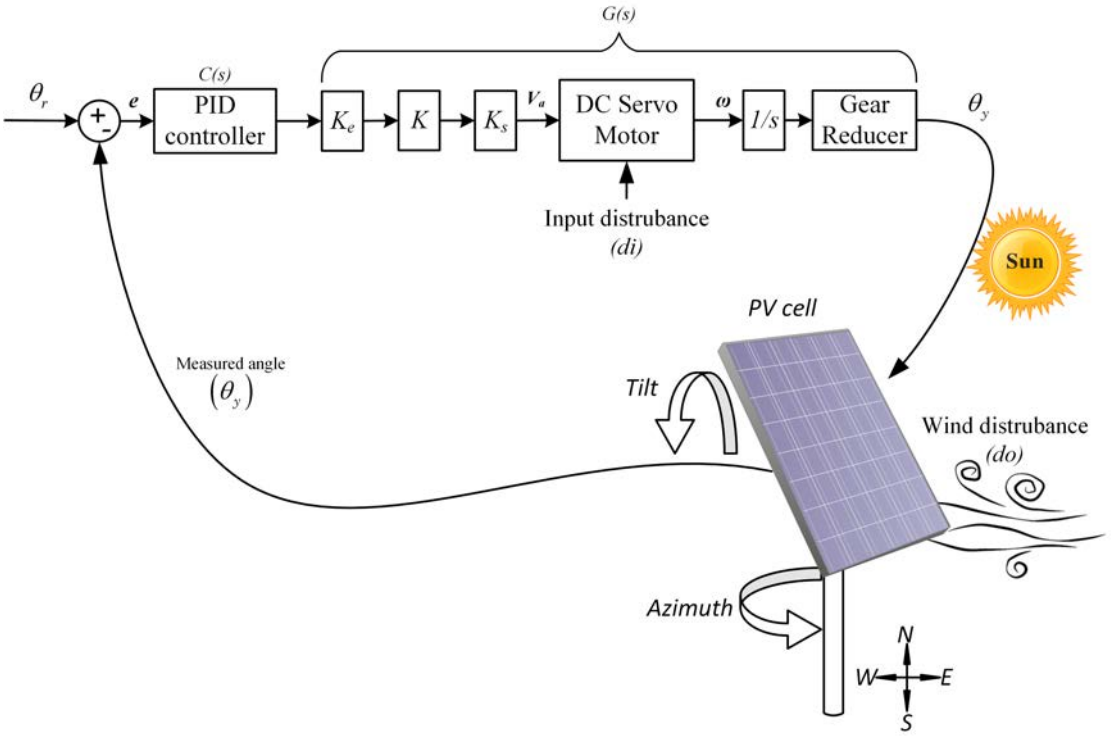

Figure 3.5: Sun tracker system layout

consider a single axis model as shown in Fig. 3.6. Applying Kirchhoff law to DC motor, we get angular velocity ($\omega(s)$)-to-armature voltage transfer function as

$$G_1(s) = \frac{\omega(s)}{V_a(s)} = \frac{K_t}{(R_a + L_a s)(Js + b) + (K_t K_b)} \tag{3.69}$$

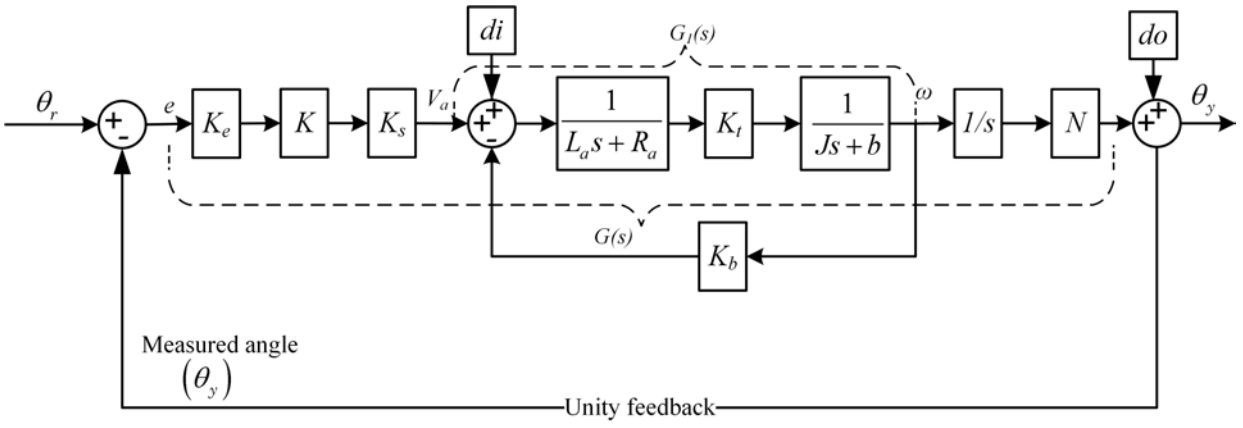

Figure 3.6: Model of solar tracker system

where, $V_a(s)$ is an armature input voltage. By integrating (3.69), the position control transfer function can be obtained as,

$$G_2(s) = \frac{\theta_y(s)}{V_a(s)} = \frac{K_t}{L_a J s^3 + (bL_a + R_a J)s^2 + (R_a b + K_t K_b)\,s} \tag{3.70}$$

Moreover, the sun tracker is interfaced with some additional components such as error discriminator (K_e), amplifier gain (K), servo amplifier (K_s) and gear ratio (N). If all these parameters are considered, then open loop transfer function for this sun tracker system becomes,

$$G(s) = \frac{\theta_y(s)}{\theta_r(s)} = \frac{K_s K K_e K_t N}{L_a J s^3 + (bL_a + R_a J)s^2 + (R_a b + K_t K_b)\,s} \tag{3.71}$$

In equation (3.71), transfer function can also be written as

$$G(s) = \frac{a_4}{b_1 s^3 + b_2 s^2 + b_3 s + b_4} \tag{3.72}$$

where, $a_4 = K_s K K_e K_t N$, $b_1 = L_a J$, $b_2 = (bL_a + R_a J)$, $b_3 = (R_a b + K_t K_b)$, and $b_4 = 0$. Equation (3.72) can be transformed into a state space model, by defining the states as, $x_1 = \theta_y$, $x_2 = \dot{\theta}_y$, and $x_3 = \ddot{\theta}_y$. The input and output variables are represented as $u = \theta_r$ and $y = \theta_y$, respectively. Using

this, the state space model can be written as

$$\begin{bmatrix} \dot{x}_1 \\ \dot{x}_2 \\ \dot{x}_3 \end{bmatrix} = \begin{bmatrix} 0 & 1 & 0 \\ 0 & 0 & 1 \\ -\frac{b_4}{b_1} & -\frac{b_3}{b_1} & -\frac{b_2}{b_1} \end{bmatrix} \begin{bmatrix} x_1 \\ x_2 \\ x_3 \end{bmatrix} + \begin{bmatrix} 0 \\ 0 \\ \frac{a_4}{b_1} \end{bmatrix} u$$
$$y = \begin{bmatrix} 1 & 0 & 0 \end{bmatrix} \begin{bmatrix} x_1 \\ x_2 \\ x_3 \end{bmatrix} \tag{3.73}$$

3.4.1 Optimal PID design using QRAWCP scheme

The quadratic regulator approach with compensatory pole (QRAWCP) approach to tune PID controller is described in a series of distinct steps as follows.

Table 3.2: Parameters of sun tracker system

Parameter	Value	Unit
Error discriminator(K_e)	0.001	V/rad
Amplifier gain(K)	10000	V/V
Servo amplifier(K_s)	1	V/V
Armature resistance(R_a)	6.25	ohm
Armature inductance(L_a)	0.001	H
Torque constant(K_t)	0.01125	Nm/A
Back emf constant(K_b)	0.0125	Nm/A
Inertia of motor rotor(J)	1×10^{-6}	kgm^2/rad
Friction coefficient(b)	0.000001	Nm
Gear ratio(N)	1/800	-

Step 1: The transfer function of the sun tracker system model $G(s)$ is given in (3.72), and the respective parameters are given in Table 3.2. The proportional (K_p), integral (K_i) and derivative (K_d) (PID) controller $C(s)$ can be written as

$$C(s) = \frac{K_d s^2 + sK_p + K_i}{s} \tag{3.74}$$

Step 2: The closed-loop characteristic polynomial for PID controller $C(s)$ and plant $G(s)$ is given as,

$$\Delta(s) = 1 + G(s)C(s) \tag{3.75}$$

Simplifying (3.75) and equating to zero, we get, the closed loop characteristic equation as,

$$s^4 + \frac{b_2}{b_1}s^3 + \left(\frac{b_3 + a_4K_d}{b_1}\right)s^2 \quad + \left(\frac{b_4 + a_4K_p}{b_1}\right)s + \frac{a_4}{b_1}K_i = 0 \tag{3.76}$$

Step 3: The state space form for sun tracker system is given in (3.73). Using this, the design procedure of PID is given in step 4 to step 7 below.

Step 4: *Determination of performance index in terms of initial conditions*:

The quadratic regulator approach is an optimal state feedback controller which can be designed to minimize a specific quadratic cost function, also known as performance index (PI). The PI is designed for constraints like control voltage (u), output signal (y), error (e) or unconstrained objectives of linear time invariant (LTI) system. The optimal control vector $u(t)$ can be obtained by using the following equation:

$$u(t) = -K_l x(t) \tag{3.77}$$

Here, unconstrained optimal action is considered. Therefore, cost function of the system is defined as

$$J_l = \int_0^\infty \left(x^T Q x + u^T R u\right) dt \tag{3.78}$$

where $Q \in \mathbb{R}^{l\times l}$ and $R \in \mathbb{R}^{m\times m}$ are symmetric positive definite matrices. Using (3.77), the LTI system equation becomes,

$$\begin{aligned} \dot{x} &= (A - BK_l)x \\ \dot{x} &= \tilde{A}x \end{aligned} \tag{3.79}$$

where, $\tilde{A} = (A - BK_l)$ If A and B are controllable, then optimal state feedback controller can be designed. Thus , $\tilde{A}$ has eigenvalues on the left of the s-plane. Substituting (3.77) in (3.78), the

performance index can be written as,

$$\begin{aligned} J_l &= \int_0^\infty \left(x^T Q x + (K_l x)^T R (K_l x) \right) dt \\ &= \int_0^\infty \left(x^T \left(Q + K_l^T R K_l \right) x \right) dt \end{aligned} \tag{3.80}$$

Let,

$$\begin{aligned} \left(x^T \left(Q + K_l^T R K_l \right) x \right) &= -\frac{d}{dt} \left(x^T P x \right) \\ &= -x^T P \dot{x} - \dot{x}^T P x \end{aligned} \tag{3.81}$$

On putting (3.79) in (3.81) and then substituting in (3.80), we get,

$$J_l = -x^T \left[P (A - B K_l) + (A - B K_l)^T P \right] x \tag{3.82}$$

In (3.82), P must be positive definite matrix. By comparing (3.81) with (3.82), we get,

$$P (A - B K_l) + (A - B K_l)^T P = -\left(Q + K_l^T R K_l \right) \tag{3.83}$$

As $(A - B K_l)$ is a stable matrix, therefore, solving for a positive definite matrix P which will satisfy (3.83), the cost function can be evaluated as,

$$J_l = \int_0^\infty \left(x^T \left(Q + K_l^T K_l \right) x \right) dt \tag{3.84}$$

From (3.81), we can write as,

$$\begin{aligned} J_l &= -x^T P x \Big|_0^\infty \\ &= -x^T (\infty) P x (\infty) + x^T (0) P x (0) \end{aligned} \tag{3.85}$$

As the system (3.79) is stable, eigenvalues of (3.85) must have negative real part. Therefore, $x(\infty) \to 0$. Thus, we get $J_l = x^T (0) P x (0)$. It is obtained in terms of initial condition.

Step 5: From (3.83), the minimization of J_l gives K_l by using feedback control law $u = -K_l x$.

The feedback gain K_l is found by using

$$K_l = R^{-1}B^T P \tag{3.86}$$

and further simplifying, we get Riccati equation as,

$$A^T P + PA - PBR^{-1}B^T P + Q = 0 \tag{3.87}$$

In (3.87), Q and R are selected in such a way that $Q = diag(q11, q22, q33)$ is $q11 > q22 > q33 > 0$ and $R = \chi^T \chi > 0$, where, χ is non singular matrix.

Step 6: Using Riccati equation (3.87) and state model from (3.73), positive definite matrix P is obtained which is given below.

$$P = \begin{bmatrix} p_{11} & p_{12} & p_{13} \\ p_{12} & p_{22} & p_{23} \\ p_{13} & p_{23} & p_{33} \end{bmatrix} \tag{3.88}$$

Step 7: Using (3.86), state feedback control gain K_l is obtained as

$$\begin{aligned} K_l &= [R]^{-1}\left[B^T\right][P] \\ &= [1]\begin{bmatrix} 0 & 0 & \frac{a_4}{b_1} \end{bmatrix}\begin{bmatrix} p_{11} & p_{12} & p_{13} \\ p_{12} & p_{22} & p_{23} \\ p_{13} & p_{23} & p_{33} \end{bmatrix} \end{aligned} \tag{3.89}$$

$$K_l = \begin{bmatrix} p_{11}\frac{a_4}{b_1} & p_{23}\frac{a_4}{b_1} & p_{33}\frac{a_4}{b_1} \end{bmatrix} \tag{3.90}$$

Step 8: Using state feedback control law for $\tilde{A}$, new system matrix can be written as,

$$(sI - \tilde{A}) = \begin{bmatrix} s & -1 & 0 \\ 0 & s & -1 \\ \left(p_{13}\frac{a_4}{b_1}+1\right)\frac{a_4}{b_1} & \left(p_{23}\frac{a_4}{b_1}+1\right)\frac{a_4}{b_1} & \left(p_{33}\frac{a_4}{b_1}+1\right)\frac{a_4}{b_1} \end{bmatrix} \tag{3.91}$$

From (3.91), the closed-loop characteristic equation can be written as

$$s^3+\left(p_{33}\frac{a_4}{b_1}+1\right)\frac{a_4}{b_1}s^2+\left(p_{23}\frac{a_4}{b_1}+1\right)\frac{a_4}{b_1}s+\left(p_{13}\frac{a_4}{b_1}+1\right)\frac{a_4}{b_1}=0 \tag{3.92}$$

Step 9: The closed-loop system in (3.76) is of fourth order and (3.92) is of third order. Therefore, in order to compare these two equations, we need to add one additional pole. The recipe of adding pole is explained below.

Let us consider fourth pole $(s+\lambda_4)$ on the left half of the s-plane. Then (3.92) can be written as,

$$\left[s^3+\left(p_{33}\frac{a_4}{b_1}+1\right)\frac{a_4}{b_1}s^2+\left(p_{23}\frac{a_4}{b_1}+1\right)\frac{a_4}{b_1}s+\left(p_{13}\frac{a_4}{b_1}+1\right)\frac{a_4}{b_1}\right](s+\lambda_4)=0 \tag{3.93}$$

The above (3.93) can also be written as

$$\begin{aligned}
&s^4+\left(\lambda_4+\left(p_{33}\frac{a_4}{b_1}+1\right)\frac{a_4}{b_1}\right)s^3+\\
&\left[\left(\lambda_4\left(p_{33}\frac{a_4}{b_1}+1\right)\frac{a_4}{b_1}\right)\left(\left(p_{23}\frac{a_4}{b_1}+1\right)\frac{a_4}{b_1}\right)\right]s^2+\\
&\left[\left(\lambda_4\left(p_{23}\frac{a_4}{b_1}+1\right)\frac{a_4}{b_1}\right)\left(\left(p_{13}\frac{a_4}{b_1}+1\right)\frac{a_4}{b_1}\right)\right]s+\\
&\left(\lambda_4\left(p_{23}\frac{a_4}{b_1}+1\right)\frac{a_4}{b_1}\right)=0
\end{aligned} \tag{3.94}$$

If (3.94) is compared with (3.93), λ_4 is calculated as

$$\lambda_4=-\left[\left(p_{33}\frac{a_4}{b_1}+1\right)\frac{a_4}{b_1}-\frac{b_2}{b_1}\right] \tag{3.95}$$

The fourth pole $(s+\lambda_4)$ is augmented by δ. Here, δ is a compensation factor which is a variable value. Thus, modified λ_4 becomes,

$$\lambda_4=-\left[\left(p_{33}\frac{a_4}{b_1}+1\right)\frac{a_4}{b_1}-\frac{b_2}{b_1}\right]+\delta \tag{3.96}$$

Before substituting (3.96) in (3.93), let

$$\tilde{p}_{13} = \left(p_{13}\frac{a_4}{b_1} + 1\right),\ \tilde{p}_{23} = \left(p_{23}\frac{a_4}{b_1} + 1\right), \tilde{p}_{33} = \left(p_{33}\frac{a_4}{b_1} + 1\right) \tag{3.97}$$

Therefore equation (3.94) becomes,

$$\begin{aligned} & s^4 + \left(\frac{b_2}{b_1} + \delta\right) s^3 \\ & + \left[\tilde{p}_{23}\frac{a_4}{b_1} + \left(\tilde{p}_{33}\frac{a_4}{b_1}\right)^2 + \left(\tilde{p}_{33}\frac{a_4}{b_1}\right)\left(\frac{b_2}{b_1} + \delta\right)\right] s^2 \\ & + \left[\tilde{p}_{13}\frac{a_4}{b_1} + \tilde{p}_{23}\tilde{p}_{33}\left(\frac{a_4}{b_1}\right)^2 + \tilde{p}_{23}\left(\frac{a_4}{b_1}\right)\left(\frac{b_2}{b_1} + \delta\right)\right] s \\ & + \left[\tilde{p}_{13}\tilde{p}_{33}\left(\frac{a_4}{b_1}\right)^2 + \tilde{p}_{13}\left(\frac{a_4}{b_1}\right)\left(\frac{b_2}{b_1} + \delta\right)\right] = 0 \end{aligned} \tag{3.98}$$

The above (3.98) can be written in simplified form as,

$$s^4 + p_1 s^3 + p_2 s^2 + p_3 s + p_4 = 0 \tag{3.99}$$

where,

$$\begin{aligned} p_1 &= \left[\frac{b_2}{b_1} + \delta\right] \\ p_2 &= \left[\hat{p}_{23} + \hat{p}_{33}^2 + \hat{p}_{33}\left(\frac{b_2}{b_1} + \delta\right)\right] \\ p_3 &= \left[\hat{p}_{13} + \hat{p}_{23}\hat{p}_{33} + \hat{p}_{23}\left(\frac{b_2}{b_1} + \delta\right)\right] \\ p_4 &= \left[\hat{p}_{13}\hat{p}_{33} + \hat{p}_{13}\left(\frac{b_2}{b_1} + \delta\right)\right] \end{aligned} \tag{3.100}$$

and

$$\hat{p}_{13} = \tilde{p}_{13}\frac{a_4}{b_1}; \quad \hat{p}_{23} = \tilde{p}_{23}\frac{a_4}{b_1}; \quad \hat{p}_{33} = \tilde{p}_{33}\frac{a_4}{b_1} \tag{3.101}$$

Step 10: By comparing (3.93) and (3.99), we get PID controller $C(s)$ parameters as follows,

$$
\begin{aligned}
K_p &= \frac{b_1}{a_4}\left[\hat{p}_{13} + \hat{p}_{23}\hat{p}_{33} + \hat{p}_{23}\left(\frac{b_2}{b_1} + \delta\right)\right] - \frac{b_4}{a_4} \\
K_i &= \frac{b_1}{a_4}\left[\hat{p}_{13}\hat{p}_{33} + \hat{p}_{13}\left(\frac{b_2}{b_1} + \delta\right)\right] \\
K_d &= \frac{b_1}{a_4}\left[\hat{p}_{23} + \hat{p}_{33}^2 + \hat{p}_{33}\left(\frac{b_2}{b_1} + \delta\right)\right] - \frac{b_3}{a_4}
\end{aligned}
\tag{3.102}
$$

3.4.2 Simulation results and analysis

Using (3.72), substitute system parameters from Table 3.2 in (3.93). Further, Q and R are considered such that $Q = diag\,[1,1,1]$ and $R = 1 \times 10^{-5}$. The gain matrix K_l can be calculated using (3.90), i.e., $K_l = [7.9958,\ 13.8156,\ 316.2278]$. The eigenvalues of closed loop system $\tilde{A}$ becomes, $\lambda_1 = -6.2354 \times 10^3$, $\lambda_2 = -23.5549$, $\lambda_3 = -2.1530 \times 10^{-3}$. The original system (3.92) is of third order. Therefore, we require one more pole which is calculated using (3.95), so we get $\lambda_4 = -1.2510 \times 10^4$. Augmenting with $\delta = 10000$ that gives $\lambda_4 = -2.5100 \times 10^3$. Using these roots, the coefficients of characteristic equation (3.99) is obtained, i.e., $p_1 = 8.7690 \times 10^3$, $p_2 = 1.5857 \times 10^7$, $p_3 = 3.6869 \times 10^8$ and $p_4 = 7.9373 \times 10^5$. Using (3.72), (3.100), then substituting in (3.102), we get QRAWCP-PID controller parameters as $K_p = 2.6218 \times 10^3$, $K_i = 5.6443$, $K_d = 111.7160$.

3.4.2.1 Time response analysis

To validate the proposed technique and to show the superiority of QRAWCP approach, we analyze step response of sun tracker system for three cases, (i) without disturbance, (ii) with input disturbance and (iii) with output disturbance. The results are compared with the recently designed PID controller schemes for sun tracker system which are based on swarm optimization approaches such as PSO [35], FFA [35] and CSA [35]. The PID parameters of proposed QRAWCP PID and PSO PID, FFA PID, and CSA PID are given in Table 3.3. The performance of proposed PID controller and other existing PID controllers is explained in case 1, case 2 and case 3 for the case without disturbance, with input disturbance and with output disturbance, respectively.

Table 3.3: PID controller parameters

Method	K_p	K_i	K_d
QRAWCP PID (Proposed)	2621.80	5.64430	111.721
PSO PID	9.51202	7.49203	0.00022
FFA PID	9.72083	7.44047	0.00010
CSA PID	9.99999	8.11378	0.00010

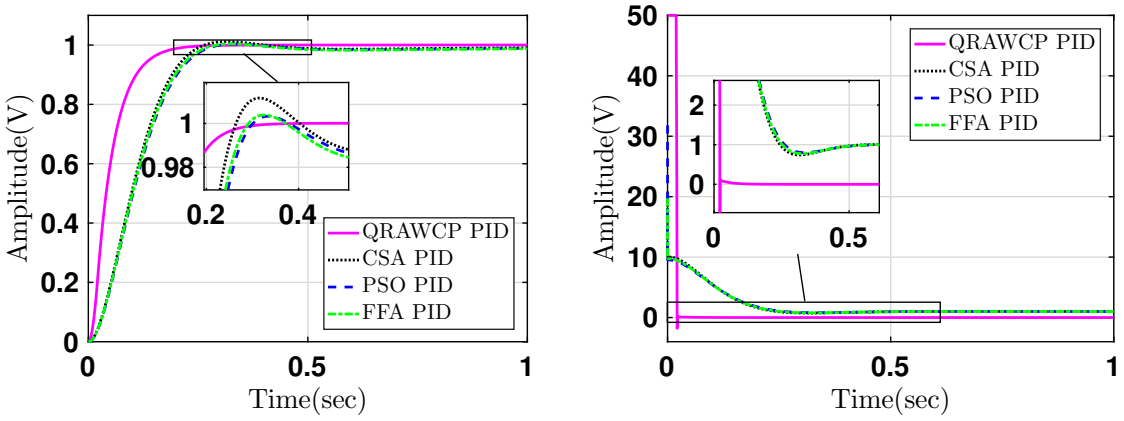

Figure 3.7: Step responses of system with PID without disturbance

Case 1: Fig. 3.7(a) depicts the step response of the closed loop system for sun tracker system in the absence of disturbance. From this figure, it can be seen that performance of the proposed QRAWCP technique is better in comparison to other PID approaches which are based on soft computing techniques.

The results are verified by performing analysis of transient performance parameters such as, rise time (t_r), settling time (t_s), peak overshoot (M_p), absolute peak value (A_{tp}), peak time (t_p) and steady state error (e_{ss}). They are tabulated in Table 3.4. From this table, it is found that, the proposed approach gives lesser value of error-based performance indices in comparison to other PIDs. Fig. 3.7(b) shows control signals using saturation limit of $\pm 50V$. It is found that overall control energy of proposed QRAWCP approach is less in comparison to other techniques. The performance of proposed PID is verified for disturbance $d_i(t)$ and $d_o(t)$, where $d_i(t)$ is input disturbance and $d_o(t)$ is output disturbance. Both these disturbances are written mathematically in

Table 3.4: Output response of system

Method	t_r(sec)	t_s(sec)	M_p(%)	A_{tp}	t_p(sec)	e_{ss}
QRAWCP PID (Proposed)	**0.09490**	**0.17750**	**0.00011**	**1.00010**	**0.79410**	**0.00011**
PSO PID	0.16640	0.25850	0.32890	1.00330	0.33550	0.01146
FFA PID	0.16300	0.25230	0.38740	1.00390	0.32720	0.01256
CSA PID	0.15670	0.23830	1.15880	1.01160	0.31580	0.00942

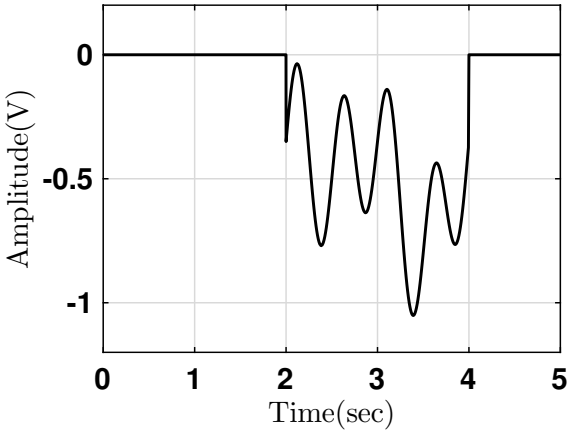

Figure 3.8: Disturbance ($d(t)$) applied to system

(3.103) as

$$d(t) = \begin{cases} 0, & t < 2 \; or \; t > 4 \\ 0.15 \times (\sin 4\pi t + \cos 2\pi t & \\ \quad + \sin \pi t + \sin 4\pi t) - 0.5, & 2 \leq t \leq 4 \end{cases} \tag{3.103}$$

The disturbance applied to the system is illustrated in Fig. 3.8. The performance analysis of the system in case of input disturbance and output disturbance is presented in case 2 and case 3, respectively.

Case 2: Fig. 3.9(a) shows the step response of the system when the disturbance ($d_i(t)$) is applied from time $t = 2s$ to $t = 4s$. The proposed approach gives better response in comparison to other PIDs. Fig. 3.9(b) shows control efforts which is quite higher for proposed controller at initial time. It is because of large inertia of system at initial time. However, during the time interval between 2 to 4 seconds. (see Fig. 3.9(b)), we found that that the control efforts are lower (see Fig. 3.9(a)) in comparison to other approaches.

Case 3: Fig. 3.10(a) shows step response of system when output disturbance ($d_o(t)$) is applied

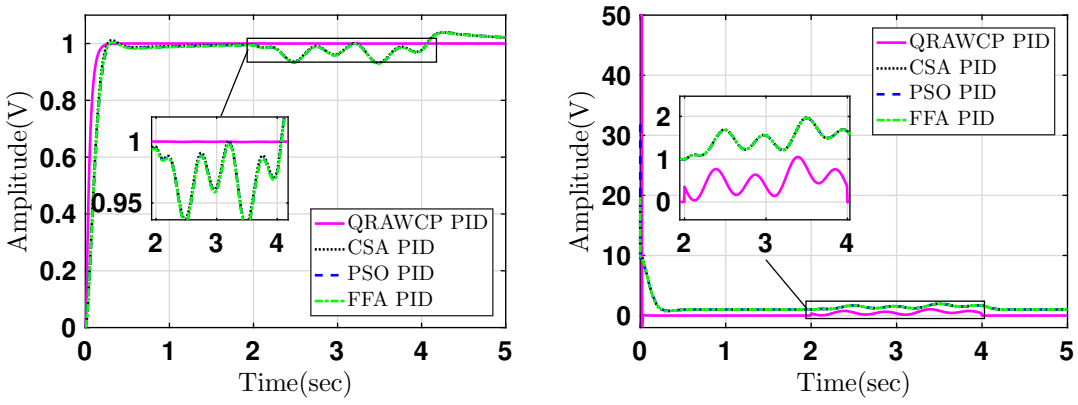

Figure 3.9: Step responses of system with input disturbance

from 2 to 4 seconds to the plant output side, i.e., the measurement noise. It is seen that, the proposed approach gives stable response with negligible e_{ss} in comparison to other PID approaches. The control efforts are shown in Fig. 3.10(a), which are quite large for proposed QRAWCP PID controller. However, during disturbance in time interval from 2 to 4 seconds, we observe that, there is less overshoot in system output, whereas other approaches have large overshoot (see Fig. 3.10(a)). Also, for safety purpose, we have considered the saturation limit of $\pm$50V. Further, loop robustness is also verified as given in next subsection.

3.4.2.2 Loop robustness

The robustness of PID controllers for sun tracker system, to calculate loop transfer function $L(s)$, is given by (3.104).

$$\Delta(s) = 1 + L(s) \tag{3.104}$$

where, $L(s)$ is obtained as,

$$L(s) = G(s)C(s) = \frac{a_4(K_d s^2 + sK_p + K_i)}{b_1 s^4 + b_2 s^3 + b_3 s^2 + b_4 s} \tag{3.105}$$

Loop robustness is determined in terms of gain margin (GM), phase margin (PM), gain crossover (ω_{gc}) and phase cross-over (ω_{pc}) frequencies. They are tabulated in Table 3.5.

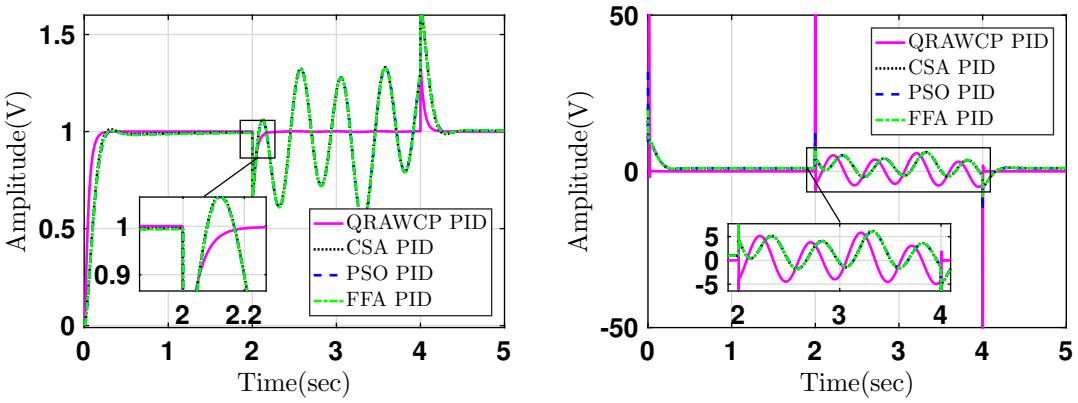

Figure 3.10: Step responses of system with output disturbance

Table 3.5: Loop robustness of PID compensated system

Method	GM (dB)	ω_{gc}(rad/s)	PM (deg)	ω_{pc}(rad/s)	$\|\|S\|\|_\infty$	DM (sec)
QRAWCP PID (Proposed)	∞	**2359.10**	**69.2549**	∞	**1.2293**	**0.0005**
PSO PID	57.8081	8.8371	69.9214	407.8013	1.2320	0.1381
FFA PID	56.8303	9.0061	69.6572	389.6705	1.2356	0.1350
CSA PID	56.5502	9.2369	68.8322	388.9042	1.2425	0.1301

Further, there is need to calculate sensitivity ($||S||_\infty$) and delay margin (DM) for robustness analysis [112]. The sensitivity (S) can be calculated as, $S = \frac{1}{1+L}$, where, $S_\infty \leq 2$ ensure robustness. However, DM is calculated using frequency domain analysis which is given by (3.106)

$$DM = \frac{PM^\circ \Pi}{180^\circ \times \omega_{gc}} \tag{3.106}$$

The above robustness test has been carried out for proposed method and existing controllers as given in Table 3.5.

It is observed that, proposed PID controller shows better stability margin, reduces delay margin, better sensitivity in comparison to other methods. Finally, the comparative studies of proposed QRAWCP approach with existing approaches[35] are carried out by calculating integral performance indices. They are explained below.

3.4.2.3 Integral performance indices

The commonly used performance measures are Integral Squared Error (ISE), Integral Absolute Error (IAE) and Integral Time-weighted Absolute Error (ITAE). Mathematically, they can be given as

$$ISE = \int_0^\infty \left(\theta_r - \theta_y\right)^2 dt; IAE = \int_0^\infty \left|\left(\theta_r - \theta_y\right)\right| dt; ITAE = \int_0^\infty t\left|\left(\theta_r - \theta_y\right)\right| dt \tag{3.107}$$

where, $\left(\theta_r - \theta_y\right)$ is the error between reference input position and measured output position (θ_y) at time 't'. All integral errors are calculated for sun tracking system which is shown in Table 3.6. From this table, it is observed that, the proposed QRAWCP method for design of PID has minimum error in comparison to PSO PID[35], FFA PID[35] and CSA PID [35].

3.4.2.4 Parametric uncertainties

We know that in real time, parameters of the system are not constant. They vary from minimum to maximum value. This is due to non-linearity, environmental variations and also due to aging. The main motto of controller design is that it should work even though there exist uncertainties in the system. Here, for sun tracker system model, its parameters are represented in terms of uncertainties as

$$\begin{aligned} &\overline{K}_e = K_e \pm \Delta K_e,\ \overline{K} = K \pm \Delta K,\ \overline{K}_s = K_s \pm \Delta K_s, \\ &\overline{L}_a = L_a \pm \Delta L_a,\ \overline{R}_a = R_a \pm \Delta R_a,\ \overline{K}_t = K_t \pm \Delta K_t, \\ &\overline{J} = J \pm \Delta J,\ \ \overline{b} = b \pm \Delta b,\ \overline{K}_b = K_b \pm \Delta K_b \end{aligned} \tag{3.108}$$

Table 3.6: Integral performance indices for ±50% perturbation without disturbance

Methods	Nominal case			-50% Lower bound			+50% Upper bound		
	ISE	IAE	ITAE	ISE	IAE	ITAE	ISE	IAE	ITAE
QRAWCP PID (Proposed)	**0.0315**	**0.0532**	**0.0024**	**0.0583**	**0.0845**	**0.0048**	**0.0260**	**0.0474**	**0.0021**
PSO PID	0.0755	0.1189	0.0137	0.2140	0.3409	0.0841	0.0464	0.1019	0.0232
FFA PID	0.0744	0.1180	0.0140	0.2110	0.3368	0.0824	0.0459	0.1016	0.0233
CSA PID	0.0727	0.1134	0.0123	0.2050	0.3280	0.0790	0.0450	0.0988	0.0218

Here, ±50% uncertainty is considered in all the parameters of the system. For this uncertainty, the upper and lower bounds are listed below.

$$
\begin{aligned}
\overline{K_e} &\in [0.00050, 0.00150] \\
\overline{K} &\in [5000.00, 15000.00] \\
\overline{K_s} &\in [0.50, 1.50] \\
\overline{L_a} &\in \left[5 \times 10^{-4}, 1.50 \times 10^{-3}\right] \\
\overline{R_a} &\in [3.125, 9.375] \\
\overline{K_t} &\in [0.005625, 0.016875] \\
\overline{J} &\in \left[5 \times 10^{-7}, 1.50 \times 10^{-6}\right] \\
\overline{b} &\in \left[0.5 \times 10^{-6}, 1.50 \times 10^{-6}\right] \\
\overline{K_b} &\in [0.00625, 0.01875]
\end{aligned}
\tag{3.109}
$$

Similar to subsection 3.4.2, the performance analysis is also carried for both lower and upper bounds. From Fig. 3.11 and Fig. 3.12, it is observed that the performance of the proposed control is better in comparison to existing controllers except that the control input is slightly more at early part of the response. Further, performance in case of parametric uncertainly is carried out by determining performance indices in case of without and with input disturbances. They are shown in Table 3.6 and 3.7, respectively. Both these tables indicate that the proposed controller approach is better in comparison to existing controllers.

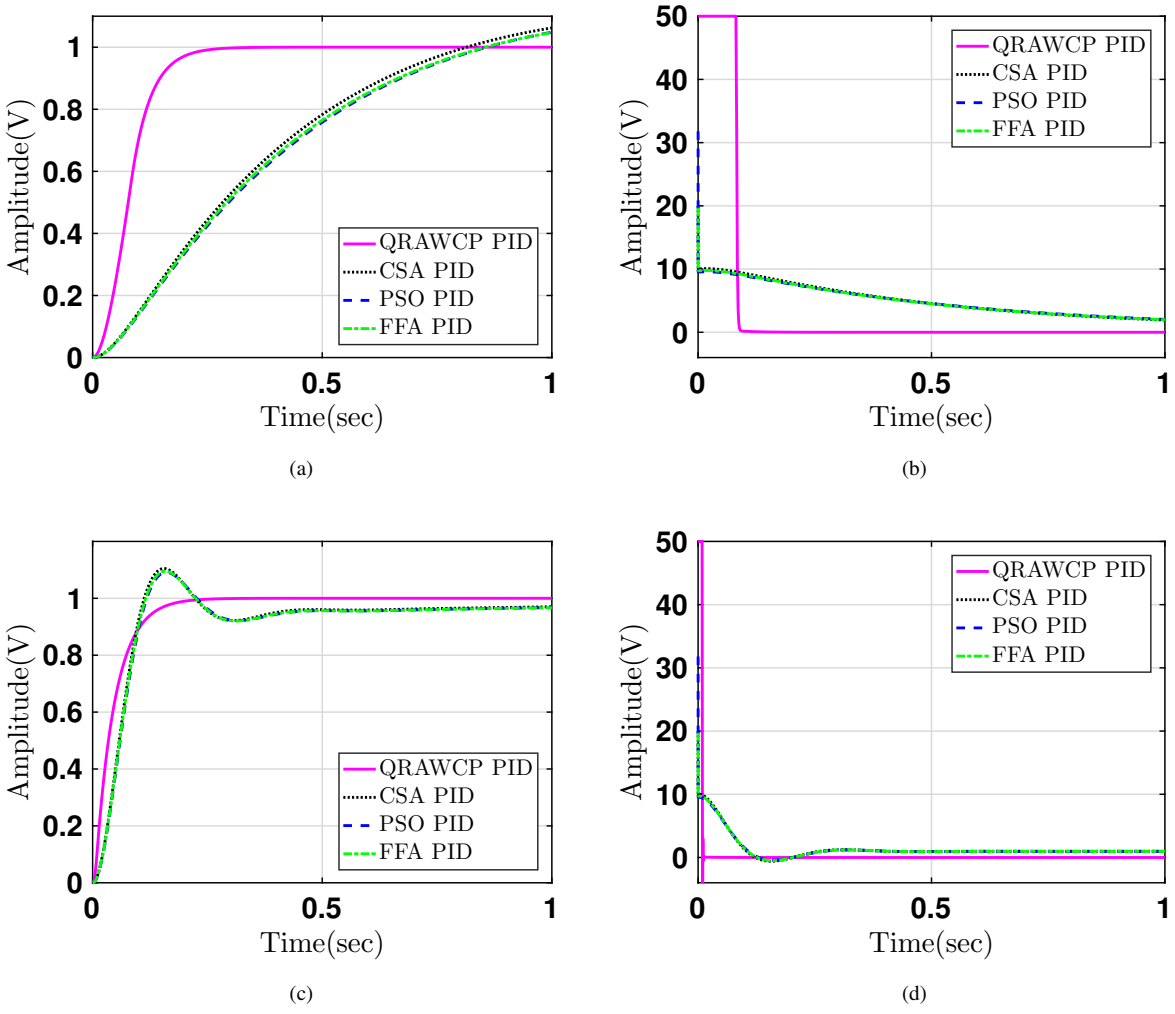

Figure 3.11: Response for ±50% parametric uncertainties in system without disturbance

Table 3.7: Integral performance indices for ± 50% perturbation with input disturbance

Methods	Nominal Plant			Lower -50% plant			Upper +50% plant		
	ISE	IAE	ITAE	ISE	IAE	ITAE	ISE	IAE	ITAE
QRAWCP PID (Proposed)	**0.0315**	**0.0536**	**0.0037**	**0.0583**	**0.0850**	**0.0063**	**0.0260**	**0.0478**	**0.0033**
PSO PID	0.0790	0.2166	0.3386	0.2275	0.5221	0.5004	0.0516	0.2250	0.3940
FFA PID	0.0779	0.2159	0.3371	0.2234	0.5114	0.4856	0.0510	0.2244	0.3913
CSA PID	0.0759	0.2043	0.3176	0.2185	0.5065	0.4831	0.0496	0.2138	0.3706

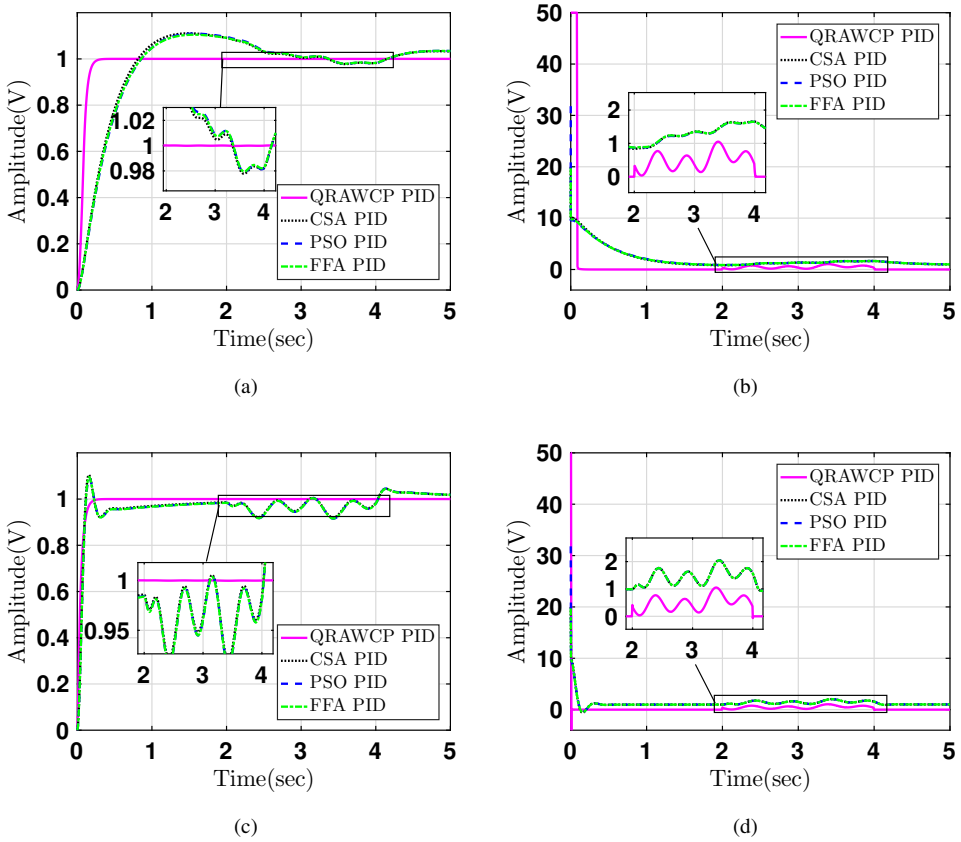

Figure 3.12: Response for $\pm 50\%$ parametric uncertainties with input disturbance in system

3.5 Observer based QRAWCP approach

The LQR solution is basically a state feedback type of controller, i.e., it requires that all states are available for feedback. In most of the situations that we encounter in real life, observability is an unreasonable assumption and is usually not valid. Hence, some form of state estimation is necessary. We know that an observer can be used in such situations, when we need to estimate the state of the system. Also, the combination of an observer and state feedback will always lead to a stable closed loop system. One could select the observer poles randomly too, but this requires an expert selection and it is quite possible that the control energy is not optimal. Further, if the system is affected by the input disturbances and the output noise, the observer chosen randomly may fail to give appreciable results. To wriggle out of such a situation, we can select an optimal observer– the Kalman filter. We can then cascade the Kalman filter with the state feedback LQR controller, and this combination is known as the Linear Quadratic Gaussian (LQG).

LQR problem is the fundamental one in the optimal control theory (discussed in section 3.1), wherein a quadratic cost function dependent on the states and the control energy has to be minimized and at the same time, the state space equation of the linear plant needs to be satisfied. It forms an important part of the LQG problem, which will be elaborated in this particular chapter. In a sense, LQG problem is a generalization of that of the LQR. The principal stumbling block in the usage of LQR controller is that the system model must be uncorrupted by noise and unaffected by any input disturbances [113], i.e, the effect of input disturbance and measurement noise is not considered in the design of a LQR controller. Further, all the states of the system must be observable, which is an unreasonable and vexatious assumption and hence, some form of state estimation is mandatory.

In [114], it is proved that a combination of observer and state feedback will always result in a closed loop system that is always stable. One can chose the desired poles for a controller via Ackermann's formula and at the same time, it is possible to obtain those poles via a closed loop system, obtained with the aid of Riccati equation using optimal control. The desired poles of the controller and observer can be independently selected for a system. But in LQG, it is the optimal control theory that will influence the choice of both the observer and the controller poles. In simpler terms, LQG is the series combination of the Kalman filter, which acts as an optimal observer and the LQR controller as illustrated in Fig. 3.13(a). In the upcoming sections of the chapter, the problem statement, mathematical equations and the analysis related to the LQG is presented.

3.5.0.1 Formulation of LQG

Consider the state space model of the linear system in the presence of input disturbance and measurement noise as follows

$$\dot{x}(t) = Ax(t) + Bu(t) + \Gamma w(t) \tag{3.110}$$

$$y(t) = Cx(t) + v(t) \tag{3.111}$$

where, the initial state is given as $x(0) = x_0$. x represents a state vector of dimension $(n \times 1)$, u

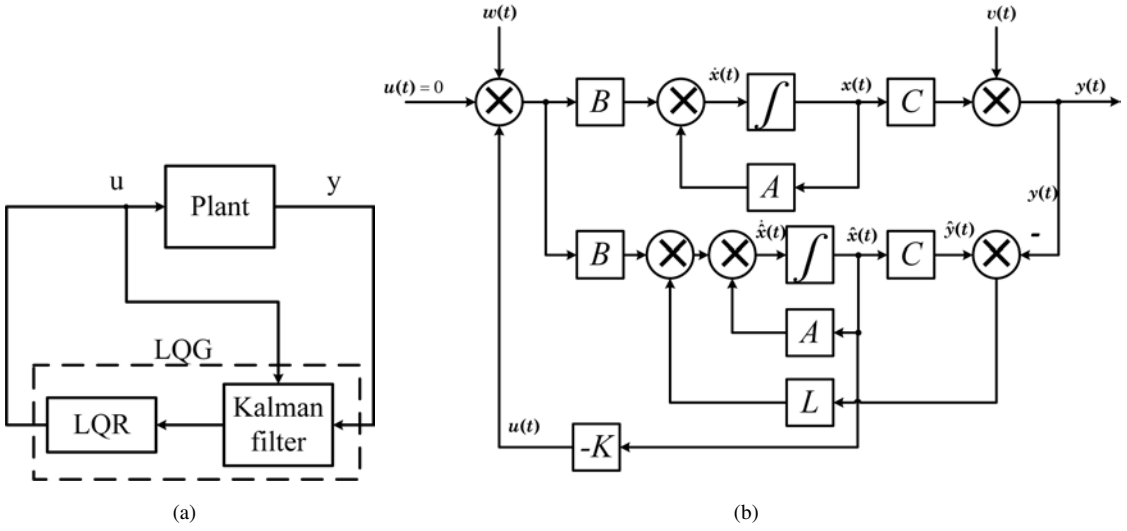

Figure 3.13: LQG structure

is an input $(m \times 1)$ vector and $w(t)$ denotes the input disturbance matrix of size p. A, B and C are the state space matrices and $v(t)$ indicates the measurement noise[115].

The following assumptions are considered

- The model of the system in (3.110) and (3.111) assumes additive noise only and the noise enters the system at two places only as shown in Fig. 3.13(b). This restriction can easily be met by making appropriate adjustments in the system model.

- The statistical nature of noise in both the state and output equations is known to us. It is assumed to be white Gaussian noise with zero mean. This assumption is valid for many naturally occurring noise and can be mathematically translated as follows

$$E(v(t)v'(\tau)) = V(t)\delta(t-\tau) \qquad E(v(t)) \equiv 0 \tag{3.112}$$

$$E(w(t)w'(\tau)) = W(t)\delta(t-\tau) \qquad E(w(t)) \equiv 0 \tag{3.113}$$

  for some non-negative definite and symmetric matrices V and W. Here, $E(v(t))$ stands for expectation of any function $v(t)$ and hence $E(v(t)v'(\tau))$ denotes the co-variance of $v(t)$. The δ term in (3.112) and (3.113) is responsible of the whiteness property of the noise.

- The terms $v(t)$ and $w(t)$ are uncorrelated.

- x_0, the initial state of the plant is also a Gaussian variable whose mean and variance are known.
- The system is controllable.

Hence, for the plant in (3.110) and (3.111), satisfying the assumptions given above, the problem is to find optimal control law $u = -K\hat{x}$, that minimizes the quadratic fitness function given as

$$J = \int_0^\infty (x(t)^T Q x(t) + u(t)^T R u(t)) dt \tag{3.114}$$

where $\hat{x}$ is the observed state of the system, estimated using a Kalman filter, such that it minimizes the performance index, given as follows

$$J_e = \int_0^\infty (x(t) - \hat{x(t)})^T (x(t) - \hat{x(t)})) dt \tag{3.115}$$

Equation (3.115) effectively implies that the observed state must be as close to the actual state as possible.

3.5.0.2 Solution of the LQG problem

The LQR problem is a well understood problem, wherein the controller K is given by [116, 117]

$$K = R^{-1} B^T P \tag{3.116}$$

Here, P is a positive definite symmetric matrix which can be computed via the algebraic Riccati equation given as

$$A^T P + PA + Q - PBR^{-1} B^T P = 0 \tag{3.117}$$

On closer observation of (3.115) and comparing it with the standard LQR problem, one can recognize that both the equations are analogous and their solutions can be found in a similar manner, which will be illustrated below.

For the LQG problem, the Kalman filter acts as a state observer, whose dynamics are given in the following equations.

$$\dot{\hat{x}}(t) = A\hat{x}(t) + Bu(t) + L(y(t) - C\hat{x}(t)) \tag{3.118}$$

Here, L is referred to as the Kalman gain. On rearranging the terms of (3.118), we obtain

$$\dot{\hat{x}}(t) = (A - LC)\hat{x}(t) + Bu(t) + Ly(t) \tag{3.119}$$

Hence, the state space solution of the above design problem is given by the solution of the Continuous filter algebraic Riccati equation, which can be given as

$$AP_e + P_eA^T - P_eC^TV^{-1}CP_e + \Gamma W\Gamma^T = 0 \tag{3.120}$$

The matrix L can be computed using the equation as given below

$$L = P_eC^TV^{-1} \tag{3.121}$$

Fig. 3.13(b) illustrates the block diagram of the overall system with LQG controller. The control input $u(t)$ can thus, be given by

$$u = -K\hat{x}(t) \tag{3.122}$$

where, K is the optimal LQR gain.

3.5.0.3 LQG transfer function

To compute the transfer function of the closed loop system, we begin with the state space equation of the observer system which is restated here for convenience.

$$\dot{\hat{x}}(t) = (A - LC)\hat{x}(t) + Bu(t) + Ly(t) \tag{3.123}$$

Substituting the value of $u(t)$ from (3.122), we get

$$\dot{\hat{x}}(t) = (A - LC - BK)\hat{x}(t) + Ly(t) \tag{3.124}$$

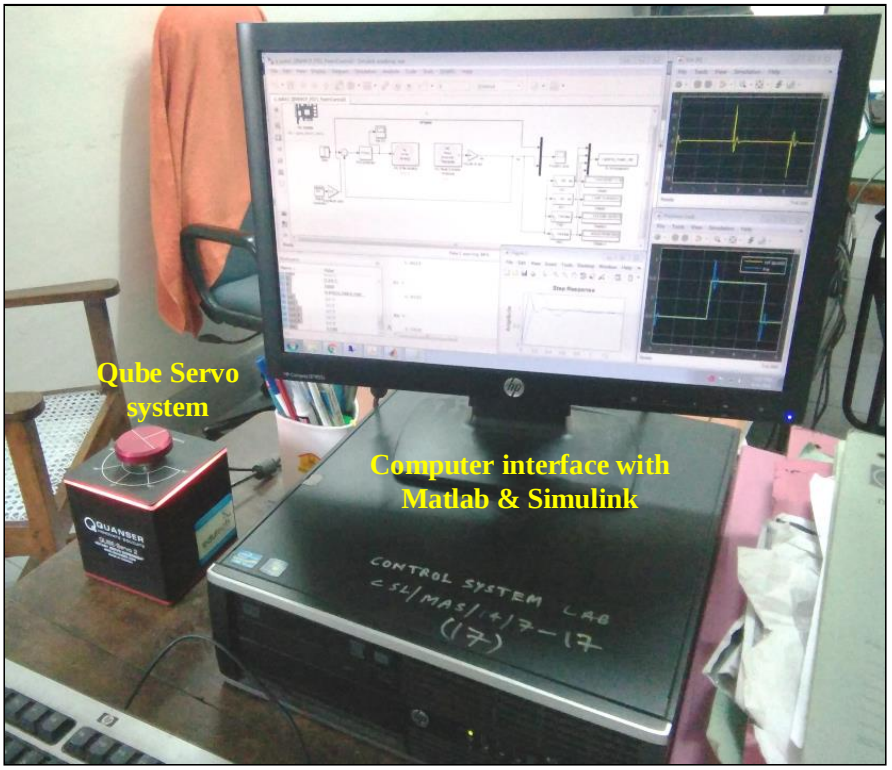

Figure 3.14: Real-time Qube-Servo2 motor set-up

Taking the Laplace transform of (3.124), we obtain

$$(sI-(A-BK-LC))\hat{X}(s)=LY(s) \tag{3.125}$$

After simplifying function(Eq3_102), we get,

$$\hat{X}(s)=(sI-(A-BK-LC))^{-1}LY(s) \tag{3.126}$$

Multiplying both sides of (3.126) by $-K$ gives

$$-K\hat{X}(s)=-K(sI-(A-BK-LC))^{-1}LY(s) \tag{3.127}$$

Using (3.126), the transfer function from $Y(s)$ to $U(s)$ can be finally given as

$$U(s)=-K(sI-(A-BK-LC))^{-1}LY(s) \tag{3.128}$$

3.6 Experimental analysis

To validate the proposed QRAWCP in real time problem, we have considered the QUBE servo system for position and speed control case. However, the limitation of LQR is that all the states are not measurable so that we have assumed these using LQG which is LQR plus full order observer, the further details are given in the upcoming section.

3.6.1 Case 1: Position control

Consider an identified model of QUBE Servo 2 (3.14), whose position-to-voltage transfer function is given as

$$G_4(s) = \frac{\Theta_m(s)}{V_m(s)} = \frac{\mathcal{K}}{\tau s^2 + a_0 s}, \tag{3.129}$$

where, $\Theta_m(s) = \mathcal{L}\left[\theta_m(t)\right]$ is the motor / disk position, $V_m(s) = \mathcal{L}\left[v_m(t)\right]$ is the applied motor voltage, $\mathcal{K}$ represents the model steady-state gain, a_0 is a coefficient and τ is the model time constant. The values of the motor parameters are given below.

$$\mathcal{K} = 26.5\ rad/(V-s),\ \tau = 0.155\ s,\ a_0 = 1 \tag{3.130}$$

If desired, the model parameters K and τ, can be obtained by conducting an experiment (e.g. by performing the Bump Test laboratory experiment). The transfer function of PID controller is $C(s) = K_p + \frac{K_i}{s} + K_d s$.

1. Proposed approach using LQG:

The closed loop characteristic equation $1 + G_4(s)C(s) = 0$ can be written as,

$$\tau s^3 + (KK_d + a_0)s^2 + KK_p s + KK_i = 0 \tag{3.131}$$

Let the state space equation for above system be $\dot{x} = Ax + Bu$, where,

$$A = \begin{bmatrix} 0 & 1 \\ -a_0 & -a_1 \end{bmatrix} \qquad B = \begin{bmatrix} 0 \\ \beta_1 \end{bmatrix} \tag{3.132}$$

From LQG(Linear Quadratic Gaussian), which is a combination of LQR and full state observer, we can obtain feedback gain matrix as $K = R^{-1}B^T P$, where, $R = [1/r]$, and $P = \begin{bmatrix} P_{11} & P_{12} \\ P_{21} & P_{22} \end{bmatrix}$. Thus, we get, $K = \begin{bmatrix} rP_{12}\beta_1 & rP_{22}\beta_1 \end{bmatrix} = [k_1 \quad k_2]$, and full state observer gain $L = P_e C^T V^{-1}$.

The overall closed loop transfer function of the LQG compensator is given by

$$H(s) = K(sI - A + BK + LC)^{-1}L \tag{3.133}$$

Using (3.133), we get the closed loop characteristic equation as $s^2 + l_1 s + l_2 = 0$. It can be seen that the order of (3.133) is one less than the order of the PID compensated system given in (3.131). Thus, we augment one pole λ_3 to the closed loop characteristic equation in (3.133) and obtain

$$(s^2 + l_1 s + l_2)(s + \lambda_3) = 0 \tag{3.134}$$

On simplification and expansion of equation (3.134), we get

$$s^3 + (l_1 + \lambda_3)s^2 + (l_2 + l_1\lambda_3)s + (l_2\lambda_2) = 0 \tag{3.135}$$

Now, select an arbitrary value of K_d in (3.131). On comparing it with (3.135), we can compute the augmented pole as $\lambda_3 = \frac{K.Kd + a0}{\tau} - l_1$. The parameters of PID can thus be calculated as, $K_p = \tau(l_2 + l_1\lambda_3)/K$ and $K_i = l2\lambda_3\tau/K$. On assuming $K_d = 0.08$, we get $\lambda_3 = -129.8462$. Subsequently, the parameters of PID controller are given as $K_p = 5.66285$, $K_i = 0.903277$. The output response and its control signal are shown in Fig. 3.15.

2. LQR-PID approach:

The closed loop characteristic equation $1 + G_4(s)C(s) = 0$ can be written as,

$$\tau s^3 + (KK_d + a_0)s^2 + KK_p s + KK_i = 0 \tag{3.136}$$

The LQR feedback gain matrix can be obtained as $K = \begin{bmatrix} rP_{12}\beta_1 & rP_{22}\beta_1 \end{bmatrix} = [k_1 \quad k_2]$.

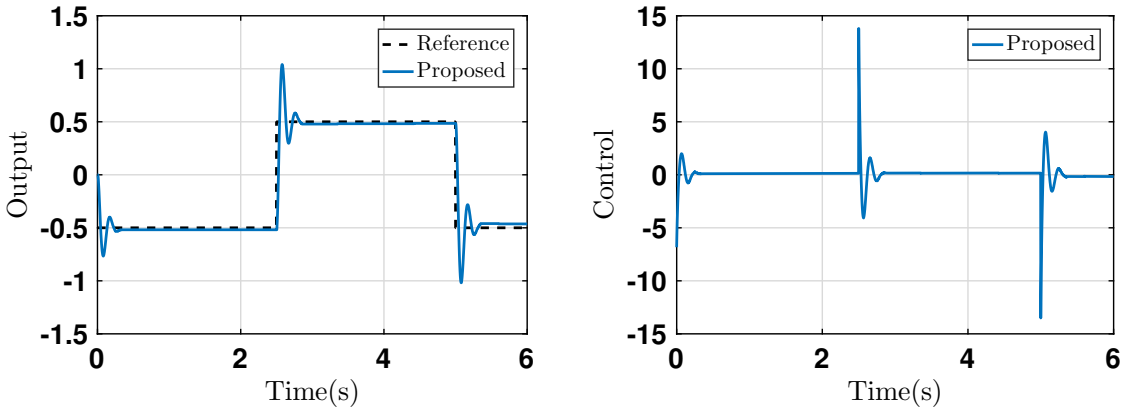

(a) (b)

Figure 3.15: Qube servo position control using proposed approach (a) output and (b) control signal response

Therefore, the closed loop characteristic equation becomes,

$$s^2 + (a_1 + k_2)s + (a_0 + k_1) = 0 \tag{3.137}$$

Now augmenting an extra pole λ_3 in (3.137), which is assumed to be six times of the real part of the dominant pole as discussed earlier, we get,

$$s^3 + (a_1 + k_2 + \lambda_3)s^2 + (a_0 + k_1 + \lambda_3(a_1 + k_2))s + (a_0 + k_1)\lambda_3 \tag{3.138}$$

Equation (3.138) can also be expressed as,

$$s^3 + (p_1)s^2 + (p_2)s + p_3 = 0 \tag{3.139}$$

Now equating eq.(3.138) and (3.139), we get the PID controller gains as, $K_p = \frac{p_2\tau}{K}$, $K_i = \frac{p_3}{K}$, and $K_d = \frac{p_1\tau - a_0}{K}$. On substituting the value of λ_3 in (3.138), we get the parameters of PID as $K_p = 2.1$ $K_i = 3.5$ $K_d = 1$. The response for set-point tracking is shown in Fig. 3.16.

It can be deduced from Fig. 3.15(a) and Fig. 3.16(a), that although LQG control scheme shows an overshoot in the output position response, but the steady state error is minimal. In contrast, LQR scheme has more steady state error accompanied with zero overshoot. The corresponding control voltages, as depicted in Fig. 3.15(b) and Fig. 3.16(b) show that the proposed approach entails the

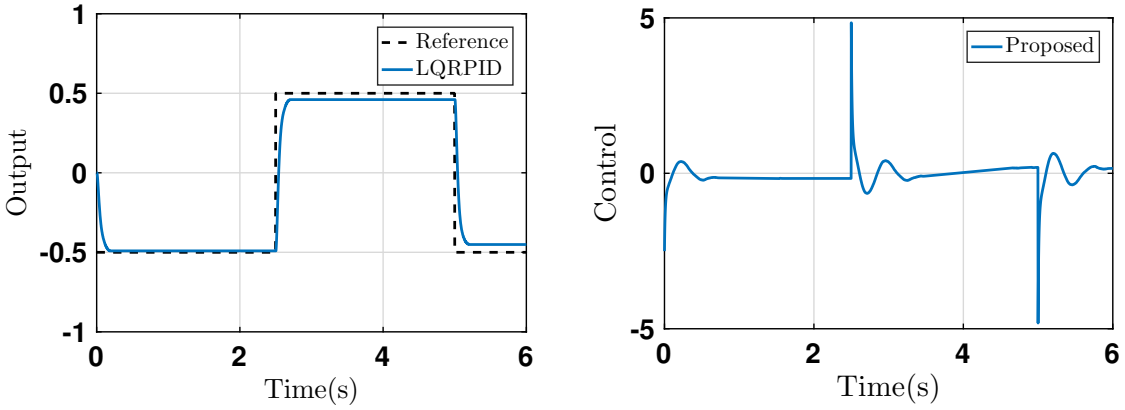

(a) (b)

Figure 3.16: Qube servo position control using LQR-PID approach output and control signal

use of minimal energy.

3.6.2 Case 2: Velocity control

Consider an identified model of QUBE Servo 2, whose speed $(\Omega_m(s))$-to-voltage $(V_m(s)$ transfer function is

$$P(s) = \frac{\Omega_m(s)}{V_m(s)} = \frac{\mathcal{K}}{(\tau s + 1)}, \tag{3.140}$$

1. Proposed approach using LQG:

The closed loop characteristic equation $1 + G_4(s)C(s) = 0$ can be written as,

$$(\tau + K_d\mathcal{K})s^2 + (\mathcal{K}K_p + a_0)s + \mathcal{K}K_i = 0 \tag{3.141}$$

From LQR, the feedback gain matrix is $K = R^{-1}B^T P$, where $R = [1/r]$, and P is the positive semi definite matrix, and from observer dynamics, we get the gain matrix as $L = \sum C^T R^{-1}$. Therefore, the overall closed-loop transfer function of the LQG compensator becomes $H(s) = K(sI - A + BK + LC)^{-1}L$. From this, we get closed-loop characteristic equation as $s + l_1 = 0$, whose order is one less than the order of PID compensated closed loop characteristic equation given in (3.141). Therefore, we augment one pole λ_2, leading to $(s + l_1)(s + \lambda_2) = 0$. On expanding, we get,

$$s^2 + (l_1 + \lambda_2)s + l_1\lambda_2 = 0 \tag{3.142}$$

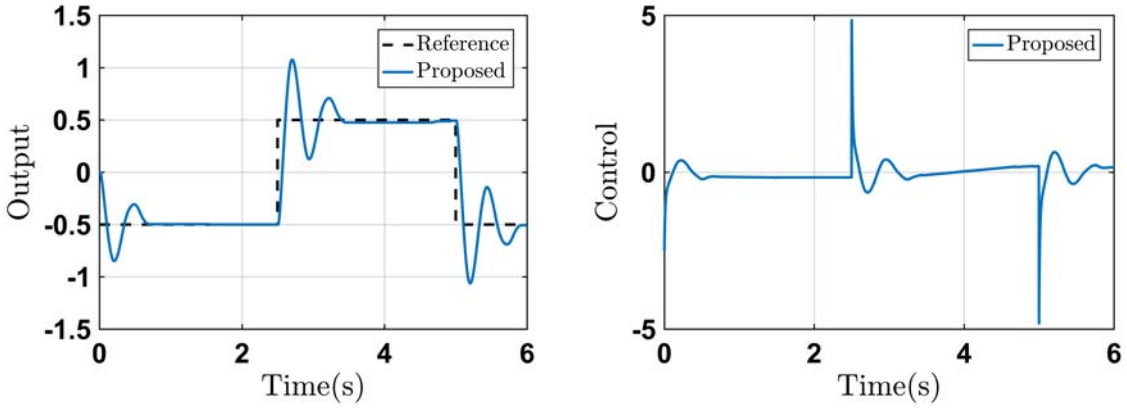

(a) (b)

Figure 3.17: Qube servo velocity control (a) output and (b) control signal

Now selecting the value of K_d and K_i in (3.141) and comparing with eq(3.142), we can calculate the augmented pole as $\lambda_2 = \frac{\mathcal{K}.Ki}{l_1\tau(1+K_d)}$, while the other parameters of PID can be calculated as $K_p = \tau(l_1 + l_1\lambda_2)(1+K_d)/\mathcal{K}$.

Thus, we assume $K_d = 1$ and $K_i = 3.5$ randomly and obtain $K_p = 2.1$ The output response and its control signal are shown in Fig. 3.17.

2. LQR-PID approach:

The closed loop characteristic equation $1 + G_4(s)C(s) = 0$ can be written as,

$$\tau(1+K_d)s^2 + (\mathcal{K}K_p + a_0)s^2 + \mathcal{K}K_i = 0 \tag{3.143}$$

As discussed earlier, λ_2 is taken as 6 times of real part of system's dominant pole and K_d is selected same as in LQG, thus we can obtain K_p and K_i. Comparing (3.141) with (3.142), we get,

$$\begin{aligned} K_p &= \frac{\tau(l_1 + l_1\lambda_2)(1+K_d)}{\mathcal{K}} \\ K_i &= \frac{\lambda_2 l_1 \tau(1+K_d)}{\mathcal{K}} \end{aligned} \tag{3.144}$$

By substituting the value of λ_2 and K_d in (3.144), we get the parameters of LQR-PID as: $K_p = 2.1$, $K_i = 3.5$, $K_d = 1$. The response for set-point tracking is shown in Fig. 3.18.

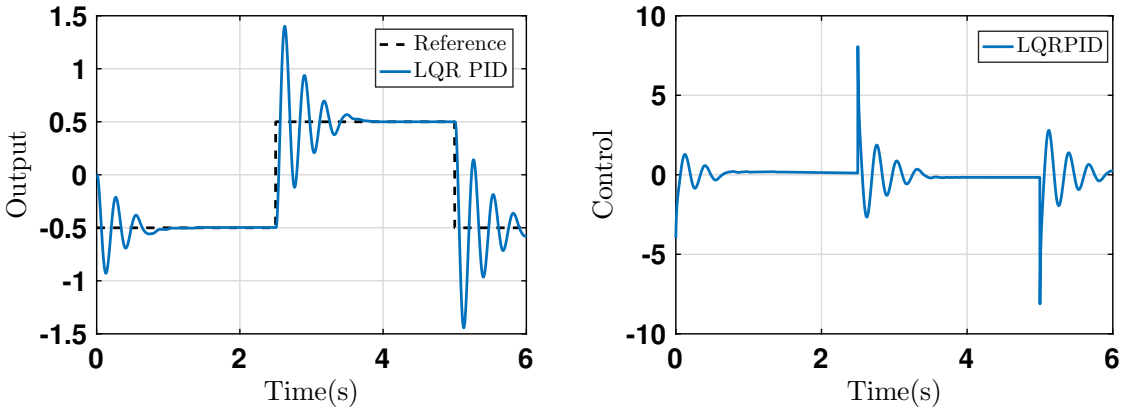

(a) (b)

Figure 3.18: Qube servo velocity by LQR-PID (a) output and (b) control signal

Table 3.8: Integral error performance indices for real time result of Qube servo

Examples	Method	Reference tracking			
		ISE	IAE	ITSE	ITAE
Position control	Proposed	1.544	2.999	4.491	8.850
	LQR-PID	1.286	2.754	3.739	8.147
Velocity control	Proposed	1.6895	3.0256	5.2030	9.1688
	LQR-PID	1.8481	3.1095	5.7513	9.4078

It can be seen from Fig. 3.17(a) and Fig. 3.18(a) that both LQR and LQG show oscillations in output velocity response. However, the oscillations in LQG approach are lesser as compared to LQR because of the noise filtering properties of Kalman filter in LQG scheme. The corresponding control voltages, as depicted in Fig. 3.17(b) and Fig. 3.18(b) show that the proposed approach needs minimal energy.

Table 3.8 enlists different performance indices for position control (Case 1) and velocity control (Case 2) of QUBE servo system via proposed LQG-QRAWCP and LQR-PID.

3.6.3 Case 3: Rotary inverted pendulum system (RIPS)

The hardware setup of Qube Servo2 Rotary inverted pendulum system control is shown in Fig. 3.19 [18, 79, 118]. The details of the mathematical modelling and the values of the parameters are given in Appendix B. We have considered balancing the pendulum in vertical direction.

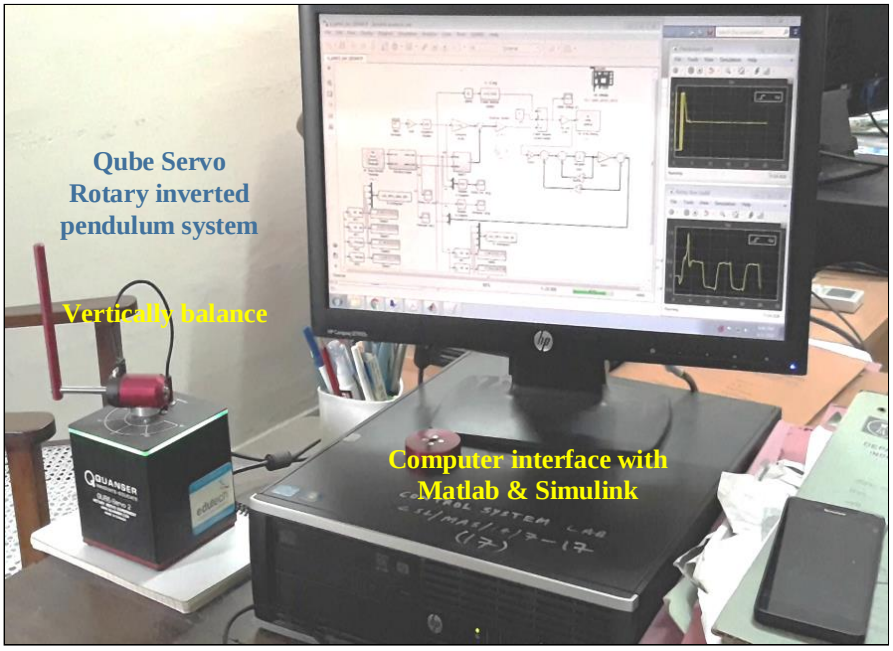

Figure 3.19: Real-time Qube-Servo2 Rotary inverted pendulum set-up

1. Proposed approach using LQG:

RIPS can be modelled by a single input - multi output (SIMO) system, wherein, the input is control voltage (U) and the output is rotary arm angle (θ) and pendulum angle (α). Hence, both the transfer functions can be written as follows:

$$\begin{aligned} P_1(s) &= \frac{\theta(s)}{U(s)} = \frac{b_1 s^2 + b_2}{s^4 + d_1 s^3 + d_2 s^2 + d_3 s} \\ P_2(s) &= \frac{\alpha(s)}{U(s)} = \frac{a_1 s^2 + a_2 s + a_3}{s^4 + d_1 s^3 + d_2 s^2 + d_3 s} \end{aligned} \tag{3.145}$$

where, $b_1 = 49.7275$, $b_2 = -5.6724$, $a_1 = 49.1493$, $a_2 = -1.7203$, $a_3 = -3.6669$, and $d_1 = 0.0104$, $d_2 = -261.6091$, $d_3 = 1.1912$.

The state space model for above system can be given by $\dot{x} = Ax + Bu$ and $y = Cx + Du$, where, the matrices are defined as:

$$A = \begin{bmatrix} 0 & 0 & 1 & 0 \\ 0 & 0 & 0 & 1 \\ 0 & 149.2751 & -0.204 & 0 \\ 0 & 261.6091 & -0.0103 & 0 \end{bmatrix} B = \begin{bmatrix} 0 \\ 0 \\ 49.7275 \\ 49.1493 \end{bmatrix} C = \begin{bmatrix} 1 & 0 & 0 & 0 \\ 0 & 1 & 0 & 0 \end{bmatrix} D = \begin{bmatrix} 0 \\ 0 \end{bmatrix} \tag{3.146}$$

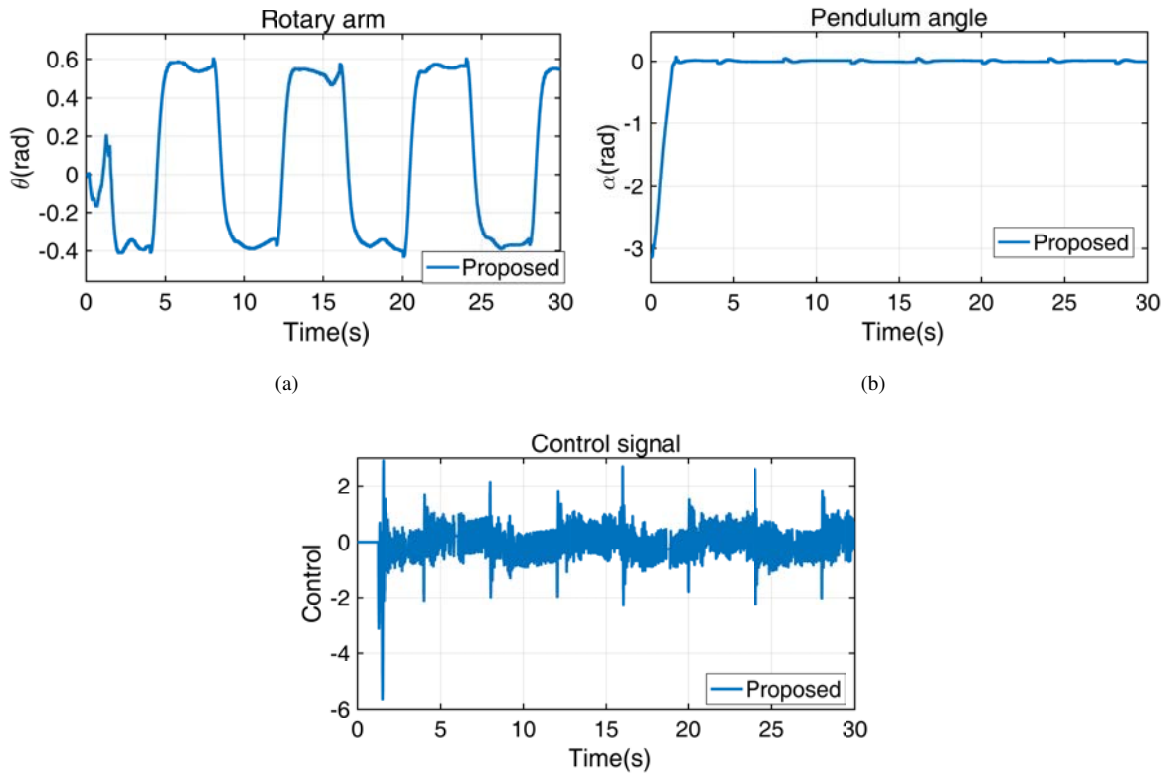

Figure 3.20: Qube servo RIPS control (a) rotary arm (b) pendulum angle and (c) control signal

Selecting the appropriate values of disturbance (w) and noise covariance (v), we obtain the LQG transfer function as $H(s) = K(sI - A + BK + LC)^{-1}L$.

Now, we implement the aforementioned approach on the hardware setup of Qube servo2 RIPS [79] and observe the stabilization of pendulum in vertical direction, for square wave input trajectory given to rotary arm. The corresponding output response of the rotary arm(θ), pendulum angle(α) and control signal(U) is shown in Fig. 3.20(a), 3.20(b) and 3.20(c), respectively.

2. LQR compensator:

To analyse the effect of LQG on RIPS, we design a standard LQR using $Q = diag([1,1,1,1])$, and $R = [1]$. Since it is not possible to measure the all the states, thus we have used a derivative function from the MATLAB and obtained all the states. The corresponding output angle response and its control signal are shown in Fig. 3.21.

From Fig. 3.20 and Fig. 3.21, it is seen that although the proposed LQG-QRAWCP approach shows less oscillations in comparison to LQR-PID, but the peak amplitude of its control signal is more.

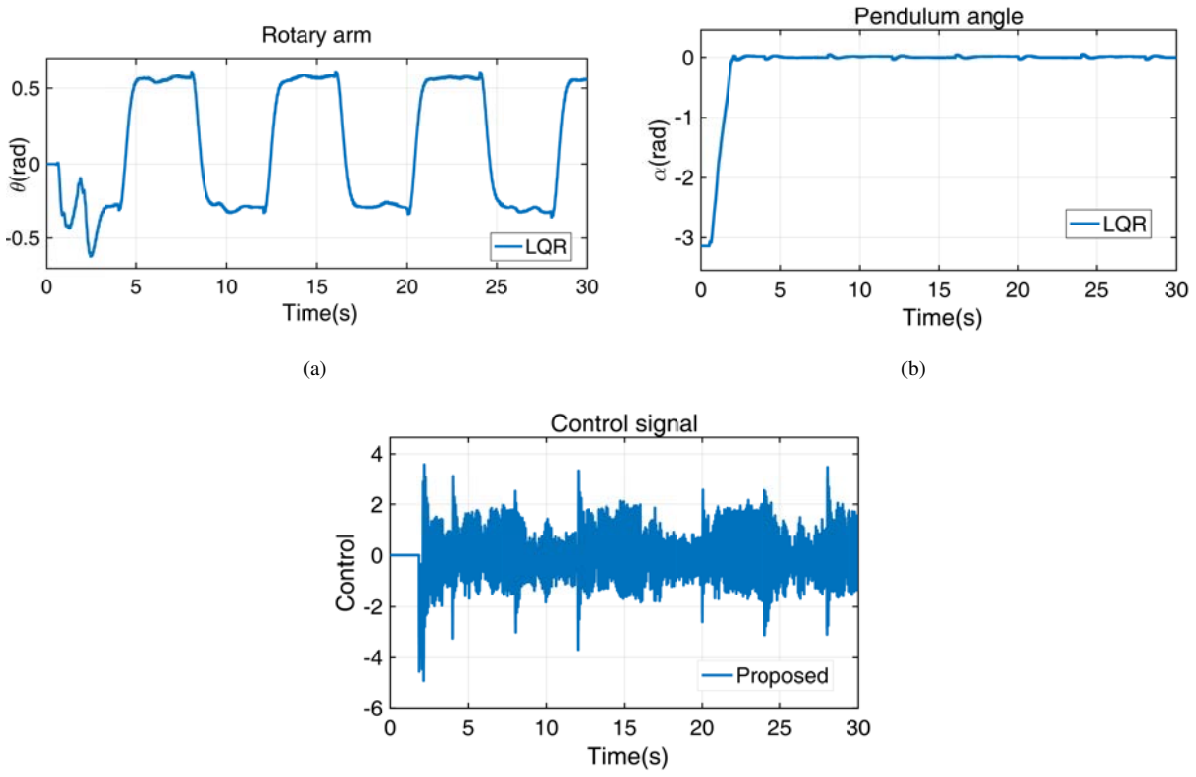

Figure 3.21: Qube servo RIPS control by LQR (a) rotary arm (b) pendulum angle and (c) control signal

Table 3.9: Performance indices for RIPS

Method	Pendulum angle(α)				Rotary arm angle(θ)			
	ISE	IAE	ITSE	ITAE	ISE	IAE	ITSE	ITAE
Proposed	5.036	2.534	1.722	5.862	3.700	6.827	52.85	96.33
LQR-PID	10.150	4.265	5.755	7.843	3.674	7.268	55.92	108.4

Table 3.9 enlists different performance indices for rotary arm angle (α) control and pendulum angle(θ) control of RIPS via proposed LQG-QRAWCP and LQR-PID.

3.7 Concluding remarks

This chapter deals with the development of a generalised and a direct formula for the design of an optimal PID controller for SISO and SIMO systems. A new technique, known as QRAWCP, that transforms an optimal LQR controller into the structure of a PID controller is proposed. It

can be deduced that the proposed QRAWCP approach outperforms the existing techniques for four illustrative examples of SISO systems. However, QRAWCP approach encounters a limitation when the system is not observable. To ameliorate this drawback, one can combine LQR and Kalman filter, resulting in LQG system. This approach is then implemented on hardware for position and velocity control of QUBE servo system and also for balancing of the rotary inverted pendulum, which is a SIMO system. The proposed LQG-PID is compared with LQR-PID. It is observed that LQG stabilises the system too, but it is required only when the states of the system are not observable and it does not guarantee better response over the LQR approach. In future, the proposed approach can be applied to various other engineering problems. In the next chapter, we discuss a rather interesting approach that proposes to combine the good properties of the controllers designed via different techniques through a weighing mechanism. This scheme will be known as the adaptive control scheme.

Chapter 4

Proposed Control Approach–II- An Adaptive control policy

The term ‘adaptive’ means ‘to change’ or to adapt to the present environment [119]. This concept has come from keen observation of natural beings to adapt to the changing environment. It is a control technique used by a particular controller setup such that it is able to acclimatise to the changing environmental conditions, as the system in certain cases are susceptible to a large scale variation in the nominal parameters. In this chapter, a generalised adaptive control scheme is proposed for linear time invariant (LTI) systems. Further, the proposed strategy is elucidated via two illustrative examples of different models. Two candidate controllers are designed for the position control of the model of a flexible robotic arm system, wherein the individual controllers are tuned via PID-LQR and SBL-PID respectively. Next, a three candidate controller is derived for the position control of a DC servo system model and the individual controllers here are tuned via LQR, SBL and ZN techniques, respectively. For each of the above cases, the results obtained via the proposed approach are compared with the design approaches of the individual controllers. It is observed that the proposed adaptive strategy outperforms the individual control techniques. Finally, the proposed scheme is further modified through the addition of a median filter and an ε term to get rid of the zero derivative problem. To validate the effectiveness and strength of the modified scheme, it is then tested on illustrative examples and on hardware setup of a Cart Inverted pendulum system.

4.1 Motivation

In control literature, the field of adaptive control, can be traced back to 1936's when a US patent was filed on self-stabilizing control mechanism by Nikolai B. *et.al* [120], and a hardware mechanism was designed to control the magnitude of variable temperature of the motor. Although in 1947 and in 1954, two US patents were filed on the control system for automatic response adjustment [121] and self-adjusting control apparatus [122] respectively, the word "adaptive" was first coined in 1958 in a survey paper [119]. Since then, various researchers such as, Whitaker *et.al*[123] have designed autopilot for automatic manoeuvring at different speeds and altitudes. In a similar fashion, adaptive pole placement technique based on linear quadratic control was suggested by Kalman [42]. Since the older times till date, various adaptive control techniques have been developed and reported in the literature [124, 125]. The main idea of adaptive control is always confined to parameter estimation and re-adjustments, to achieve desired performance. This has been done in different ways and reported by various researchers [126, 127], in order to simplify the controller design as well as achieve better response. The classification of all the reported control laws in a broad sense is of two types: Identifier-based and Non-identifier based. In the former category, the controller adaptation is on the basis of online parameter estimation. In contrast to this, non-identifier based methods do not employ online parameter estimation but use heuristic or deterministic search algorithms to determine the best controller configuration required. The popular gain scheduling technique [128] is used for faithful power system operation and comes under the category of non-identifier based control. Gain scheduling [129] basically deals with a controller block composed of multiple numbers of controllers, each possessing its own characteristics, and a switching logic block which, on the basis of some search algorithm technique, determines which controller to be preferred the most for the current scenario.

However, it is found that in most of the cases [53, 130], one type of controller gives the optimum result for some types of performance measures but may not be optimum for the rest [131, 132]. In such cases the adaptive control strategy is useful, to stabilize the system even in presence of parametric uncertainties and disturbance, or if any of the other controller fails. This is carried out by assigning an appropriate weight to the respective candidate controllers to get desired or optimum performance. The adaptive weighing principle [133–135] for prioritizing the controllers is

inspired from [136–138]. Instead of employing search algorithms for the optimum weight pairs, gradient descent algorithm can be used [139, 140], which is a efficient and relatively faster for online update of the weights [141]. Valluru et. al. [142] tuned PID by a multi-objective genetic algorithm and used adaptive particle swarm optimization (APSO) algorithm for the inverted pendulum [143].

Keeping in mind the drawbacks of the above-discussed control techniques, in this chapter, an adaptive control logic is proposed to stabilize the LTI system. The control law involves two candidate PID controllers, wherein, one is having better transient performance and the other is having better steady state performance. The adaptive weights are updated by online gradient descent algorithm. The design procedure is simplified by selecting these two types of controllers which not only reduce the mathematical intricacies, but also provide good performance of the system, both in presence and absence of matched disturbances into the system.

Summarizing the above discussion, the main contribution of this chapter is highlighted in the following points:

- A single control unit is proposed, which is to be composed of multiple number of candidate controllers, operated adaptively.
- The main motivation behind this initiative is to handle model uncertainties and external disturbances using an adaptive form of PID terminology.

4.2 Adaptive control logic scheme

For the control of systems having matched disturbances as an external input, a supervisory system, which select controller from a set of pre-designed controllers, can be used. Here, supervisory system means adaptive control logic. But in most of the practical problems, designing a supervisory control requires prior knowledge of the accurate behavior of a system, based on which it can be further trained.

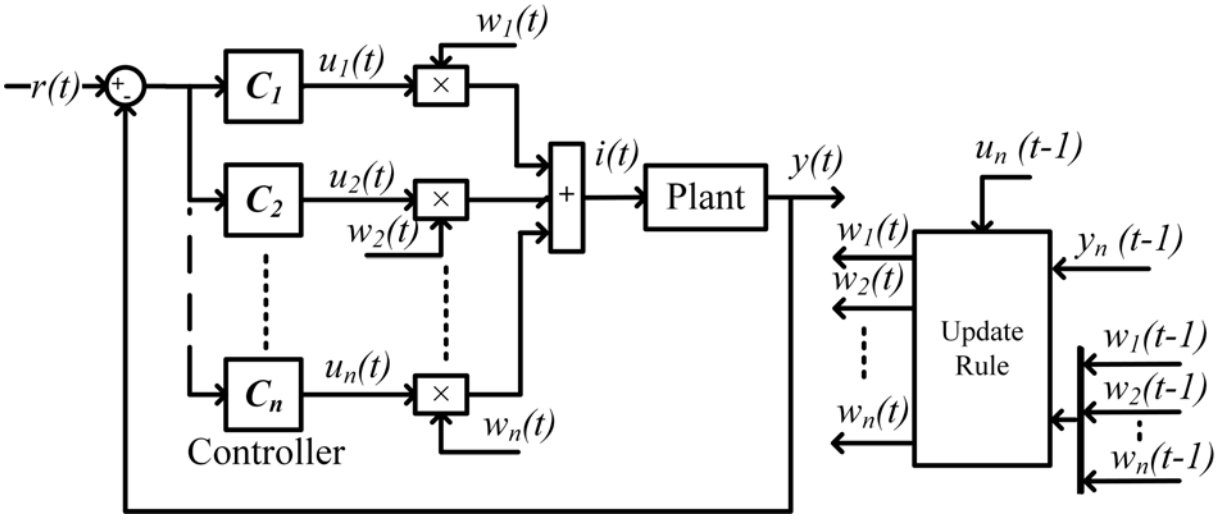

Figure 4.1: General block diagram for adaptive control logic

This training data set may not be available in every possible scenario since an accurate behaviour of a system in case of uncertain environment is not known every time. So, an approach to adaptively control a system using online gradient descent to obtain parameter estimates can be used for such problems. In an online learning model, the algorithm receives immediate feedback about each prediction and uses this feedback to improve its accuracy in subsequent predictions. Fig. 4.1 shows the block diagram of the proposed approach where to control plant G, a set of k candidate controllers have been pre-designed. The output signal from the n^{th} controller (where $n \in \mathbb{N}, n \leq k$) at time '$t$' is denoted by $u_n(t)$. This output is multiplied by weight $w_n(t)$ before it is fed as an input to the plant. So the net control input to the plant at time 't' can be written as:

$$i(t) = w(t)^T u(t) \tag{4.1}$$

where,

$$\begin{aligned} u(t) &= [u_1(t)\ \ u_2(t)\ \ u_3(t)\ \ \ldots\ \ u_k(t)]^T \\ w(t) &= [w_1(t)\ \ w_2(t)\ \ w_3(t)\ \ \ldots\ \ w_k(t)]^T \end{aligned} \tag{4.2}$$

In order to carry out dynamic adaptive control among a set of candidate controllers, the weight vector is updated at every iteration to mask inactive controllers. This update is carried out by means of gradient descent algorithm [139], which is a first order optimization algorithm that aims at finding a local minimum of a function by moving in the direction of negative gradient of a function, calculated at the current point.

Consider a general plant of order q, which is represented in the transfer function form as follows:

$$G(s) = \frac{b_0 + b_1 s + b_2 s^2 + ... + b_m s^m}{a_0 + a_1 s + a_2 s^2 + ... + a_q s^q} \qquad m < q \tag{4.3}$$

Let the set of pre-defined candidate controllers $[C]$ for the given plant be formulated as

$$C(s) = [C_1(s)\ \ C_2(s)\ \ C_3(s)\ \ ...\ \ C_k(s)] \tag{4.4}$$

The output of n^{th} controller $C_n(s)$ at any time 't' is given by $u_n(t)$, and the net control input $i(t)$ that is to be applied to the plant is given in (4.1). The output $y(t)$ of plant $G(s)$ can be written in s-domain as: $Y(s) = G(s)I(s)$ where, $Y(s) \equiv \mathscr{L}(y(t)) = \int_0^\infty e^{-st} y(t)dt$ and $I(s) \equiv \mathscr{L}(i(t)) = \int_0^\infty e^{-st} i(t)dt$, Thus, we get,

$$Y(s)[a_0 + a_1 s + a_2 s^2 + ... + a_q s^q] = I(s)[b_0 + b_1 s + b_2 s^2 + ... + b_m s^m] \tag{4.5}$$

Taking inverse laplace transform and converting (4.5) into a differential equation, we write

$$a_0 y(t) + a_1 \frac{dy(t)}{dt} + ... + a_q \frac{d^q y(t)}{dt^q} = b_0 i(t) + b_1 \frac{di(t)}{dt} + ... + b_m \frac{d^m i(t)}{dt^m} \tag{4.6}$$

with zero initial conditions, i.e., $\frac{dy^{q-1}(t)}{dt^{q-1}}|_{t=0^+} = 0$, $\forall q$ and $\frac{di^{m-1}(t)}{dt^{m-1}}|_{t=0^+} = 0$, $\forall m$.

To find the optimum value of the weight vector $w_n(t)$ iteratively, using gradient descent method, let us define an error function as:

$$e(t) = \frac{1}{2} \int_0^\infty (r(t) - y(t))^2 dt \tag{4.7}$$

where, $r(t)$ is the reference input to the plant at time 't' and $y(t)$ is the actual output.

To improve the system performance in uncertain noisy environment, we must choose the weights (see (4.2)) such that, the error function $e(t)$, at any time 't', is minimized. For that, the weights are iteratively updated using gradient descent [144] and the update rules can be written as:

$$w_n(t+1) \leftarrow \left[w_n(t) - \alpha \frac{\partial e(t)}{\partial w_n(t)} \right] \tag{4.8}$$

From equation (4.8), $\frac{\partial e(t)}{\partial w_n(t)}$ is written using chain rule. This is shown in (4.9).

$$\frac{\partial e(t)}{\partial w_n(t)} = \frac{\partial e(t)}{\partial y(t)} \frac{\partial y(t)}{\partial i(t)} \frac{\partial i(t)}{\partial w_n(t)} \quad n \in \{1,2,3,...,k\} \tag{4.9}$$

Here, α is the learning rate, $\{\alpha \in \mathbb{R} \,|\, 0 < \alpha < 1\}$. Using (4.7), we can write $\frac{\partial e(t)}{\partial y(t)} = -(r(t) - y(t))$ and using (4.1), we get $\frac{\partial i(t)}{\partial w_n(t)} = u_n(t)$. Since y and i are functions of time t alone, hence the following holds true:

$$\frac{\partial y}{\partial t} = \frac{dy}{dt}; \quad \frac{\partial i}{\partial t} = \frac{di}{dt} \implies \frac{\partial y}{\partial i} = \frac{dy}{di} \tag{4.10}$$

Rearranging the terms of (4.6), we get

$$i(t) = \frac{1}{b_0}\left(a_0 y(t) + a_1 \frac{dy(t)}{dt} + a_2 \frac{d^2y(t)}{dt^2} + ... + a_q \frac{d^q y(t)}{dt^q} - \left(b_1 \frac{di(t)}{dt} + b_2 \frac{d^2 i(t)}{dt^2} + ... + b_m \frac{d^m i(t)}{dt^m}\right)\right) \tag{4.11}$$

Differentiating both sides of (4.11) and simplifying, we get

$$\frac{di(t)}{dy(t)} = \frac{1}{b_0}\left(a_0 \frac{dy(t)}{dt} + a_1 \frac{d^2y(t)}{dt^2} + ... + a_q \frac{d^{q+1} y(t)}{dt^q} - \left(b_1 \frac{d^2 i(t)}{dt^2} + ... + b_m \frac{d^m i(t)}{dt^{m+1}}\right)\right) \tag{4.12}$$

Substituting the values from (4.9) and (4.12) in (4.8), we obtain the final weights as

$$w_n(t+1) = w_n(t) - \frac{\alpha(y(t) - r(t)) u_n b_0 \frac{dy}{dt}}{v(t)} \tag{4.13}$$

where,

$$v(t) = \left(a_0 \frac{dy(t)}{dt} + a_1 \frac{d^2y(t)}{dt^2} + ... + a_q \frac{d^{q+1} y(t)}{dt^q} - \left(b_1 \frac{d^2 i(t)}{dt^2} + ... + b_m \frac{d^m i(t)}{dt^{m+1}}\right)\right) \tag{4.14}$$

Note: The number of controllers (C_n) depends upon desired specifications and also on the performance of the corresponding individual candidate controllers.

4.3 Illustrative Examples

The superiority of the proposed approach is demonstrated through illustrative examples and via the comparison of the performance indices with the existing methodologies in control theory literature.

4.3.1 Example 1: two candidate controller

To illustrate the proposed adaptive control policy, we consider an example of a flexible robotic arm model [145], wherein two candidate controllers are designed, one using SBL-PID[57] and other via LQR-PID[1] scheme.

Following steps need to be followed to formulate an adaptive policy for flexible robotic arm.

The transfer function of a flexible robotic arm [57] is given as

$$G_1(s) = \frac{s+500}{s(s+0.0325)(s^2+2.57s+6.667)} \tag{4.15}$$

Fig. 4.2 depicts the block diagram for implementing the proposed control logic. The proposed

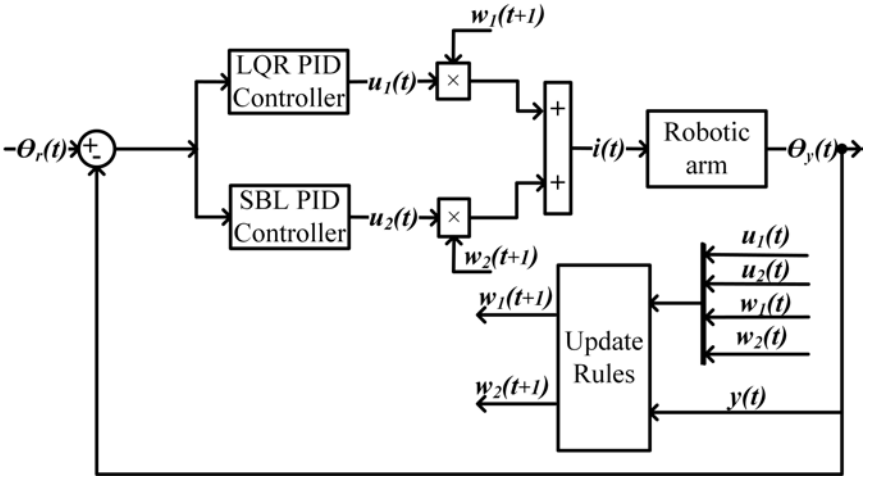

Figure 4.2: Block diagram of proposed adaptive control technique for example 1

adaptive logic is based on two contrasting candidate PID controllers. They are designed based on LQR[1, 50] and SBL based [57] approaches respectively. The design methodology is explained as follows:

(i) First candidate controller(C_1): Design by LQR-PID

The first candidate controller is a PID, represented as $C_1(s)$ and is tuned by pole placement technique. Let $C_1(s)$ be written as: $C_1(s) = \frac{K_{d1}s^2+sK_{p1}+K_{i1}}{s}$. The flexible robotic arm transfer function (4.15) can be written in generalised coefficient form as,

$$G_2(s) = \frac{s+b_0}{s^4+a_3s^3+a_2s^2+a_1s} \tag{4.16}$$

The closed-loop characteristic equation using $C_1(s)$ and (4.16) becomes $1+G_2(s)C_1(s)=0$, which is simplified as

$$s^5+a_3s^4+(a_2+K_d)s^3+(K_db_0+a_1+K_p)s^2+(K_pb_0+K_i)s+K_ib_0=0 \tag{4.17}$$

Equation (4.17) is of fifth order. Therefore, we select five poles on the left half of the s-plane. The characteristic equation of the system having these poles is shown in eq.(4.18).

$$(s+\lambda_1)(s+\lambda_2)(s+\lambda_3)(s+\lambda_4)(s+\lambda_5)=0 \tag{4.18}$$

The above equation can also be written as

$$s^5+p_4s^4+p_3s^3+p_2s^2+p_1s+p_0=0 \tag{4.19}$$

where,

$$\begin{aligned}
p_4 &= (\lambda_1+\lambda_2+\lambda_3+\lambda_4+\lambda_5)\\
p_3 &= \left(\lambda_1\lambda_2+(\lambda_1+\lambda_2)\lambda_3+(\lambda_1+\lambda_2+\lambda_3)\lambda_4+(\lambda_1+\lambda_2+\lambda_3+\lambda_4)\lambda_5\right)\\
p_2 &= \lambda_1\lambda_2\lambda_3+\left(\lambda_1\lambda_2+(\lambda_1+\lambda_2)\lambda_3\right)\lambda_4+\left(\lambda_1\lambda_2+(\lambda_1+\lambda_2)\lambda_3+(\lambda_1+\lambda_2+\lambda_3)\lambda_4\right)\lambda_5\\
p_1 &= \lambda_1\lambda_2\lambda_3\lambda_4+\left(\lambda_1\lambda_2\lambda_3+\left(\lambda_1\lambda_2+(\lambda_1+\lambda_2)\lambda_3\right)\lambda_4\right)\lambda_5\\
p_0 &= \lambda_1\lambda_2\lambda_3\lambda_4\lambda_5
\end{aligned}$$

By comparing (4.17) and (4.19), parameters of $C_1(s)$ are calculated as

$$K_{p1} = \frac{p_1 b_1}{a_4}, \quad K_{i1} = \frac{p_0 b_1}{a_4}, \quad K_{d1} = \frac{p_2 b_1 - b_3}{a_4} \tag{4.20}$$

(ii) The second PID controller $C_2(s)$ is tuned by SBL method [57]. The mathematical explanation of the SBL-PID is given in chapter 2 and is not included here for avoidance of repetition.

4.3.1.1 Proposed methodology

After designing the two candidate controllers C_1 and C_2, such that one performs better during the transient part and other in steady state part, now design the proposed adaptive scheme for the flexible robotic arm system, which is given in (4.16). From Fig. 4.2 the system input $i(t)$ can be written as:

$$i(t) = w_1(t)u_1(t) + w_2(t)u_2(t) \tag{4.21}$$

where, $u_1(t)$ is the output of C_1 controller and $u_2(t)$is the output of the C_2 controller.
The Laplace transform of the output $\theta_y(t)$ can be written as

$$\theta_y(s) = i(s) \times \frac{s + b_0}{s^4 + a_3 s^3 + a_2 s^2 + a_1 s} \tag{4.22}$$

Equation (4.22), in time domain form, can be written as:

$$i(t) = \frac{\frac{d^4\theta_y(t)}{dt^4} + a_3\frac{d^3\theta_y(t)}{dt^3} + a_2\frac{d^2\theta_y(t)}{dt^2} + a_1\frac{d\theta_y(t)}{dt} - \frac{di(t)}{dt}}{b_0} \tag{4.23}$$

Defining the objective function $e(t)$ such that

$$e(t) = \frac{1}{2}\left(\theta_r - \theta_y\right)^2(t) \tag{4.24}$$

where, $\theta_r(t)$ is the reference position and $\theta_y(t)$ is the actual output angular position. The main objective is to minimize $e(t)$. The rules to update weights $w_n(t+1)$ are decided by using on-line

gradient descent function which is represented in (4.25).

$$w_n(t+1) = \left(w_n(t) - \alpha \frac{de(t)}{dw_n(t)} \right) \tag{4.25}$$

where, $n = 1, 2$ and α is the rate of convergence. Substituting $n = 1$ in (4.25), we get $w_1(t+1)$ that can be written as:

$$w_1(t+1) = \left(w_1(t) - \alpha \frac{de(t)}{dw_1(t)} \right) \tag{4.26}$$

In order to find $\frac{de(t)}{dw_1(t)}$, the following steps are to be followed:

$$\frac{de(t)}{dw_1(t)} = \frac{de(t)}{d\theta_y(t)} \times \frac{d\theta_y(t)}{di(t)} \times \frac{di(t)}{dw_1(t)} \tag{4.27}$$

For $\frac{de(t)}{d\theta_y(t)}$, differentiating (4.24) with respect to θ_y, we get,

$$\frac{de(t)}{d\theta_y(t)} = -1 \left(\theta_r(t) - \theta_y(t) \right) \tag{4.28}$$

Differentiating (4.21) with respect to w_1, the following equation is obtained:

$$\frac{di(t)}{dw_1(t)} = u_1(t) \tag{4.29}$$

To find $\frac{d\theta_y(t)}{di(t)}$, differentiating (4.23) by $\theta_y(t)$, we get

$$\begin{aligned} \frac{di(t)}{d\theta_y(t)} &= \frac{d}{d\theta_y(t)} \left(\frac{d^4\theta_y(t)}{dt^4} \right) + \frac{d}{d\theta_y(t)} \left(\frac{a_3}{b_0} \frac{d^3\theta_y(t)}{dt^3} \right) \\ &+ \frac{d}{d\theta_y(t)} \left(\frac{a_2}{b_0} \frac{d^2\theta_y(t)}{dt^2} \right) + \frac{d}{d\theta_y(t)} \left(\frac{a_1}{b_0} \frac{d\theta_y(t)}{dt} \right) - \frac{d}{d\theta_y(t)} \left(\frac{1}{b_0} \frac{di(t)}{dt} \right) \end{aligned} \tag{4.30}$$

Simplifying using chain rule, (4.30) becomes

$$\begin{aligned} \frac{di(t)}{d\theta_y(t)} &= \frac{d}{dt}\frac{dt}{d\theta_y(t)} \left(\frac{d^4\theta_y(t)}{dt^4} \right) + \frac{d}{dt}\frac{dt}{d\theta_y(t)} \left(\frac{a_3}{b_0} \frac{d^3\theta_y(t)}{dt^3} \right) \\ &+ \frac{d}{dt}\frac{dt}{d\theta_y(t)} \left(\frac{a_2}{b_0} \frac{d^2\theta_y(t)}{dt^2} \right) + \frac{d}{dt}\frac{dt}{d\theta_y(t)} \left(\frac{a_1}{b_0} \frac{d\theta_y(t)}{dt} \right) - \frac{d}{dt}\frac{dt}{d\theta_y(t)} \left(\frac{1}{b_0} \frac{di(t)}{dt} \right) \end{aligned} \tag{4.31}$$

Equation (4.31) can also be written as

$$\frac{di(t)}{d\theta_y(t)} = \frac{\frac{1}{b_0}\left[\begin{array}{l}\left(\frac{d^5\theta_y(t)}{dt^5}\right)+\left(a_3\frac{d^4\theta_y(t)}{dt^4}\right)\\ +\left(a_2\frac{d^3\theta_y(t)}{dt^3}\right)+\left(a_1\frac{d^2\theta_y(t)}{dt^2}\right)-\left(\frac{d^2i(t)}{dt^2}\right)\end{array}\right]}{\frac{d\theta_y(t)}{dt}} \tag{4.32}$$

To obtain $\frac{d\theta_y(t)}{di(t)}$, rearranging (4.32), we get,

$$\frac{d\theta_y(t)}{di(t)} = b_0 \frac{\frac{d\theta_y(t)}{dt}}{\left(\frac{d^5\theta_y(t)}{dt^5}\right)+\left(a_3\frac{d^4\theta_y(t)}{dt^4}\right)+\left(a_2\frac{d^3\theta_y(t)}{dt^3}\right)+\left(a_1\frac{d^2\theta_y(t)}{dt^2}\right)-\left(\frac{d^2i(t)}{dt^2}\right)} \tag{4.33}$$

By substituting (4.28), (4.29), (4.33) in equation (4.27), we get,

$$\begin{aligned}\frac{de(t)}{dw_1(t)} &= \left(\theta_y(t)-\theta_r(t)\right)\times u_1(t)\\ &\times b_0 \frac{\frac{d\theta_y(t)}{dt}}{\left(\frac{d^5\theta_y(t)}{dt^5}\right)+\left(a_3\frac{d^4\theta_y(t)}{dt^4}\right)+\left(a_2\frac{d^3\theta_y(t)}{dt^3}\right)+\left(a_1\frac{d^2\theta_y(t)}{dt^2}\right)-\left(\frac{d^2i(t)}{dt^2}\right)}\end{aligned} \tag{4.34}$$

To obtain next state value of weight $w_1(t+1)$, we substitute (4.52) in (4.26), which yields,

$$\begin{aligned}w_1(t+1) \leftarrow \Bigg\{ w_1(t) - \alpha \Bigg[&\left(\theta_y(t)-\theta_r(t)\right) u_1(t)\\ &\times b_0 \frac{\frac{d\theta_y(t)}{dt}}{\left(\frac{d^5\theta_y(t)}{dt^5}\right)+\left(a_3\frac{d^4\theta_y(t)}{dt^4}\right)+\left(a_2\frac{d^3\theta_y(t)}{dt^3}\right)+\left(a_1\frac{d^2\theta_y(t)}{dt^2}\right)-\left(\frac{d^2i(t)}{dt^2}\right)} \Bigg] \Bigg\}\end{aligned} \tag{4.35}$$

Similarly, weight $w_2(t+1)$ is calculated as below:

$$\begin{aligned}w_2(t+1) \leftarrow \Bigg\{ w_2(t) - \alpha \Bigg[&\left(\theta_y(t)-\theta_r(t)\right) \times u_2(t)\\ &\times b_0 \frac{\frac{d\theta_y(t)}{dt}}{\left(\frac{d^5\theta_y(t)}{dt^5}\right)+\left(a_3\frac{d^4\theta_y(t)}{dt^4}\right)+\left(a_2\frac{d^3\theta_y(t)}{dt^3}\right)+\left(a_1\frac{d^2\theta_y(t)}{dt^2}\right)-\left(\frac{d^2i(t)}{dt^2}\right)} \Bigg] \Bigg\}\end{aligned} \tag{4.36}$$

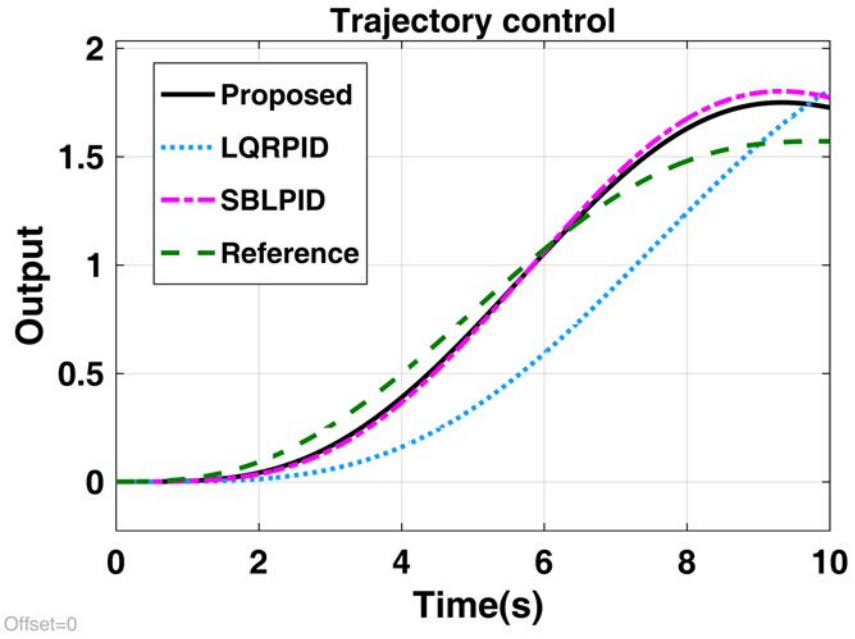

Figure 4.3: Output response for example 1

These two weights $w_1(t+1)$ and $w_2(t+1)$ are multiplied with $i(t+1)$ at time $(t+1)$. This will be the future state control signal value given to the system.

4.3.1.2 Results and analysis

The output response of the adaptive controller and the individual candidate controllers is illustrated in Figure 4.3. It can be observed that the controller designed via the adaptive scheme follows the reference more closely as compared to the controller that is tuned by the individual control approach. Figure 4.4(a) and Figure 4.4(b) depict the control signal response and the weight update plot for example respectively. It can be seen that although the control energy for LQR-PID is minimum, but its response does not track the reference. The proposed approach tracks the reference and uses fairly minimum energy as well.

Table 4.1 enlists different performance indices for the proposed adaptive policy and the individual candidate controllers in Example 1. It can be observed that the proposed logic gives the least value of ISE, IAE, ITAE and ITSE.

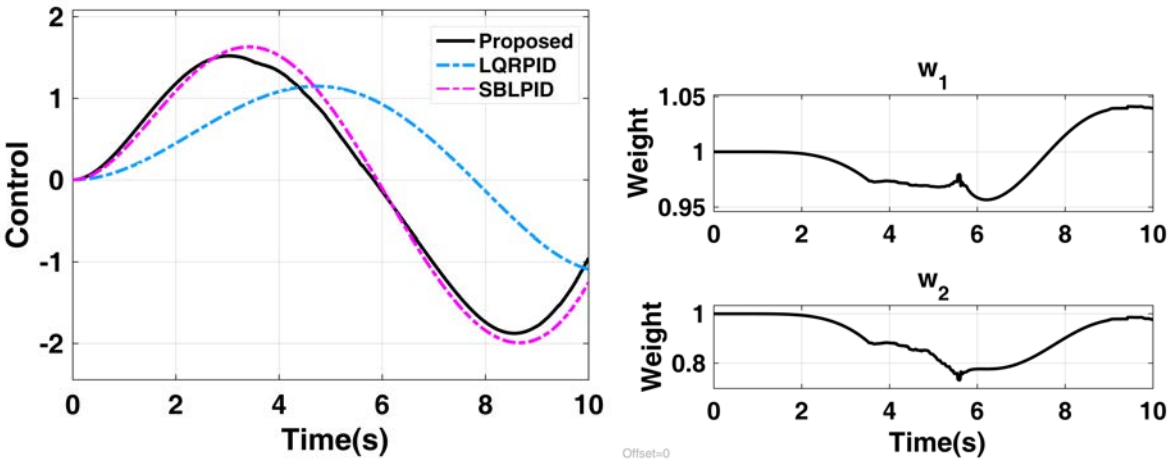

(a) (b)

Figure 4.4: Control signal and weight response for example 1

Table 4.1: Performance indices for example 1

Examples	Method	Reference tracking			
		ISE	IAE	ITSE	ITAE
Example1	Proposed	0.107482281	0.857726399	0.784649916	5.554876783
Reference	LQR-PID	0.835963702	2.348153083	4.797519615	13.3877223
tracking	SBL-PID	0.170506727	1.06822442	1.270615494	7.042755378

4.3.2 Example 2: three candidate controllers

In this example, three candidate controllers, C_1 (LQR-PID[1]), C_2 (SBL-PID [57]), and C_3 (ZNPID[26]) with each having a distinct advantage have been considered for DC servo motor control problem. The design steps for each of these candidate controllers are designed previously. C_1 is discussed in example 1 as well as in chapter 3, and C_2 and C_3 are given in chapter 2.

Here, we have considered the DC servo motor position control transfer function from user manual of precision modular servo (PMS) system [146] manufactured by Feedback instruments Ltd., UK.

$$G_2(s) = \frac{0.042}{2.424 \times 10^{-8} s^3 + 0.0001755 s^2 + 0.001764 s} \tag{4.37}$$

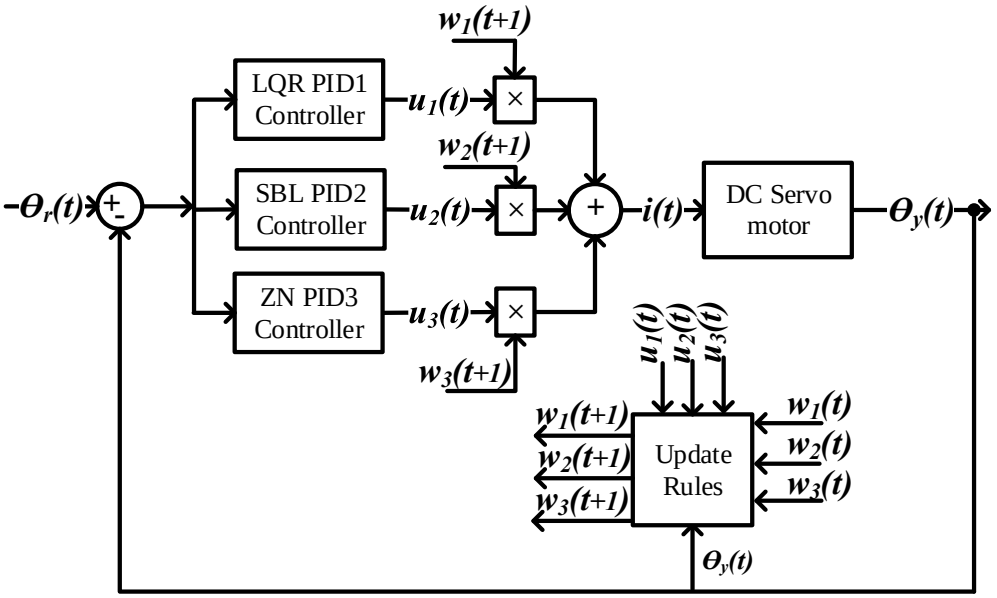

Figure 4.5: Block diagram of proposed adaptive control technique for example 2

4.3.2.1 Proposed methodology

Let the transfer function, be written as (4.37),

$$G_2(s) = \frac{b_0}{a_3 s^3 + a_2 s^2 + a_1 s} \tag{4.38}$$

From Fig. 4.5, the plant input $i(t)$ to the servo motor can be written as:

$$i(t) = w_1(t)u_1(t) + w_2(t)u_2(t) + w_3(t)u_3(t) \tag{4.39}$$

where, $u_1(t)$ is the output of C_1 controller, $u_2(t)$is the output of the C_2 controller and $u_3(t)$is the output of the C_3 controller. Similarly, the output $\theta_y(t)$ can be written as

$$\theta_y(s) = i(s)\frac{b_0}{a_3 s^3 + a_2 s^2 + a_1 s} \tag{4.40}$$

Equation (4.40), in time domain form, can be written as:

$$i(t) = \frac{a_3 \frac{d^3\theta_y(t)}{dt^3} + a_2 \frac{d^2\theta_y(t)}{dt^2} + a_1 \frac{d\theta_y(t)}{dt}}{b_0} \tag{4.41}$$

Let us define the objective function $e(t)$ as

$$e(t) = \frac{1}{2}\left(\theta_r - \theta_y\right)^2(t) \tag{4.42}$$

where, $\theta_r(t)$ is the reference position and $\theta_y(t)$ is the actual output angular position. The main objective is to minimize $e(t)$. The rules to update weights $w_n(t+1)$ are decided by using on-line gradient descent function which is represented in (4.43).

$$w_n(t+1) = \left(w_n(t) - \alpha \frac{\partial e(t)}{\partial w_n(t)}\right) \tag{4.43}$$

where, $n = 1, 2, 3$ and α is the rate of convergence.

For first weight $n = 1$ in (4.43), we get $w_1(t+1)$ that can be written as:

$$w_1(t+1) = \left(w_1(t) - \alpha \frac{de(t)}{dw_1(t)}\right) \tag{4.44}$$

In order to find $\frac{de(t)}{dw_1(t)}$, the following steps are to be followed:

$$\frac{de(t)}{dw_1(t)} = \frac{de(t)}{d\theta_y(t)} \times \frac{d\theta_y(t)}{di(t)} \times \frac{di(t)}{dw_1(t)} \tag{4.45}$$

For $\frac{de(t)}{d\theta_y(t)}$, differentiating (4.42) with respect to θ_y, we get

$$\frac{de(t)}{d\theta_y(t)} = -1\left(\theta_r(t) - \theta_y(t)\right) \tag{4.46}$$

Differentiating (4.39) with respect to w_1, the following equation is obtained:

$$\frac{di(t)}{dw_1(t)} = u_1(t) \tag{4.47}$$

To find $\frac{d\theta_y(t)}{di(t)}$, differentiating (4.41) by $\theta_y(t)$, we get,

$$\begin{aligned}\frac{di(t)}{d\theta_y(t)} &= \frac{d}{d\theta_y(t)}\left(\frac{d^4\theta_y(t)}{dt^4}\right) + \frac{d}{d\theta_y(t)}\left(\frac{a_3}{b_0}\frac{d^3\theta_y(t)}{dt^3}\right) \\ &+ \frac{d}{d\theta_y(t)}\left(\frac{a_2}{b_0}\frac{d^2\theta_y(t)}{dt^2}\right) + \frac{d}{d\theta_y(t)}\left(\frac{a_1}{b_0}\frac{d\theta_y(t)}{dt}\right) - \frac{d}{d\theta_y(t)}\left(\frac{1}{b_0}\frac{di(t)}{dt}\right)\end{aligned} \tag{4.48}$$

Simplifying using chain rule, (4.48) becomes,

$$\frac{di(t)}{d\theta_y(t)} = \frac{d}{dt}\frac{dt}{d\theta_y(t)}\left(\frac{d^4\theta_y(t)}{dt^4}\right) + \frac{d}{dt}\frac{dt}{d\theta_y(t)}\left(\frac{a_3}{b_0}\frac{d^3\theta_y(t)}{dt^3}\right) + \frac{d}{dt}\frac{dt}{d\theta_y(t)}\left(\frac{a_2}{b_0}\frac{d^2\theta_y(t)}{dt^2}\right) + \frac{d}{dt}\frac{dt}{d\theta_y(t)}\left(\frac{a_1}{b_0}\frac{d\theta_y(t)}{dt}\right) - \frac{d}{dt}\frac{dt}{d\theta_y(t)}\left(\frac{1}{b_0}\frac{di(t)}{dt}\right) \tag{4.49}$$

Equation (4.49) can also be written as

$$\frac{di(t)}{d\theta_y(t)} = \frac{\frac{1}{b_0}\left[\begin{array}{l}\left(\frac{d^5\theta_y(t)}{dt^5}\right) + \left(a_3\frac{d^4\theta_y(t)}{dt^4}\right) \\ + \left(a_2\frac{d^3\theta_y(t)}{dt^3}\right) + \left(a_1\frac{d^2\theta_y(t)}{dt^2}\right) - \left(\frac{d^2i(t)}{dt^2}\right)\end{array}\right]}{\frac{d\theta_y(t)}{dt}} \tag{4.50}$$

Further, simplified form of (4.50) is represented so as to obtain $\frac{d\theta_y(t)}{di(t)}$, rearranging (4.50), we get,

$$\frac{d\theta_y(t)}{di(t)} = b_0\frac{\frac{d\theta_y(t)}{dt}}{\left(\frac{d^5\theta_y(t)}{dt^5}\right) + \left(a_3\frac{d^4\theta_y(t)}{dt^4}\right) + \left(a_2\frac{d^3\theta_y(t)}{dt^3}\right) + \left(a_1\frac{d^2\theta_y(t)}{dt^2}\right) - \left(\frac{d^2i(t)}{dt^2}\right)} \tag{4.51}$$

By substituting (4.28), (4.29), (4.51) in equation (4.27), we get,

$$\begin{aligned}\frac{de(t)}{dw_1(t)} &= \left(\theta_y(t) - \theta_r(t)\right) \times u_1(t) \\ &\times b_0\frac{\frac{d\theta_y(t)}{dt}}{\left(\frac{d^5\theta_y(t)}{dt^5}\right) + \left(a_3\frac{d^4\theta_y(t)}{dt^4}\right) + \left(a_2\frac{d^3\theta_y(t)}{dt^3}\right) + \left(a_1\frac{d^2\theta_y(t)}{dt^2}\right) - \left(\frac{d^2i(t)}{dt^2}\right)}\end{aligned} \tag{4.52}$$

To obtain next state value of weight $w_1(t+1)$, we substitute (4.52) in (4.26), which yields,

$$\begin{aligned}w_1(t+1) \leftarrow \Bigg\{ & w_1(t) - \alpha\left[\left(\theta_y(t) - \theta_r(t)\right) u_1(t)\right. \\ & \left.\times b_0\frac{\frac{d\theta_y(t)}{dt}}{\left(\frac{d^5\theta_y(t)}{dt^5}\right) + \left(a_3\frac{d^4\theta_y(t)}{dt^4}\right) + \left(a_2\frac{d^3\theta_y(t)}{dt^3}\right) + \left(a_1\frac{d^2\theta_y(t)}{dt^2}\right) - \left(\frac{d^2i(t)}{dt^2}\right)}\right]\Bigg\}\end{aligned} \tag{4.53}$$

Similarly, weights $w_2(t+1)$ and $w_3(t+1)$ are calculated as below:

$$w_2(t+1) \leftarrow \left\{ w_2(t) - \alpha \left[\left(\theta_y(t) - \theta_r(t)\right) u_2(t) \right.\right. \\ \left.\left. \times b_0 \frac{\frac{d\theta_y(t)}{dt}}{\left(\frac{d^5\theta_y(t)}{dt^5}\right) + \left(a_3 \frac{d^4\theta_y(t)}{dt^4}\right) + \left(a_2 \frac{d^3\theta_y(t)}{dt^3}\right) + \left(a_1 \frac{d^2\theta_y(t)}{dt^2}\right) - \left(\frac{d^2 i(t)}{dt^2}\right)} \right] \right\} \tag{4.54}$$

$$w_3(t+1) \leftarrow \left\{ w_3(t) - \alpha \left[\left(\theta_y(t) - \theta_r(t)\right) u_3(t) \right.\right. \\ \left.\left. \times b_0 \frac{\frac{d\theta_y(t)}{dt}}{\left(\frac{d^5\theta_y(t)}{dt^5}\right) + \left(a_3 \frac{d^4\theta_y(t)}{dt^4}\right) + \left(a_2 \frac{d^3\theta_y(t)}{dt^3}\right) + \left(a_1 \frac{d^2\theta_y(t)}{dt^2}\right) - \left(\frac{d^2 i(t)}{dt^2}\right)} \right] \right\} \tag{4.55}$$

These three weights $w_1(t+1)$, $w_2(t+1)$ and $w_3(t+1)$ are multiplied with $i(t+1)$ at time $(t+1)$. This will be the next state $(t+1)$ control signal value given to the system.

4.3.2.2 Results and analysis

Here, the three candidate controllers are considered as follows: $C_1(s)$ is LQRPID1 designed using steps considered in chapter 3, $C_2(s)$ is SBLPID2 designed using steps considered from [57] which are discussed in chapter 3, and $C_3(s)$ is ZNPID1 designed using conventional tuning method discussed in chapter 2 section 4.

The output response of the adaptive controller and the individual candidate controllers are illustrated in Figure 4.6. It is observed that the controller designed via the adaptive scheme follows the reference more closely as compared to the controller that is tuned by the individual control approach. Fig. 4.7(a), and Fig. 4.7(b) depict the control signal response and the weight update plot, respectively.

It is seen that at initial time, more weight is assigned to SBLPID2($C_2(s)$), whose rise time is less than others, then, because of less overshoot, the adaptive policy assigns more weight to LQRPID1($C_1(s)$) and further, in the next state the weights has been assigned to ZNPID3 which has better steady state performance. The proposed approach tracks the reference and uses fairly

Table 4.2: Performance indices for example 2

Example	Method	Reference tracking			
		ISE	IAE	ITSE	ITAE
Example 2 Reference tracking	Proposed	6.427×10^{-03}	8.350×10^{-03}	2.473×10^{-05}	4.045×10^{-05}
	LQR-PID	2.678×10^{-02}	5.766×10^{-02}	1.050×10^{-03}	4.256×10^{-03}
	SBL-PI	5.617×10^{-02}	1.280×10^{-01}	5.912×10^{-03}	2.093×10^{-02}
	ZNPID	1.699×10^{-02}	3.361×10^{-02}	2.454×10^{-04}	2.173×10^{-03}

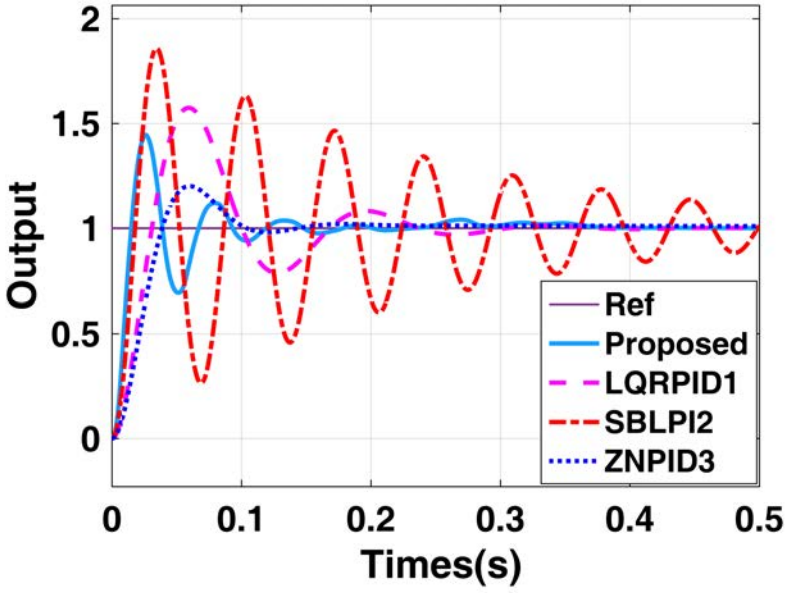

Figure 4.6: Output response for example 2

minimum energy as well in comparison to other candidate controllers. This can also be verified using performance indices in Table 4.2.

4.4 Modified Adaptive control policy

The generalised form of the adaptive control logic given in [140] is shown in Fig. 4.8. This control logic is briefly discussed, together with the modifications to the existing method, in the following set of equations:

$$Y(s) = G(s)I_c(s) \qquad (I_c(s) = \mathcal{L}[i_c(t)]) \tag{4.56}$$

$$i_c(t) = \sum_{i=1}^{k} w_i C_i{}^T(s) Z(s) \tag{4.57}$$

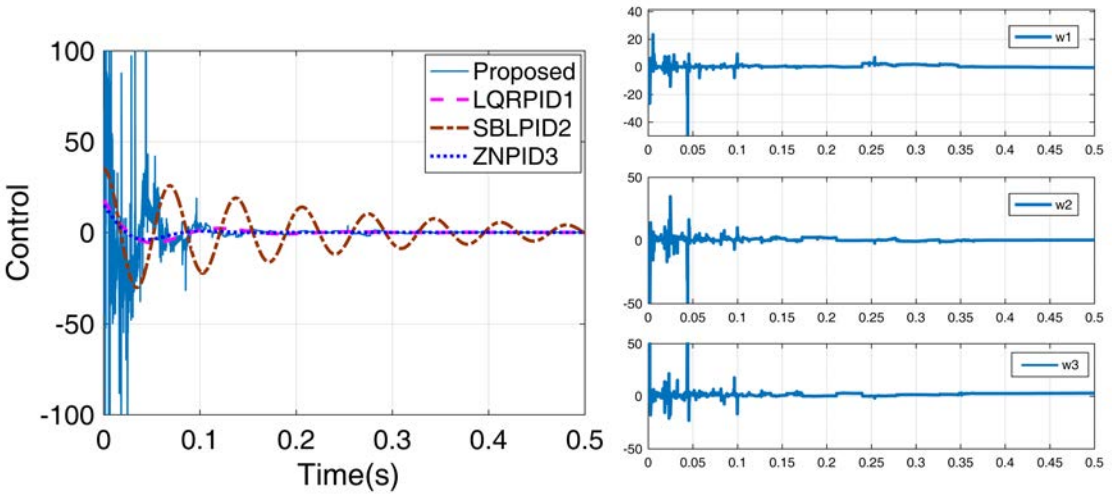

(a) (b)

Figure 4.7: Control signal and weight response for example 2

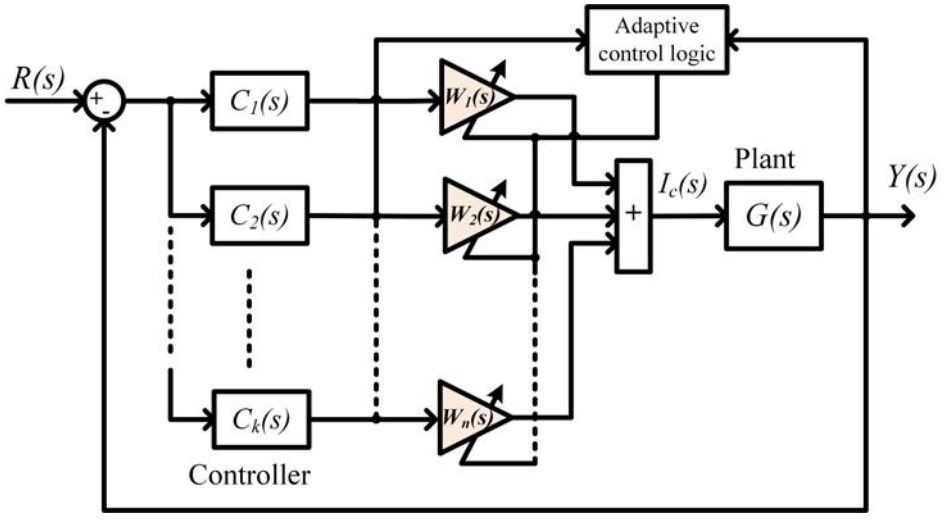

Figure 4.8: Proposed modified adaptive policy general structure

In (4.56), $G(s)$ represents the plant's transfer function having input as $i_c(t)$ and output $y(t)$, whose Laplace Transform is $Y(s)$. In (4.57), the expression for $i_c(t)$ is given, where $Z(s)$ is the Laplace Transform of the state vector $z(t)$ of $G(s)$, with dimension $p \times 1$ ($p \in \mathbb{N}$). The number of candidate controllers used is $k \in \mathbb{N}$ and $C_i(s) = \left[C_{i1}\ C_{i2}\ C_{i3} \ldots C_{ip}\right]^T(s)$, where $\{i \in \mathbb{N} \,|\, i \leq k\}$. Each $C_{ip}(s)$ represents the Laplace Transform of the controller for each state of the plant. The corresponding weight for each C_i is given by $w_i(t)$, where $w_i(t) \in w_c(t) = [w_1\ w_2 \ldots w_k]^T(t)$. The error function $e(t)$ is obtained as $e(t) = (r(t) - y(t))$, where $r(t)$ is the reference input to the system, and its Laplace Transform is represented by $R(s)$ in Fig. 4.8.

The objective function used to carry out the adaptive control logic is given by $J_o(e(t)) = 0.5\|e(t)\|_2^2$. The weights are updated according to the gradient descent algorithm, as given below:

$$w_c(t+1) = w_c(t) - \alpha \nabla J_o(t) \tag{4.58}$$

where, α ($\alpha \in \mathbb{R}_{>0} \,|\, \alpha < 1$) is the learning rate. The expression for $\nabla J_o(t)$ can be obtained using the chain rule of derivatives

$$\nabla J_o(t) = \frac{\partial J_o}{\partial e(t)} \cdot \frac{\partial e}{\partial i_c(t)} \cdot \frac{\partial i_c}{\partial w_c(t)} \tag{4.59}$$

Also, to avoid the flat spots in the error surface, the following equation is adopted for the eradication [147]:

$$w_c(t+1) = (2-\varepsilon)w_c(t) + (2\varepsilon - 1)w_c(t-1) - \varepsilon w_c(t-2) \tag{4.60}$$

where, ε is a positive real number such that $\varepsilon \in (0,1)$.

To illustrate the modified adaptive policy, we have considered the problem of balancing the pendulum angle and cart position of CIPS in chapter 5 and load frequency control of power system in chapter 6. For CIPS, simulation and real time hardware implementation is done, whereas for LFC, simulation results are carried out.

4.5 Concluding remarks

In this chapter, a novel adaptive technique is proposed consisting of a single control unit, which is further composed of multiple candidate controllers, each tuned via a different technique. Appropriate weights are assigned to each controller via gradient descent algorithm in such a manner that the merits of each individual controller are replicated in the final output response as far as possible. It is observed that, in the two illustrative examples that are undertaken here, the proposed adaptive strategy outperforms the individual control techniques. Further, the proposed adaptive control scheme is modified via the incorporation of a median filter and an epsilon(ε) term and it can be seen from the hardware simulation of CIPS, that the proposed technique is implementable

and it shows improvement in performance over the proposed adaptive control scheme. Inclusion of an epsilon term preserves the analytic properties of the weights and median filter minimises the switching frequency of the control signal. From the next chapter onwards, the focus of our discussion shifts from the proposition of new techniques to their applications to real world systems. Therefore, for the purpose of illustration of the proposed techniques, an example of inverted pendulum is considered. This is presented in next chapter.

Chapter 5

Application–I: Stabilization of Inverted pendulum system

The inverted pendulum system is an important benchmark problem in control system engineering because of non-minimum phase and unstable nature of the system [34, 148, 149]. Hence, it is arduous to design a controller for such class of systems [150, 151]. Moreover, even if controller is verified in simulation, it is difficult to implement it in real time application due to various constraints such as track length, rotary arm rotational limit, applied voltage and pendulum angle.

5.1 Introduction

The primary objective of this chapter is the design and implementation of different control strategies [53] that have been developed in the preceding chapters to a cart inverted pendulum system (CIPS)[54, 55]. First, a simplified model of the CIPS is derived. Then, the QRAWCP approach, is used to design a PID controller for the obtained model. To tackle the problem of parametric uncertainties, a combination of Kharitonov's theorem [56] and SBL technique [57] is applied to tune the PID controller. Further, an adaptive control policy[2], comprising of two candidate PID controllers that are tuned via SBL and LQR respectively is applied to the given system and the

effects of input disturbance, variation in input gain and input time delay are also explored. To investigate the effectiveness of the adaptive scheme to real life situations, it is also implemented on the hardware setup of CIPS system [152]. Further, a modified adaptive control policy is also used to tune a PID controller. Finally, an interactive and animated graphical user interface is developed for analysis, design and validation of controllers for cart inverted pendulum system (CIPS).

5.2 Motivation

Earlier in control literature [9], classical control techniques were widely used in stability analysis and controller of design for linear systems [153]. But, when the system belongs to non-linear or interval type [154], researchers found it difficult to design a classical controller. In order to solve these problems, various advanced control techniques have been developed for tuning of controller such as linear quadratic optimal approach [43], sliding mode control [155], feedback linearization [156] and Kharitonov's theorem [154]. As we know inverted pendulum system is highly non-linear plant [157], thus, it is difficult to design classical controllers such as PI/PID, Lag/lead, etc.

Recently in [1], it is shown that classical PID controller can be designed for inverted pendulum system using linear quadratic regulator (LQR) approach. This work has also been referred by various authors [47, 158–160]. In [1], robustness is studied via investigation and computation of gain margin, phase margin, delay margin, and sensitivity. However, in [1], parameter variations are not considered, but they are essential to probe in real time applications. For example, in guided missile system, the mass of the system changes due to the consumption of fuel. The variation in cart mass is an important element in cart inverted pendulum system. It may be possible that the controller stabilizes the inverted pendulum for some specific cart mass but becomes unstable if some additional load is applied. Further, variations in length of the pendulum and force applied to it are also crucial. Therefore, in this chapter, mathematical conditions have been developed for LQR based PID controller and stability boundary locus (SBL) based PID controller for stabilization of CIPS. This approach is based on well-known V. Krishnamurthi's corollary [161] on Routh stability criterion [34, 162]. The proposed condition gives the information about the additional

load (mass) either minimum or maximum which can be bore by the CIPS [163, 164]. The proposed condition has been verified in simulation and also in real time environment. It is shown that SBL based PID controller can be a useful aid in carrying more additional cart mass in comparison to LQR based PID controller. Further, the effectiveness of both the controllers is scrutinized in the presence of increase in pendulum length and applied force. Herein, the effect of increase in pendulum length is shown in hardware and the effect of increase of applied force is shown in simulation. Finally, practical issues have been discussed by comparing simulation and real time results.

The cart inverted pendulum has been used in research as well as pedagogical settings. The basis of this setup is to sustain a weight suspended from the pivot in a vertical upright position. Control of an inverted pendulum is akin to the attitude control of robot [165]. Since the pendulum system is nonlinear, under-actuated and has a non-minimum phase, therefore it serves as a physical example of several types of control systems.

5.3 Mathematical modelling of CIPS

In [1], authors have reported linearized model of CIPS. It is observed that this model is not generalized. Moreover, minor correction is required in equation (2) of [1]). Although, this does not affect the final result, but can be helpful to the research community. The apt approach for obtaining linearized model is presented below.

Table 5.1: Parameters of the CIPS

Symbol	Parameter	Value	Unit
M_c	Cart mass	2.4	kg
m	Mass of pendulum	0.23	kg
l	Length of pendulum	0.4	m
g	Gravitational constant	9.8	m/s^2
F	Applied force to cart	± 20	N
b	Cart friction	0.055	Ns/m
J	Moment of Inertia	0.099	kgm^2
d	Damping coefficient	0.005	Nms/rad

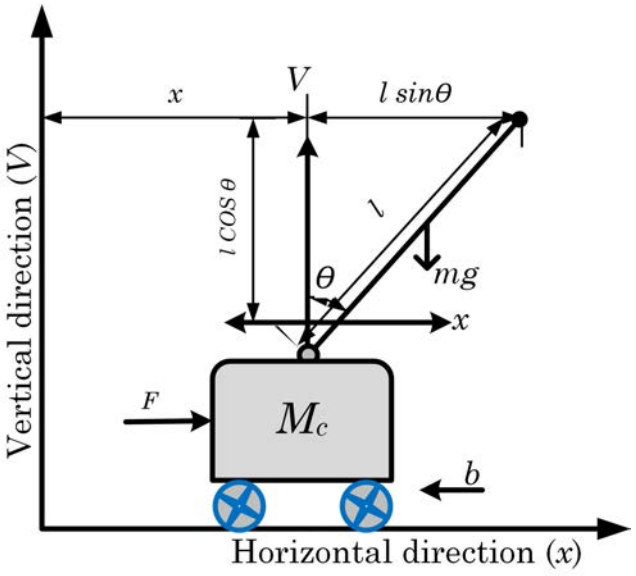

Figure 5.1: Model of cart inverted pendulum

Figure 5.1 shows the cart inverted pendulum system and its parameters are given in Table 5.1 [152]. Let, $\tilde{M}_c$ is actual cart mass and M_c is total cart mass. From this figure, horizontal (x) and rotating (θ) motions of CIPS are determined. Equation (5.1) and (5.2) given below shows the linear motion of the cart in the X-axis and rotation of the pendulum about the X-Y plane, respectively.

$$\ddot{x} = \frac{\begin{pmatrix} J+ml^2\left(F-b\dot{x}+ml\dot{\theta}^2\sin\theta\right) \\ 1 \quad -m^2l^2g\cos\theta\sin\theta+d\dot{\theta}\left(ml\cos\theta\right) \end{pmatrix}}{J\left(M_c+m\right)+M_cml^2+m^2l^2\sin^2\theta} \tag{5.1}$$

$$\ddot{\theta} = \frac{\begin{pmatrix} -ml\left(\left(F-b\dot{x}\right)\cos\theta-\left(M_c+m\right)g\sin\theta \right. \\ 1 \qquad \left. +ml\dot{\theta}^2\cos\theta\sin\theta\right)+\left(M_c+m\right)d\dot{\theta} \end{pmatrix}}{J\left(M_c+m\right)+M_cml^2-m^2l^2\sin^2\theta} \tag{5.2}$$

It is observed that above equations are non-linear. Therefore, for analysis and design purpose, there is a need to linearize above equations using Taylor series expansion about the equilibrium point. Here, the equilibrium point of a pendulum is considered as $(\theta = 0)$ in a vertical plane that gives $\sin\theta = \theta$, $\cos\theta = 1$ and higher order term as $\dot{\theta}^2 = 0$. Thus, by linearising (5.1) and (5.2) about the equilibrium point for small angle of θ from a vertical plane, we get equations, (5.3) and (5.4).

$$\ddot{x} = \frac{(J+ml^2)F-m^2l^2g\theta}{J\left(M_c+m\right)+M_cml^2} \tag{5.3}$$

$$\ddot{\theta} = \frac{-mlF + (M_c + m)\, mgl\theta}{J(M_c + m) + M_c ml^2} \tag{5.4}$$

As the damping coefficient(d) and friction coefficient(b) are small in comparison to other parameters, therefore, they are neglected. By taking Laplace transform of (5.3) and (5.4), the transfer function(TF) of position(x) versus input force (F) and angle (θ) versus input force (F) can be determined and are given in (5.5) and (5.6), respectively. The proof of equations (5.5) and (5.6) is given in appendix A.

$$\frac{x(s)}{F(s)} = \frac{\left(J + ml^2\right) s^2 - mgl}{\psi s^4 - \left(mgl(M_c + m)\right) s^2} \tag{5.5}$$

where, $\psi = J(M_c + m) + M_c ml^2$.

$$\frac{\theta(s)}{F(s)} = \frac{mls^2}{\psi s^4 - \left(mgl(M_c + m)\right) s^2} \tag{5.6}$$

On simplification of equation (5.5), we obtain

$$\frac{x(s)}{F(s)} = \frac{\left(J + ml^2\right)\left(s^2 - \frac{mgl}{\left(J + ml^2\right)}\right)}{\psi\left(s^4 - \frac{mgl(M_c + m)}{\psi} s^2\right)} \tag{5.7}$$

In (5.7), we can write $\sigma(M_c + m) = \psi + m^2 l^2$, where, $\sigma = \left(J + ml^2\right)$. From Table 5.1, it is found that $m^2 l^2 = 0.0085$. This is a small quantity which can be neglected. Here, M_c shows the total mass, i.e., $M_c = \tilde{M}_c + \Delta M_c$ where $\tilde{M}_c$ is the actual cart mass and ΔM_c is the additional perturbation mass. Therefore, equation(5.7) can be written as

$$\frac{x(s)}{F(s)} \simeq \frac{\sigma\left(s^2 - \frac{mgl}{\sigma}\right)}{\sigma(M_c + m)\left(s^4 - \frac{mgl(M_c + m)}{\sigma(M_c + m)} s^2\right)} \tag{5.8}$$

On further simplifying above equation, we get,

$$\begin{aligned} \frac{x(s)}{F(s)} &= \frac{1}{(M_c + m)\, s^2} \\ P_1(s) = \frac{x(s)}{F(s)} &= \frac{b_1}{s^2} \\ \text{where, } b_1 &= \frac{1}{(M_c + m)} \end{aligned} \tag{5.9}$$

Similarly, for angle control$(\theta(s)/F(s))$, we get transfer function as given in equation (5.10). Further, simplification leads to equation (5.11).

$$\frac{\theta(s)}{F(s)} \simeq \frac{mls^2}{\sigma\left(M_c+m\right)\left(s^4-\frac{mgl(M_c+m)}{\sigma(M_c+m)}s^2\right)} \tag{5.10}$$

$$\begin{aligned} \frac{\theta(s)}{F(s)} &= \frac{mls^2}{\sigma\left(M_c+m\right)\left(s^4-\frac{mgl}{\sigma}s^2\right)} \\ P_2(s) &= \frac{\theta(s)}{F(s)} = \frac{b_2}{s^2-a_2} \end{aligned} \tag{5.11}$$

where,

$$b_2 = \frac{ml}{\sigma\left(M_c+m\right)}, \qquad a_2 = \frac{mgl}{\sigma} \tag{5.12}$$

State space model of CIPS: The minimum states required to represent the complete model of CIPS are cart position $(x_1 = x)$, pendulum angle $(x_3 = \theta)$ and their respective velocities $(x_2 = \dot{x})$ and $(x_4 = \dot{\theta})$.

$$\begin{aligned} \begin{bmatrix} \dot{x}_1 \\ \dot{x}_2 \\ \dot{x}_3 \\ \dot{x}_4 \end{bmatrix} &= \begin{bmatrix} 0 & 1 & 0 & 0 \\ 0 & 0 & \frac{M_c+m}{M_c l}g & 0 \\ 0 & 0 & 0 & 1 \\ 0 & 0 & -\frac{m}{M_c}g & 0 \end{bmatrix} \begin{bmatrix} x \\ \dot{x} \\ \theta \\ \dot{\theta} \end{bmatrix} + \begin{bmatrix} 0 \\ -\frac{1}{M_c l} \\ 0 \\ \frac{1}{M_c} \end{bmatrix} u(t); \\ y(t) &= \begin{bmatrix} 1 & 0 & 0 & 0 \\ 0 & 0 & 1 & 0 \end{bmatrix} \begin{bmatrix} x \\ \dot{x} \\ \theta \\ \dot{\theta} \end{bmatrix} \end{aligned} \tag{5.13}$$

Control structure logic:

In [1], two loop PID control scheme has been designed. Figure 5.2 shows the two loop PID controller for CIPS. In this figure, $C_1(s)$, $C_2(s)$ denote the PID controllers for position control and angle control respectively and $P_1(s)$ and $P_2(s)$ are the position and angle transfer functions,

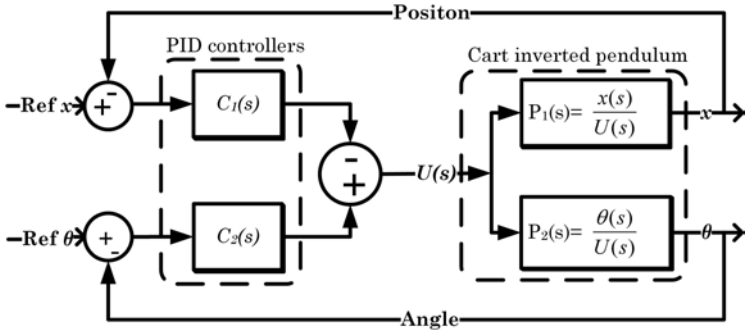

Figure 5.2: Two loop PID control scheme

respectively. From this figure, the closed-loop characteristic equation can be written as

$$1 - P_1(s)C_1(s) + P_2(s)C_2(s) = 0 \tag{5.14}$$

In above equation, $C_1(s)$ and $C_2(s)$ are represented as

$$C_n(s) = K_{pn} + \frac{K_{in}}{s} + sK_{dn}; \quad n = 1,2 \tag{5.15}$$

Using equation (5.14) and equation (5.15), the closed-loop characteristic equation can be written as

$$\begin{aligned} &s^5 + (-b_1K_{d1} + b_2K_{d2})\,s^4 + \left(-a_2 - b_1K_{p1} + b_2K_{p2}\right)s^3 \\ &+ (-b_1K_{i1} + a_2b_1K_{d1} + b_2K_{i2})\,s^2 + \left(a_2b_1K_{p1}\right) + (a_2b_1K_{i1}) = 0 \end{aligned} \tag{5.16}$$

Here, stability analysis in the presence of parametric uncertainty is carried out using two PID based control approaches. First PID controller design for CIPS is carried out using linear quadratic regulator approach and second PID controller design is carried out using stability boundary locus. The details of PID controller design using LQR approach and stability boundary locus approach are reported in [1], and [57, 166], respectively. The PID tuning parameters using both these approaches are enlisted below.

1. The LQR PID gain values for position control PID (C_1) and angle control PID (C_2) are determined in [1]. They are given below.

$$\begin{aligned} K_{p1} &= 43.3, K_{i1} = 33.796, K_{d1} = 2.254 \\ K_{p2} &= 120.9, K_{i2} = 247.43, K_{d2} = 10. \end{aligned} \tag{5.17}$$

2. The SBL PID gain values for position control PID ($C_1(s)$) and angle control PID ($C_2(s)$) are determined in [57, 166]. Design steps are given in appendix 2.

$$\begin{aligned} K_{p1} &= 6.9964, K_{i1} = 0.2, K_{d1} = 5 \\ K_{p2} &= 50.3294, K_{i2} = 5, K_{d2} = 10. \end{aligned} \tag{5.18}$$

The stability analysis in presence of uncertainty such as increment and decrement of additional cart mass is presented below.

5.4 Stability Analysis for M_c and m

The proposed stability analysis is carried out using various steps. They are elucidated below.

Step 1 : Determination of closed-loop characteristic equation in terms of variation in cart mass. The controller design which has been carried out in [1] is only applicable for the fixed system. However, in [1], robustness analysis is carried out by determining the gain margin and phase margin via the introduction of a gain block and a delay block, respectively. This has been done through software simulation. Along with this, the main focus is on the parametric variations in the actual CIP plant. Here, the stability analysis has been carried out by considering variation in the cart mass (M_c). As shown in Table 1, cart mass is represented as $\tilde{M}_c$. Suppose, the perturbation in M_c is represented by $(\tilde{M}_c - \Delta M_c)$ and $(\tilde{M}_c + \Delta M_c)$. However, in available set-up of CIP system [152], there is no provision to reduce cart mass. Therefore, for the analysis purpose, only additional mass, i.e., $(\tilde{M}_c + \Delta M_c)$ is considered. By substituting values of b_1, b_2 and a_2 from (5.9), (5.12) in

(5.16), we get,

$$s^5+\left(-\frac{K_{d1}}{(M_c+m)}+\frac{mlK_{d2}}{\sigma(M_c+m)}\right)s^4+\left(-\frac{mgl}{\sigma}+\frac{1}{(M_c+m)}\left(-K_{p1}+\frac{mlK_{p2}}{\sigma}\right)\right)s^3 \\ +\frac{1}{(M_c+m)}\left(-K_{i1}+\frac{mglK_{d1}}{\sigma}+\frac{mlK_{i2}}{\sigma}\right)s^2+\left(\frac{mgl}{\sigma(M_c+m)}\right)(K_{p1}+K_{i1})=0 \tag{5.19}$$

Further simplifying, we get,

$$(M_c+m)s^5+\left(-K_{d1}+\frac{mlK_{d2}}{\sigma}\right)s^4+\left(-\frac{(M_c+m)mgl}{\sigma}-K_{p1}+\frac{mlK_{p2}}{\sigma}\right)s^3 \\ +\left(-K_{i1}+\frac{mglK_{d1}}{\sigma}+\frac{mlK_{i2}}{\sigma}\right)s^2+\left(\frac{mglK_{p1}}{\sigma}\right)+\left(\frac{mglK_{i1}}{\sigma}\right)=0 \tag{5.20}$$

In above equation, let us consider, $\tilde{J}=J+ml^2$ and $\hat{J}=\frac{ml}{\sigma}$. Equation (5.20) can be expressed as,

$$(M_c+m)s^5+\left(-K_{d1}+\hat{J}K_{d2}\right)s^4+\left(-(M_c+m)\hat{J}g-K_{p1}+\hat{J}K_{p2}\right)s^3 \\ +\left(-K_{i1}+\hat{J}gK_{d1}+\hat{J}K_{i2}\right)s^2+\left(\hat{J}gK_{p1}\right)+\left(\hat{J}gK_{i1}\right)=0 \tag{5.21}$$

The above equation (5.21) can also be written as

$$p_5s^5+p_4s^4+p_3s^3+p_2s^2+p_1s+p_0=0 \tag{5.22}$$

where,

$$\begin{aligned}
&(M_c+m)=p_5\\
&\left(-K_{d1}+\hat{J}K_{d2}\right)=p_4\\
&\left(-(M_c+m)\hat{J}g-K_{p1}+\hat{J}K_{p2}\right)=p_3\\
&\left(-K_{i1}+\hat{J}gK_{d1}+\hat{J}K_{i2}\right)=p_2\\
&\left(\hat{J}gK_{p1}\right)=p_1\\
&\left(\hat{J}gK_{i1}\right)=p_0
\end{aligned} \tag{5.23}$$

Step 2 : The proposed analysis is based on Krishnamurthi's approach on Routh stability criterion. This is explained below.

Routh stability criterion is normally used for absolute stability of the system. But in [161], V. Krishnamurthi showed that Routh criterion is useful for the relative stability analysis. It is explained in corollary 1.

Corollary 1:[161] *According to Routh criterion, the test function in the s^1 row of the Routh array is proportional to the characteristic vector $1+G(s)H(s)$ and if the test function in the s^1 row of the Routh array is zero, a pair of imaginary roots exists.*

Using this corollary, the marginal gain (K_m) is obtained by equating the test function in the s^1 row to zero. By knowing the actual gain K of the system, the gain margin can be determined.

Step 3 : Application of Krishamurthi's approach on Routh stability criterion to CIP System.

Applying Routh criterion to equation (5.22), we get,

$$
\begin{array}{lccc}
s^5 \rightarrow & p_5 & p_3 & p_1 \\
s^4 \rightarrow & p_4 & p_2 & p_0 \\
s^3 \rightarrow & \left(\frac{p_4p_3-p_2p_5}{p_4}\right) & \left(\frac{p_1p_4-p_0p_5}{p_4}\right) & 0 \\
s^2 \rightarrow & \frac{p_2\left(\frac{p_4p_3-p_2p_5}{p_4}\right)-p_4\left(\frac{p_1p_4-p_0p_5}{p_4}\right)}{\left(\frac{p_4p_3-p_2p_5}{p_4}\right)} & p_0 & \\
s^1 \rightarrow & \frac{\mathcal{Q}\left(\frac{p_1p_4-p_0p_5}{p_4}\right)-p_0\left(\frac{p_4p_3-p_2p_5}{p_4}\right)}{\mathcal{Q}} & 0 & \\
s^0 \rightarrow & p_0 & &
\end{array}
\tag{5.24}
$$

where,

$$
\mathcal{Q}=\frac{p_2\left(\frac{p_4p_3-p_2p_5}{p_4}\right)-p_4\left(\frac{p_1p_4-p_0p_5}{p_4}\right)}{\left(\frac{p_4p_3-p_2p_5}{p_4}\right)} \tag{5.25}
$$

Using Krishnamurthi's approach [161], we write,

$$s^1 \rightarrow \frac{\mathcal{Q}\left(\frac{p_1p_4-p_0p_5}{p_4}\right)-p_0\left(\frac{p_4p_3-p_2p_5}{p_4}\right)}{\mathcal{Q}} \geq 0$$
$$\frac{\left(\begin{array}{l}\left(\frac{p_2\left(\frac{p_4p_3-p_2p_5}{p_4}\right)-p_4\left(\frac{p_1p_4-p_0p_5}{p_4}\right)}{\left(\frac{p_4p_3-p_2p_5}{p_4}\right)}\right)\left(\frac{p_1p_4-p_0p_5}{p_4}\right) \\ -p_0\left(\frac{p_4p_3-p_2p_5}{p_4}\right)\end{array}\right)}{\left(\frac{p_2\left(\frac{p_4p_3-p_2p_5}{p_4}\right)-p_4\left(\frac{p_1p_4-p_0p_5}{p_4}\right)}{\left(\frac{p_4p_3-p_2p_5}{p_4}\right)}\right)} \geq 0 \tag{5.26}$$

$$\left(p_2\left(\frac{p_4p_3-p_2p_5}{p_4}\right)-p_4\left(\frac{p_1p_4-p_0p_5}{p_4}\right)\right)$$
$$\left(\frac{p_1p_4-p_0p_5}{p_4}\right)-p_0\left(\frac{p_4p_3-p_2p_5}{p_4}\right)^2 \geq 0 \tag{5.27}$$

Further simplifying,

$$\Big[\left\{p_2\left(p_4p_3-p_2p_5\right)-p_4\left(p_1p_4-p_0p_5\right)\right\}$$
$$\left(p_1p_4-p_0p_5\right)\Big]-p_0\left(p_4p_3-p_2p_5\right)^2 \geq 0 \tag{5.28}$$

Simplifying (5.28), we get,

$$p_2\left(p_4p_3-p_2p_5\right)\left(p_1p_4-p_0p_5\right)$$
$$-p_4\left(p_1p_4-p_0p_5\right)^2-p_0\left(p_4p_3-p_2p_5\right)^2 \geq 0 \tag{5.29}$$

Equation (5.29) can also be written as

$$p_2\Theta\Gamma-p_4\Gamma^2-p_0\Theta^2 \geq 0 \tag{5.30}$$

where, $\Theta=\left(p_4p_3-p_2p_5\right)$ and $\Gamma=\left(p_1p_4-p_0p_5\right)$. Substituting coefficients from (5.23) in Θ and Γ, we get

$$\Theta=\left(p_4p_3-p_2p_5\right)$$
$$=-\left(\hat{J}K_{d1}g+\hat{J}K_{i2}K_{i1}\right)\left(M_c+m\right)$$
$$+\left(-(M_c+m)\hat{J}-K_{p1}+\hat{J}K_{p2}\right)\left(\hat{J}K_{d2}-K_{d1}\right) \tag{5.31}$$

$$\begin{aligned}\Gamma &= (p_1 p_4 - p_0 p_5) \\ &= -\hat{J} g K_{i1} (M_c + m) + \hat{J} g K_{p1} \left(\hat{J} K_{d2} - K_{d1} \right)\end{aligned} \tag{5.32}$$

Suppose, $\Upsilon = p_2 \Theta \Gamma - p_4 \Gamma^2$ and $\Lambda = -p_0 \Theta^2$. Thus (5.30) can be written as

$$\Upsilon - \Lambda \geq 0 \tag{5.33}$$

where,

$$\begin{aligned}\Upsilon &= p_4 (p_4 p_3 - p_0 p_5)(p_1 p_4 - p_0 p_5) \\ &= \left(\hat{J} K_{d1} g + \hat{J} K_{i2} - K_{i1} \right) \\ &\left(- \left(\hat{J} K_{d1} g + \hat{J} K_{i2} - K_{i1} \right) (M_c + m) \right. \\ &\left. + \left(-\hat{J} (M_c + m) - K_{p1} + \hat{J} K_{p2} \right) \left(\hat{J} K_{d2} - K_{d1} \right) \right) \\ &\left(-\hat{J} g K_{i1} (M_c + m) + \hat{J} g K_{p1} \left(\hat{J} K_{d2} - K_{d1} \right) \right)\end{aligned} \tag{5.34}$$

$$\begin{aligned}\Lambda &= p_0 (p_4 p_3 - p_0 p_5)^2 \\ &= \frac{mlgK_{i1} \left(\begin{array}{l} - \left(\frac{mlK_{d1}g}{\sigma} + \frac{mlKi2}{\sigma} - K_{i1} \right) p5 \\ + \left(- \frac{(M_c+m)ml}{\sigma} - K_{p1} + \frac{mlKp2}{\sigma} \right) p4 \end{array} \right)^2}{\sigma}\end{aligned} \tag{5.35}$$

Now, we check stability condition (5.33) for two different controllers, i.e., LQR based PID controller and SBL based PID controller, which are shown in equations (5.16) and (5.17). The stability condition for these controllers are explained below in step 4 and step 5.

Step 4: LQR based PID analysis [1]:

Substituting values of C_1, C_2 from (5.16), and Υ, Λ from equation (5.34) and (5.35) in (5.33) and replacing parameters values from Table 5.1, we get,

$$\begin{aligned}&-8.4639 \times 10^{30} {M_c}^2 - 1.0059 \times 10^{32} M_c \\ &+ 2.1467 \times 10^{33} \geq 0\end{aligned} \tag{5.36}$$

From (5.36), we write,

$$f(M_c) = -M_c^2 - 11.8843M_c + 253.6351 = 0 \tag{5.37}$$

The roots of above equation are calculated as $M_{c1} = -22.9405$ and $M_{c2} = 11.0562$.

The significance of the roots of the equations is given below.

$$\begin{aligned} \tilde{M}_c + \Delta M_{c1} &= -22.9405 \\ 2.4 + \Delta M_{c1} &= -22.9405 \\ \Delta M_{c1} &= -20.5405 \end{aligned} \tag{5.38}$$

$$\begin{aligned} \tilde{M}_c + \Delta M_{c2} &= 11.0562 \\ 2.4 + \Delta M_{c2} &= 11.0562 \\ \Delta M_{c2} &= 8.6562 \end{aligned} \tag{5.39}$$

Equations (5.38) and (5.39) give the limits for the minimum and maximum additional mass (ΔM_c), respectively. Now, we verify the above equation by considering different cases as shown below.

Case (i): M_c = - 23

$$\begin{aligned} f(-23) &= -4.4774 \times 10^{33} + 2.3136 \times 10^{33} \\ &\quad + 2.1467 \times 10^{33} \\ &= -1.7133 \times 10^{31} < 0 \end{aligned} \tag{5.40}$$

Case (ii): M_c = - 2

$$\begin{aligned} f(-2) &= -3.3856 \times 10^{31} + 2.0118 \times 10^{32} \\ &\quad + 2.1467 \times 10^{33} \\ &= 2.3140 \times 10^{33} > 0 \end{aligned} \tag{5.41}$$

Case (iii.a): M_c = 3

$$\begin{aligned} f(3) &= -7.6175 \times 10^{31} - 3.0177 \times 10^{32} \\ &\quad + 2.1467 \times 10^{33} \\ &= 1.7688 \times 10^{33} > 0 \end{aligned} \tag{5.42}$$

Case (iii.b): M_c = 4.3

$$\begin{aligned} f(4.3) &= -1.5650 \times 10^{32} - 4.3254 \times 10^{32} \\ &\quad + 2.1467 \times 10^{33} \\ &= 1.5577 \times 10^{33} > 0 \end{aligned} \tag{5.43}$$

Case (iv): M_c = 12

$$\begin{aligned} f(12) &= -1.2188 \times 10^{33} - 1.2071 \times 10^{33} \\ &\quad + 2.1467 \times 10^{33} \\ &= -2.7918 \times 10^{32} < 0 \end{aligned} \tag{5.44}$$

From above, it is proved that for all $M_{c1} < \tilde{M}_c < M_{c2} \Rightarrow f(M_c) > 0 \Rightarrow$ are stable. The bound of M_c for stability is shown as follows

$$\begin{aligned} &-22.9405 < M_c < 11.0562 \\ &-22.9405 < 2.4 + \Delta M_c < 11.0562 \\ &-20.5405 < \Delta M_c < 8.6562 \end{aligned} \tag{5.45}$$

From equation (5.45), it is found that, for negative values of ΔM_c, i.e., for reducing a cart mass M_c, system can also be stable. Therefore, the stability margin of lower to higher values of cart mass is shown in Figure 5.3.

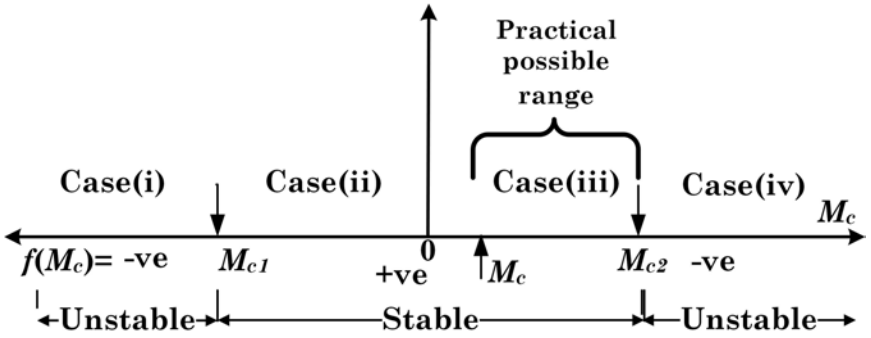

Figure 5.3: Different stability cases for total cart mass M_c

Step 5: SBL based PID analysis [57, 166]:

Similarly, substituting values of SBL PIDs C_1, C_2 from (5.17) and replacing parameters values

from Table 5.1 in (5.33), we get,

$$\begin{aligned} -2.9348 \times 10^{50} {M_c}^2 - 2.8079 \times 10^{53} M_c \\ + 3.8432 \times 10^{54} \geq 0 \end{aligned} \tag{5.46}$$

From (5.46), we write,

$$f(M_c) = -M_c^2 - 956.7615 M_c + 13095 = 0 \tag{5.47}$$

The roots of above equation (5.47) are calculated as $M_{c1} = -970.2583$ and $M_{c2} = 13.4968$. The roots of the equation (5.47), are represented by M_{c1} and M_{c2} and provide the limits for the minimum and maximum values of ΔM_{c1} in (5.48) and ΔM_{c2} in (5.49), respectively

$$\begin{aligned} \tilde{M}_c + \Delta M_{c1} &= -970.2583 \\ 2.4 + \Delta M_{c1} &= -970.2583 \\ \Delta M_{c1} &= -967.8583 \end{aligned} \tag{5.48}$$

$$\begin{aligned} \tilde{M}_c + \Delta M_{c2} &= 13.4968 \\ 2.4 + \Delta M_{c2} &= 13.4968 \\ \Delta M_{c2} &= 11.0968 \end{aligned} \tag{5.49}$$

Now we can verify ΔM_{c1} and ΔM_{c2} conditions by considering different cases such as,

Case (i): M_c = - 971

$$\begin{aligned} f(-971) &= -2.7670 \times 10^{56} + 2.7265 \times 10^{56} \\ &+ 3.8432 \times 10^{54} \\ &= -2.1467 \times 10^{53} < 0 \end{aligned} \tag{5.50}$$

Case (ii): M_c = - 23

$$\begin{aligned} f(-23) &= -1.5525 \times 10^{53} + 6.4582 \times 10^{54} \\ &+ 3.8432 \times 10^{54} \\ &= 1.0146 \times 10^{55} > 0 \end{aligned} \tag{5.51}$$

Case (iii.a): M_c = 4.3

$$\begin{aligned} f(4.3) &= -5.4264 \times 10^{51} - 1.2047 \times 10^{54} \\ &\quad + 3.8432 \times 10^{54} \\ &= 2.6304 \times 10^{54} > 0 \end{aligned} \tag{5.52}$$

Case (iii.b): M_c = 12

$$\begin{aligned} f(12) &= -4.2261 \times 10^{52} - 3.3695 \times 10^{54} \\ &\quad + 3.8432 \times 10^{54} \\ &= 4.3146 \times 10^{53} > 0 \end{aligned} \tag{5.53}$$

Case (iv): M_c = 14

$$\begin{aligned} f(14) &= -5.7522 \times 10^{52} - 3.9311 \times 10^{54} + 3.8432 \times 10^{54} \\ &= -1.4538 \times 10^{53} < 0 \end{aligned} \tag{5.54}$$

From above, it is proved that for all $M_{c1} < \tilde{M}_c < M_{c2} \Rightarrow f(M_c) > 0 \Rightarrow$ are stable. The bound of M_c for stability is shown in (5.55).

$$\begin{aligned} &-970.2583 < M_c < 13.4968 \\ &-970.2583 < (2.4 + \Delta M_c) < 13.4968 \\ &-967.8583 < \Delta M_c < 11.0968 \end{aligned} \tag{5.55}$$

From equation (5.55), it is found that, for negative values of ΔM_c, system can also be stable. Therefore, the stability margin of lower to higher values of cart mass can also be represented by Figure 5.3. Thus, from equation (5.45), which is LQR based PID, maximum additional cart mass to be carried is 8.6562 kg and from equation (5.55), which is based on SBL based PID, maximum additional cart mass to be carried is 11.0968kg. Thus, SBL based PID controller shows better robustness in comparison to LQR based PID. However, in the practical set-up which we have considered here, it is not possible to reduce the actual cart mass $\tilde{M}_c$. Therefore, reduction of cart mass analysis is carried out through simulation only, whereas effect of addition of cart mass is carried out through both simulation and also on real time set-up of CIPS.

5.4.1 Results and Analysis

Here, the digital cart inverted pendulum set-up has been considered, which is provided by Feedback Instruments Ltd. UK ® company [152]. The CIPS parameters are given in Table 5.1. According to user manual of the set-up[152], maximum output voltage (in v) and force (in N) are given, which are shown in equation (5.56). As per [1], the actuator DC motor gain is considered to be 15, which when multiplied with applied force, leads to the position transfer function as, $P_1(s) = x(s)/U(s)$ and angle TF $P_2(s) = \theta(s)/U(s)$. The cart rail limit is ± 0.5m and angle θ should be less than 0.2 rad. The stability margin or bounds for the additional mass are verified through simulation and hardware set-up.

$$\begin{aligned} -2.5 \text{ V to } 2.5 \text{ V} &\simeq 0 \text{ to } 5 \text{ V} \\ -20\,N \text{ to } 20\,N &\simeq 0 \text{ to } 40\,N \end{aligned} \tag{5.56}$$

As discussed earlier, $\tilde{M}_c$ is the actual cart mass and ΔM_c is the additional perturbation mass and M_c is the total mass. So, we can write

$$M_c = \tilde{M}_c + \Delta M_c \tag{5.57}$$

Using equation (5.57), total mass of the cart for additional mass are shown in (5.58). Here, seven cases have been considered. They are given below.

$$\begin{aligned} \Delta M_c &= 0, & M_c &= 2.4 + 0 \Rightarrow 2.4\text{kg} \\ \Delta M_c &= -1.4, & M_c &= 2.4 - 1.4 \Rightarrow 1\text{kg} \\ \Delta M_c &= 1, & M_c &= 2.4 + 1 \Rightarrow 3.4\text{kg} \\ \Delta M_c &= 1.9, & M_c &= 2.4 + 1.9 \Rightarrow 4.3\text{kg} \\ \Delta M_c &= 8.5, & M_c &= 2.4 + 8.5 \Rightarrow 10.9\text{kg} \\ \Delta M_c &= 8.7, & M_c &= 2.4 + 8.7 \Rightarrow 11.1\text{kg} \\ \Delta M_c &= 9.6, & M_c &= 2.4 + 9.6 \Rightarrow 12\text{kg} \\ \text{and } \Delta M_c &= 11, & M_c &= 2.4 + 11 \Rightarrow 13.4\text{kg} \end{aligned} \tag{5.58}$$

Table 5.2: Maximum value at different cases for LQR PID

ΔM_c(kg)	M_c(kg)	x(m)	θ(rad)	u(v)
0	2.4	-0.3271	-0.1201	-12.09
-1.4	1	-0.3024	-0.1038	-12.09
1	3.4	-0.3496	-0.1346	-12.09
1.9	4.3	-0.3684	-0.147	-12.09
8.5	10.9	0.4943	0.2608	-12.2358
8.7	11.1	0.5083	0.2679	-12.2379
9.6	12	0.5717	-0.3065	13.8448

4.1 Simulation results:

For all the cases, simulation analysis are carried out for initial angle $\theta_0 = 0.1$ rad.

i) LQR based PID results:

The additional mass ΔM_c and cart mass (M_c) are shown in (5.58). Initially, small variations around cart mass $\tilde{M}_c$ have been considered, i.e., $\Delta M_c = 0, -1.4, 1$ and 1.9 kg. Using equations (5.9), (5.11) and (5.16), the responses of LQR PID controlled cart position (x) are shown in Figure 5.4(a), and corresponding to this, pendulum angle (θ) in Figure 5.4(b) and the control voltages (u) in Figure 5.4(c) are shown. In proposed approach, it is shown that for some values of ΔM_c, i.e., up to additional mass $\Delta M_c = 1.9$ kg, the LQR PID controller stabilizes the system effectively. This is shown in Figures 5.4((a)-(c)). We further check the extreme condition of additional mass after which CIPS become unstable. It is explained below.

Earlier, it is shown that at $\Delta M_c = 8.6562$ kg, the system is on the verge of instability. Therefore, additional mass ΔM_c such as 8.5 kg is considered, which shows that the cart position (x), pendulum angle (θ) and also control voltage (u) are within the prescribed limits. It is shown in Table 5.2. As the additional mass increases to 8.7kg and 9.6kg, it is found that the cart position, pendulum angle and control voltage cross the maximum limits. This is depicted in Figures 5.5(a), 5.5(b), 5.5(c), respectively. The actual values are shown in Table 5.2. Thus, the proposed analysis is verified through simulation.

(ii) SBL based PID results:

SBL-based PID tuning parameters are shown in (5.18). The variations of $\Delta M_c(0, -1.4, 1.9,$ and 9.6kg) from (5.58) have been considered. Then system responses are obtained for x, θ, and u,

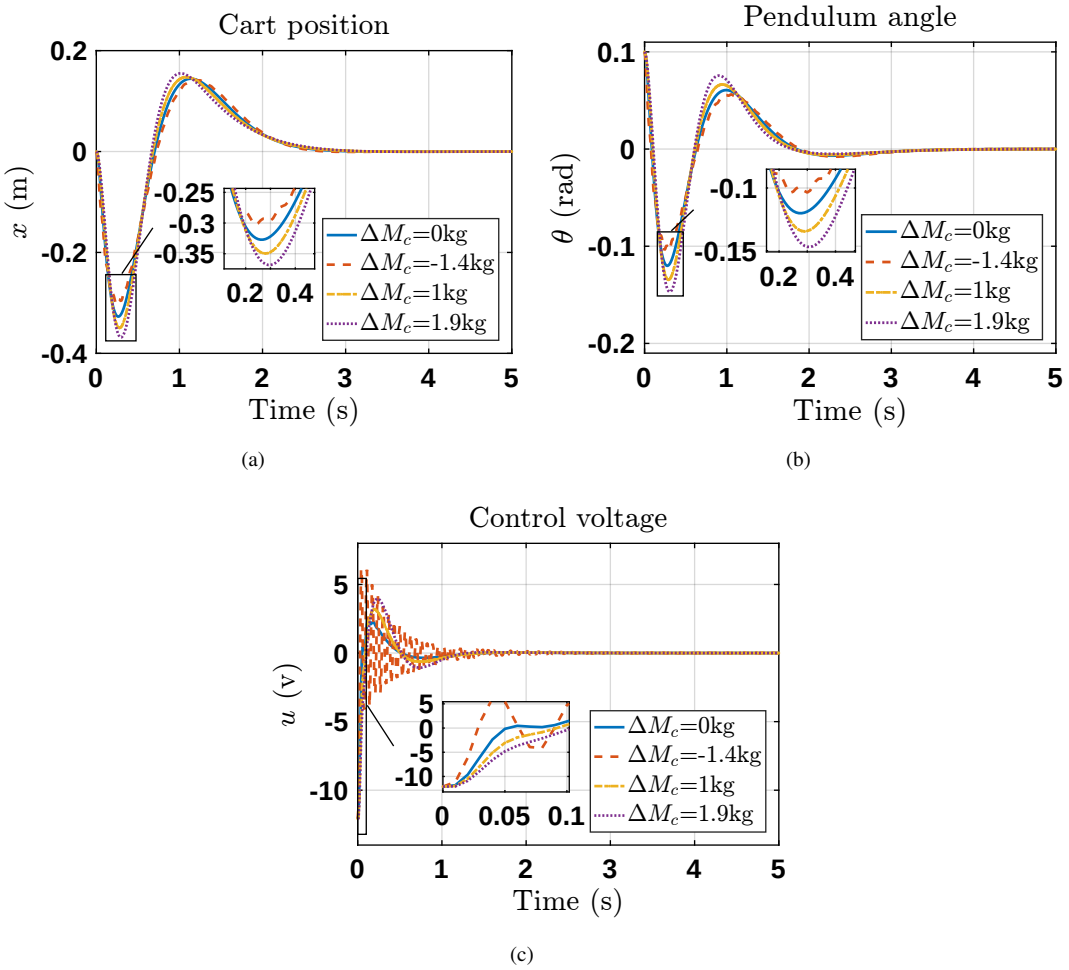

Figure 5.4: Response of CIPS using LQR PID for ΔM_c

which are shown in Figure 5.6((a)-(c)) respectively and their maximum values are tabulated in Table 5.3.

Earlier using equation (5.55), it is shown that when $\Delta M_c = 11.0968$ kg, the system is on the verge of instability. Therefore, additional extreme mass ΔM_c of 11 kg is considered, that shows that the cart position (x), pendulum angle (θ) and also control voltage (u) are within the prescribed limits. They are shown in Table 5.3. As the additional mass increases to 11.5kg and 12kg, it is found that the cart position, pendulum angle and control voltage cross the maximum limits. They are shown in Figures 5.7((a)-(c)), respectively. Thus, the proposed analysis is verified through simulation. The actual values are shown in Table 5.3.

(iii) Comparison between LQR based PID and SBL based PID with reference cart mass uncertainty :

The responses of cart position for extreme cart mass M_c in case of LQR based PID controller and

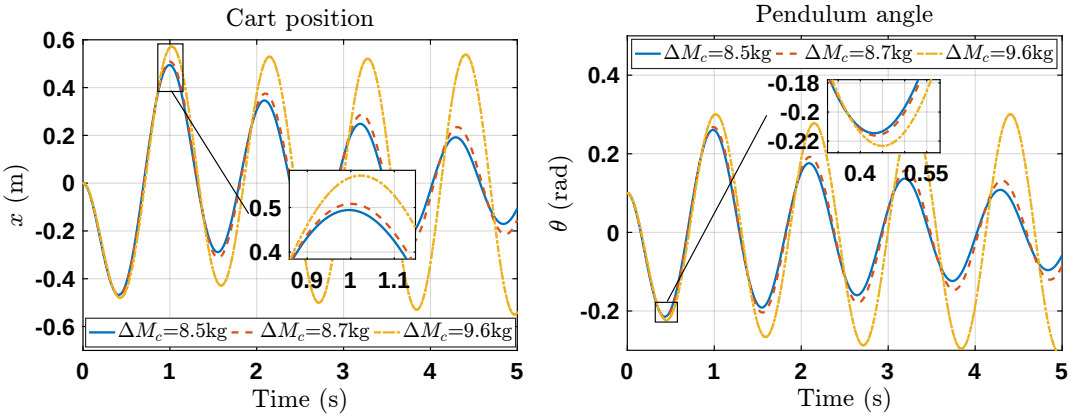

(a)

(b)

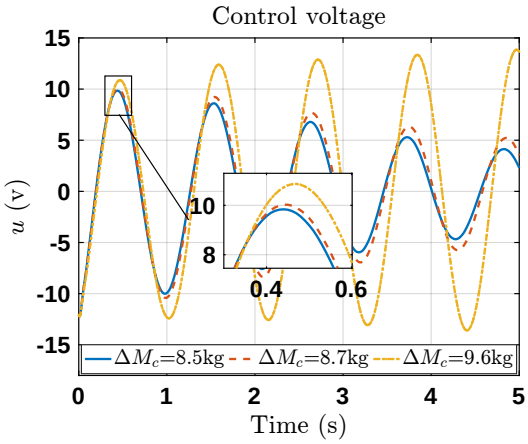

(c)

Figure 5.5: Response of CIPS using LQR PID for extreme ΔM_c

Table 5.3: Maximum value at different cases for SBL PID

ΔM_c(kg)	M_c(kg)	x(m)	θ(rad)	u(v)
0	2.4	-0.2609	0.1	-5.0329
-1.4	1	-0.2168	0.1	-5.0329
1.9	4.3	-0.3009	0.1	-5.0329
9.6	12	-0.4027	-0.1389	-5.0329
11	13.4	-0.418	0.1584	-5.4784
11.5	13.9	-0.4235	0.2051	-7.5368
12	14.4	-0.6509	0.3247	-11.9064

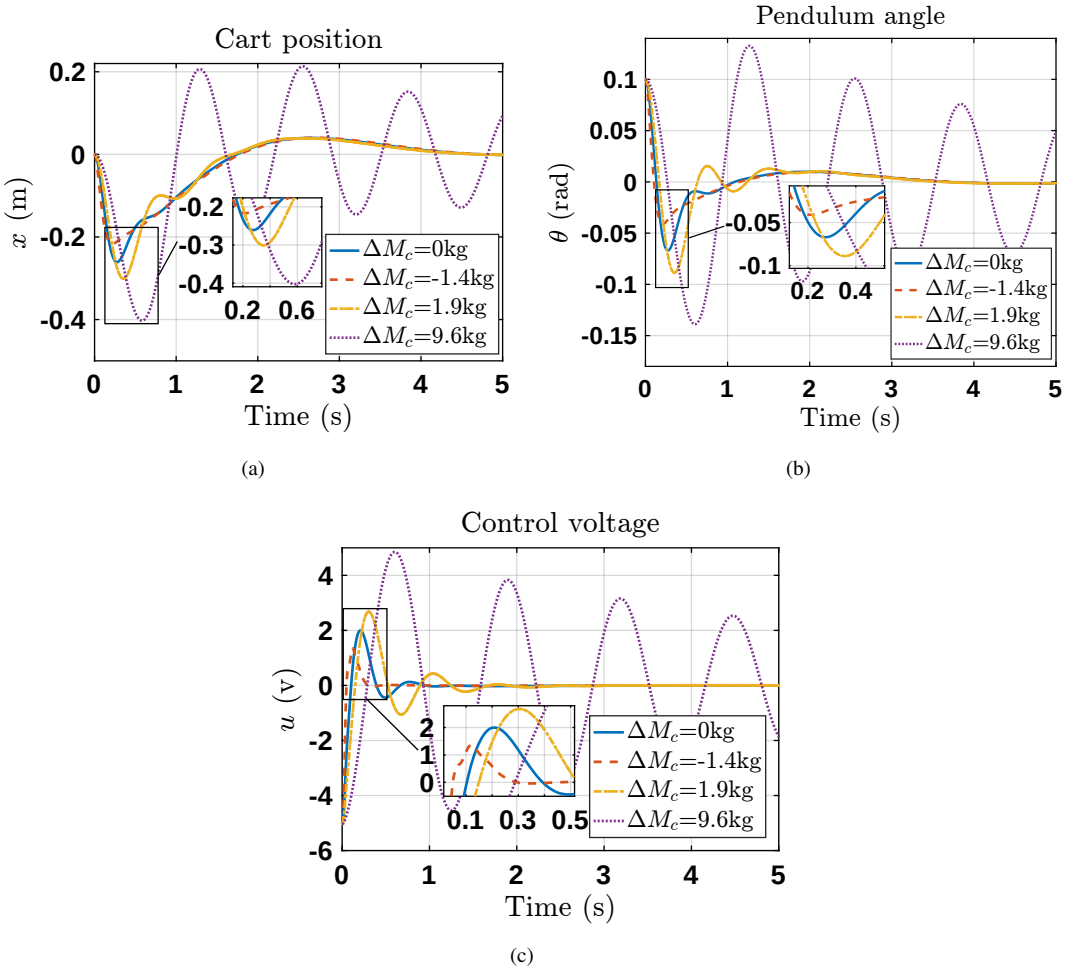

Figure 5.6: Response of CIPS using SBL PID for ΔM_c

SBL based PID controller are shown in Figure 5.5(a) and 5.7(a), respectively. It is found that LQR based PID controller stabilized the system till additional mass $\Delta M_c = 8.5$kg, whereas, SBL based PID controller stabilized CIPS till $\Delta M_c = 11$kg. Thus, SBL based PID controller is more robust than LQR based PID controller. We have already obtained the stability margin in section 3 for both the PIDs, for LQR PID is $\Delta M_c < 8.6565$, and for SBL PID is $\Delta M_c < 11.0968$. Thus, the mathematical approach is verified through simulation.

iv) Comparison between LQR based PID and SBL based PID with respect to uncertainty in length of pendulum and force applied to the cart:

The effect of additional increase of length of pendulum $\Delta l = 0.08m$ for both type of PID controllers is considered when $\Delta M_c = 0$ and $\Delta M_c = 1.9$kg. The performance of LQR based PID controller and SBL based PID controller are shown in figure 5.8(a)-(c). In this figure 5.8(a) shows cart

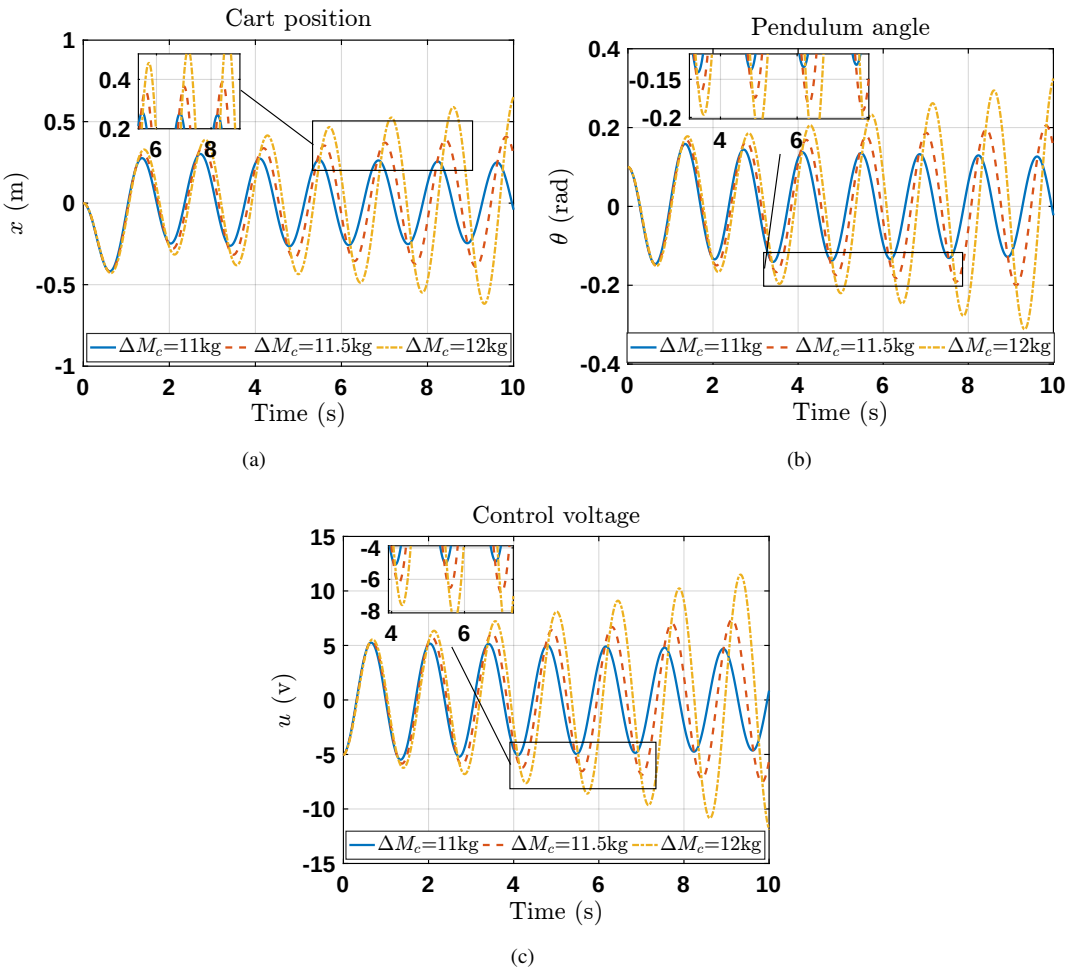

Figure 5.7: Response of CIPS using SBL PID for extreme ΔM_c

position, figure 5.8(b) shows pendulum angle and figure 5.8(c) shows the corresponding control voltage. In this, the actual length of pendulum is 0.4m. It is observed that for additional length of pendulum (Δl) equal to 0.08m,(total length of pendulum$= 0.4 + 0.08 = 0.48$m), complete CIPS system is stable. However, performance of SBL based PID is better than LQR based PID controller. Similar to above, effect of increase and decrease of applied force (F) to the cart has been verified when additional cart mass is at $\Delta M_c = 1.9$kg and additional length $\Delta l = 0.08$m. The actual force is 15N and perturbation in force is considered as $\pm 50\%$. Thus, the variation in actual force is in between $[7.5 \;\; 22.5]N$. The results are shown in figure 5.9(a)-(c). Fig. 5.9(a) shows cart position, figure 5.9(b) shows pendulum angle and figure 5.9(c) shows control voltage. Here, it is also observed that performance of CIPS system based on SBL based PID is better than LQR based PID.

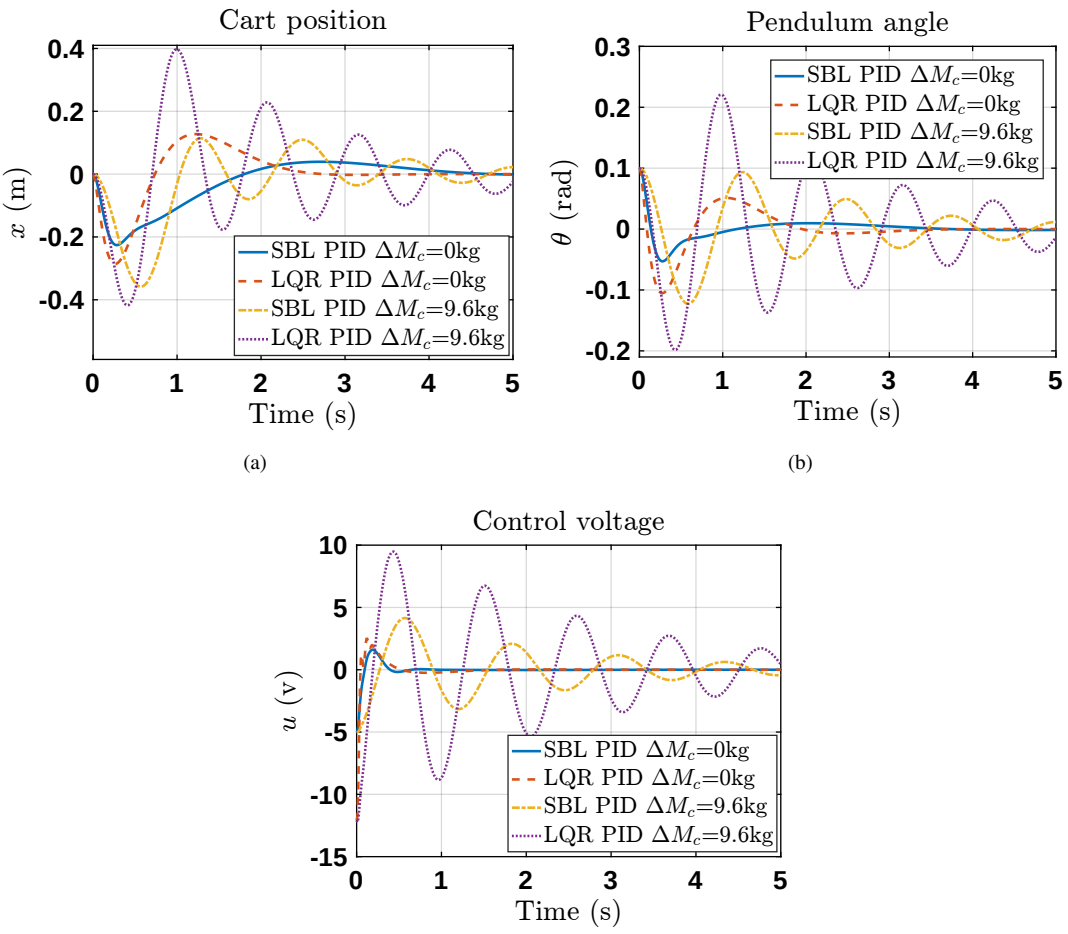

Figure 5.8: Comparison of SBL and LQR PIDs response for ΔM_c at $\Delta l = 0.08$m

4.2 Hardware results:

For the experimental results, pendulum is swung up by hand to bring it to the stabilization zone. The angular plots in these responses start from π rad which is a point of stable equilibrium. From the user manual of actual hardware, the actuator (DC motor) capacity is calculated in terms of total cart mass(M_c). This capacity shows that the actuator can carry maximum load irrespective of control algorithm. It is elucidated below. We know that,

$$F = M_x \times a \tag{5.59}$$

where, M_x is the total mass across the motor shaft, which includes cart mass(M_c) and pendulum assembly mass $(m + m_b)$, where, m_b is a bob mass$(m_b \approx 0.1\text{kg})$ and 'a' is an acceleration due to

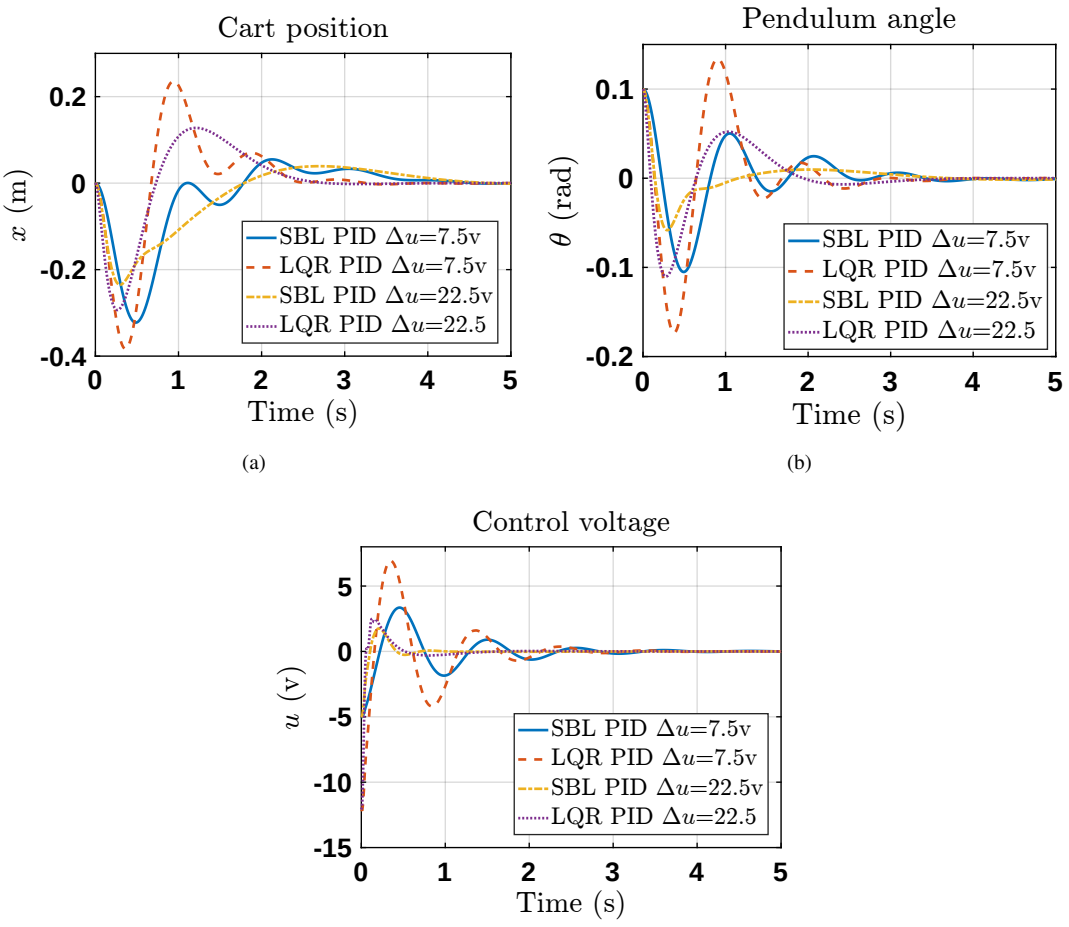

Figure 5.9: Comparison of system response for Δu using SBL and LQR PID for $\Delta M_c = 1.9$kg at $\Delta l = 0.08$m

gravity, i.e., $a = 9.81\ ms^{-2}$. We write,

$$M_x = M_c + (m + m_b) \tag{5.60}$$

Equation (5.59) can be written as,

$$40 = (M_c + 0.33) \times 9.81 \tag{5.61}$$

Solving above equation, we get,

$$M_c \simeq 3.7475\text{kg} \tag{5.62}$$

In the real time environment, maximum mass perturbation ($\Delta\mathcal{P}_{M_c}$) is obtained using equation (5.63).

$$\Delta\mathcal{P}_{M_c} = min\ \left[\Omega_{M_c}, \Pi_{M_c}\right] \tag{5.63}$$

where, $\Delta\mathcal{P}_{M_c}$ is the maximum cart mass perturbation, Ω_{M_c} is the stability margin of designed controller (SMDC) with respect to cart mass(M_c) and Π_{M_c} is practical actuator rating (PAR) with respect to M_c.

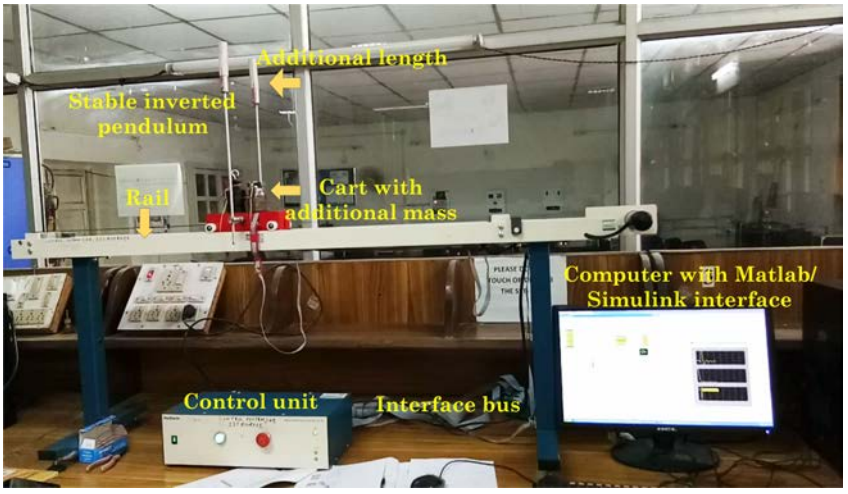

Figure 5.10: Hardware set-up of cart inverted pendulum system

i) LQR based PID results :

For LQR PID, SMDC Ω_{M_c} = 8.6562 kg is obtained in (5.45) and PAR Π_{M_c}= M_c = 3.7475 kg is calculated in (5.62). Hence, using equation (5.63), maximum cart mass perturbation allowed is nothing but the minimum of Ω_{M_c} and Π_{M_c}. Thus, using (5.62), we get $\Delta\mathcal{P}_{M_c}$ = 3.7475 kg.

Table 5.4: Real-time maximum values of LQR PID for different cases

ΔM_c(kg)	M_c(kg)	x(m)	θ(rad)	u(v)
0	2.4	0.2564	0.9879	-24.2642
0.5	2.9	0.2322	0.9940	-24.2708
1	3.4	0.1896	0.9942	-24.2116
1.9	4.3	0.1044	0.9913	-24.1556

The hardware set-up of cart inverted pendulum is shown in Figure 5.10. The hardware results are carried out for different masses (M_c) equal to 2.4, 2.9, 3.4 and 4.3 kg considering additional

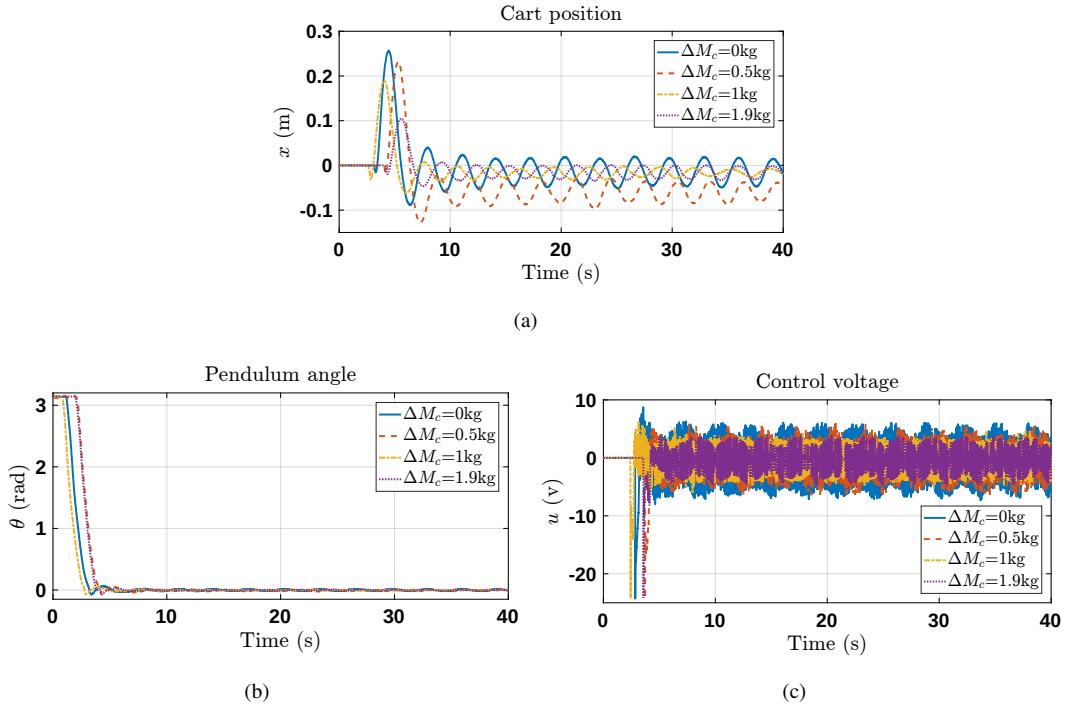

Figure 5.11: LQR PID real-time response of CIPS system for ΔM_c

mass as (ΔM_c) 0, 0.5, 1 and 1.9 kg, respectively. Here, we have not considered all the additional mass which we have considered in the simulation due to limitation imposed by (5.63). This is important from the safety point of view of CIPS. The effect of additional cart mass on position of cart(x), pendulum angle(θ) and corresponding control voltage(u) are shown in figure 5.11((a)-(c)), respectively. From these figures, it is found that for the additional variation in cart mass (ΔM_c), stable cart position(x) and pendulum angle(θ) of CIPS have been obtained. Similar to simulation results, in hardware results, maximum values of x, θ and u for additional mass ΔM_c are tabulated in Table 5.4. Thus, hardware results satisfied the bounded range of cart mass as determined in (5.62).

Further, real time analysis is carried by increasing pendulum length ($\Delta l = 0.08$m) when there is no additional cart mass and also when there is an additional cart mass $\Delta M_c = 1.9$kg. The response of CIPS system is shown in Figures 5.12(a,b,c). Figure 5.12(a) shows x, figure 5.12(b) shows θ and figure 5.12(c) shows u. From these figures, it is found that the LQR based PID controller stabilized the CIPS, however their exist small oscillation across x and θ and increased control voltage (u) level.

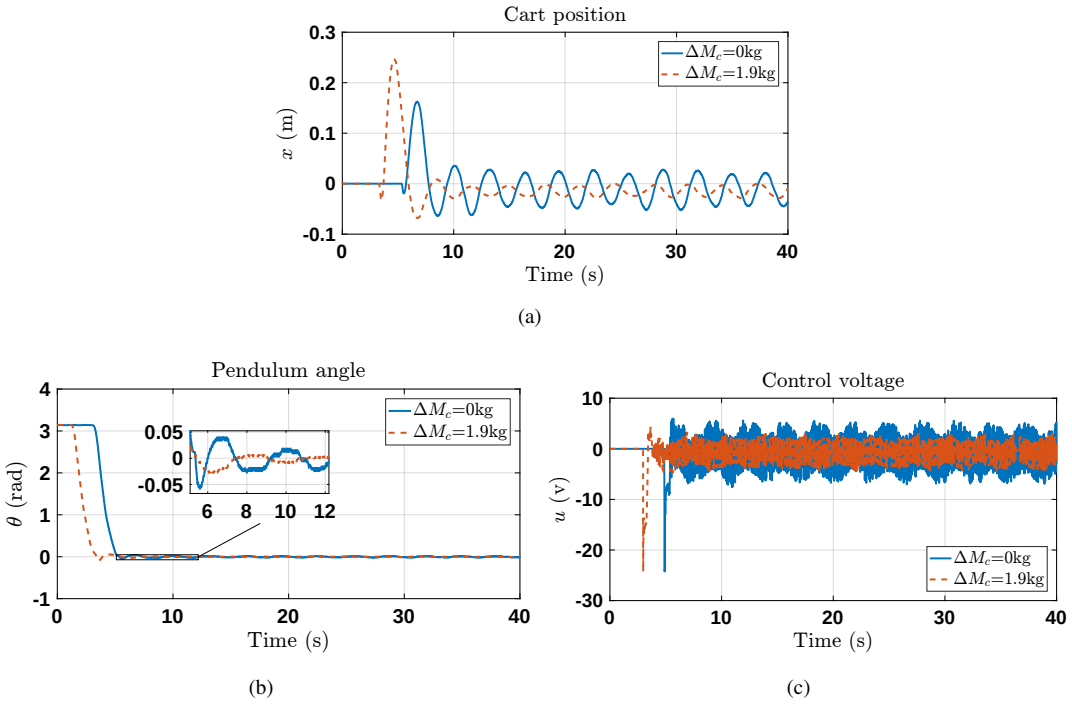

Figure 5.12: Real time CIPS response with LQR PID for ΔM_c at $\Delta l = 0.08$m

ii) SBL based PID results :

For SBL PID, SMDC Ω_{M_c}= 11.0968 kg is obtained in (5.55) and PAR Π_{M_c} = 13.4968 kg is calculated in (5.62). Hence, similarly using equation (5.63), maximum ΔM_c allowed is nothing but the minimum of SMDC $\Omega_{M_c}$and PAR Π_{M_c}. Thus, using (5.62), we get $\Delta\mathcal{P}_{M_c}$ = 3.7475 kg. The real-time results are carried out for different masses (M_c) 2.4 kg, and 4.3 kg considering additional mass as $\Delta M_c = 0$, and $\Delta M_c = 1.9$ kg, respectively. Here, we have not considered all the additional mass which we have considered in the simulation due to (5.63), as this is important from the safety point of view of CIPS. The effect of additional cart mass on x, θ and corresponding u are shown in Figure 5.13(a), 5.13(b) and 5.13(c), respectively. From these figures, it is found that for the additional variation in cart mass (ΔM_c), SBL based PID stabilized the cart position(x) and pendulum angle(θ). However, small oscillations can be seen across the cart position. Moreover, hardware results satisfy the bounded range of cart mass as determined in (5.62). Further, real time analysis is carried for increasing pendulum length ($\Delta l = 0.08$m), when there is no additional cart mass and also when there is additional cart mass is $\Delta M_c = 1.9$kg. The responses of CIPS system are shown in figures 5.13(a,b,c), Figure 5.13(a)shows x, figure 5.13(b) shows θ and figure 5.13(c) shows u. From these figures, it is found that the SBL based PID controller stabilised the CIPS

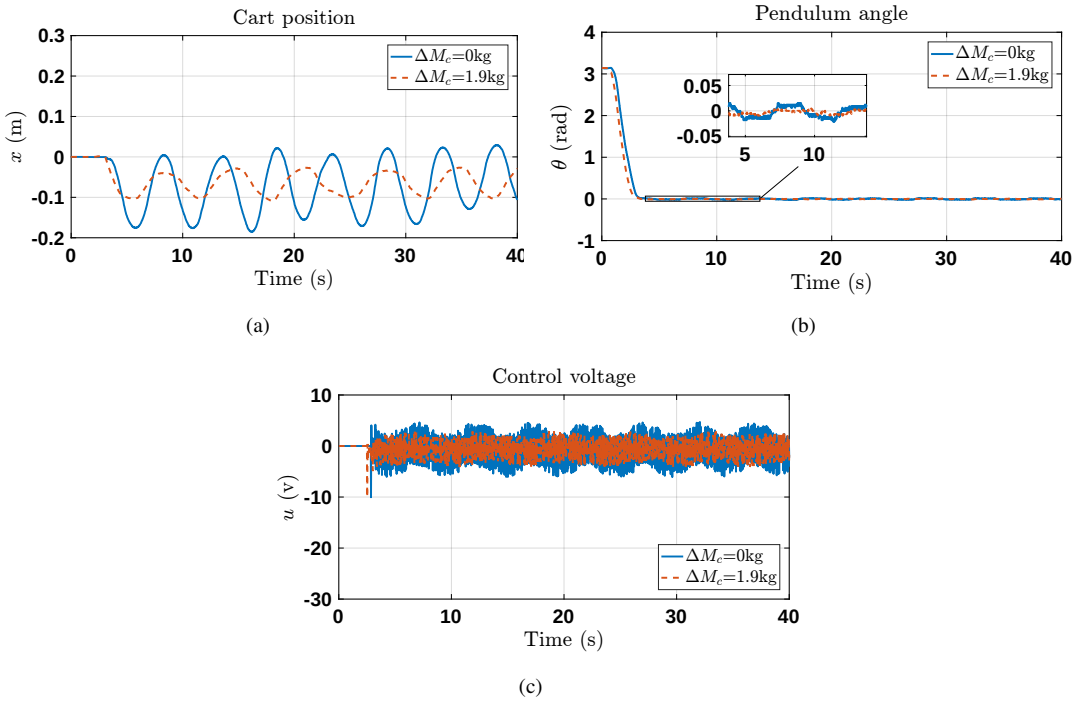

Figure 5.13: Real time CIPS response with SBL PID for ΔM_c at $\Delta l = 0.08$m

system, but still small oscillations are present across x and θ.

iii) Comparison between LQR based PID and SBL based PID :

From above discussion and from figures 5.12(a,b,c) and figures 5.13(a,b,c), it can be deduced that the performance based on SBL based PID is better in comparison to LQR based PID when additional cart mass and increase of pendulum length are considered. Particularly, control input voltage u and oscillation across pendulum angle θ are also found minimum in case of SBL based PID controller.

5.5 Proposed controller design techniques

In this section, we propose three different techniques for the control of cart inverted pendulum system. Initially, for an interval system, SBL-PID has been designed via Kharitonov's theorem. Then, adaptive control policy has been used to extract the best features of the individual candidate controllers. Further, the existing adaptive scheme has been modified and implemented on real time CIPS setup. Finally, QRAWCP-PID is designed and compared with existing LQR-PID.

5.5.1 SBL for perturbed CIPS

Let the perturbed model of CIPS be given as

$$\frac{x(s)}{F(s)} = \frac{\left((J\pm\delta_J)+(m\pm\delta_m)(L\pm\delta_L)^2\right)}{\left((J\pm\delta_J)+(m\pm\delta_m)(L\pm\delta_L)^2\right)\left((M\pm\delta_M)+(m\pm\delta_m)\right)}\times \frac{\left[s^2-\frac{(m\pm\delta_m)g(L\pm\delta_L)}{\left((J\pm\delta_J)+(m\pm\delta_m)(L\pm\delta_L)^2\right)}\right]}{\left[s^4-\frac{(m\pm\delta_m)g(L\pm\delta_L)((M\pm\delta_M)+(m\pm\delta_m))}{\left((J\pm\delta_J)+(m\pm\delta_m)(L\pm\delta_L)^2\right)\left((M\pm\delta_M)+(m\pm\delta_m)\right)}s^2\right]} \tag{5.64}$$

Simplification of (5.64) gives,

$$\frac{x(s)}{F(s)} = \frac{1}{\left((M\pm\delta_M)+(m\pm\delta_m)\right)s^2} \tag{5.65}$$

Further (5.65), can be written as

$$P_1 = \frac{x(s)}{F(s)} = \frac{b_1}{s^2} \tag{5.66}$$

where,

$$b_1 = \frac{1}{\left((M\pm\delta_M)+(m\pm\delta_m)\right)}$$

Similarly, the transfer function for angle control is determined as,

$$\frac{\theta(s)}{F(s)} = \frac{\left[(m\pm\delta_m)(L\pm\delta_L)\right]s^2}{\left[(J\pm\delta_J)(M\pm\delta_M+m\pm\delta_m)+(M\pm\delta_M)(m\pm\delta_m)(L\pm\delta_L)^2\right]s^4} \times\frac{1}{-\left[(m\pm\delta_m)(M\pm\delta_M+m\pm\delta_m)(L\pm\delta_L)\right]gs^2} \tag{5.67}$$

Equation (5.67) is simplified as,

$$\frac{\theta(s)}{F(s)} \simeq \frac{(m\pm\delta_m)(L\pm\delta_L)s^2}{\left((J\pm\delta_J)+(m\pm\delta_m)(L\pm\delta_L)^2\right)\left((M\pm\delta_M)+(m\pm\delta_m)\right)}\times \frac{1}{\left[s^4-\frac{(m\pm\delta_m)g(L\pm\delta_L)((M\pm\delta_M)+(m\pm\delta_m))}{\left((J\pm\delta_J)+(m\pm\delta_m)(L\pm\delta_L)^2\right)\left((M\pm\delta_M)+(m\pm\delta_m)\right)}s^2\right]} \tag{5.68}$$

$$\frac{\theta(s)}{F(s)} \simeq \frac{(m\pm\delta_m)(L\pm\delta_L)s^2}{\Big((J\pm\delta_J)+(m\pm\delta_m)(L\pm\delta_L)^2\Big)\Big((M\pm\delta_M)+(m\pm\delta_m)\Big)} \times \frac{1}{\left[s^4 - \frac{(m\pm\delta_m)g(L\pm\delta_L)}{\Big((J\pm\delta_J)+(m\pm\delta_m)(L\pm\delta_L)^2\Big)}s^2\right]} \tag{5.69}$$

Further, (5.69) can be written as

$$P_2 = \frac{\theta(s)}{F(s)} = \frac{b_2}{s^2 - a_3} \tag{5.70}$$

where,

$$\begin{aligned} b_2 &= \frac{(m\pm\delta_m)(L\pm\delta_L)}{\Big((J\pm\delta_J)+(m\pm\delta_m)(L\pm\delta_L)^2\Big)\Big((M\pm\delta_M)+(m\pm\delta_m)\Big)} \\ a_3 &= \frac{(m\pm\delta_m)g(L\pm\delta_L)}{\Big((J\pm\delta_J)+(m\pm\delta_m)(L\pm\delta_L)^2\Big)} \end{aligned} \tag{5.71}$$

Design of SBL-PID using Kharitonov's theorem The design of SBL based PID for various systems is discussed in [57, 166–168]. Two PID controllers are designed, one for position control i.e., $\text{PID}_1(C_1)$ and other for angle control i.e., $\text{PID}_2(C_2)$.

The closed-loop characteristics equation for both the transfer function are derived below.

1. **Position control (x):**

$$1 + P_1(s)C_1(s) = 0 \tag{5.72}$$

Using (5.66) and $C_1(s) = K_{p1} + \frac{K_{i1}}{s} + K_{d1}.s$, (5.72) can be written as

$$1 + \left\{\frac{b_1}{s^2}\right\}\left\{K_{p1} + \frac{K_{i1}}{s} + K_{d1}.s\right\} = 0 \tag{5.73}$$

Simplification of (5.73) gives,

$$s^3 + b_1K_{d1}s^2 + b_1K_{p1}.s + b_1K_{i1} = 0 \tag{5.74}$$

2. **Angle control(θ):**

$$1 + P_2(s)C_2(s) = 0 \tag{5.75}$$

Using (5.70) and $C_2(s) = K_{p2} + \frac{K_{i2}}{s} + K_{d2}.s$, (5.75) can be written as

$$1 + \left\{ \frac{b_2}{s^2 - a_3} \right\} \left\{ K_{p2} + \frac{K_{i2}}{s} + K_{d2}.s \right\} = 0 \tag{5.76}$$

Further simplification of (5.76) gives,

$$s^3 + b_2 K_{d2} s^2 + \left(b_2 K_{p2} - a_3 \right) s + b_2 K_{i2} = 0 \tag{5.77}$$

Now using Kharitonov's theorem which has been discussed in [56, 169, 170], the four extreme polynomials for closed-loop characteristic equations (5.74) and (5.77) can be obtained, as given below.

5.5.1.1 Kharitonov polynomials

Applying Kharitonov's theorem to position control transfer function (TF) (5.66), the four polynomials are written as,

$$\begin{aligned}
K_x^1 &= \underline{b_1} K_{i1}^1 + \underline{b_1} K_{p1}^1 s + \overline{b_1} K_{d1}^1 s^2 + s^3 \\
K_x^2 &= \underline{b_1} K_{i1}^2 + \overline{b_1} K_{p1}^2 s + \overline{b_1} K_{d1}^2 s^2 + s^3 \\
K_x^3 &= \overline{b_1} K_{i1}^3 + \underline{b_1} K_{p1}^3 s + \underline{b_1} K_{d1}^3 s^2 + s^3 \\
K_x^4 &= \overline{b_1} K_{i1}^4 + \overline{b_1} K_{p1}^4 s + \underline{b_1} K_{d1}^4 s^2 + s^3
\end{aligned} \tag{5.78}$$

Where, $\underline{b_1}$ and $\overline{b_1}$ are the minimum and maximum values of $b_1 \in [x_1, y_1]$, respectively. x_1 and y_1 can be written as,

$$\begin{aligned}
x_1 &= \frac{1}{\left((M + \delta_M) + (m + \delta_m) \right)} \\
y_1 &= \frac{1}{\left((M - \delta_M) + (m - \delta_m) \right)}
\end{aligned} \tag{5.79}$$

Equation (5.78) can be written as,

$$\begin{aligned}
K_x^1 &= x_1 K_{i1}^1 + x_1 K_{p1}^1 s + y_1 K_{d1}^1 s^2 + s^3 \\
K_x^2 &= x_1 K_{i1}^2 + y_1 K_{p1}^2 s + y_1 K_{d1}^2 s^2 + s^3 \\
K_x^3 &= y_1 K_{i1}^3 + x_1 K_{p1}^3 s + x_1 K_{d1}^3 s^2 + s^3 \\
K_x^4 &= y_1 K_{i1}^4 + y_1 K_{p1}^4 s + x_1 K_{d1}^4 s^2 + s^3
\end{aligned} \tag{5.80}$$

Similarly for angle control, applying Kharitonov's theorem to (5.77), the four polynomials can be written as

$$\begin{aligned}
K_\theta^1 &= \underline{b_2}K_{i2}^1 + \underline{\left(b_2K_{p2}^1 - a_3\right)}s + \overline{b_2}K_{d2}^1 s^2 + s^3 \\
K_\theta^2 &= \underline{b_2}K_{i2}^2 + \overline{\left(b_2K_{p2}^2 - a_3\right)}s + \overline{b_2}K_{d2}^2 s^2 + s^3 \\
K_\theta^3 &= \overline{b_2}K_{i2}^3 + \underline{\left(b_2K_{p2}^3 - a_3\right)}s + \underline{b_2}K_{d2}^3 s^2 + s^3 \\
K_\theta^4 &= \overline{b_2}K_{i2}^4 + \overline{\left(b_2K_{p2}^4 - a_3\right)}s + \underline{b_2}K_{d2}^4 s^2 + s^3
\end{aligned} \tag{5.81}$$

where, $\underline{b_2}$ and $\overline{b_2}$ shows minimum and maximum values of $b_2 \in [x_2, y_2]$ respectively, and similarly $\underline{\left(b_2K_{p2} - a_3\right)}$ and $\overline{\left(b_2K_{p2} - a_3\right)}$ shows minimum and maximum values of $a_3 \in [x_3, y_3]$. Using eq.(5.71), x_2, y_2, x_3, and y_3 can be written as,

$$\begin{aligned}
x_2 &= \frac{(m-\delta_m)(l-\delta_l)}{\left((J+\delta_J)+(m+\delta_m)(L+\delta_L)^2\right)\left((M+\delta_M)+(m+\delta_m)\right)} \\
y_2 &= \frac{(m+\delta_m)(L+\delta_L)}{\left((J-\delta_J)+(m-\delta_m)(L-\delta_L)^2\right)\left((M-\delta_M)+(m-\delta_m)\right)} \\
x_3 &= \frac{(m-\delta_m)g(L-\delta_L)}{\left((J+\delta_J)+(m+\delta_m)(L+\delta_L)^2\right)} \\
y_3 &= \frac{(m+\delta_m)g(L+\delta_L)}{\left((J-\delta_J)+(m-\delta_m)(L-\delta_L)^2\right)}
\end{aligned} \tag{5.82}$$

Similarly, (5.81) can be written as,

$$\begin{aligned}
K_\theta^1 &= x_2K_{i2}^1 + \left(x_2K_{p2}^1 - y_3\right)s + y_2K_{d2}^1 s^2 + s^3 \\
K_\theta^2 &= x_2K_{i2}^2 + \left(y_2K_{p2}^2 - x_3\right)s + y_2K_{d2}^2 s^2 + s^3 \\
K_\theta^3 &= y_2K_{i2}^3 + \left(x_2K_{p2}^3 - y_3\right)s + x_2K_{d2}^3 s^2 + s^3 \\
K_\theta^4 &= y_2K_{i2}^4 + \left(y_2K_{p2}^4 - x_3\right)s + x_2K_{d2}^4 s^2 + s^3
\end{aligned} \tag{5.83}$$

5.5.1.2 Obtaining SBL regions

For designing SBL for position control and angle control, SBL is obtained for (5.80) and (5.83), respectively. The SBL based PID controllers are as given below.

For **PID**$_1$

1. Substituting $s = jw$ in (5.80) for first polynomial $K_x^1(s)$. Thus, the closed loop characteristic equation is given as

$$x_1 K_{i1}^1 + x_1 K_{p1}^1(j\omega) + y_1 K_{d1}^1(-\omega^2) + j\omega(-\omega^2) = 0 \tag{5.84}$$

On equating real and imaginary parts of (5.84) to zero, (5.85) and (5.86) can be obtained as,

$$x_1 K_{i1}^1 = y_1 K_{d1}^1(\omega^2) \tag{5.85}$$

and

$$x_1 K_{p1}^1(j\omega) = j\omega(\omega^2) \tag{5.86}$$

Now arbitrarily selecting the value of K_{d1}^1, other parameters of PID_1 can be obtained for $K_x^1(s)$ using (5.85) and (5.86) as,

$$K_{i1}^1 = \frac{y_1 K_{d1}^1 \omega^2}{x_1} \tag{5.87}$$

and

$$K_{p1}^1 = \frac{\omega^2}{x_1} \tag{5.88}$$

By varying ω from $(0, \infty)$, the SBL plot is obtained.

Similarly for other three polynomials $K_x^2(s)$,$K_x^3(s)$, and $K_x^4(s)$, K_{p1} and K_{i1} are computed, which are given below.

2. Taking second polynomial K_x^2 from (5.80), (5.89) can be obtained as,

$$x_1 K_{i1}^2 + y_1 K_{p1}^2(j\omega) + y_1 K_{d1}^2(-\omega^2) + j\omega(-\omega^2) = 0 \tag{5.89}$$

For above polynomial, K_{p1}^2 and K_{i1}^2 can be determined, by equating real and imaginary parts of $K_x^2(jw)$ (5.89) to zero and arbitrarily selecting K_{d1}^2, (5.90) and (5.91) are obtained as,

$$K_{i1}^2 = \frac{y_1 K_{d1}^2 \omega^2}{x_1} \tag{5.90}$$

and

$$K_{p1}^{2} = \frac{\omega^2}{y_1} \tag{5.91}$$

3. Consider the third polynomial of K_x^3 from (5.80), as

$$y_1 K_{i1}^{3} + x_1 K_{p1}^{3}(j\omega) + x_1 K_{d1}^{3}(-\omega^2) + j\omega(-\omega^2) = 0 \tag{5.92}$$

For above polynomial, K_{p1}^3 and K_{i1}^3 can be determined, by equating real and imaginary parts of (5.92) to zero and arbitrarily selecting K_{d1}^3, (5.93) and (5.94) are obtained as,

$$K_{i1}^{3} = \frac{x_1 K_{d1}^{3} \omega^2}{y_1} \tag{5.93}$$

and

$$K_{p1}^{3} = \frac{\omega^2}{x_1} \tag{5.94}$$

4. Similarly, using the fourth polynomial of K_x^4 from (5.80), (5.95) is obtained.

$$y_1 K_{i1}^{4} + y_1 K_{p1}^{4}(j\omega) + x_1 K_{d1}^{4}(-\omega^2) + j\omega(-\omega^2) = 0 \tag{5.95}$$

For above polynomial, K_{p1}^4 and K_{i1}^4 can be determined, by equating real and imaginary parts of (5.95) to zero and arbitrarily selecting K_{d1}^4, (5.96) and (5.97) can be obtained as,

$$K_{i1}^{4} = \frac{x_1 K_{d1}^{4} \omega^2}{y_1} \tag{5.96}$$

and

$$K_{p1}^{4} = \frac{\omega^2}{y_1} \tag{5.97}$$

For **PID**$_2$

1. In eq.(5.83), the first polynomial is represented as K_θ^1 . In this equation, substituting $s = jw$, (5.98) is obtained.

$$x_2 K_{i2}^{1} + \left(x_2 K_{p2}^{1} - y_3\right)(j\omega) + y_2 K_{d2}^{1}(-\omega^2) + j\omega(-\omega^2) = 0 \tag{5.98}$$

By equating real and imaginary parts of (5.98) to zero, (5.99) and (5.100) are obtained as,

$$x_2 K_{i2}^1 = y_2 K_{d2}^1(\omega^2) \tag{5.99}$$

and

$$\left(x_2 K_{p2}^1 - y_3\right)(j\omega) = j\omega(\omega^2) \tag{5.100}$$

By arbitrarily selecting K_{d2}^1 , other parameters of PID_2 can be obtained for K_θ^1 polynomial as,

$$K_{i2}^1 = \frac{y_2 K_{d2}^1 \omega^2}{x_2} \tag{5.101}$$

and

$$K_{p2}^1 = \frac{\omega^2 + y_3}{x_2} \tag{5.102}$$

By varying ω from $(0,\infty)$, the SBL plot is obtained.

Similarly, for other three polynomials, K_θ^2 ,K_θ^3 and K_θ^4 are obtained which are given below.

2. The second polynomial K_θ^2 from (5.83) is written as

$$x_2 K_{i2}^2 + \left(y_2 K_{p2}^2 - x_3\right)(j\omega) + y_2 K_{d2}^2(-\omega^2) + j\omega(-\omega^2) = 0 \tag{5.103}$$

In above equation, K_{p2}^2 and K_{i2}^2 can be determined, by equating real and imaginary parts of (5.103) to zero and arbitrarily selecting K_{d2}^2, (5.104) and (5.105) are obtained as,

$$K_{i2}^2 = \frac{y_2 K_{d2}^2 \omega^2}{x_2} \tag{5.104}$$

and

$$K_{p2}^2 = \frac{\omega^2 + x_3}{y_2} \tag{5.105}$$

3. Taking the third polynomial K_θ^3 from (5.83), (5.106) is obtained as,

$$y_2 K_{i2}^3 + \left(x_2 K_{p2}^3 - y_3\right)(j\omega) + x_2 K_{d2}^3(-\omega^2) + j\omega(-\omega^2) = 0 \tag{5.106}$$

Table 5.5: Perturb parameters of cart inverted pendulum system

Parameter	Nominal	Perturbation	[Min δ Max δ]
Cart mass (M)	2.4 kg	$\delta_M = \pm 0.480$ kg	$[1.92, 2.88]$kg
Pendulum mass (m)	0.23 kg	$\delta_m = \pm 0.040$ kg	$[0.184, 0.276]$kg
Pendulum length (L)	0.4 m	$\delta_L = \pm 8$ cm	$[0.32, 0.48]$m

In above equation, K_{p2}^3 and K_{i2}^3 can be determined, by equating real and imaginary parts of $K_\theta^3(jw)$ (5.106) to zero and arbitrarily selecting K_{d2}^3, (5.107) and (5.108) are obtained as,

$$K_{i2}^3 = \frac{x_2 K_{d2}^3 \omega^2}{y_2} \tag{5.107}$$

and

$$K_{p2}^3 = \frac{\omega^2 + y_3}{x_2} \tag{5.108}$$

4. Similarly, using the fourth polynomial of K_θ^4 from (5.83), (5.109) is obtained as,

$$y_2 K_{i2}^4 + \left(y_2 K_{p2}^4 - x_3\right)(j\omega) + x_2 K_{d2}^4(-\omega^2) + j\omega(-\omega^2) = 0 \tag{5.109}$$

In above equation, K_{p2}^4 and K_{i2}^4 can be determined by equating real and imaginary parts of (5.109) to zero and arbitrarily selecting K_{d2}^4, (5.110) and (5.111) are obtained as,

$$K_{i2}^4 = \frac{x_2 K_{d2}^4 \omega^2}{y_2} \tag{5.110}$$

and

$$K_{p2}^4 = \frac{\omega^2 + x_3}{y_2} \tag{5.111}$$

5.5.1.3 Plotting stability boundary locus

For CIP system, 20% variations are considered in the cart mass, pendulum mass and pendulum length from the nominal value. The lower and upper bounds of parameters are listed in Table 5.5.

Using Table 5.1, Table 5.5 and from eq.(5.79), (5.82), $x_1 = 0.31686$, $y_1 = 0.47529$, $x_2 = 0.10229$, $y_2 = 0.64224$, $x_3 = 3.16690$ and $y_3 = 13.25589$ are calculated. Further, for performing an experiment on hardware setup, a conversion factor α is also required. In user manual [152], conversion factor is given as $\alpha = 15$. Therefore, the coefficients b_1, b_2 and a_3 become

$$\begin{aligned} b_1 &\in [4.7529, 7.1293] \\ b_2 &\in [1.5343, 9.6335] \\ a_3 &\in [3.1669, 13.2559] \end{aligned} \tag{5.112}$$

The design of PID controller is carried out using stability boundary locus for cart control and angle control for CIP system. As mentioned earlier, PID_1 is for cart control and PID_2 is for angle control. For cart control, derivative gain is fixed as $K_{d1} = 5$. The stability boundary locus, i.e., locus between K_{p1} verses K_{i1} is determined for four Kharitonov polynomials as given in eq.(5.78). For first polynomial, SBL determined using eq.(5.87) and eq.(5.88). Similarly, for second, third, and fourth polynomials, SBL is determined using eq.(5.90) (5.91), (5.93) (5.94), (5.96) and (5.97), respectively. In order to find the parameters of PID_1, in Fig. 5.14, the intersection region, i.e., $K_x^1 \cap K_x^2 \cap K_x^3 \cap K_x^4$ is selected. In this, two regions are obtained, i.e., one above the K_x^2 and other below the K_x^3. By selecting, one value from each of these regions, stability of cart control system is checked. Here, it is found that the value from below K_x^3 region gives stable response. Afterwards, using trial and error procedure, a suitable value is selected which gives satisfactory performance. The selected value is shown by the marker '▷'in Fig. 5.14. Thus, from this figure, the PID_1 values are selected as $K_{p1} = 6.9964$, $K_{i1} = 0.2$ and $K_{d1} = 5$.

Similar to above procedure, SBL is determined for angle control system. For angle control, derivative gain is fixed at $K_{d2} = 10$. The stability boundary locus i.e., locus between K_{p2} versus K_{i2} is determined for four Kharitonov polynomials. For first polynomial, SBL determined using eq.(5.101) and (5.102). Similarly, for second, third, and fourth polynomials, SBL is determined using eq.(5.104) (5.105), eq.(5.107) (5.108) and eq.(5.110) (5.111), respectively. In order to find the parameters of PID_2, in Fig. 5.15, the intersection region of $K_\theta^1 \cap K_\theta^2 \cap K_\theta^3 \cap K_\theta^4$ is selected. In this, enclosed regions which lie between above K_θ^1, K_θ^3 and below K_θ^2, K_θ^4 are determined. By selecting one value from enclosed region and one value from outside this region,

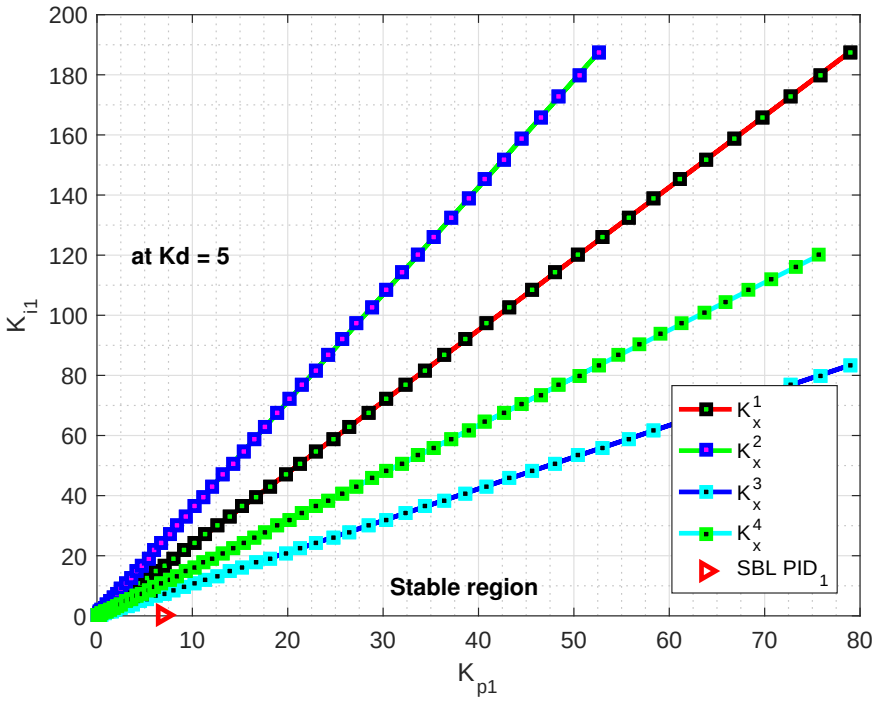

Figure 5.14: SBL of four Kharitonov polynomials for cart control

the enclosed region gives stable response. Subsequently, using trial and error procedure, suitable value is selected which gives satisfactory performance. The selected value is shown by marker '▷'in Fig. 5.15. Thus, from this figure, the PID$_2$ values are selected as $K_{p2} = 50.3294$, $K_{i2} = 5$, and $K_{d2} = 10$.

5.5.1.4 Stability analysis of Kharitonov's polynomials

The two PID control structure for CIP are shown in Fig.5.2. From this figure, the closed-loop characteristic equation becomes $1 - P_1C_1(s) + P_2C_2(s)$. From eq.(5.80) and (5.83), the open loop transfer functions with controllers are given in eq.(5.113) and (5.114), respectively.

$$\begin{aligned}
\{P_1C_1\}_x^1 &= \frac{x_1 K_{i1}}{y_1 K_{d1} s^2 + x_1 K_{p1} s + s^3} \\
\{P_1C_1\}_x^2 &= \frac{x_1 K_{i1}}{y_1 K_{d1} s^2 + y_1 K_{p1} s + s^3} \\
\{P_1C_1\}_x^3 &= \frac{y_1 K_{i1}}{x_1 K_{d1} s^2 + x_1 K_{p1} s + s^3} \\
\{P_1C_1\}_x^3 &= \frac{y_1 K_{i1}}{x_1 K_{d1} s^2 + y_1 K_{p1} s + s^3}
\end{aligned} \tag{5.113}$$

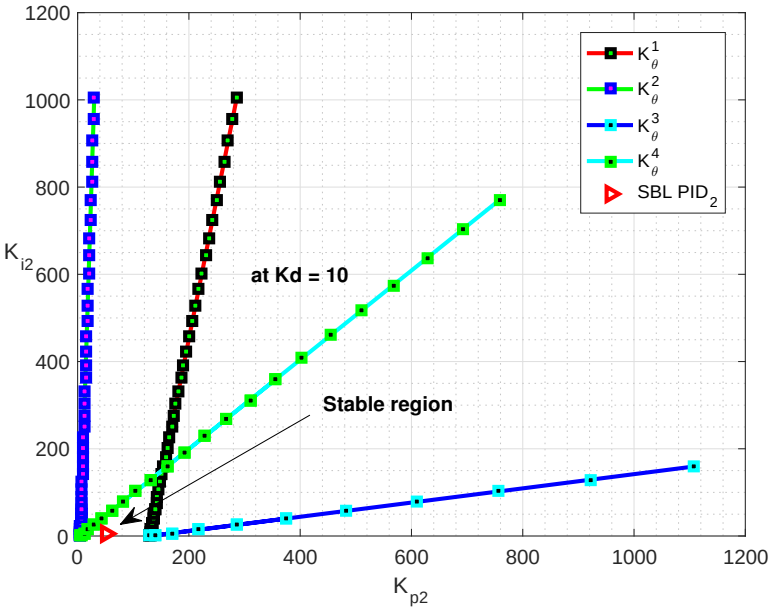

Figure 5.15: SBL of four Kharitonov polynomials for angle control

$$
\begin{aligned}
\{P_2C_2\}_\theta^1 &= \frac{x_2\,K_{i2}}{s^3 + y_2\,K_{d2}\,s^2 + \left(K_{p2}\,x_2 - y_3\right)s} \\
\{P_2C_2\}_\theta^2 &= \frac{x_2\,K_{i2}}{s^3 + y_2\,K_{d2}\,s^2 + \left(y_2\,K_{p2} - x_3\right)s} \\
\{P_2C_2\}_\theta^2 &= \frac{y_2\,K_{i2}}{s^3 + x_2\,K_{d2}\,s^2 + \left(K_{p2}\,x_2 - y_3\right)s} \\
\{P_2C_2\}_\theta^2 &= \frac{y_2\,K_{i2}}{s^3 + x_2\,K_{d2}\,s^2 + \left(y_2\,K_{p2} - x_3\right)s}
\end{aligned}
\tag{5.114}
$$

Using above eq.(5.113) and (5.114), sixteen possible combinations of Kharitonov polynomials are written as

$$
\begin{aligned}
&1 - \{P_1C_1\}_x^1 + \{P_2C_2\}_\theta^1 = 0; \\
&s^5 + \left(K_{d1}\,y_1 + x_2\,K_{d2}\right)s^4 + \left(K_{d1}\,K_{d2}\,x_2\,y_1 + K_{p1}\,x_1 + y_2\,K_{p2} - x_3\right)s^3 \\
&\quad + \Big(\left(K_{d2}\,K_{p1}\,x_2 - K_{i1}\right)x_1 + \left(K_{d1}\,K_{p2}\,y_1 + K_{i2}\right)y_2 - K_{d1}\,x_3\,y_1\Big)\,s^2 \\
&\quad + \Big(\left(-K_{d2}\,K_{i1}\,x_2 + K_{p1}\,K_{p2}\,y_2 - K_{p1}\,x_3\right)x_1 + K_{d1}\,K_{i2}\,y_1\,y_2\Big)\,s \\
&\quad + x_1\,\Big(\left(-K_{i1}\,K_{p2} + K_{i2}\,K_{p1}\right)y_2 + x_3\,K_{i1}\Big) = 0
\end{aligned}
\tag{5.115}
$$

$$
\begin{aligned}
&1-\{P_1C_1\}_x^1+\{P_2C_2\}_\theta^2=0;\\
&s^5+(K_{d1}y_1+K_{d2}y_2)s^4+\Big(K_{p1}x_1+\big(K_{d1}K_{d2}y_1+K_{p2}\big)y_2-x_3\Big)s^3\\
&\quad+\Big(\big(K_{d2}K_{p1}y_2-K_{i1}\big)x_1+K_{d1}K_{p2}y_1y_2-K_{d1}x_3y_1+x_2K_{i2}\Big)s^2\\
&\quad+\Big(\Big(\big(-K_{d2}K_{i1}+K_{p1}K_{p2}\big)y_2-K_{p1}x_3\Big)x_1+K_{i2}x_2y_1K_{d1}\Big)s\\
&\quad+x_1\left(-K_{i1}K_{p2}y_2+K_{i2}K_{p1}x_2+x_3K_{i1}\right)=0
\end{aligned}
\tag{5.116}
$$

$$
\begin{aligned}
&1-\{P_1C_1\}_x^1+\{P_2C_2\}_\theta^3=0;\\
&s^5+(K_{d1}y_1+x_2K_{d2})s^4+\Big(K_{p1}x_1+\big(K_{d1}K_{d2}y_1+K_{p2}\big)x_2-y_3\Big)s^3\\
&\quad+\Big(\big(K_{d2}K_{p1}x_2-K_{i1}\big)x_1+K_{p2}x_2y_1K_{d1}-y_1y_3K_{d1}+y_2K_{i2}\Big)s^2\\
&\quad+\Big(\Big(\big(-K_{d2}K_{i1}+K_{p1}K_{p2}\big)x_2-K_{p1}y_3\Big)x_1+K_{d1}K_{i2}y_1y_2\Big)s\\
&\quad+x_1\left(-K_{i1}K_{p2}x_2+K_{i2}K_{p1}y_2+K_{i1}y_3\right)=0
\end{aligned}
\tag{5.117}
$$

Similarly, the other combinations of Kharitonov polynomials can be obtained as,

$$
\begin{aligned}
&1-\{P_1C_1\}_x^1+\{P_2C_2\}_\theta^4=0;\\
&s^5+(K_{d1}y_1+x_2K_{d2})s^4+\big(K_{d1}K_{d2}x_2y_1+K_{p1}x_1+y_2K_{p2}-x_3\big)s^3\\
&\quad+\Big(\big(K_{d2}K_{p1}x_2-K_{i1}\big)x_1+\big(K_{d1}K_{p2}y_1+K_{i2}\big)y_2-K_{d1}x_3y_1\Big)s^2\\
&\quad+\Big(\big(-K_{d2}K_{i1}x_2+K_{p1}K_{p2}y_2-K_{p1}x_3\big)x_1+K_{d1}K_{i2}y_1y_2\Big)s\\
&\quad+x_1\Big(\big(-K_{i1}K_{p2}+K_{i2}K_{p1}\big)y_2+x_3K_{i1}\Big)=0
\end{aligned}
\tag{5.118}
$$

$$
\begin{aligned}
&1-\{P_1C_1\}_x^2+\{P_2C_2\}_\theta^1=0;\\
&s^5+(K_{d1}y_1+x_2K_{d2})s^4+\Big(\big(K_{d1}K_{d2}x_2+K_{p1}\big)y_1+y_2K_{p2}-x_3\Big)s^3\\
&\quad+\Big(\big(K_{d1}K_{p2}y_2+K_{d2}K_{p1}x_2-K_{d1}x_3\big)y_1+y_2K_{i2}-x_1K_{i1}\Big)s^2\\
&\quad+\Big(\Big(\big(K_{d1}K_{i2}+K_{p1}K_{p2}\big)y_2-K_{p1}x_3\Big)y_1-K_{d2}K_{i1}x_1x_2\Big)s\\
&\quad+K_{i2}K_{p1}y_1y_2-x_1K_{i1}\left(y_2K_{p2}-x_3\right)=0
\end{aligned}
\tag{5.119}
$$

$$
\begin{aligned}
&1-\{P_1C_1\}_x^2+\{P_2C_2\}_\theta^2=0;\\
&s^5+(K_{d1}\,y_1+K_{d2}\,y_2)\,s^4+\Big(\big(K_{d1}\,K_{d2}\,y_2+K_{p1}\big)\,y_1+y_2\,K_{p2}-x_3\Big)\,s^3\\
&\quad+\Big(\Big(\big(K_{d1}\,K_{p2}+K_{d2}\,K_{p1}\big)\,y_2-K_{d1}\,x_3\Big)\,y_1+x_2\,K_{i2}-x_1\,K_{i1}\Big)\,s^2\\
&\quad+\Big(\big(K_{d1}\,K_{i2}\,x_2+K_{p1}\,K_{p2}\,y_2-K_{p1}\,x_3\big)\,y_1-x_1\,y_2\,K_{d2}\,K_{i1}\Big)\,s\\
&\quad+K_{i2}\,K_{p1}\,x_2\,y_1-x_1\,K_{i1}\,\big(y_2\,K_{p2}-x_3\big)=0
\end{aligned}
\tag{5.120}
$$

$$
\begin{aligned}
&1-\{P_1C_1\}_x^2+\{P_2C_2\}_\theta^3=0;\\
&s^5+(K_{d1}\,y_1+x_2\,K_{d2})\,s^4+\Big(\big(K_{d1}\,K_{d2}\,x_2+K_{p1}\big)\,y_1+K_{p2}\,x_2-y_3\Big)\,s^3\\
&\quad+\Big(\Big(\big(K_{d1}\,K_{p2}+K_{d2}\,K_{p1}\big)\,x_2-y_3\,K_{d1}\Big)\,y_1+y_2\,K_{i2}-x_1\,K_{i1}\Big)\,s^2\\
&\quad+\Big(\big(K_{d1}\,K_{i2}\,y_2+K_{p1}\,K_{p2}\,x_2-K_{p1}\,y_3\big)\,y_1-K_{d2}\,K_{i1}\,x_1\,x_2\Big)\,s\\
&\quad+K_{i2}\,K_{p1}\,y_1\,y_2-x_1\,K_{i1}\,\big(K_{p2}\,x_2-y_3\big)=0
\end{aligned}
\tag{5.121}
$$

$$
\begin{aligned}
&1-\{P_1C_1\}_x^2+\{P_2C_2\}_\theta^4=0;\\
&s^5+(K_{d1}\,y_1+x_2\,K_{d2})\,s^4+\Big(\big(K_{d1}\,K_{d2}\,x_2+K_{p1}\big)\,y_1+y_2\,K_{p2}-x_3\Big)\,s^3\\
&\quad+\Big(\big(K_{d1}\,K_{p2}\,y_2+K_{d2}\,K_{p1}\,x_2-K_{d1}\,x_3\big)\,y_1+y_2\,K_{i2}-x_1\,K_{i1}\Big)\,s^2\\
&\quad+\Big(\Big(\big(K_{d1}\,K_{i2}+K_{p1}\,K_{p2}\big)\,y_2-K_{p1}\,x_3\Big)\,y_1-K_{d2}\,K_{i1}\,x_1\,x_2\Big)\,s\\
&\quad+K_{i2}\,K_{p1}\,y_1\,y_2-x_1\,K_{i1}\,\big(y_2\,K_{p2}-x_3\big)=0
\end{aligned}
\tag{5.122}
$$

$$
\begin{aligned}
&1-\{P_1C_1\}_x^3+\{P_2C_2\}_\theta^1=0;\\
&s^5+(K_{d1}\,x_1+x_2\,K_{d2})\,s^4+\Big(\big(K_{d1}\,K_{d2}\,x_2+K_{p1}\big)\,x_1+y_2\,K_{p2}-x_3\Big)\,s^3\\
&\quad+\Big(\big(K_{d1}\,K_{p2}\,y_2+K_{d2}\,K_{p1}\,x_2-K_{d1}\,x_3\big)\,x_1+y_2\,K_{i2}-y_1\,K_{i1}\Big)\,s^2\\
&\quad+\Big(\Big(\big(K_{d1}\,K_{i2}+K_{p1}\,K_{p2}\big)\,y_2-K_{p1}\,x_3\Big)\,x_1-x_2\,y_1\,K_{d2}\,K_{i1}\Big)\,s\\
&\quad+K_{i2}\,K_{p1}\,x_1\,y_2-y_1\,K_{i1}\,\big(y_2\,K_{p2}-x_3\big)=0
\end{aligned}
\tag{5.123}
$$

$$
\begin{aligned}
&1-\{P_1C_1\}_x^3+\{P_2C_2\}_\theta^2=0;\\
&s^5+(K_{d1}x_1+K_{d2}y_2)s^4+\Big(\big(K_{d1}K_{d2}y_2+K_{p1}\big)x_1+y_2K_{p2}-x_3\Big)s^3\\
&\quad+\Big(\Big(\big(K_{d1}K_{p2}+K_{d2}K_{p1}\big)y_2-K_{d1}x_3\Big)x_1+x_2K_{i2}-y_1K_{i1}\Big)s^2\\
&\quad+\Big(\big(K_{d1}K_{i2}x_2+K_{p1}K_{p2}y_2-K_{p1}x_3\big)x_1-y_1y_2K_{d2}K_{i1}\Big)s\\
&\quad+K_{i2}K_{p1}x_1x_2-y_1K_{i1}\left(y_2K_{p2}-x_3\right)=0
\end{aligned}
\tag{5.124}
$$

$$
\begin{aligned}
&1-\{P_1C_1\}_x^3+\{P_2C_2\}_\theta^3=0;\\
&s^5+(K_{d1}x_1+x_2K_{d2})s^4+\Big(\big(K_{d1}K_{d2}x_2+K_{p1}\big)x_1+K_{p2}x_2-y_3\Big)s^3\\
&\quad+\Big(\Big(\big(K_{d1}K_{p2}+K_{d2}K_{p1}\big)x_2-y_3K_{d1}\Big)x_1+y_2K_{i2}-y_1K_{i1}\Big)s^2\\
&\quad{}^{+}\Big(\big(K_{d1}K_{i2}y_2+K_{p1}K_{p2}x_2-K_{p1}y_3\big)x_1-x_2y_1K_{d2}K_{i1}\Big)s\\
&\quad+K_{i2}K_{p1}x_1y_2-y_1K_{i1}\left(K_{p2}x_2-y_3\right)=0
\end{aligned}
\tag{5.125}
$$

$$
\begin{aligned}
&1-\{P_1C_1\}_x^3+\{P_2C_2\}_\theta^4=0;\\
&s^5+(K_{d1}x_1+x_2K_{d2})s^4+\Big(\big(K_{d1}K_{d2}x_2+K_{p1}\big)x_1+y_2K_{p2}-x_3\Big)s^3\\
&\quad+\Big(\big(K_{d1}K_{p2}y_2+K_{d2}K_{p1}x_2-K_{d1}x_3\big)x_1+y_2K_{i2}-y_1K_{i1}\Big)s^2\\
&\quad+\Big(\Big(\big(K_{d1}K_{i2}+K_{p1}K_{p2}\big)y_2-K_{p1}x_3\Big)x_1-x_2y_1K_{d2}K_{i1}\Big)s\\
&\quad+K_{i2}K_{p1}x_1y_2-y_1K_{i1}\left(y_2K_{p2}-x_3\right)=0
\end{aligned}
\tag{5.126}
$$

$$
\begin{aligned}
&1-\{P_1C_1\}_x^4+\{P_2C_2\}_\theta^1=0;\\
&s^5+(K_{d1}x_1+x_2K_{d2})s^4+\big(K_{d1}K_{d2}x_1x_2+K_{p1}y_1+y_2K_{p2}-x_3\big)s^3\\
&\quad+\Big(\big(K_{d2}K_{p1}x_2-K_{i1}\big)y_1+\big(K_{d1}K_{p2}x_1+K_{i2}\big)y_2-x_1x_3K_{d1}\Big)s^2\\
&\quad+\Big(\big(-K_{d2}K_{i1}x_2+K_{p1}K_{p2}y_2-K_{p1}x_3\big)y_1+K_{i2}x_1y_2K_{d1}\Big)s\\
&\quad+y_1\Big(\big(-K_{i1}K_{p2}+K_{i2}K_{p1}\big)y_2+x_3K_{i1}\Big)=0
\end{aligned}
\tag{5.127}
$$

$$
\begin{aligned}
&1-\{P_1C_1\}_x^4+\{P_2C_2\}_\theta^2=0;\\
&s^5+(K_{d1}x_1+K_{d2}y_2)s^4+\Big(K_{p1}y_1+\big(K_{d1}K_{d2}x_1+K_{p2}\big)y_2-x_3\Big)s^3\\
&\quad+\Big(\big(K_{d2}K_{p1}y_2-K_{i1}\big)y_1+K_{p2}x_1y_2K_{d1}-x_1x_3K_{d1}+x_2K_{i2}\Big)s^2\\
&\quad+\Big(\Big(\big(-K_{d2}K_{i1}+K_{p1}K_{p2}\big)y_2-K_{p1}x_3\Big)y_1+K_{i2}x_1x_2K_{d1}\Big)s\\
&\quad+y_1\left(-K_{i1}K_{p2}y_2+K_{i2}K_{p1}x_2+x_3K_{i1}\right)=0
\end{aligned}
\tag{5.128}
$$

$$
\begin{aligned}
&1-\{P_1C_1\}_x^4+\{P_2C_2\}_\theta^3=0;\\
&s^5+(K_{d1}x_1+x_2K_{d2})s^4+\Big(K_{p1}y_1+\big(K_{d1}K_{d2}x_1+K_{p2}\big)x_2-y_3\Big)s^3\\
&\quad+\Big(\big(K_{d2}K_{p1}x_2-K_{i1}\big)y_1+K_{p2}x_1x_2K_{d1}-x_1y_3K_{d1}+y_2K_{i2}\Big)s^2\\
&\quad+\Big(\Big(\big(-K_{d2}K_{i1}+K_{p1}K_{p2}\big)x_2-K_{p1}y_3\Big)y_1+K_{i2}x_1y_2K_{d1}\Big)s\\
&\quad+y_1\left(-K_{i1}K_{p2}x_2+K_{i2}K_{p1}y_2+K_{i1}y_3\right)=0
\end{aligned}
\tag{5.129}
$$

$$
\begin{aligned}
&1-\{P_1C_1\}_x^4+\{P_2C_2\}_\theta^4=0;\\
&s^5+(K_{d1}x_1+x_2K_{d2})s^4+\big(K_{d1}K_{d2}x_1x_2+K_{p1}y_1+y_2K_{p2}-x_3\big)s^3\\
&\quad+\Big(\big(K_{d2}K_{p1}x_2-K_{i1}\big)y_1+\big(K_{d1}K_{p2}x_1+K_{i2}\big)y_2-x_1x_3K_{d1}\Big)s^2\\
&\quad+\Big(\big(-K_{d2}K_{i1}x_2+K_{p1}K_{p2}y_2-K_{p1}x_3\big)y_1+K_{i2}x_1y_2K_{d1}\Big)s\\
&\quad+y_1\Big(\big(-K_{i1}K_{p2}+K_{i2}K_{p1}\big)y_2+x_3K_{i1}\Big)=0
\end{aligned}
\tag{5.130}
$$

After substituting the values of perturbations from (5.112) and parameters of PID_1 and PID_2 in (5.115) to (5.130), the roots of these closed loop characteristics equation are obtained. They are shown in appendix Table 5.6. It is found that for all sixteen combinations, roots are lying on the left half of the s-plane. Hence, system is stable. Further, the results of proposed PID scheme are verified using simulation and also on real time hardware setup. For $\pm 20\%$ parametric variations in system model as shown in Table 5.5, performance of the controllers is discussed in the next section.

Table 5.6: Roots of sixteen Kharitonov polynomials

From eq.	Closed loop characteristic equation	Roots	Remark
(5.115)	$s^5+92.54s^4+2078s^3+5823s^2+4451s+325.9=0$	-58.9260,-30.4950,-1.8081,-1.2278,-0.0817	Stable
(5.116)	$s^5+92.54s^4+2266s^3+1.178\times10^4s^2+1.127\times10^4s+131.1=0$	-55.4134,-30.4950,-5.3984,-1.2199,-0.0118	Stable
(5.117)	$s^5+56.16s^4+925.5s^3+4521s^2+5065s+985.8=0$	-30.4950,-18.3714,-5.8162,-1.2301,-0.2459	Stable
(5.118)	$s^5+56.16s^4+1113s^3+1.047\times10^4s^2+1.188\times10^4s+790.9=0$	-30.4950, -12.1856 +12.2748i, -12.1856 -12.2748i,-1.2214 ,-0.0710	Stable
(5.119)	$s^5+92.54s^4+2086s^3+6314s^2+5368s+424.6=0$	-58.9260,-30.2173,-1.8042,-1.5032,-0.0879	Stable
(5.120)	$s^5+92.54s^4+2274s^3+1.227\times10^4s^2+1.37\times10^4s+229.7=0$	-55.4134,-30.2173,-5.3984,-1.4924,-0.0170	Stable
(5.121)	$s^5+56.16s^4+933.5s^3+4719s^2+5982s+1231=0$	-30.2173,-18.3714,-5.8161,-1.4996,-0.2543	Stable
(5.122)	$s^5+56.16s^4+1121s^3+1.067\times10^4s^2+1.431\times10^4s+1036=0$	-30.2173, -12.1856 +12.2748i, -12.1856 -12.2748i,-1.4934,-0.0768	Stable
(5.123)	$s^5+86.78s^4+1728s^3+5167s^2+4367\times10^4s+299.7=0$	-58.9260,-24.4381,-1.7983,-1.5399,-0.0752	Stable
(5.124)	$s^5+86.78s^4+1916s^3+1.004\times10^4s^2+1.118\times10^4s+61.58=0$	-55.4134,-24.4381,-5.3984,-1.5220,-0.0055	Stable
(5.125)	$s^5+50.4s^4+784.4s^3+3866s^2+4884s+959.6=0$	-24.4381,-18.3714,-5.8157,-1.5326,-0.2398	Stable
(5.126)	$s^5+50.4s^4+972.4s^3+8737s^2+1.17\times10^4s+721.4=0$	-24.4381, -12.1856 +12.2748i, -12.1856 -12.2748i,-1.5235,-0.0648	Stable
(5.127)	$s^5+86.78s^4+1736s^3+5658s^2+5283s+398.4=0$	-58.9260, -24.0813,-1.8439 + 0.0538i, -1.8439 - 0.0538i,-0.0825	Stable
(5.128)	$s^5+86.78s^4+1924s^3+1.053\times10^4s^2+1.361\times10^4s+160.2=0$	-55.4134,-24.0813,-5.3984,-1.8725,-0.0119	Stable
(5.129)	$s^5+50.4s^4+792.5s^3+4063s^2+5801s+1205=0$	-24.0813,-18.3715,-5.8156,-1.8802,-0.2491	Stable
(5.130)	$s^5+50.4s^4+980.4s^3+8934s^2+1.413\times10^4s+966.7=0$	-24.0813, -12.1856 +12.2748i, -12.1856, -12.2748i,-1.8735,-0.0716	Stable

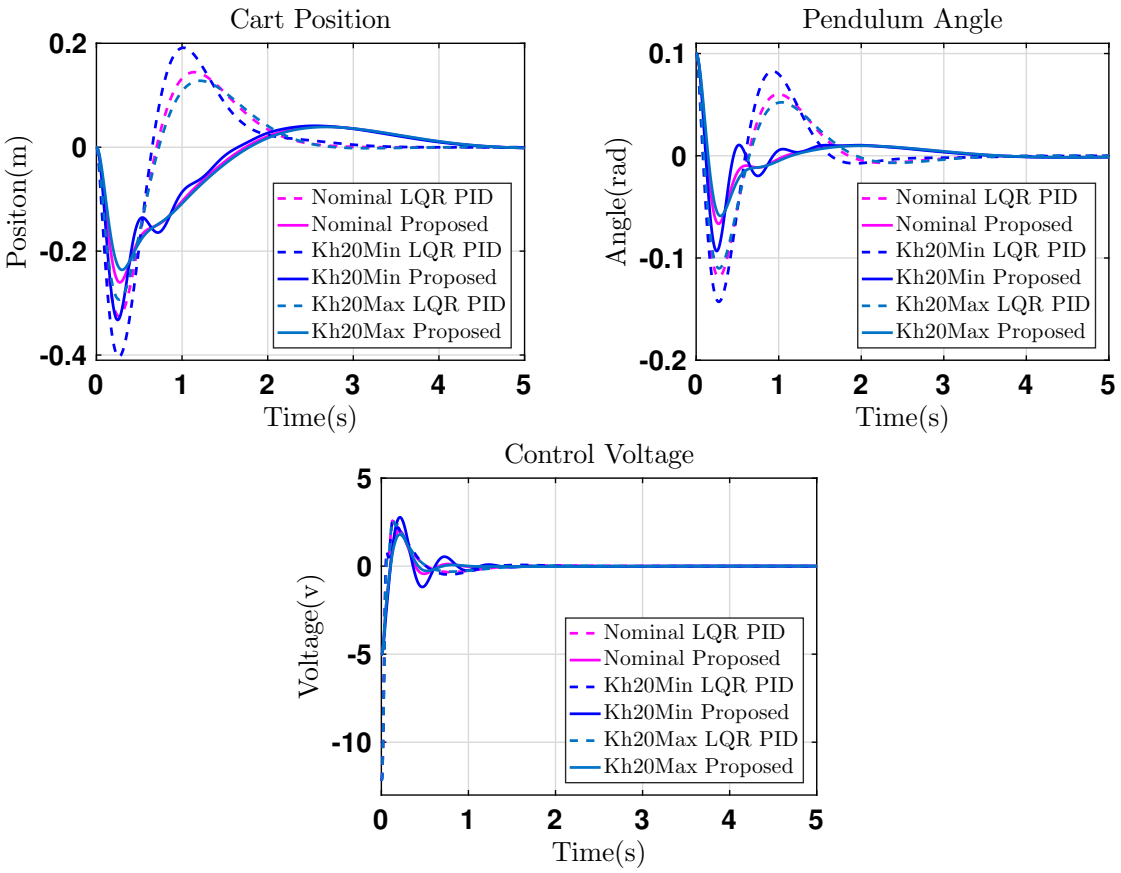

Figure 5.16: Response of CIPS without disturbance

5.5.1.5 Simulation results and discussion

For the verification of proposed PID scheme for interval CIP system, two cases have been considered for simulation. One is for linear interval model and other is for non-linear interval model.

(a) Linear interval model:

In order to verify the performance of controllers for uncertainties as mentioned in Table 5.5, the linear interval model is considered. The linear model equations are shown in (5.66) and (5.70). In this, three conditions are examined. One is nominal value, other conditions are minimum (Min δ) and maximum(Max δ), values respectively. The proposed results are compared with the results based on LQR PID approach as presented in [1]. In this, initial condition is considered as $\theta = 0.1$ rad. The results are shown in Fig. 5.16. Fig. 5.16(a) shows cart position response, which shows minimal overshoot for all three conditions. Fig. 5.16(b) shows pendulum angle at $\theta = 0$ rad without oscillations in all three conditions. Fig. 5.16(c) shows control efforts (u) required

Table 5.7: Performance indices using LQR PID [1] for linear model

Perfor. indices	Nominal values		Min δ		Max δ	
	x	θ	x	θ	x	θ
ISE	0.04705	0.005891	0.06808	0.008462	0.03929	0.005056
IAE	0.2672	0.09242	0.3115	0.1054	0.2497	0.08714
ITSE	0.02744	0.003191	0.03618	0004521	0.02406	0.002738
ITAE	0.2268	0.07666	0.2517	0.08034	0.2231	0.07492

Table 5.8: Performance indices using proposed PID for linear model

Perfor. indices	Nominal values		Min δ		Max δ	
	x	θ	x	θ	x	θ
ISE	0.03406	0.00159	0.04	0.002091	0.03195	0.001547
IAE	0.2773	0.04674	0.2842	0.04986	0.2736	0.04737
ITSE	0.02186	0.0005518	0.02238	0.0006813	0.02177	0.0005547
ITAE	0.436	0.05606	0.4297	0.05585	0.4385	0.05742

to stabilize the pendulum vertically, which are less as compared to LQR PID [1] control efforts. Further, results are compared for commonly used integral performance indices such as integral square error (ISE), integral absolute error (IAE), integral time square error (ITSE) and integral time absolute error (ITAE). Here, for all there conditions, LQR PID performance indices are listed in Table 5.7 and for proposed PID are listed in Table 5.8. The proposed approach also shows minimum values in all three conditions in comparison to LQR PID [1].

Robustness analysis using input gain and time delay:

Further, robustness analysis is carried out for +20% perturbation for two cases. One is by introducing gain and other is by adding time delay at plant input (u). For first case, effects on CIP when plant input gain decreases and increases are observed, which is shown in Fig. 5.16 and 5.17, respectively. From these figures, it is shown that, proposed controller design has less overshoot in comparison to LQR PID design [1]. For second case, time delay is introduced at plant input and their effects are shown in Fig.5.18, which shows proposed controller design has less overshoot in comparison to LQR PID design[1].

(b) Non-linear interval model:

Further, the non-linear model using (5.64) and (5.67) is considered for three physically possible conditions, i.e., nominal, extreme min δ and extreme max δ. The results of proposed PID are

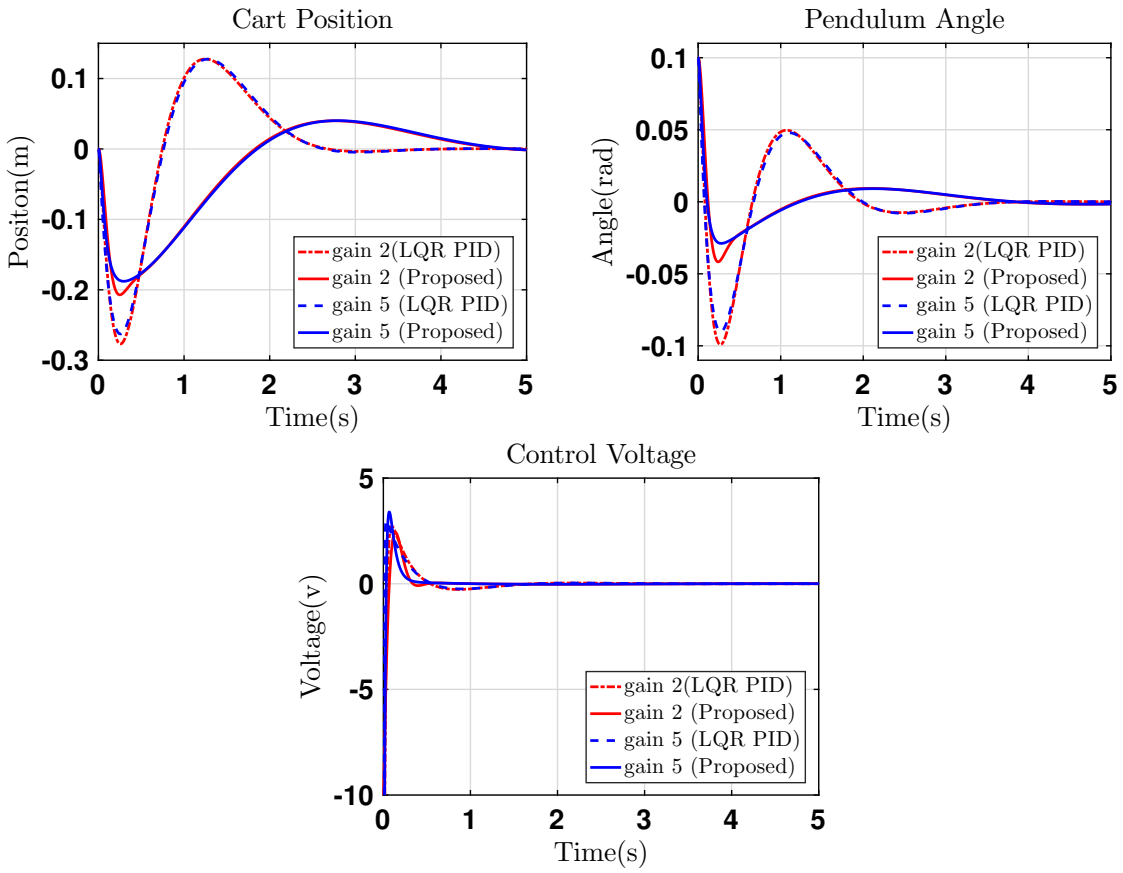

Figure 5.17: Effects of decreasing input gain at +20% perturbed CIP linear model

shown in Fig. 5.19 and it is also compared with LQR PID designed as given in [1] for the initial condition of $\theta = 0.1$ rad pendulum angle. Fig.5.19(a) shows cart position response with less overshoot for all three conditions. Fig. 5.19(b) shows pendulum angle at $\theta = 0$ rad exhibits nil oscillations in all three conditions. Fig. 5.19(c) gives amount of control effort required to stabilize the pendulum vertically, which is less as compared to LQR PID control voltage. Further, integral performance indices such as ISE, IAE, ITSE and ITAE are calculated. For all three conditions, performance indices of LQR PID and proposed PID are listed in Table 5.9 and Table 5.10, respectively. It also shows that the proposed PID design has minimum error values, in all three conditions compared to LQR PID design [1].

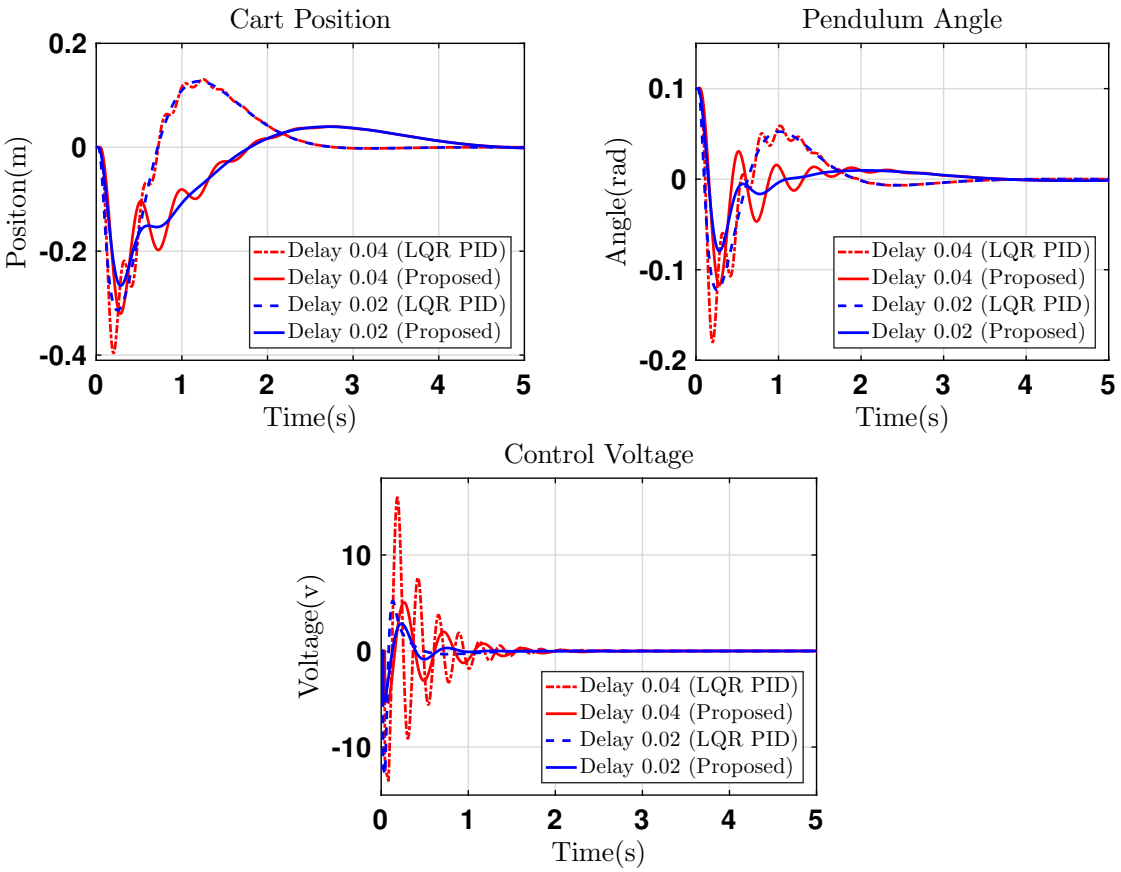

Figure 5.18: Effect of time delay input at +20% perturbed CIP linear model

Table 5.9: Performance indices using LQR PID [1] for non-linear model

Perfor. indices	Nominal values		Min δ		Max δ	
	x	θ	x	θ	x	θ
ISE	0.06048	0.009675	0.09656	0.01505	0.04965	0.008391
IAE	0.3007	0.1104	0.3614	0.1323	0.2771	0.1049
ITSE	0.03526	0.005107	0.05471	0.008522	0.02974	0.004344
ITAE	0.2546	0.08271	0.2866	0.09479	0.2435	0.08103

Table 5.10: Performance indices using proposed PID for non-linear model

Perfor. indices	Nominal values		Min δ		Max δ	
	x	θ	x	θ	x	θ
ISE	0.03908	0.003051	0.04971	0.004829	0.03635	0.00288
IAE	0.2749	0.06315	0.2901	0.08476	0.2713	0.06075
ITSE	0.0233	0.001081	0.02752	0.002406	0.02282	0.001113
ITAE	0.4262	0.06408	0.4431	0.08385	0.4252	0.0623

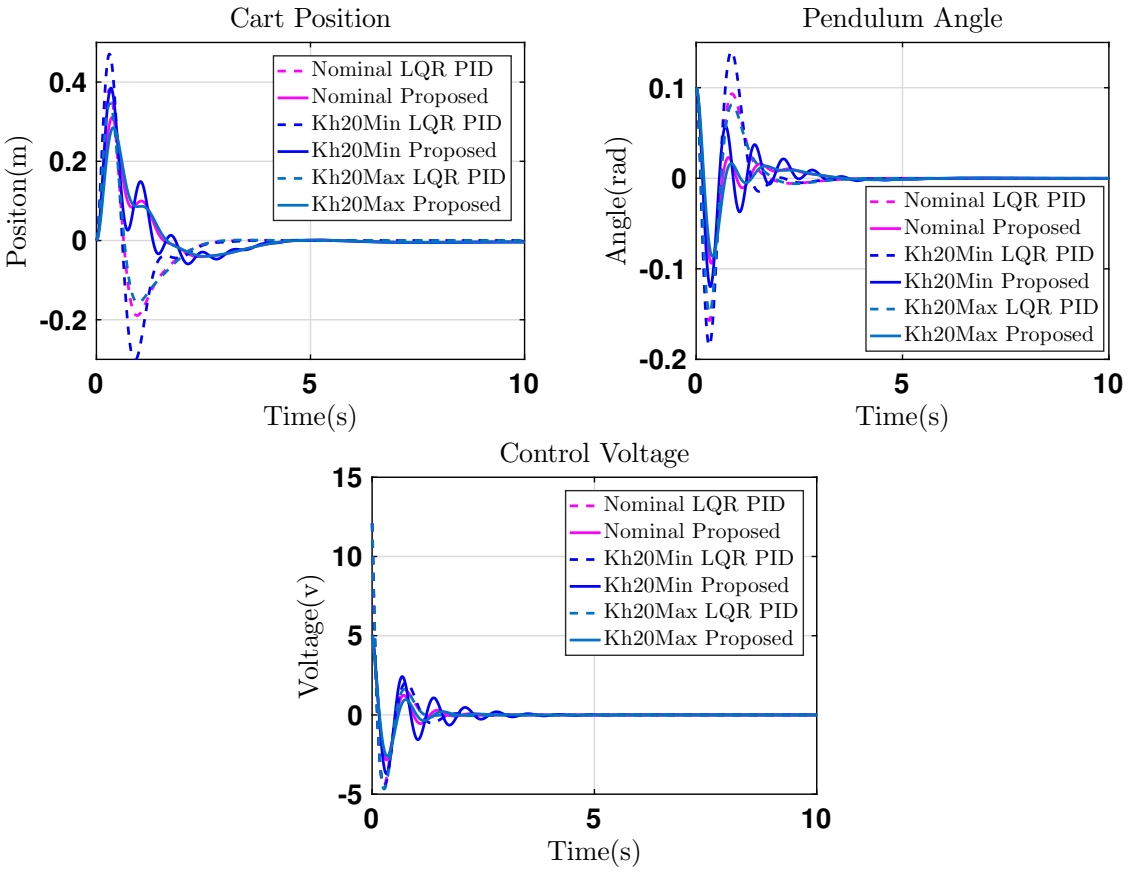

Figure 5.19: Response of non-linear model using LQR PID and Proposed PID

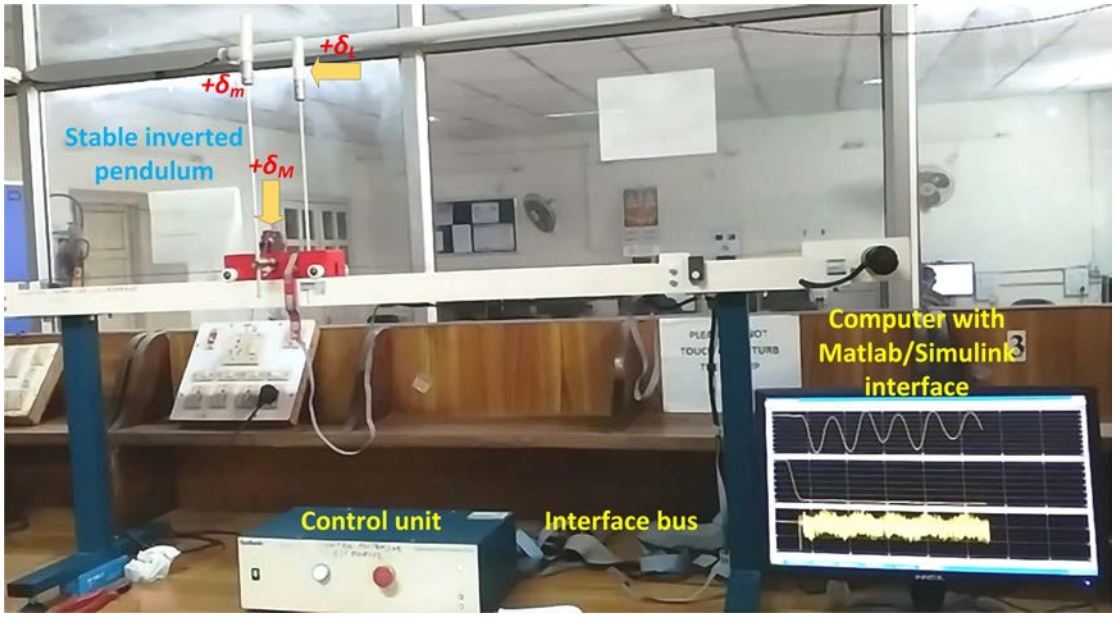

Figure 5.20: Hardware setup with +20% perturbed parameters of CIP system

Table 5.11: Performance indices analysis for proposed PID on hardware setup

Performance indices	Nominal values		Max δ	
	x	θ	x	θ
ISE	0.4408	20.19	0.2309	24.07
IAE	3.24	7.683	2.31	8.769
ITSE	9.479	21.36	4.701	29.9
ITAE	70.08	18.25	49.29	18.8

5.5.1.6 Real time hardware results

The proposed method is also validated on a real time hardware setup of digital cart inverted pendulum system [152], in which two physical conditions are possible, one is nominal and other is extreme $+\delta$ parameters. The hardware setup is shown in Fig. 5.20. Practically, the cart mass($+\delta_M$), pendulum mass ($+\delta_m$) and pendulum length ($+\delta_L$) are externally added AND is shown in Fig. 5.20. The hardware results are obtained by following procedure. In the beginning, pendulum is manually lifted from stable position ($\theta = \pi$) to its stabilization zone at $\theta = \pm 0.2$ rad, from where proposed controller take over to stabilize the pendulum at unstable position ($\theta = 0$). Now two possible conditions can be checked. They are as given below.

In the first condition, performance of pendulum angle (θ), cart position (x) and control voltage(u) have been verified without adding uncertainties. The results are shown in Fig. 5.21. It can be seen that the proposed controller stabilizes pendulum vertically at $\theta = 0$ angle with the minimum control energy. However, small oscillations are observed in cart position.

For second condition, on adding physical uncertainties, $+\delta_M$, $+\delta_m$ and $+\delta_L$, the proposed PID controller stabilizes the perturbed CIP plant. The results are shown in Fig. 5.21. Further, the integral performance indices for both conditions are tabulated in Table 5.11. Hence, proposed controller is robust and stabilizes interval CIP system in both conditions.

5.5.2 Adaptive policy for CIPS

This section describes the working and implementation of the proposed adaptive control logic for CIPS and derives the mathematical update rules for this system.

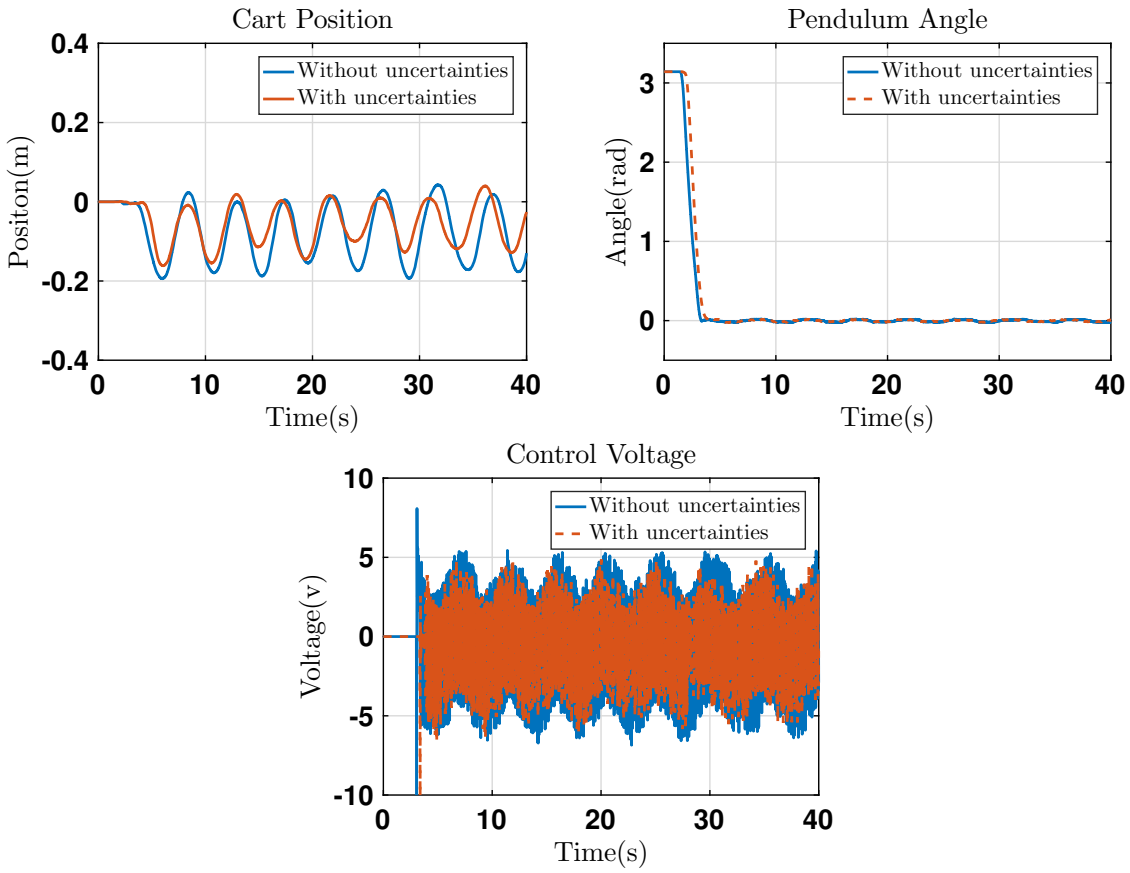

Figure 5.21: Response of proposed PID for nominal and perturbed parameters of CIP system

5.5.2.1 Dynamics of CIPS

CIPS is highly non-linear, unstable, under-actuated and non-minimum phase system [171, 172]. This system exhibits two types of motions-linear and rotational [1, 152]. The linear motion of the cart is in the horizontal direction, while the rotational one is of the pendulum about its hinge. Fig. 5.1 shows the model of CIPS. Parameters of CIPS are shown in Table 5.1. The linearised models are given in (5.8) and (5.10).

Finally, the position control $\frac{x(s)}{F(s)}$ angle control $(\theta(s)/F(s))$ transfer function, has obtained in (5.9) and (5.11), respectively.

5.5.2.2 Design of candidate controllers

The following section describes the design of different candidate controllers, as explained below.

(a) LQR based PID controller [1]:

The first candidate controller is chosen from [1] which is a PID controller. It has been designed using Linear Quadratic Regulator (LQR) and pole placement technique, where the dominant closed-loop poles are obtained from an LQR design. The tuned parameter values of position control PID (C_1^1), are $K_{p1}^1 = 43.3,\ K_{i1}^1 = 33.796,\ K_{d1}^1 = 2.254$. Similarly, for the angle control PID (C_2^1), the tuned controller parameters are $K_{p2}^1 = 120.9,\ K_{i2}^1 = 247.43,\ K_{d2}^1 = 10$.

(b) SBL based PID controller [2, 57]:

The second candidate controller is determined using Stability Boundary Locus approach [57]. Using this approach, two PID controllers are designed. One is for position control (C_1^2) and the other for angle control (C_2^2). The method is briefly explained below.

1) Position control: The closed-loop characteristic equation is written as

$$1 + P_1(s)C_1^2(s) = 0 \tag{5.131}$$

Using $C_1^2(s) = K_{p1}^2 + \frac{K_{i1}^2}{s} + K_{d1}^2 s$, (5.131) can be written as

$$1 + \left(\frac{b_1}{s^2}\right)\left(K_{p1}^2 + \frac{K_{i1}^2}{s} + K_{d1}^2.s\right) = 0 \tag{5.132}$$

Simplification of (5.132) gives,

$$s^3 + b_1 K_{d1}^2 s^2 + b_1 K_{p1}^2.s + b_1 K_{i1}^2 = 0 \tag{5.133}$$

For C_1^2, substituting $s = jw$ in (5.132) gives,

$$b_1 K_{i1}^2 + b_1 K_{p1}^2(j\omega) + b_1 K_{d1}^2(-\omega^2) + j\omega(-\omega^2) = 0 \tag{5.134}$$

Equating real and imaginary parts of (5.134) to zero, the following equations are obtained:

$$b_1 K_{i1}^2 = b_1 K_{d1}^2(\omega^2) \tag{5.135}$$

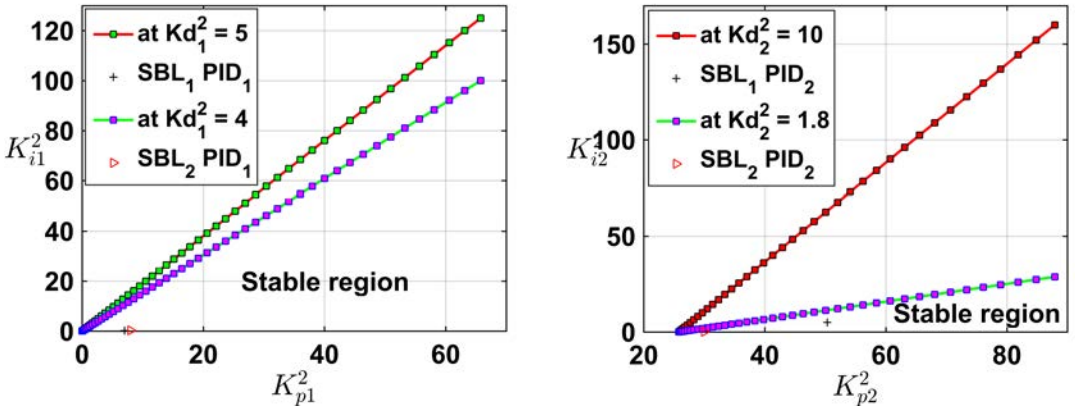

(a) (b)

Figure 5.22: Stability boundary locus for CIP system (a) Cart position control (b) Angle control

and

$$b_1 K_{p1}^2(j\omega) = j\omega(\omega^2) \tag{5.136}$$

For any arbitrarily chosen value of K_{d1}^2, (5.135) and (5.136) can be expressed as,

$$K_{i1}^2 = K_{d1}^2 \omega^2 \tag{5.137}$$

and as physical mass of CIPS $(M_c + m) \neq 0$, $b_1 \neq 0$

$$K_{p1}^2 = \frac{\omega^2}{b_1} \tag{5.138}$$

Taking the values of $K_{d1}^2 = 5$ and $K_{d1}^2 = 4$, and by varying ω in $[0,5]$, SBL plot between K_{p1}^2 and K_{i1}^2 is obtained in Fig. 5.22(a).

2) Angle control: The closed-loop characteristic equation can be written as

$$1 + P_2(s) C_2^2(s) = 0 \tag{5.139}$$

Using (5.11) and $C_2^2(s) = K_{p2}^2 + \frac{K_{i2}^2}{s} + K_{d2}^2 s$, (5.139) can be written as

$$1 + \left(\frac{b_2}{s^2 - a_3}\right)\left(K_{p2}^2 + \frac{K_{i2}^2}{s} + K_{d2}^2 s\right) = 0 \tag{5.140}$$

Further simplification of (5.140) gives,

$$s^3 + b_2K_{d2}^2 s^2 + \left(b_2K_{p2}^2 - a_3\right)s + b_2K_{i2}^2 = 0 \tag{5.141}$$

For C_2^2, substituting $s = jw$ in (5.141) gives,

$$b_2K_{i2}^2 + \left(b_2K_{p2}^2 - a_3\right)(j\omega) + b_2K_{d2}^2(-\omega^2) + j\omega(-\omega^2) = 0 \tag{5.142}$$

Equating real and imaginary parts of (5.142) to zero, equations obtained are:

$$b_2K_{i2}^2 = b_2K_{d2}^2(\omega^2) \tag{5.143}$$

and

$$\left(b_2K_{p2}^2 - a_3\right)(j\omega) = j\omega(\omega^2) \tag{5.144}$$

For any arbitrarily chosen value of K_{d2}^2, (5.143) and (5.144) can be expressed as,

$$K_{i2}^2 = K_{d2}^2\omega^2 \tag{5.145}$$

and since $b_2 \neq 0$, thus

$$K_{p2}^2 = \frac{\omega^2 + a_3}{b_2} \tag{5.146}$$

Using $K_{d2}^2 = 10$ and $K_{d2}^2 = 1.8$, and by varying ω in $[0,1]$, SBL plot between K_{p2}^2 and K_{i2}^2 is obtained in Fig. 5.22(b). Figures 5.22(a) and 5.22(b) consist of two regions separated by the stability boundary locus. Stability of the cart and angle control in these regions can be checked by arbitrarily selecting any value from the two regions. Here, it is found that the values K_{d1}^2 and K_{d2}^2 from the region give stable response. Thus, by selecting any arbitrarily values from the stable regions of the plots Figure 5.22(a) and 5.22(b), PID parameters for C_1^2 and C_2^2 can be obtained. Two values, one from Fig. 5.22(a) and the other from Fig. 5.22(b), are selected arbitrarily from the large stability regions of the respective plots, as shown with marker '+'in Fig.5.22(a) and Fig.5.22(b). For these values, PID parameters are obtained[2] for C_1^2 as $K_{p1}^2 = 6.9964$, $K_{i1}^2 = 0.2$ and $K_{d1}^2 = 5$; and for C_2^2 , $K_{p2}^2 = 50.3294$, $K_{i2}^2 = 5$ and $K_{d2}^2 = 10$.

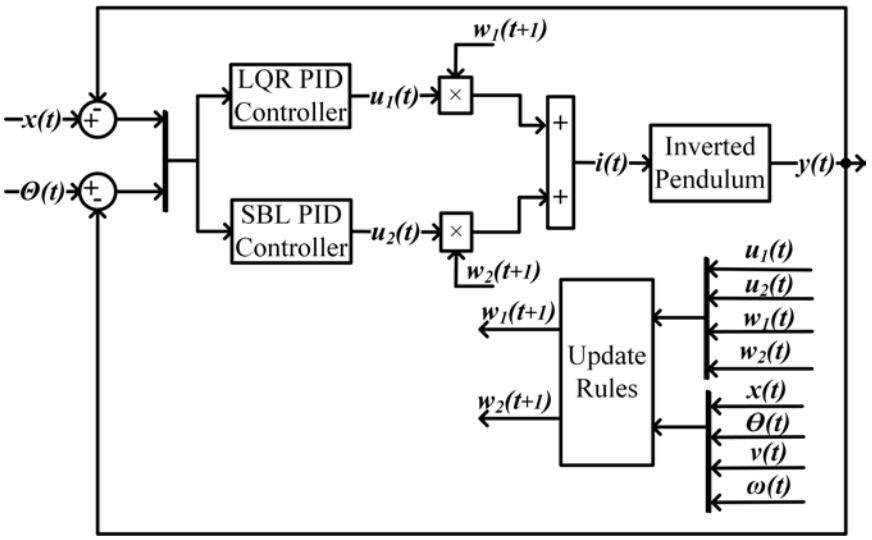

Figure 5.23: Block diagram of proposed adaptive control technique for CIPS

5.5.2.3 Implementation of Adaptive policy

Fig. 5.23 shows the block diagram of the proposed adaptive control logic technique for CIPS. In this figure, the output $y(t)$ involves cart position $(x(t))$ and pendulum angle $(\theta(t))$.The states are identified as $x(t)$, $\theta(t)$, $v(t)$, $\omega(t)$, and $w(t+1)$ where, $v(t)$ is cart velocity, $\omega(t)$ is angular velocity of pendulum and $w(t+1)$ implies future time value of the weight. In the following section, we derive the update rules for CIPS.

Equations of motion:

By summing up all the forces acting on the CIPS in the horizontal direction, the equation of rectilinear motion can be written as:

$$(M_c+m)\frac{d^2x}{dt^2}+b\frac{dx}{dt}+ml\cos\theta\frac{d^2\theta}{dt^2}-ml\frac{d^2\theta}{dt^2}\sin\theta=F(t) \tag{5.147}$$

The equation for curvilinear motion is obtained by considering forces perpendicular to the pendulum axis and can be written as:

$$(J+ml^2)\frac{d^2\theta}{dt^2}+mgl\sin\theta=-ml\cos\theta\frac{d^2x}{dt^2} \tag{5.148}$$

Further, for performing experimental analysis on hardware setup [152], a conversion factor of DC motor gain equal to 15 is multiplied [1]. Therefore, after linearisation at equilibrium point $\theta=0$,

and $b, \zeta \approx 0$, (5.147) and (5.148) can be expressed as:

$$(M_c + m)\frac{d^2x}{dt^2} + ml\frac{d^2\theta}{dt^2} = u_n(t) \tag{5.149}$$

$$(J + ml^2)\frac{d^2\theta}{dt^2} - mgl\theta = -ml\frac{d^2x}{dt^2} \tag{5.150}$$

From Fig. 5.23, plant input can be written as

$$i(t) = u_1(t)w_1(t) + u_2(t)w_2(t) \tag{5.151}$$

Using (5.149), (5.150), (5.151) and substituting system parameter values from Table 5.1, update rules for weights $w_1(t)$ and $w_2(t)$ are derived in the following section.

Formulation of update rules using online gradient descent algorithm:

Let us first define the objective function, which needs to be optimized. To control CIPS, we need to minimize errors $(e(t))$ in the pendulum angle (θ) and the cart position (x). Therefore, the objective function to control CIPS can be written as:

$$e(t) = \int_0^\infty (\theta^2(t) + x^2(t))dt \tag{5.152}$$

where, $\theta(t)$ is the pendulum angle, measured from the reference angle $(\theta_r = 0)$ at time 't'and $x(t)$ is the cart position, measured from the reference cart position $(x_r = 0)$ at time 't'. The weight update rules for the CIPS can be written as:

$$w_1(t+1) \leftarrow \left[w_1(t) - \alpha\frac{\partial e(t)}{\partial w_1(t)}\right] \tag{5.153}$$

$$w_2(t+1) \leftarrow \left[w_2(t) - \alpha\frac{\partial e(t)}{\partial w_2(t)}\right] \tag{5.154}$$

Using (5.152) and the chain rule of derivative, $\frac{\partial e(t)}{\partial w_1(t)}$ and $\frac{\partial e(t)}{\partial w_2(t)}$ can be expressed as,

$$\frac{\partial e(t)}{\partial w_1(t)} = \frac{\partial e(t)}{\partial \theta(t)}\frac{\partial \theta(t)}{\partial i(t)}\frac{\partial i(t)}{\partial w_1(t)} + \frac{\partial e(t)}{\partial x(t)}\frac{\partial x(t)}{\partial i(t)}\frac{\partial i(t)}{\partial w_1(t)} \tag{5.155}$$

$$\frac{\partial e(t)}{\partial w_2(t)} = \frac{\partial e(t)}{\partial \theta(t)}\frac{\partial \theta(t)}{\partial i(t)}\frac{\partial i(t)}{\partial w_2(t)} + \frac{\partial e(t)}{\partial x(t)}\frac{\partial x(t)}{\partial i(t)}\frac{\partial i(t)}{\partial w_2(t)} \tag{5.156}$$

From (5.149) and (5.150),we get two transfer functions, one is control voltage $u_j(t)$ to angle $\theta(t)$, which is written as,

$$u_j(t) = (M_c + m)g\theta(t) - \left(\frac{\sigma}{ml}\right)\frac{d^2\theta(t)}{dt^2}(j = 1,2) \tag{5.157}$$

$$\frac{du_j(t)}{d\theta(t)} = (M_c + m)g - \left(\frac{\sigma}{ml}\right)\frac{d^3\theta(t)}{dt^3}\Big/\frac{d\theta(t)}{dt} \tag{5.158}$$

and other is angle $\theta(t)$ to position $x(t)$. Using chain rule $\frac{du(t)}{dx(t)} = \frac{du(t)}{d\theta(t)}\frac{d\theta(t)}{dx(t)}$, so, (5.150) becomes,

$$\frac{d\theta(t)}{dx(t)} = \frac{\left[(J + ml^2)\frac{d^3\theta(t)}{dt^3} + ml\frac{d^3x(t)}{dt^3}\right]}{(mgl\frac{dx(t)}{dt})} \tag{5.159}$$

So, at every time instant 't', using (5.151), (5.152), (5.158) and (5.159) the weights $w_1(t)$ and $w_2(t)$ are updated. Therefore, (5.153) and (5.154) can be written as,

$$w_1(t+1) \leftarrow \left[w_1(t) - \alpha u_1(t)\left(\frac{2\theta(t)}{\frac{du_1(t)}{d\theta(t)}} + \frac{2x(t)}{\frac{du_1(t)}{d\theta(t)}\frac{d\theta(t)}{dx(t)}}\right)\right] \tag{5.160}$$

$$w_2(t+1) \leftarrow \left[w_2(t) - \alpha u_2(t)\left(\frac{2\theta(t)}{\frac{du_2(t)}{d\theta(t)}} + \frac{2x(t)}{\frac{du_2(t)}{d\theta(t)}\frac{d\theta(t)}{dx(t)}}\right)\right] \tag{5.161}$$

where, α is the learning rate.

To summarize, the following steps are to be followed for implementing the proposed logic are given below,

- Initialize w_1, w_2 and α to one and obtain inputs $u_1(t)$ and $u_2(t)$ from Fig. 5.23.
- Using (5.152), define the performance indices to be minimized.
- Calculate $\frac{\partial e(t)}{\partial w_1(t)}$, and $\frac{\partial e(t)}{\partial w_2(t)}$ using (5.155) and (5.156) respectively.
- Use the calculated values of $\frac{\partial e(t)}{\partial w_1(t)}$, and $\frac{\partial e(t)}{\partial w_2(t)}$ to update the weights $w_1(t+1)$, and $w_2(t+1)$ for next iteration, as per (5.160) and (5.161) respectively.

5.5.2.4 Simulation results and analysis

The analysis of CIPS (for parameter values, refer to Table 5.1) with the proposed control logic and the individual controllers is carried out using simulation in the MATLAB© and Simulink environment. Based on this analysis, the comparative conclusions are also drawn. The results are obtained for $\alpha = 1$ and initial angle 0.1 rad which are discussed below.

Case 1: In absence of disturbance

The trajectories of the cart's position (x), pendulum angle (θ) and control signal (u) are obtained in Fig. 5.24. Referring to this figure on cart position, it can be seen that with LQR-PID[1], the rise time and settling time are less, but at the cost of increased deviation with respect to the steady-state value. On the other hand, the response begins with a slower start, with reduced deviation from the steady-state value, but takes a longer time to settle, when controlled with SBL-PID[2]. Hence, comparing the responses with two individual controllers, in terms of rise time and settling time, LQR-PID[1] performs better, while SBL-PID[2] rules over LQR-PID[1] when it comes to the peak deviations from the steady-state value. Similar result can be observed from the response of the pendulum's angle. Now, coming to the system's response with the proposed logic, starting with the cart's position with time, the curve almost matches that with the one with LQR-PID[1]. Next, in terms of the peak deviations from the steady-state value, if the figure is observed closely, it can be seen that the magnitudes of the deviations are smaller than that with LQR-PID[1], and comparable with that achieved using SBL-PID[2]. Progressing further ahead in time, the response with proposed logic settles almost as quick as the response with LQR-PID[1]. Thus, summarizing the description on the traversal of the curve, the proposed logic assigns more weight to w_1, then to w_2, and lastly to w_1 again, in order to resemble the behaviour of the system with LQR-PID[1] at first, following by SBL-PID[2] and LQR-PID[1] till the response settles.

Same conclusion can be drawn from the trajectory of the pendulum's angle. The more interesting point can be seen from the profile of the control signal, where the peak control voltage lies within that using LQR-PID[1], thus implying that the performance is improved but not at the cost of excess control energy. The weight update profile for this operating condition is shown in Fig. 5.25.

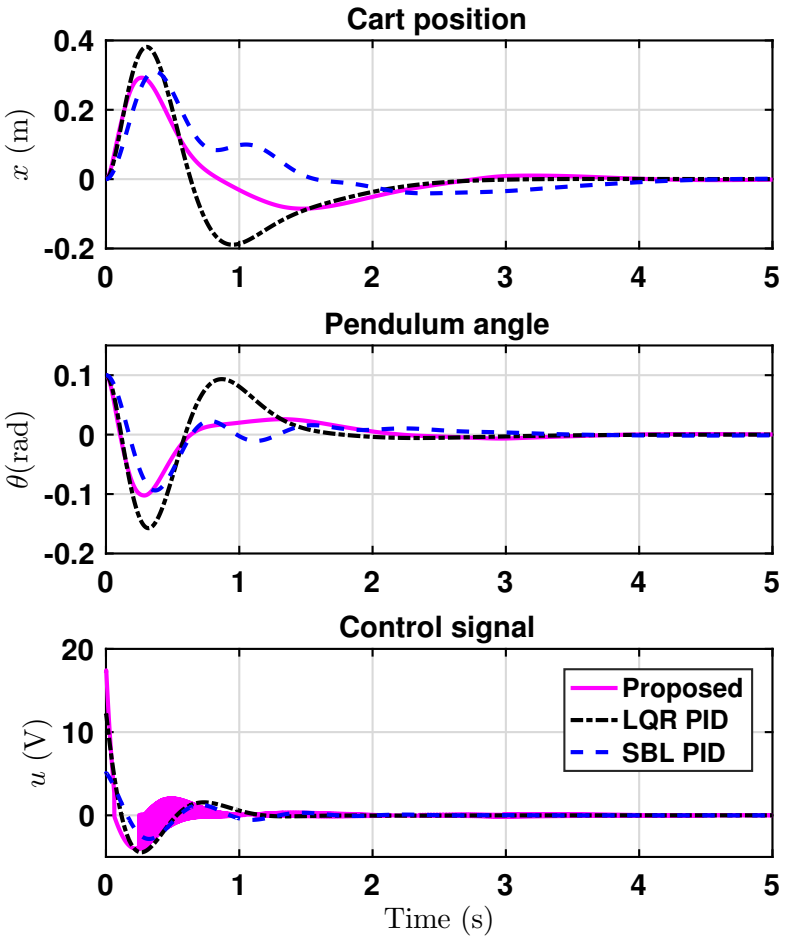

Figure 5.24: Time domain responses without disturbance

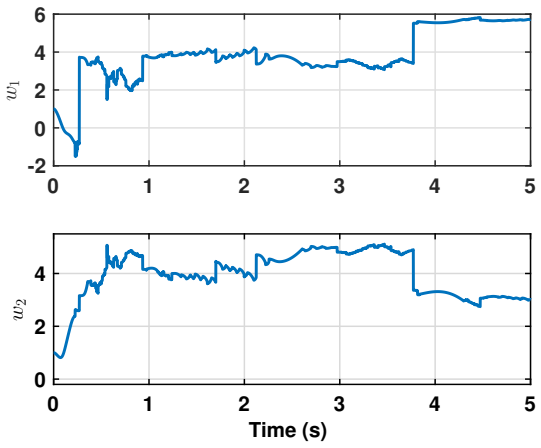

Figure 5.25: Weights w_1, w_2 responses without disturbance

Case 2: In presence of disturbance

The disturbance profile used is a white Gaussian noise with power intensity 0.01, seed value 23341 at sample time 0.001 sec. is used to mimic the external disturbances in real-time. Fig. 5.27 shows the disturbance profile, which is applied to plant input.

In previous case, the performance analysis is done with the nominal system model. Now a fabricated disturbance (the profile is shown in Fig. 5.27(a)) is introduced in the input channel for the entire period of the simulation. The performance of the system under this condition is analysed via Fig. 5.26, with respect to the three different control strategies. The responses of x and θ in this figure resemble to that of Fig. 5.24, if the small bumps caused by the input channel disturbance are omitted. Referring to the weight assignment profile under this condition, the close resemblance to the update of weights when analysed using the nominal model (given in Fig. 5.25) proves that the proposed adaptive logic assigns more value to w_1, then w_2, and lastly to w_1 again, till the settling point is reached. The reason behind this kind of operation of the proposed logic is explained as follows, with reference to Fig. 5.27(b). As the process begins, with LQR-PID[1], rise time is comparatively lesser than with SBL-PID[2], so LQR-PID[1] appears to be the best out of the two, during this span of time. As time progresses, LQR-PID[1] causes larger cart position deviations about $x = 0$, in comparison with that caused by SBL-PID[2]. Hence adaptive logic allots more weight to w_2 to prioritize SBLPID over LQRPID[1], therefore it shows minimum oscillation across cart. After $t = 2$ seconds, x, when controlled by LQR-PID[1] alone, settles down quicker than when controlled by SBL-PID[2] only. Therefore, proposed adaptive logic assigns more weight to LQR-PID[1] to obtain desired performance.

Case 3: Change in input gain:

In this case, the plant input is amplified and attenuated with time (as shown in Fig. 5.28 to 5.30), to analyse the system performance under faulty operation of the actuator, thus supplying the plant with tampered actuated signal. Assuming this situation, the stabilization of the same CIPS is achieved using the three control strategies. The plots of x and θ, when controlled by the respective control strategies, are shown in Fig. 5.29. Studying this figure, it can be observed that, if the actuator signal is attenuated by a factor of 0.4, then the system stability fails, under the influence of LQR-PID[1] alone, but not, when it is SBL-PID[2]. So the best of the two for this situation is SBL-PID[2], and more value should be assigned to w_2 so that the proposed logic behaves like

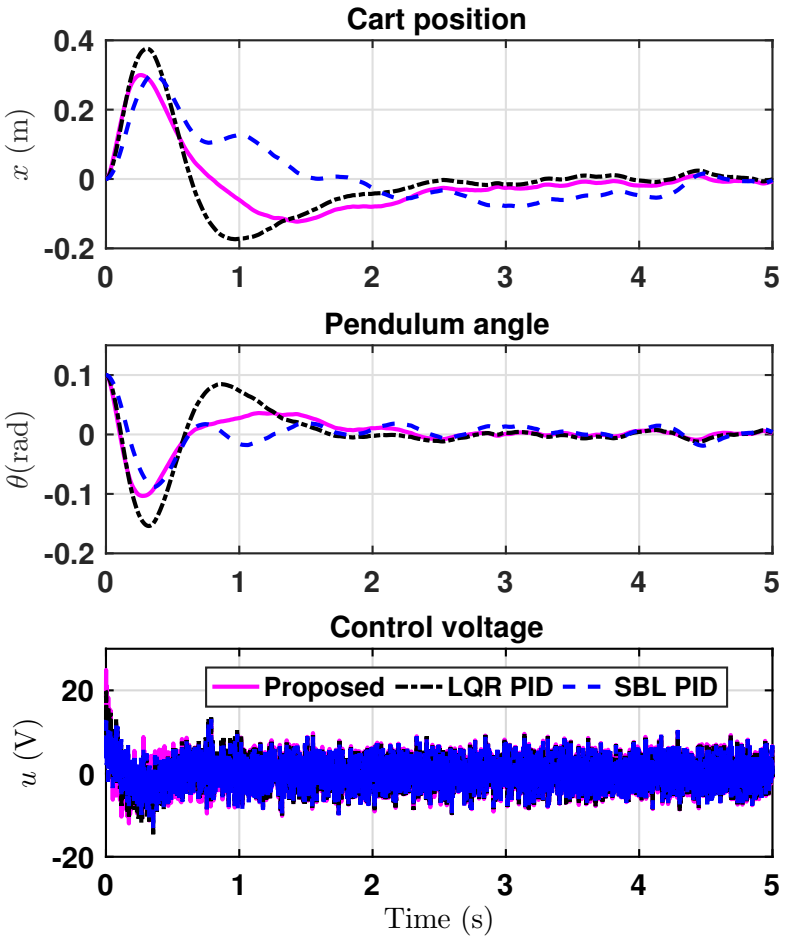

Figure 5.26: Time domain responses in presence of disturbance

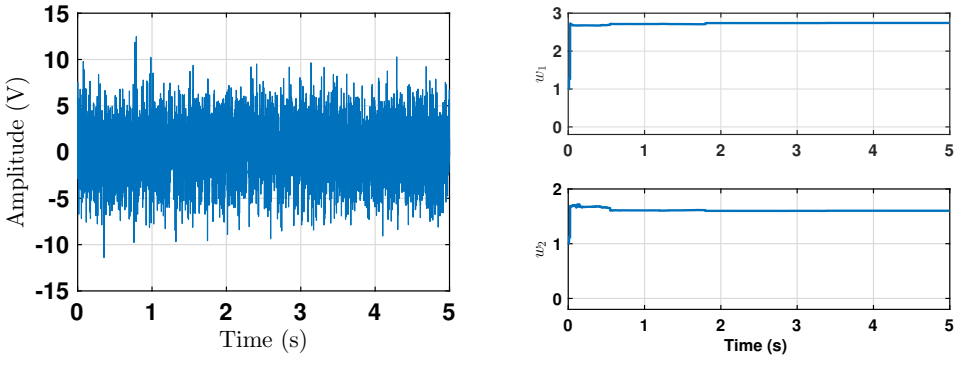

(a) (b)

Figure 5.27: Input Gaussian disturbance and weight response

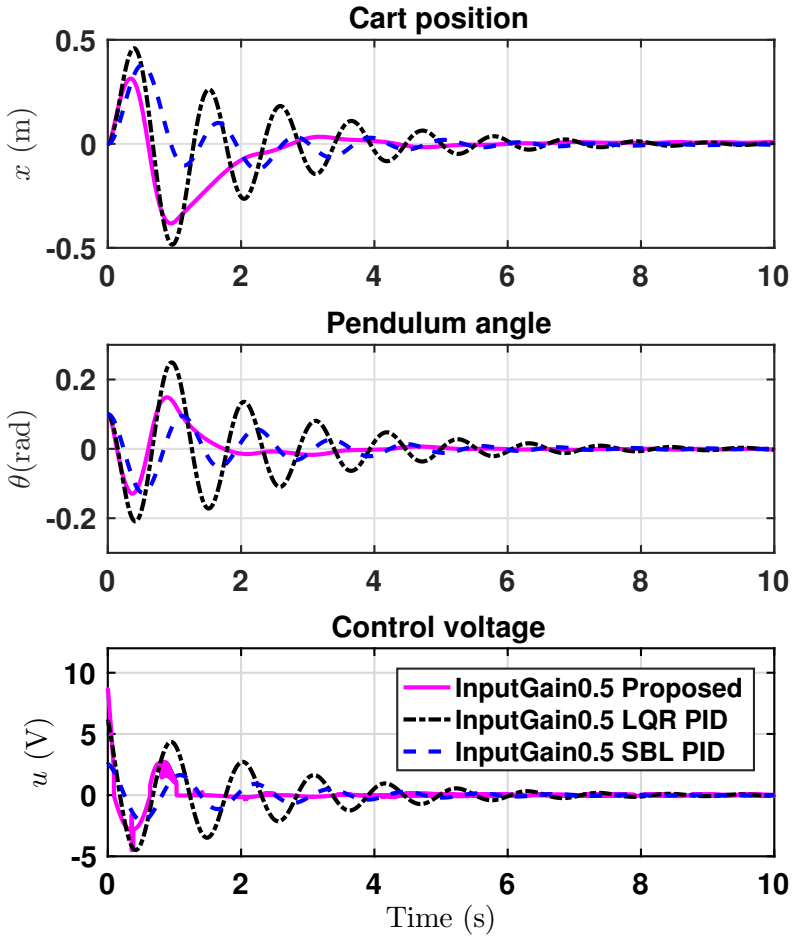

Figure 5.28: Time domain responses as input gain decreases to 0.5

this controller. This can be confirmed from the same figure, where it is evident that the system is stabilized using the proposed logic. This also proves the efficacy of the proposed control law, that the overall controller output can be maintained stable, despite having some candidate controllers unstable under certain circumstances. Furthermore, the system is also tested with increment in input gain 2. Referring to Fig. 5.30, it can be concluded that, although the increasing input gain hinders the appropriate working of the adaptive weight assignment process, however, the gain sensitivity is improved compared to both the candidate controllers, at different instants of time.

Case 4: Introduction of input time delay

In this case, an intentional time delay of 0.02 second is introduced in the input channel of the plant, to analyse the performance using the proposed logic in presence of input time delays. The system's performance under this operating condition is depicted in Fig. 5.31. By observing this figure, it is

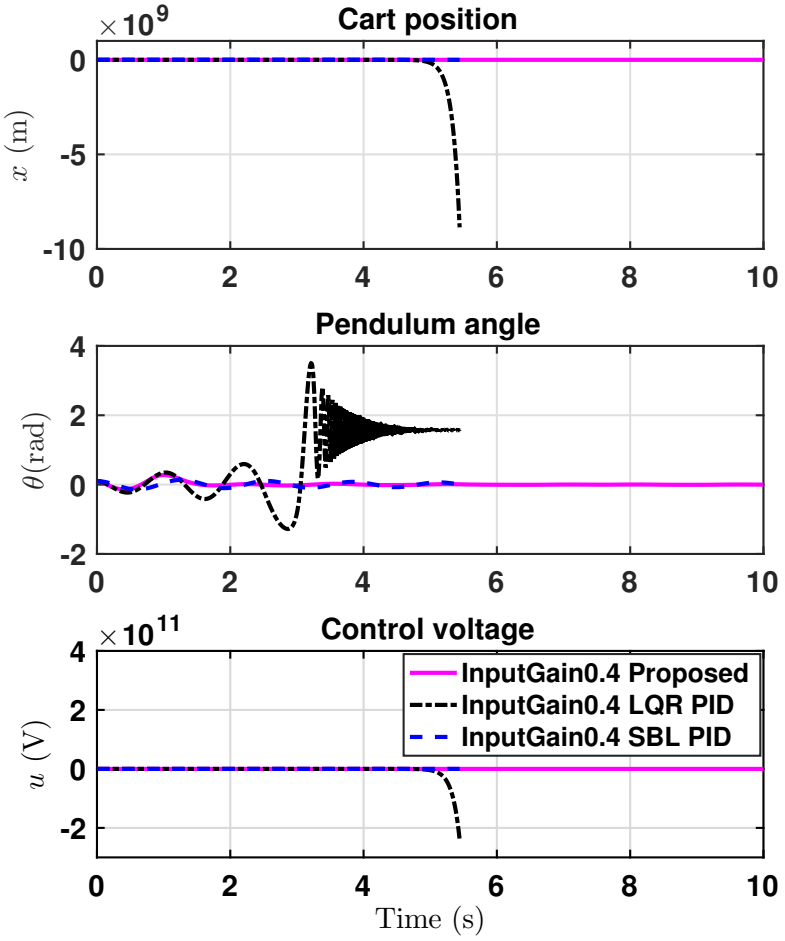

Figure 5.29: Time domain response as input gain decreases to 0.4

Table 5.12: Integral performance indices for CIPS using proposed approach

Perf. Indices	Without disturbance		With disturbance		Decreasing gain 0.5		Increasing gain 2		Input dealy 0.02	
	x	θ	x	θ	x	θ	x	θ	x	θ
ISE	0.03209	0.00342	0.04105	0.00404	0.12052	0.01335	0.03265	0.00286	0.05070	0.00687
IAE	0.23286	0.07099	0.34825	0.10043	0.53579	0.15935	0.24850	0.07304	0.27425	0.09334
ITSE	0.01754	0.00149	0.03531	0.00302	0.11879	0.01041	0.02204	0.00172	0.03045	0.00281
ITAE	0.29455	0.07949	0.78425	0.24678	0.85672	0.21373	0.28624	0.08376	0.30002	0.08560

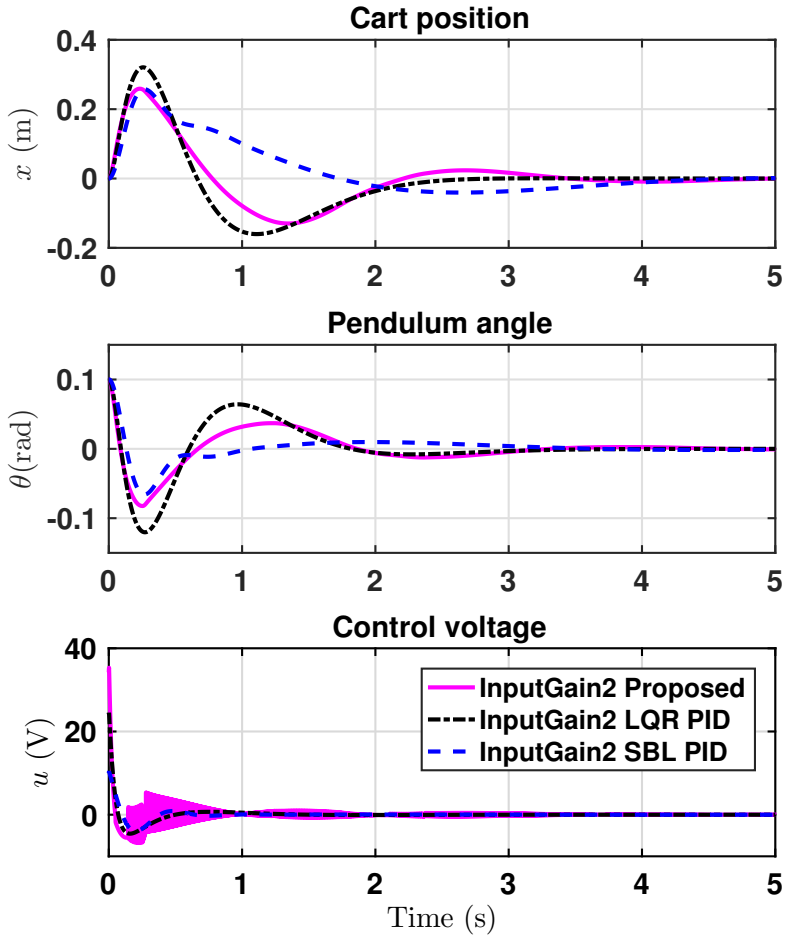

Figure 5.30: Time domain responses as input gain increases to 2

Table 5.13: Integral performance indices for CIPS using LQR PID[1] controller

Perf. Indices	Without disturbance		With disturbance		Decreasing gain 0.5		Increasing gain 2		Input delay 0.02	
	x	θ	x	θ	x	θ	x	θ	x	θ
ISE	0.06045	0.00967	0.05946	0.00926	0.19118	0.05046	0.04759	0.00605	0.06696	0.01133
IAE	0.30073	0.11033	0.36323	0.13945	0.79867	0.42657	0.27362	0.09457	0.30590	0.11736
ITSE	0.03525	0.00510	0.04064	0.00627	0.23182	0.06887	0.03012	0.00336	0.03593	0.00541
ITAE	0.25481	0.08263	0.68697	0.29755	1.64569	0.92324	0.23900	0.07968	0.25487	0.08487

evident that the curve of $x(t)$ and $\theta(t)$ experience slight oscillatory behaviour, inherited from the SBL-PID's nature, but makes up to the performance using LQR-PID[1], as time approaches the settling time.

Moreover, performances of all these three cases are compared using integral performance indices, such as integral square error (ISE), integral absolute error (IAE), integral time square error (ITSE)

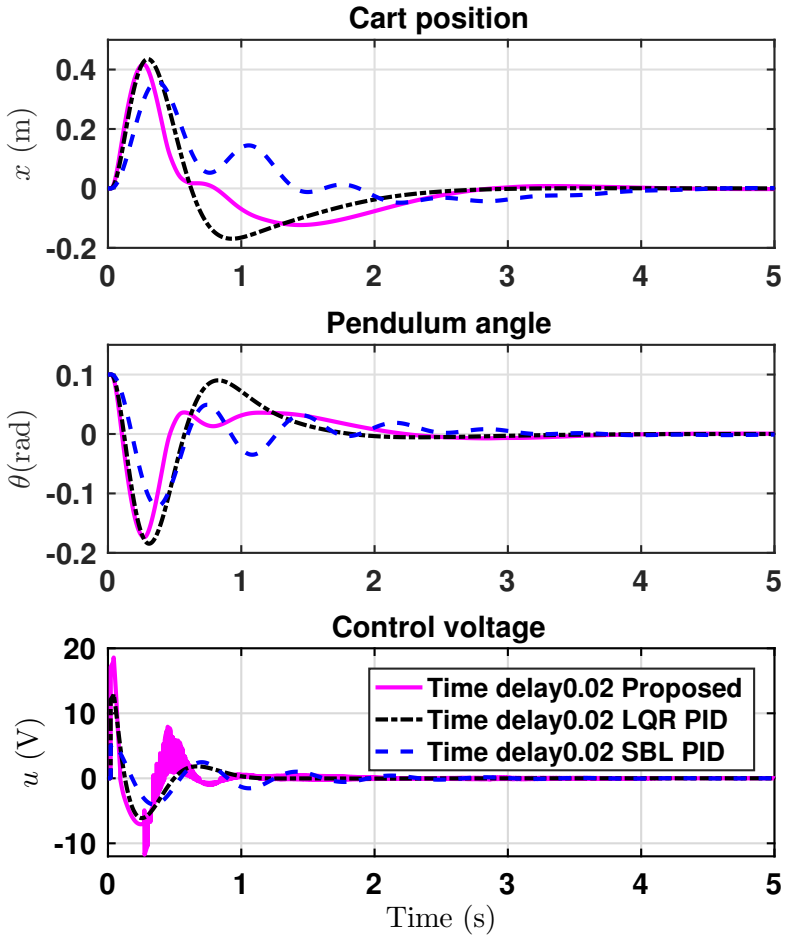

Figure 5.31: Time domain responses with time delay 0.02 sec

Table 5.14: Integral performance indices for CIPS using SBL PID[2] controller

Perf. Indices	Without disturbance		With disturbance		Decreasing gain 0.5		Increasing gain 2		Input dealy 0.02	
	x	θ	x	θ	x	θ	x	θ	x	θ
ISE	0.03908	0.00305	0.04706	0.00342	0.06936	0.01109	0.03287	0.00154	0.04613	0.00494
IAE	0.27492	0.06315	0.42547	0.11335	0.40018	0.18577	0.27538	0.04583	0.28306	0.08396
ITSE	0.02330	0.00118	0.06212	0.00559	0.05685	0.01166	0.02135	0.00053	0.02716	0.00230
ITAE	0.42619	0.06408	1.26629	0.42233	0.71799	0.35113	0.44557	0.05557	0.42451	0.08183

and integral time absolute error (ITAE), for more clarification. Table 5.12, 5.13, and 5.14 represent the performance indices of the proposed adaptive logic, LQR PID[1] and SBL PID[2], respectively.

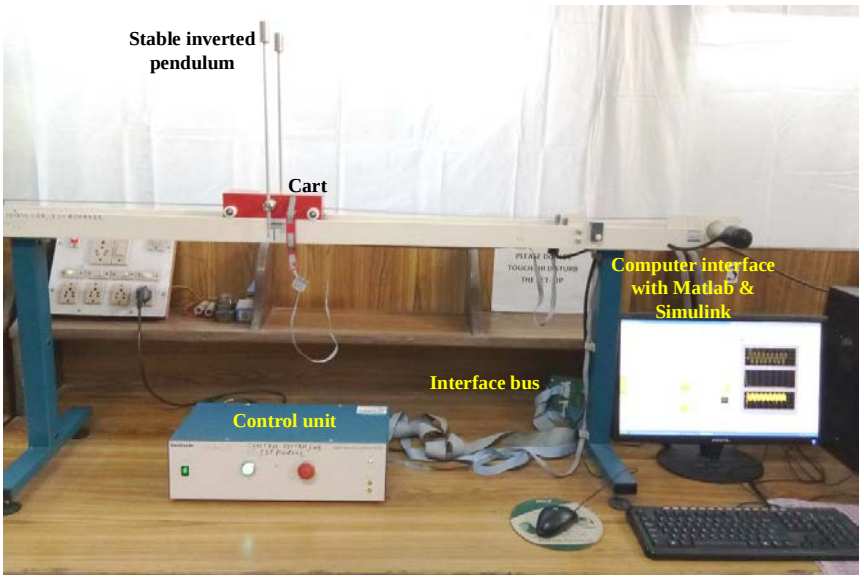

Figure 5.32: Experimental setup of CIPS

5.5.2.5 Real-Time experimental results

A Real-Time experimental hardware setup of CIPS, developed by the Feedback Instruments, is used to prove and extend the applicability of the proposed adaptive control strategy in real-world engineering applications. Assuming a unity input gain, Fig. 5.32 shows the experimental setup of CIPS. The proposed adaptive logic and both candidate controllers are implemented using MATLAB© and Simulink, which is interfaced with the control unit of the hardware setup. Initially, pendulum is lifted up to the stabilization zone, i.e., $\theta = 0.2$ rad, and then the control action starts which stabilizes it in a vertical direction by sending the appropriate control signal. Two situations-without and with external disturbances-are considered in the following two cases:

Case 1: Without external disturbances:

In Fig. 5.33, it is shown that the proposed adaptive logic has extracted the best feature of each candidate controller which stabilized pendulum effectively in comparison to individual candidate controller LQR PID[1] and SBL PID[2] controller. This is verified by determining performance indices which are shown in Table 5.15. Thus, from this table, it is concluded that the proposed controller outperforms the individual candidate controllers. The change in weights w_1 and w_2 with time is shown in Fig. 5.34.

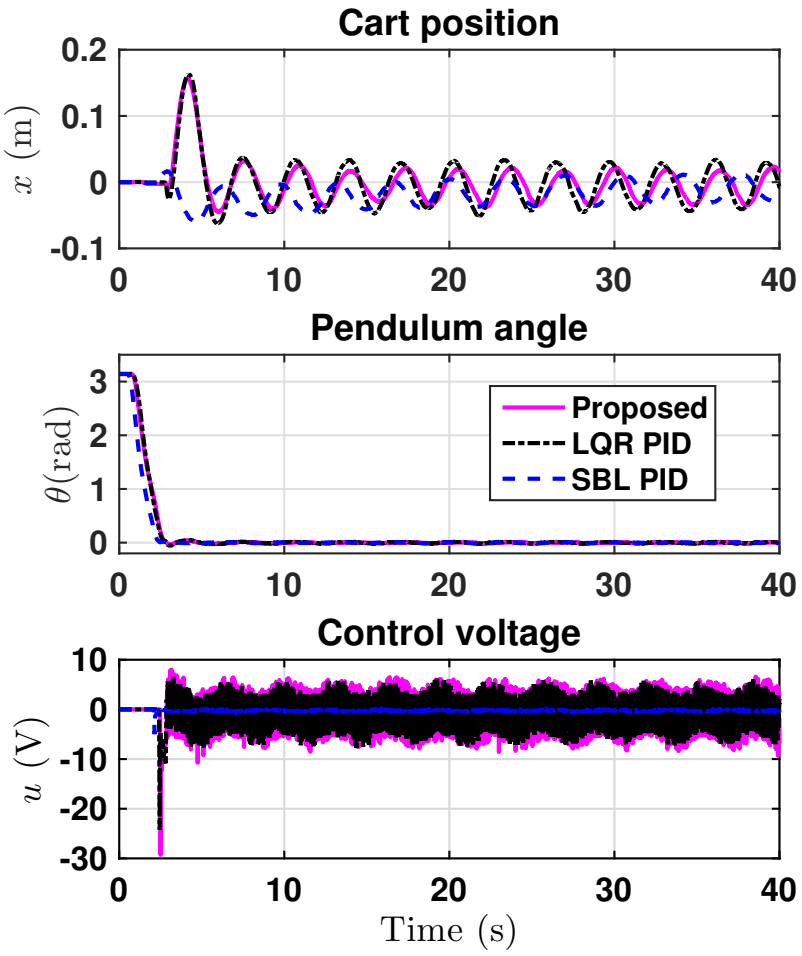

Figure 5.33: Performance of the hardware setup using the proposed method, LQR PID and, SBL PID in absence of external disturbances

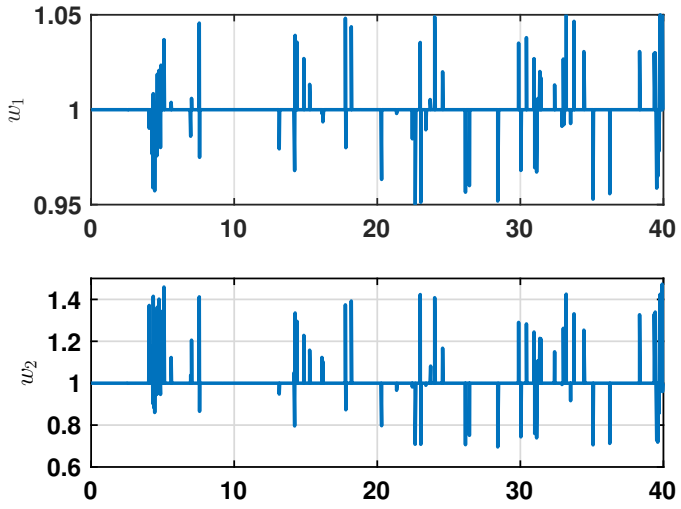

Figure 5.34: Variations of w_1, w_2 with time during the experimental validation

Table 5.15: Performance indices of experimental CIPS for various controllers

Perf. Indices	Proposed		LQR PID		SBL PID	
	x	θ	x	θ	x	θ
ISE	0.146114578	14.95432964	0.053774928	14.08492555	0.369564756	15.73201068
IAE	1.857065971	6.271232529	1.083638613	5.720373892	3.017500154	6.192373645
ITSE	2.185765629	12.22071198	0.702349346	10.7293046	7.314059263	13.12570964
ITAE	36.15661772	17.29642657	20.03770789	12.35830865	62.67149012	14.63843352

Case 2: With external disturbances:

Applying manually a small perturbation to the CIPS at $t = 20$ seconds and again at $t = 30$ seconds. The real-time experimentation is carried out in presence of these disturbances.

In Fig. 5.35, it is clear that the sudden effect of disturbances at $t = 20$ and $t = 30$ seconds are alleviated swiftly by means of the proposed adaptive control logic, thereby proving its effectiveness in presence of external disturbances. The corresponding variation in weights during the entire stabilization process is shown in Fig. 5.36.

5.5.3 Modified adaptive policy for CIPS

From (5.149), (5.150), $z(t) = [x\ \theta]^T(t)$. The objective function is chosen to be $J_o(t)$. Following from (5.153) and (5.155), and also (5.149) and (5.150), the weight update rule for updating each weight $w_i(t)$ of $w_c(t)$, for the CIPS is obtained as follows:

$$w_i(t+1) = w_i(t) - \alpha u_i(t) \left(\frac{2\theta(t)}{\frac{du_i(t)}{d\theta(t)}} + \frac{2x(t)}{\frac{du_i(t)}{d\theta(t)} \frac{d\theta(t)}{dx(t)}} \right) \tag{5.162}$$

where $i = 1, 2$, and $u_i(t)$ represent the output signal of each individual state's controller.

Note: For handling the flat spots, the weights are updated where λ is taken to be 0.9.

5.5.3.1 Stability analysis of modified approach

The system's stability analysis is carried out by using Corollary I of [161]. Following from this corollary, for a particular candidate controller $C_k(s)$, the closed-loop characteristic equation is $1 + \sum_{i=1}^{p} C_{ki}(s) G_i(s) = 0$. The systems $G_i(s)(i = 1, 2)$ are control-to-position and control-to-angle

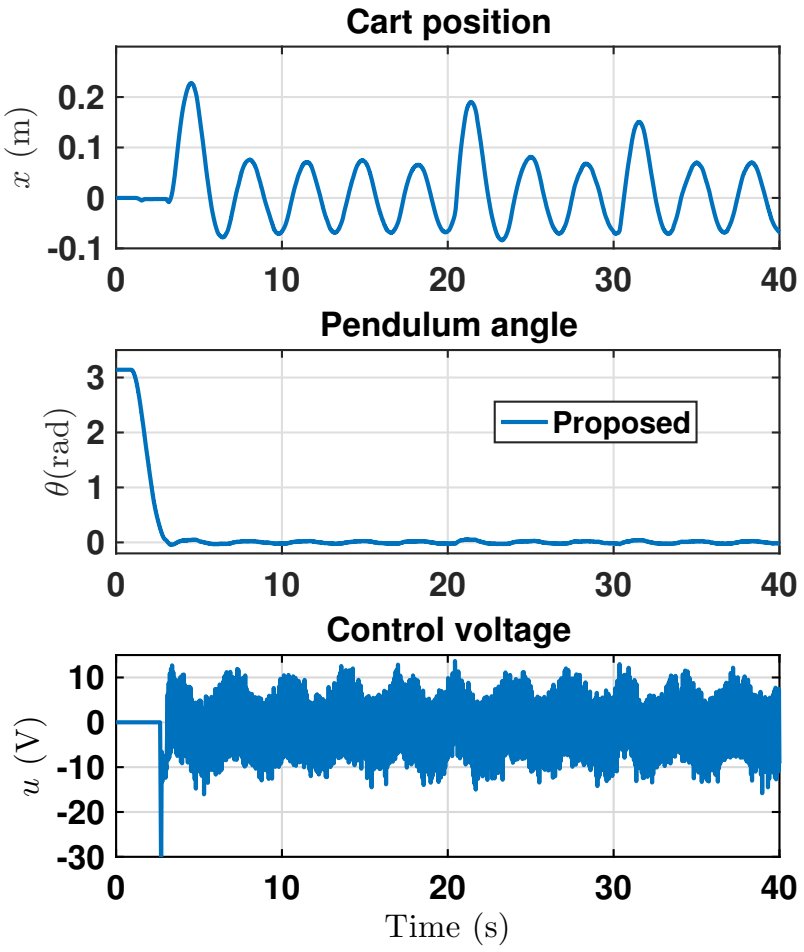

Figure 5.35: Experimental analysis of hardware setup in presence of external disturbances

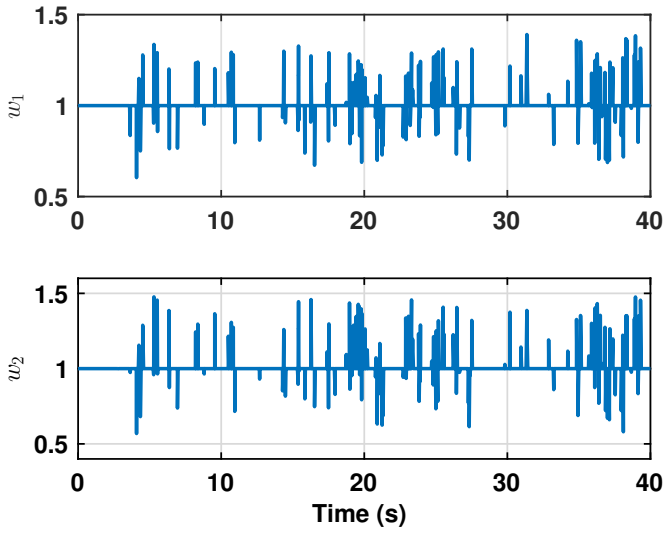

Figure 5.36: Weight update profile during experimental analysis in presence of external disturbances

transfer functions respectively. Hence, for the system under consideration, the characteristic equation is represented as follows:

$$s^5 + \delta_4 s^4 + \delta_3 s^3 + \delta_2 s^2 + \delta_1 s + \delta_0 = 0 \tag{5.163}$$

where,

$$\begin{aligned}
\delta_4 &= \left(-K_{d11} w_1 - K_{d21} w_2\right) b_1 + b_2 \left(K_{d12} w_1 + K_{d22} w_2\right) \\
\delta_3 &= \left(-K_{p11} w_1 - K_{p21} w_2\right) b_1 + b_2 K_{p12} w_1 + K_{p22} b_2 w_2 - a_2 \\
\delta_2 &= \left(\left(K_{d11} a_2 - K_{i11}\right) w_1 - w_2 \left(-K_{d21} a_2 + K_{i21}\right)\right) b_1 \\
&\quad + b_2 \left(K_{i12} w_1 + K_{i22} w_2\right) \\
\delta_1 &= a_2 b_1 \left(K_{p11} w_1 + K_{p21} w_2\right) \\
\delta_0 &= a_2 b_1 \left(K_{i11} w_1 + K_{i21} w_2\right)
\end{aligned}$$

The Routh array for (5.163) is obtained in equation (5.164).

$$\begin{array}{lccc}
s^5 & 1 & \delta_3 & \delta_1 \\
s^4 & \delta_4 & \delta_2 & \delta_0 \\
s^3 & \dfrac{\delta_4\delta_3 - \delta_2}{\delta_4} & \dfrac{\delta_4\delta_1 - \delta_0}{\delta_4} & 0 \\
s^2 & \dfrac{\gamma_1\delta_2 - \delta_4\gamma_2}{\gamma_1} & \dfrac{\gamma_1\delta_0 - 0}{\gamma_1} & 0 \\
s^1 & \dfrac{\beta_1\gamma_2 - \gamma_1\delta_0}{\beta_1} & 0 & 0 \\
s^0 & \dfrac{\psi\delta_0}{\psi} & 0 & 0
\end{array} \tag{5.164}$$

where, $\beta_1 = \frac{\gamma_1\delta_2 - \delta_4\gamma_2}{\gamma_1}$; $\gamma_1 = \frac{\delta_4\delta_3 - \delta_2}{\delta_4}$; $\gamma_2 = \frac{\delta_4\delta_1 - \delta_0}{\delta_4}$, and $\psi = \frac{\beta_1\gamma_2 - \gamma_1\delta_0}{\beta_1}$. Using Krishnamurthi's approach [161], for stability of the system, ψ must be positive, which is given as,

$$\psi = \frac{\beta_1\gamma_2 - \gamma_1\delta_0}{\beta_1} > 0 \tag{5.165}$$

Since $w_1, w_2 > 0$, further simplifying above, we get

$$\beta_1\gamma_2 - \gamma_1\delta_0 > 0 \tag{5.166}$$

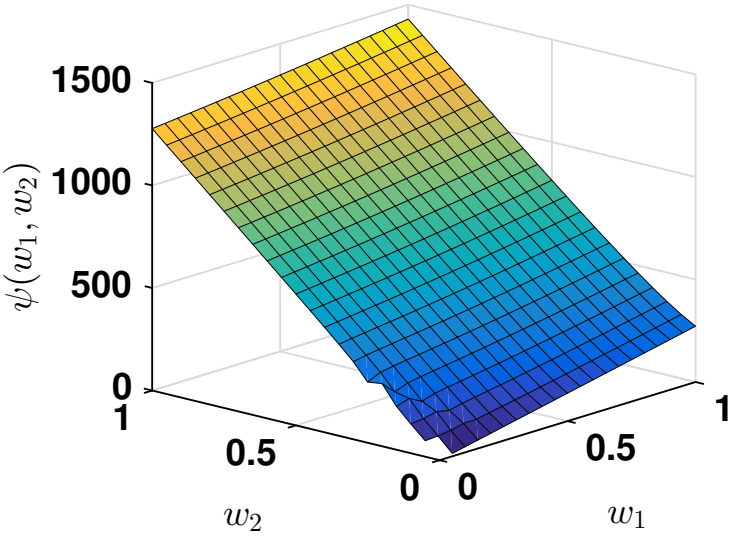

Figure 5.37: Plot of ψ vs w_1 and w_2 for CIPS

By varying w_1 and w_2 from 0 to 1, stability condition (5.166) has been verified. It is found that $\psi(w_1, w_2) > 0$. Thus, $\forall w_1, w_2 \in [0, 1]$, the system is stable. This is also verified graphically which is shown in Fig. 5.37. Hence, it shows that the stability condition is satisfied.

5.5.3.2 Simulation results and analysis

The application of the proposed control on CIPS is tested in MATLAB-Simulink© environment and on a Real-Time hardware setup. The results obtained are discussed and analyzed as follows:

(i) Without disturbance: In absence of external disturbances, the performance of CIPS, controlled by the proposed logic, shows significant improvement in both transient and steady-state regions. From Fig. 5.38, it is clear that the modified control action performs better, by providing early corrections, thus reducing the magnitudes of the deviations. Fig. 5.38(c)shows the control energy's variations, which infer that the chattering caused by the control given in [2], is reduced by using the proposed control logic.

(ii) With disturbance: Adding Gaussian white noise as an external disturbance to the CIPS, setting aside the small spontaneous crests and troughs caused by the noise, the improvement in performance is clearly evident from Fig. 5.38. The system converges to the equilibrium point quicker than when controlled using the existing adaptive control [2].

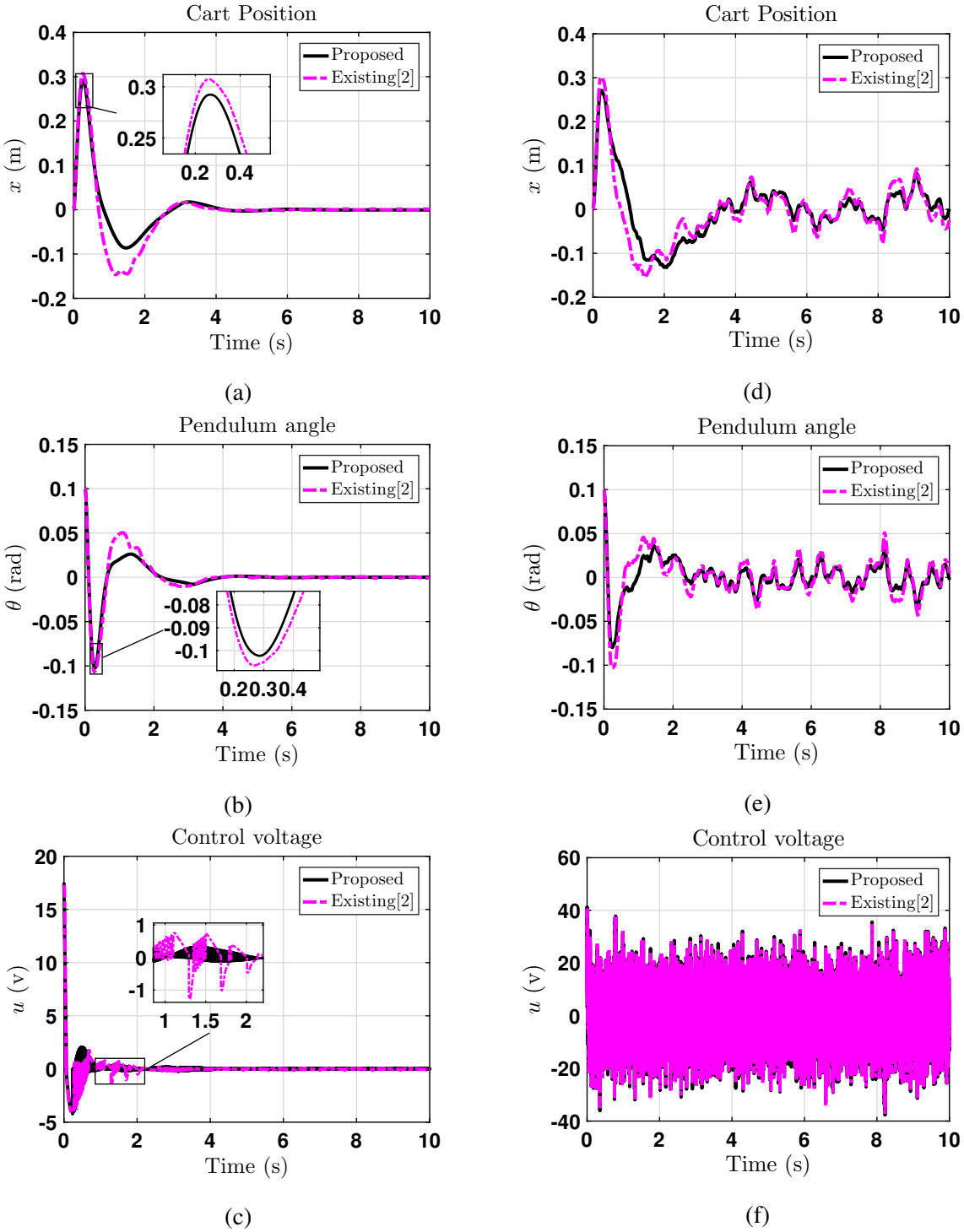

Figure 5.38: Response of CIPS without and with disturbance

Table 5.16: Proposed Adaptive Logic with Median filter

Perf.	Without dist.		With dist.		⇓ gain 0.5		⇑ gain 2		Input time delay 0.02	
Indices	x	θ	x	θ	x	θ	x	θ	x	θ
ISE	0.03222	0.00343	0.04979	0.00357	0.05807	0.00613	0.01361	0.00121	0.05049	0.00583
IAE	0.23266	0.07109	0.48149	0.13004	0.31902	0.09732	0.18665	0.05228	0.29319	0.08657
ITSE	0.01787	0.00153	0.08049	0.00781	0.03794	0.00309	0.01294	0.00078	0.03377	0.00262
ITAE	0.27028	0.07455	1.47192	0.49972	0.36925	0.10047	0.32629	0.08940	0.33650	0.08733

Table 5.17: Existing Adaptive control logic [2]

Perf.	Without noise		With noise		⇓ gain 0.5		⇑ gain 2		Input time dealy 0.02	
Indices	x	θ	x	θ	x	θ	x	θ	x	θ
ISE	0.04929	0.00504	0.05562	0.00617	0.05859	0.00741	0.03818	0.00303	0.05352	0.00679
IAE	0.31464	0.09667	0.50852	0.17581	0.32349	0.10811	0.29196	0.07708	0.31168	0.09744
ITSE	0.03717	0.00299	0.10004	0.01597	0.04073	0.00420	0.03031	0.00187	0.03511	0.00299
ITAE	0.37206	0.11276	1.72741	0.71863	0.33858	0.10206	0.37036	0.08998	0.38138	0.09929

(iii) Changing input gain: The improvement in performance in terms of the gain sensitivity can be verified from Figs. 5.39. Both the transient and steady-state responses are smoothened, which marks the superiority of the modified adaptive logic.

(iv) Effect due to input delay: The plots of each variable's variation with time, when an input delay of 0.02 second is introduced, are shown in Figs.5.39. The peaks attained by $x(t)$ and $\theta(t)$ are lesser, when driven by the proposed control law. The more significant improvement can be observed from the improvement in the variations of the control input, as compared to the undesirable chattering that occurs with adaptive logic of [2].

5.5.3.3 Experimental results

For validation of the effectiveness of introducing the proposed modifications to the existing adaptive control logic, the modified control is applied on a Real-Time CIPS, developed by the Feedback Instruments© (shown in Fig. 5.40). The stabilization of the pendulum of this setup is carried out, subject to a mild disturbance given to it externally. The results of the variations in each state variable are obtained in Fig. 5.41. Referring to this figure, it is ensured that the primary objective of the problem, that is the stabilization of the CIPS is achieved using the modified adaptive control. The improvements, as expected from the simulation-based analysis, can be

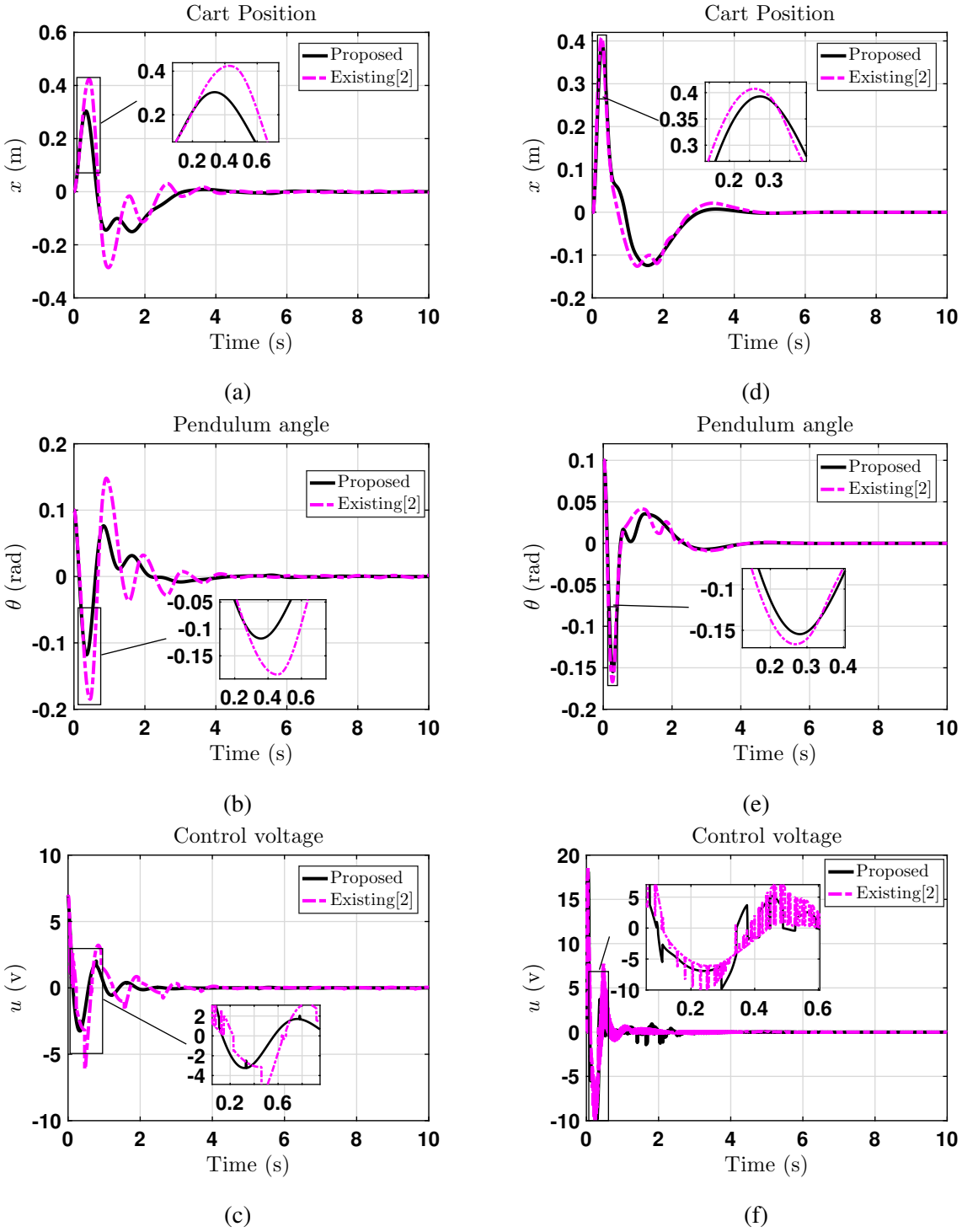

Figure 5.39: Response of CIPS without and with input gain 0.04 and input time delay 0.02sec

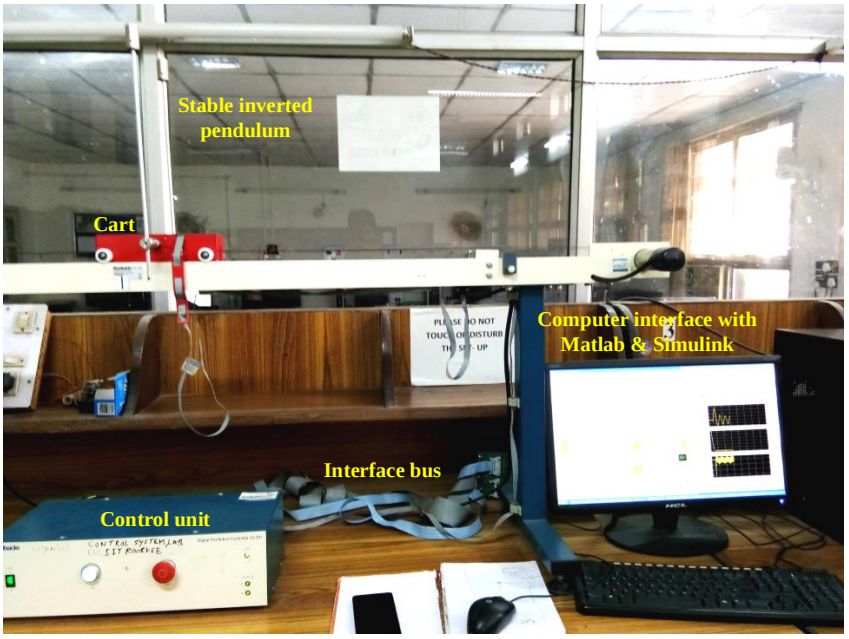

Figure 5.40: CIPS real-time hardware setup

seen in the trajectories of $x(t)$ and $\theta(t)$, where the former shows reduction in the amplitude of the oscillatory motion of the cart, while in the latter, though both the curves seem to be superimposed, yet the response under the influence of the modified control shows improvement as compared to that using the existing one. Next, focusing on the control signal's variations, although $\inf_{t\in\mathbb{R}^+}\left\{u_{proposed}-u_{existing}\right\}(t)>0$, still the fluctuations are limited to the safety bounds for the system. This implies that the proposed modifications can improve the system's performance at the cost of increased control energy, but the increment is not high enough to cross the safety limits, rather limited to a level well below the maximum control energy applicable for the hardware setup.

Analysis using Integral performance indices

The performance analysis of the CIPS is also carried out using the commonly used integral performance indices-ISE, IAE, ITSE, and ITAE. In this analysis, the values of these indices are obtained for both x and θ, working under different operating conditions. Table 5.17 shows the results when controlled using the proposed control logic, and Table 5.16 contains the values of the indices, when controlled using the conventional adaptive logic. To show the improvement in performance, the ISE values for x are compared between these tables, for each operating condition. Taking a closer look of the values, it can be observed that the ISE values of x in Table 5.16 are approximately

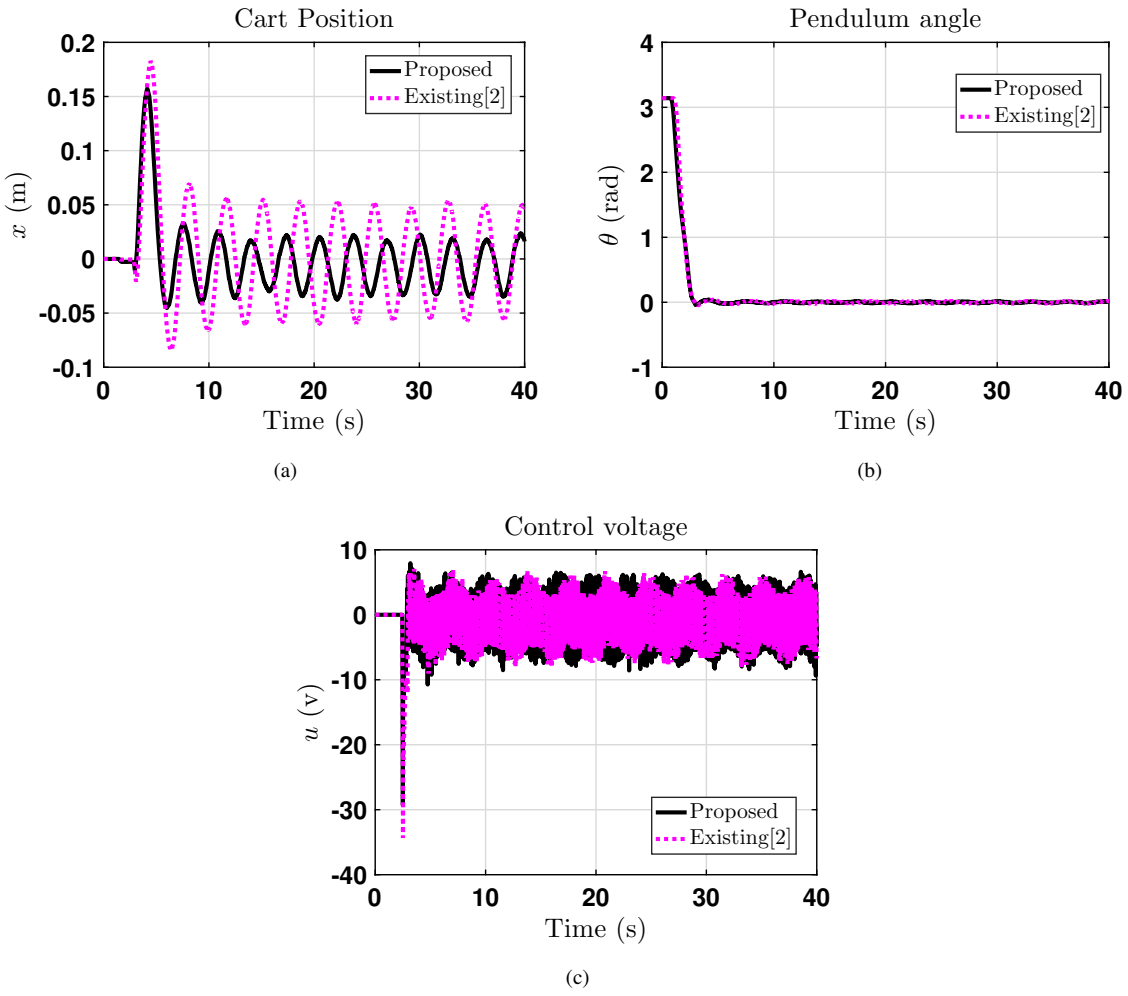

Figure 5.41: Response of real time setup of CIPS

65%, 89%, 98%, 38%, 94% of the ISE values of x in Table 5.16 , for each respective operating condition, starting with performance in absence of noise. The best of all these is when the input gain is increased.

5.5.4 QRAWCP-PID

The stabilisation of pendulum and the control of cart position in a CIPS system is a classical benchmark problem in the area of control engineering. It is characterized by high non-linearity, non-minimum phase characteristics [173], instability [9] as well as under-actuation [3]. Hence, it has been a challenging task for control practitioners to design a controller for this problem so that the desired performance is achieved and the control strategy used is not too complex to

comprehend [174, 175]. A comprehensive review of the techniques for the control of an inverted pendulum is presented in [53].

The CIPS has two types of motions-linear and rotational [1, 152]. The linear motion of the cart is in the horizontal direction, while the rotational motion of the pendulum is about its hinge. Fig. 5.1 shows the model of CIPS system.

On linearising the model of CIPS about its equilibrium point, for small angular displacement θ, we get the equations of motion as follows:

$$\ddot{x} \approx \frac{(J+ml^2)F - m^2l^2g\theta}{J(M_c+m)+M_cml^2} \tag{5.167}$$

$$\ddot{\theta} \approx \frac{-mlF + (M_c+m)mgl\theta}{J(M_c+m)+M_cml^2} \tag{5.168}$$

On further simplification, we get the transfer functions as $P_1(s) = \frac{x(s)}{F(s)} = \frac{b_1}{s^2}$ and $P_2(s) = \frac{\theta(s)}{F(s)} = \frac{b_2}{s^2-a_2}$.The parameters of CIPS are shown in Table 5.1. From appendix A, the values of the transfer function parameters are $b_1 = 5.841, b_2 = 3.957$ and $a_2 = 6.807$. For the purpose of illustration in this example, the model of the inverted pendulum has been taken from [1]. In [1], effect of the filter in derivative term has been neglected while designing a LQR-PID controller. But, in this example, the effect of filter has also been analyzed.

As discussed earlier, the closed-loop characteristic equation of the Cart inverted pendulum system can be given by, $1 - P_1C_1 + P_2C_2 = 0$, where $C_n(s) = \frac{K_{dn}s^2+sK_{pn}+K_{in}}{s}, n = 1,2$.

Thus, the characteristic equation becomes,

$$1 - \frac{b_1}{s^2}(K_{p_1} + \frac{K_{i_1}}{s} + K_{d_1}s) + \frac{b_2}{s^2-a_2}(K_{p_2} + \frac{K_{i_2}}{s} + K_{d_2}s) = 0 \tag{5.169}$$

On further simplification, finally, we get the closed loop characteristic equation as

$$\begin{aligned} s^5 + (-b_1K_{d_1} + b_2K_{d_2})s^4 + (-a_2 - b_1K_{p_1} + b_2K_{p_2})s^3 + \\ (-b_1K_{i_1} + a_2b_1K_{d_1} + b_2K_{i_2})s^2 + (a_2b_1Kp_1)s + a_2b_1K_{i_1} = 0 \end{aligned} \tag{5.170}$$

(1) Proposed approach

Initially, we obtain the state feedback gain matrix using LQR. We know that $K = R^{-1}B^T P$. On substituting the values of the variables, we get, $K = [p_{12} \quad p_{22}]$. Thus, the closed loop characteristic equation of the system can be given by

$$s^4 + p_1 s^3 + p_2 s^2 + p_3 s + p_4 = 0 \tag{5.171}$$

Equation (5.170), that represents a PID compensated closed loop system is of fifth order, whereas, (5.171) has an order of four. Therefore, to effectively compare (5.170) and (5.171), we augment (5.171) with one extra pole. On augmenting the pole λ_5 to (5.171), we obtain,

$$(s+\lambda_5)(s^4 + p_1 s^3 + p_2 s^2 + p_3 s + p_4) \tag{5.172}$$

Simplification of (5.172) yields,

$$s^5 + (p_1+\lambda_5)s^4 + (p_2 + K_1\lambda_5)s^3 + (p_3 + p_2\lambda_5)s^2 + (p_4 + p_3\lambda_5)s + p_4\lambda_5 \tag{5.173}$$

We set K_{d1} and K_{d2} to desired values, depending on the actuator rate constant. Consequently, the additional pole can be determined as,

$$\lambda_5 = K_{d1}b_1 + p_1 - b_2 K_{d2} \tag{5.174}$$

Substitution of λ_5 in (5.172) yields,

$$s^5 + k_1 s^4 + k_2 s^3 + k_3 s^2 + k_4 s + k_5 \tag{5.175}$$

On comparing (5.170) and (5.175), the gain parameters of the PID controller are obtained as

$$K_{p1} = \frac{k_4}{a_2 b_1}; \qquad K_{i1} = \frac{k_5}{a_2 b_1} \tag{5.176}$$

$$K_{p2} = \frac{k_2 + b1K_{p1}}{b_2}; \qquad K_{i2} = \frac{(k_3 - (a_2 b_1 K_{d1}) + b_1 K_{i1})}{b_2} \tag{5.177}$$

(2) LQR PID approach

In [1], Ghosh et al. have designed a LQR-PID controller, wherein they have chosen the additional pole to be six times of the dominant real pole of the closed loop system. But they have not discussed the reason for the random choice of the additional pole and the effect of this extra pole on the stability of the system. Further, the effect of the filter on the derivative term of the PID controller has also not been taken into consideration in the design phase. For the purpose of comparison, the values of the controller gains are taken from [1].

5.5.4.1 Results and analysis

To perform a fair comparison between LQR-PID and the proposed approach, the values of K_{d1}, K_{d2} for the proposed PID are assumed to be the same as computed by LQR-PID in [1]. The values are $K_{d1} = 2.254$ and $K_{d2} = 10$. Thus, $\lambda_5 = -46.1606$.

The gains of the proposed PID controller are computed from (5.176) (5.177) and are enlisted as follows:

$$\begin{aligned} K_{p1} = 124.8050,\ K_{i1} = 100.7733,\ K_{d1} = 2.254 \\ K_{p2} = 325.9798,\ K_{i2} = 782.5889,\ K_{d2} = 10 \end{aligned} \tag{5.178}$$

The parameters of the LQR-PID controller [1] are given as

$$\begin{aligned} K_{p1} = 44.3,\ K_{i1} = 33.796,\ K_{d1} = 2.254 \\ K_{p2} = 120.9,\ K_{i2} = 247.43,\ K_{d2} = 10 \end{aligned} \tag{5.179}$$

We have undertaken two case studies, one in the absence of output noise and the other in the presence of output noise. The step noise, having an amplitude of 0.05 units has been applied to the system at time $t = 5s$ for the duration of 0.5 seconds to the pendulum angle channel.

Fig. 5.42(a-c) depicts the comparison of the response of cart position, pendulum angle and control energy for proposed approach and LQR-PID respectively. In a similar manner, Fig. 5.42(d-f) depicts the same responses, but in the presence of noise. It can be seen that the proposed approach shows less overshoot as compared to LQR-PID for cart position and pendulum angle control respectively. On a closer look at the control energy plots in the presence of noise, it can be observed

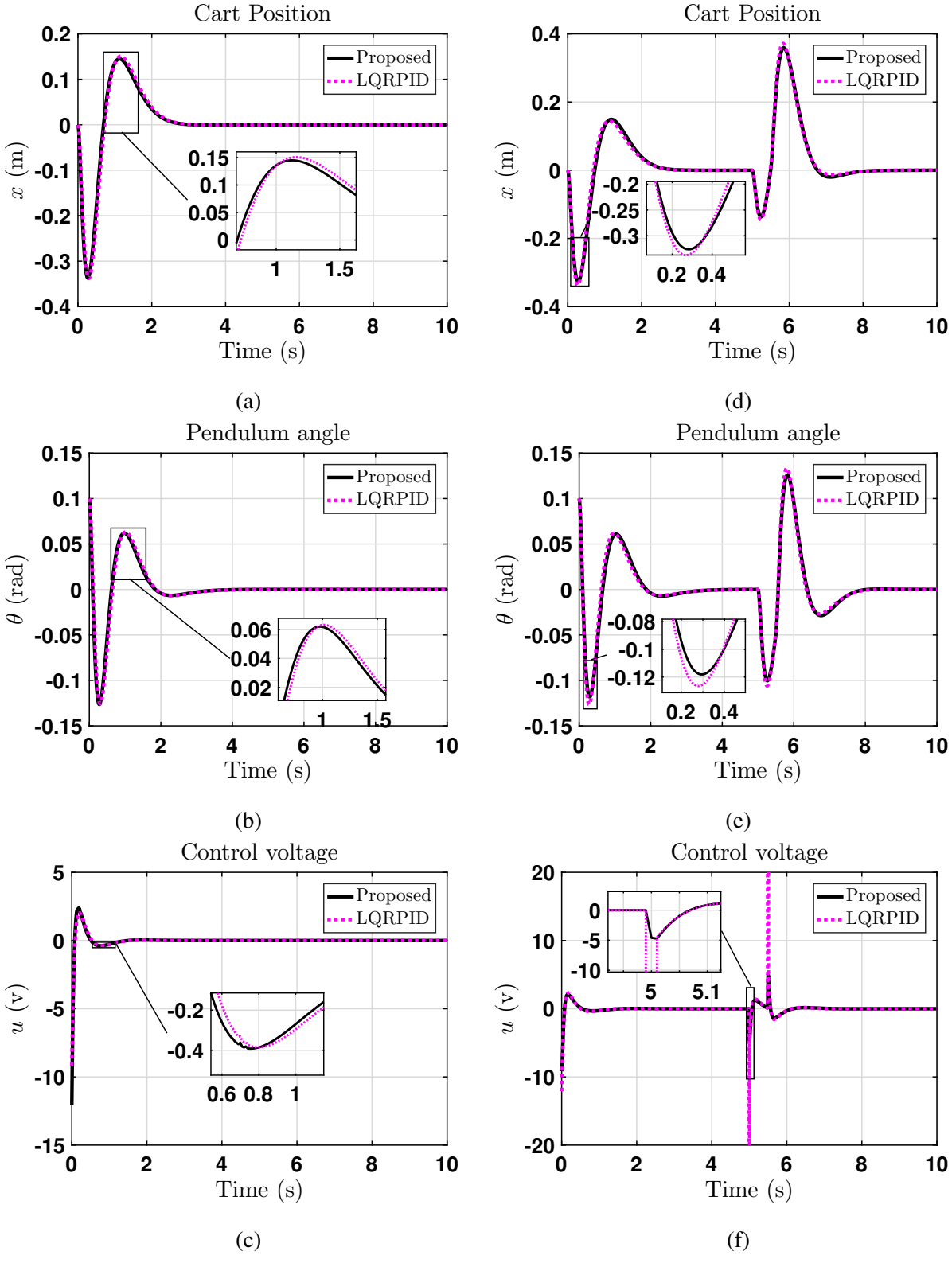

Figure 5.42: Output CIPS for D-filter cases (a) cart position, (b) pendulum angle, and (c) control action for wihtout filter case and (d) cart position, (e) pendulum angle, and (f) control action for with D-filter of Example 3

that the LQR-PID technique needs a large amount of control energy, whereas for the proposed approach, the control energy requirement is minimal. Hence, there is a large reduction in the control energy on implementing the proposed approach.

5.6 Interactive and Animated GUI for CIPS

To design and validate these control techniques, there are various mathematical computational software that are available in market such as: MATLAB® [48], Scilab [176], SageMath®[177], MAPLE® [178], and MATHEMATICA® [179]. However, MATLAB® is popular, because it is a multidisciplinary software which is widely used in all the branches of engineering and has large number of inbuilt toolboxes. Basically, MATLAB stands for MATrix LABoratory. Matrix is the fundamental building block of this software. MATLAB® has varieties of products such as Simulink, Simmechanics, Graphical User Interface (GUI) editor, application development, etc, [180]. Many interactive GUI have been developed in past. In [181], a GUI is developed for Computer controlled systems (CCSDEMO) with Virtual interactive system, whereas in [182], the description of GUI for root locus and bode design and classical control is given. In [183, 184], interacting tools (IC Tools) for linear control system analysis and for modelling of level control system are elucidated. There are GUI on servo systems [180], linear systems [185, 186] and Quadrotor [187]. In [188], an interactive GUI is designed for cart-pendulum system but it has limited functionalities and gives very less freedom in system and controller design.

GUI's have certain advantages over traditional learning. It gives necessary freedom on system parameters and other inputs to the user. This gives user a chance to see the effects of these parameters on system performance. In this GUI, we have given necessary freedom for user to design its own system and controllers. Various researchers reported about the programming difficulties in [181, 183], which have been overcome in this GUI. User friendly graphical application and in-build functions, also, eliminates complex mathematics calculations for user.

In this section, an interactive and animated graphical user interface is developed for analysis, design and validation of controllers for cart inverted pendulum system (CIPS) and rotary inverted pendulum system (RIPS). User can design the pendulum system, as linear or non-linear model,

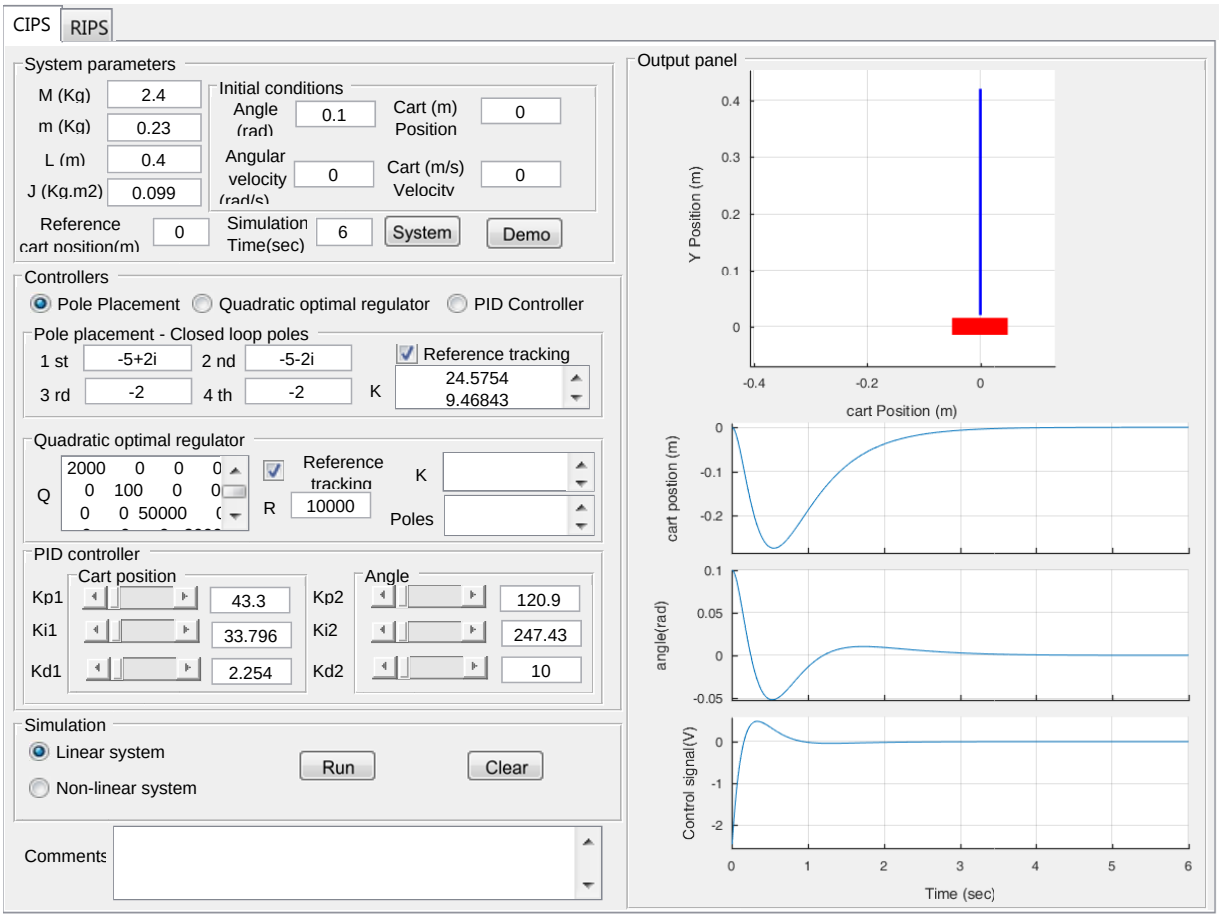

Figure 5.43: Graphical user interface of CIPS

and controllers by providing various system controller parameters, respectively. User can also design three types of controllers: pole-placement, linear quadratic regulator (LQR) and parallel structure Proportional Integral Derivative (PID) controller. Further, user can analyse controller-based systems in time domain by obtaining transient plot of various signals like position, pendulum angle etc. Further, it facilitates the animation of CIPS which depicts the behaviour or motion of system in 3-D space subjected to aforementioned control techniques.

5.6.1 Description of CIPS GUI toolbox :

This Tab is used for designing controllers for linear and non-linear model of CIPS and for the analysis of the resultant system. Figure 5.1 shows *CIPS* tab, with an example. The various panels of this tab are explained hereinafter.

(i) System parameters: This panel takes the input variables which defines the CIPS such as, cart mass (M), pendulum mass (m), length of pendulum (L) and movement of inertia (J). Few other standard system parameters are assumed internally inside the GUI function. Here, user, also, has to provide the initial conditions, reference input for cart position and simulation run time of the pendulum setup considered. Once all input parameters are entered, user can see the free body diagram, state space model and transfer function of CIPS by clicking *'System'* push button. One demonstration example can be loaded, to help the user, by clicking *'Demo'* push button which loads all the values in desired syntax at corresponding input edit boxes.

(ii) Controllers: In this panel, user can design the three different control methodologies such as, pole placement, LQR and PID for CIPS. For pole placement method, user need to enter four desired closed loop poles, since, order of the system is four. For designing LQR, user need to provide Q and R matrices. Once these controllers are designed, K and *Poles* edit boxes give state feedback gain and closed loop poles of the system. Since, a controller designed by pole placement and LQR method do not provide reference tracking, so *Reference tracking* check box provide an option to choose reference tracking. Here, reference tracking is done by multiplying a gain to reference input. In PID controller sub-panel, the user can manually enter the gain values of proportional gain (K_p), integral gain (K_i), and derivative gain (K_d). The control law has been considered from [1], where two loop PID control scheme has been designed.

(iii) Simulation: This panel simulates the controller based closed loop CIPS. User can select either linear or non-linear model of CIPS for simulation. In this version of GUI, we have considered the linear system for all the three controllers from *controller* panel, and only PID controller with non-linear model. Once all system parameters and all controller parameters of chosen controller are entered correctly, user can press *Run* push button to run simulation the system. This simulation will run for the specified time entered by the user in *System parameter* panel.

(iv) Output: This panel is for displaying the animation of CIPS's motion in 2-D space, where horizontal direction is cart position (x) and vertical direction is Y-position. Transient behaviour of three signals is also displayed for analysis purpose in three plots. First plot is for cart position (x) in meters (m) vs time in seconds (s). Second plot is for pendulum angle (θ) in radian (rad) vs time (s), and last plot is for control signal (u) in voltage (v) vs time (s). As user press *Run* push button,

animation and plotting begins simultaneously. As the time progresses, plots also get updated or drawn further, means at any time, cart position, pendulum angle and control signal are according to corresponding spatial arrangement of animated CIPS. In other words, plots are plotted according to animation as time passes. In this panel, transient behaviour of signals for multiple controllers can be compared and studied. Moreover, there are other functions such as, save, print, zoom-in, zoom-out, data cursor, pan, rotate 3-D are given in tool-bar of GUI to facilitate the user. We have stored the necessary results or data in workspace, so that the data can be used by user for plotting and analysis the results separately. There is *Comment* edit box which displays the useful suggestions and errors that occur, while operating this GUI.

5.7 Concluding remarks

In this chapter, different control strategies developed in the earlier chapters have been applied to a cart inverted pendulum system. A mathematical model of the CIPS is derived, followed by the stability analysis of the system. It is observed that the QRAWCP approach, that transforms the optimal LQR or LQG controller into a classical PID controller outperforms the soft computing techniques for a solar tracker system. Next, fixed robust PID controllers have been designed by using stability boundary locus and Kharitonov's theorem for perturbed CIP system. The performance of proposed controllers have been verified using simulation and also on a real time hardware setup. The effectiveness of proposed controllers have been checked by determining various performance indices such as ISE, IAE, ITSE, ITAE. Further, adaptive control logic has also been utilised to combine two PID controllers having good properties in different regions and it was observed, that the resultant system is able to replicate the good properties of the individual candidate controllers. An extensive and a comprehensive analysis is conducted, which highlights the effectiveness and strength of the proposed techniques. Furthermore, an interactive and animated GUI is developed and illustrated with an example. In the next chapter, we study the importance of the load frequency control in power systems and the manner in which the techniques proposed in the preceding chapters are applied to the load frequency control problem in power system.

Chapter 6

Application–II-Load Frequency Control

6.1 Introduction

Nowadays, electricity demand of every country is increasing continuously, due to industrial revolution, technological developments, etc. However, in power delivery, the most critical issue is to provide uninterrupted power supply to the consumers in-spite of the presence of any parametric uncertainties or external disturbances [189]. For stable and continuous operation, one of the ancillary services is the 'frequency regulation' or 'load following' for the Load Frequency Control (LFC).

The frequency of the generated voltage should be kept within the permissible limits [190]. If the input-output power balance is not maintained, change in the frequency occurs. Hence, frequency control is an essential issue, which is achieved via speed governor mechanism. The role of the governor is to control the speed of generator according to load. If the load on the turbine increases, the speed of the governor decreases and vice-versa. Fig. 6.1 shows the general scheme of a generating unit, where V_r is the voltage demand and f is the reference frequency as discussed in [191].

LFC has been in practice for several years as part of the automatic generation control (AGC) unit in electric power systems. AGC is a system for adjusting the power output of multiple generators at different power plants, in response to changes in the load [192, 193]. Whenever there is a

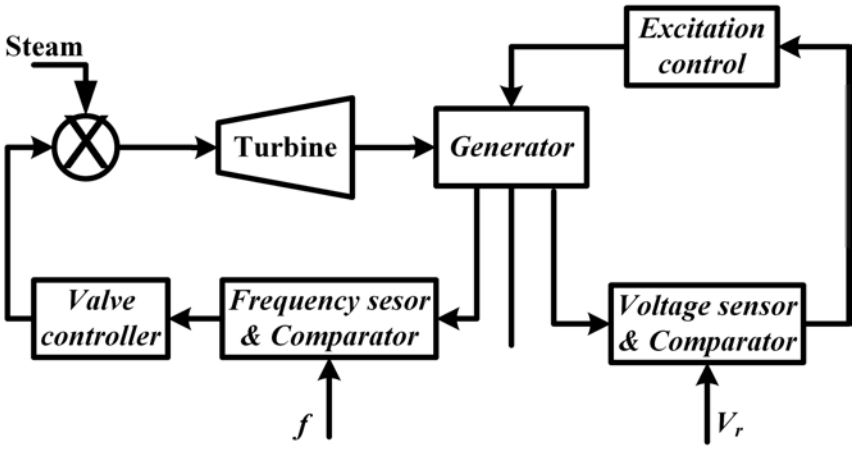

Figure 6.1: General scheme of a generating unit

change in load, frequency of the system changes from its nominal value. In the control literature, various control techniques have been implemented on the LFC problem. This frequency regulation concept can be traced back nearly hundred years from today[194–196].

6.2 Motivation

In the last two decades, the electricity demand has increased steeply due to population explosion, industrialisation, urbanisation, etc. So, it is observed that, because of the frequency mismatches, we can see occurrences of interruption in power supply have become a new normal.

To overcome it, researchers have proposed numerous methodologies to guarantee the uninterrupted power flow. Internal Model Control (IMC) scheme has been proposed in [61] and it uses model order reduction for uncertain model [190, 197]. In [58], a unified tuning of proportional–integral–derivative (PID) control was presented, and in [59], a PID design technique using frequency response matching with direct synthesis technique was proposed. In [198], PID controller was designed using Kharitonov's theorem for, perturbed multi-area systems and in [140], adaptive policy for LFC was explained. Apart from these techniques, there are various other non-linear control strategies reported in the control literature till date, which can outperform linear controllers;

however, most of these are mathematically complicated and difficult to implement in real time applications. Since, PID is one of the simplest linear controller till date, it is also used in conjunction with optimal control.

The PID controller offers simplicity, ease of functionality, past good record of success, and the most profound solution to process industry and also to many real-time control problems, as elucidated in [5, 11]. The three control actions of the PID controller provide improvement in both the transient and steady-state specifications of the control system response, as described in [199–201]. The first tuning method for PID controllers was presented in [26]. Since then a lot of research has been carried out on PID, leading to the development of new techniques such as, Cohen-Coon, Chien, Hrones and Reswick (C-H-R), Internal Model Control (IMC), optimization methods such as, Particle Swarm Optimization (PSO) [202], Big-Bang Big-Crunch (BBBC) techniques [203], Linear Quadratic Regulator (LQR)-PID [2], Fuzzy PID, ANN-PID [204], SBL-PID [57], FOPID [205, 206], etc. However, all these methods have certain merits and demerits, and attempt to improve upon previous method either in terms of transient or steady state response. In [192], LQR and Linear Quadratic Gaussian (LQG) controllers were designed, but only for a single area system, and non-linear constraints were not taken into consideration. Recently, a quadratic regulator based PID for Sun tracker system, was proposed in [207], however this technique did not consider the effect of non-linearities on the performance of the system.

So, in this chapter, we first design an optimal PID controller for load frequency control using direct model based formula via Quadratic Regulator Approach with Compensating Pole (QRAWCP) approach. To demonstrate the superiority of proposed technique, we compare the results for the single and multi-area cases, in the presence of practical issues such as non-linearities Generation Rate Constraint (GRC), Governor Dead Band (GDB) and parametric uncertainties, with the recently designed PID controller and other control techniques. The comparison is carried out for three different cases, which are discussed later in the chapter. Further, an adaptive control scheme that gives a guaranteed performance improvement by combining the merits of different control schemes is proposed. Different case studies for single and multi-area power systems have been conducted to verify the accuracy and efficiency of the proposed method.

Table 6.1: Nomenclature of LFC

Δf	Incremental frequency deviation (Hz)
ΔP_d	Load disturbance (p.u.MW)
f	Reference load frequency input
u	Control signal
K_P	Electric system gain
T_P	Electric system time constant (s)
K_G	Governor gain constant
T_G	Governor time constant (s)
K_T	Turbine gain constant
T_T	Turbine time constant (s)
R	Speed regulation due to governor action (Hz/p.u.MW)
ΔP_G	Incremental change in generator output (p.u.MW)
ΔX_G	Incremental change in governor valve position

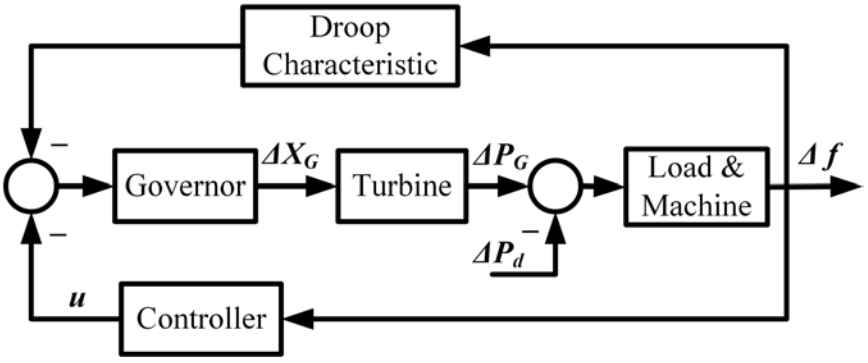

Figure 6.2: Schematic of the proposed control system

6.3 Mathematical modelling of LFC

The mathematical models of LFC depend on the nature of turbine as well as the number of control areas. For different types of turbines, one can obtain various mathematical models like, single area non-reheated, single area-reheated, two area- non-reheated, two area reheated, etc. They are explained individually below.

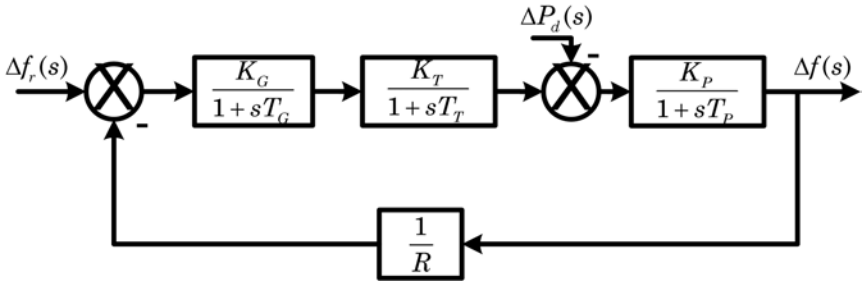

Figure 6.3: Model of single area power system

6.3.1 Single area power system

6.3.1.1 Non-reheated turbine based model

The mathematical modelling of single area thermal power system is described in [58, 208]. The plant for LFC system consists of governor, turbine, rotating mass generating unit and load [59]. An electric power system is a complex large scale system comprising of nonlinear dynamics. But for LFC problem, it can be represented by a linear system, linearized about the operating point since the load changes during its normal operation are assumed to be small.

The linearised model of the plant is shown in Fig. 6.3. The transfer function of plant for non-reheated turbine with droop characteristics is written as:

$$G(s) = \frac{G_G(s)G_T(s)G_P(s)}{1+G_G(s)G_T(s)G_P(s)/R} \tag{6.1}$$

$$G(s) = \frac{RK_P}{\left\{\begin{array}{l}(T_PT_GT_Ts^3+(T_PT_G+T_PT_T+T_GT_T)s^2\\+(T_P+T_G+T_T)s+1)R+K_P\end{array}\right\}} \tag{6.2}$$

where, Governor dynamics, $G_G(s) = 1/(sT_G+1)$, Turbine dynamics, $G_T(s) = 1/(sT_T+1)$, rotating mass generating unit and load with dynamic, $G_P(s) = K_P/(sT_P+1)$ and R is speed regulation due to governor action (Hz/p.u.MW), ΔP_d is load disturbance(p.u.MW), K_P is electric system gain, T_P is electrical system time constant, T_T is turbine time constant, T_G is governor time constant, Δf is frequency deviation, u is load reference.

6.3.1.2 Reheated turbine model

The dynamics of reheated turbine are given as

$$G_T(s) = \frac{cT_R + 1}{(T_R s + 1)(T_T s + 1)} \tag{6.3}$$

Here, T_R is time constant and c is percentage of the power generated by the reheated turbine to the total generated power. In such case, the closed loop transfer function with droop characteristics is given as

$$G(s) = \frac{RK_P(cT_R + 1)}{(T_R s + 1)(T_T s + 1)(T_G s + 1)(T_P s + 1)R + K_P(cT_R + 1)} \tag{6.4}$$

6.3.2 Multi-area power system

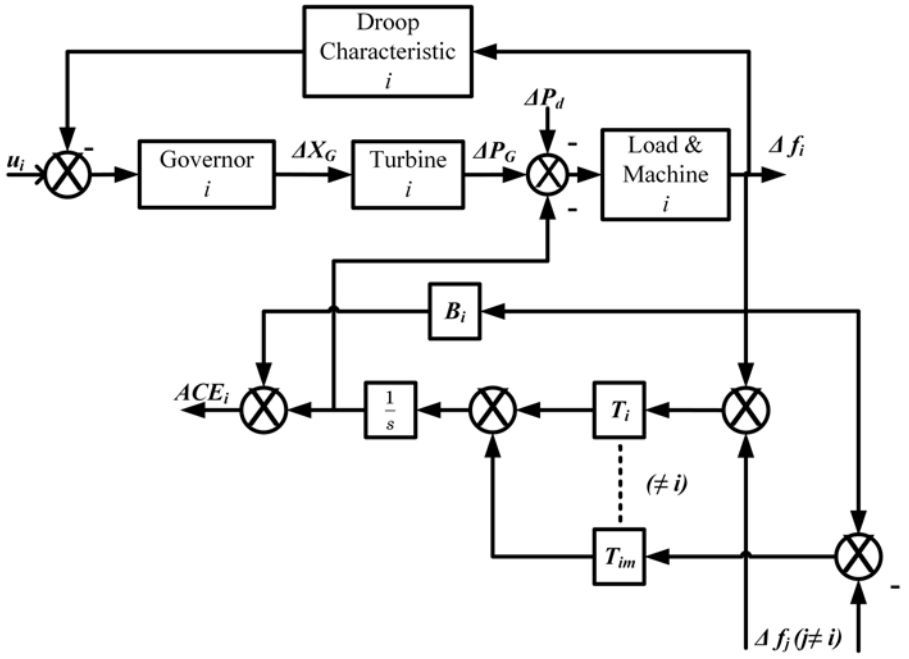

Figure 6.4: Schematic block-diagram of i^{th} control area for LFC design

6.3.2.1 Two-Area power system with non-reheated turbine

In two area power system, frequency and tie line power are main variables in LFC design. The values of these variables in each area should be in specified limits i.e., any deviations in frequency

must be restored to its nominal value and the tie line power should be returned to scheduled power value. So a composite factor, area control error (ACE) is used as a feedback variable in LFC studies. The ACE is defined as (for ith control area)

$$ACE_i = B_i \Delta f_i + \Delta P_{tielinei} \tag{6.5}$$

Here, B_i is feedback bias setting and $\Delta P_{tielinei}$ is tie line power of i^{th} control area and is defined as

$$\sum_{\substack{j=1 \\ j\neq i}}^{N} \Delta P_{tielineij} = \frac{2\pi}{s} \left[\sum_{\substack{j=1 \\ j\neq i}}^{N} T_{ij} \Delta f_i(s) - \sum_{\substack{j=1 \\ j\neq i}}^{N} T_{ij} \Delta f_j(s) \right] \tag{6.6}$$

where, T_{ij} is a tie-line synchronizing parameter between area i and j (p.u. MW/radian). Similarly, for a single area power system, the plant dynamics for multi area power system of each control area becomes (for ith control area)

$$G_i(s) = B_i \frac{G_{G,i}(s) G_{T,i}(s) G_{P,i}(s)}{1 + G_{G,i}(s) G_{T,i}(s) G_{P,i}(s)/R_i} \tag{6.7}$$

6.3.3 Worst-case plant selection approach

This section presents the controller synthesis scheme using the worst-case plant selection. It has been observed that in order to test the robust stability of low degree polynomial family, there is no need to investigate all four Kharitonov's polynomials. The analysis can be done with the help of 1, 2, and 3 Kharitonov polynomials for polynomials of degree 3, 4 and 5, respectively [209, 210]. Also, in [39] , the authors have proposed a worst-case polynomial selection theorem for interval polynomial given by

$$\mathcal{G}(s,\Delta) = \{ g(s,\delta) = \delta_0 + \delta_1 s + ... + \delta_n s^n \} \tag{6.8}$$

having uncertain parameter vector $\delta = [\delta_1, \delta_2 ... \delta_n]^T$ and
$\Delta = \left\{ \delta \mid \delta_i \in \left[\underline{\delta}_i, \overline{\delta}_i \right], \ \underline{\delta}_i > 0, \ \ i = 0, 1, ..., n \right\}$ is robustly stable if and only if the Kharitonov's four extreme polynomials are Hurwitz.

$$g_1(s, \delta^{--}) = \underline{\delta}_0 + \underline{\delta}_1 s + \overline{\delta}_2 s^2 + \overline{\delta}_3 s^3 + \underline{\delta}_4 s^4 + ... \tag{6.9}$$

$$g_2(s,\delta^{-+}) = \underline{\delta}_0 + \overline{\delta}_1 s + \overline{\delta}_2 s^2 + \underline{\delta}_3 s^3 + \underline{\delta}_4 s^4 + \ldots \tag{6.10}$$

$$g_3(s,\delta^{+-}) = \overline{\delta}_0 + \underline{\delta}_1 s + \underline{\delta}_2 s^2 + \overline{\delta}_3 s^3 + \overline{\delta}_4 s^4 + \ldots \tag{6.11}$$

$$g_4(s,\delta^{++}) = \overline{\delta}_0 + \overline{\delta}_1 s + \underline{\delta}_2 s^2 + \underline{\delta}_3 s^3 + \overline{\delta}_4 s^4 + \ldots \tag{6.12}$$

Theorem 6.1 ([198, 209]). *For the interval polynomial described in (6.8) having $\sigma(\mathcal{P}) = 3$, the testing set is $\Delta_T = \delta^{+-}$ that means only $g_3(s,\delta^{+-})$ described by (6.11) is sufficient to investigate the robust stability of the entire family of polynomials in $\mathcal{P}$.*

Theorem 6.2 ([198, 209]). *Let $G(s)$ be interval plant as defined in (20) from [198]. Then the entire family is $G(s)$ stabilized by a particular PID controller, if the worst-case plant $G_{23}(s)$ defined in (21) from [198] is stabilized by that same PID controller.*

Therefore, using theorem 1 and 2, we simplify the system model and from that we select the $g_3(s)$ polynomial and carried out further analysis to design optimal QRAWCP-PID controller.

6.4 Proposed controller approach for LFC

Fig. 6.2, shows the schematic of load frequency control using controller to compensate the deviation Δf using a proper control signal u.

6.4.1 QRAWCP-PID approach

The steps of QRAWCP scheme for the single area and multi-area power system model consisting of a non-reheated turbine are described simultaneously as follows:

Step 1: For a single area power system, comprising of a non-reheated turbine, the transfer function $G(s)$ of LFC is given in the generalised form as

$$G(s) = \frac{\mathcal{K}}{s^3 + b_2 s^2 + b_1 s + b_0} \tag{6.13}$$

where, $\mathcal{K} = K_P K_T K_G/\sigma$, $b_0 = 1 + K_P K_T K_G/\sigma R$, $b_1 = (T_G + T_T + T_P)/\sigma$, $b_2 = (T_G T_T + T_G T_P + T_T T_P)/\sigma$ and $\sigma = T_G T_T T_P$. For multi-area power system, the system model of each control area is $B_i G$.

Further, the state space model is given in (6.14). Table 6.1 provides the nomenclature of LFC variables, which are taken from [198].

$$\begin{bmatrix} \dot{x}_1 \\ \dot{x}_2 \\ \dot{x}_3 \end{bmatrix} = \begin{bmatrix} 0 & 1 & 0 \\ 0 & 0 & 1 \\ -b_0 & -b_1 & b_2 \end{bmatrix} \begin{bmatrix} x_1 \\ x_2 \\ x_3 \end{bmatrix} + \begin{bmatrix} 0 \\ 0 \\ \mathcal{K} \end{bmatrix} u$$
$$y = \begin{bmatrix} 1 & 0 & 0 \end{bmatrix} \begin{bmatrix} x_1 \\ x_2 \\ x_3 \end{bmatrix} \tag{6.14}$$

In (6.14), $A \in \mathbb{R}^{3\times 3}$, $B \in \mathbb{R}^{3\times l}$, and $C \in \mathbb{R}^{l\times 3}$.

The transfer function of a PID controller is given by $C(s) = (\rho_d s^2 + s\rho_p + \rho_i)/s$, where, ρ_p = proportional gain, ρ_i= integral gain and ρ_d = derivative gain.

Step 2: The closed-loop characteristic polynomial for the closed loop plant with controller is given as $\Delta(s) = 1 + G(s)C(s)$, and equating $\Delta(s)$ to zero, we get the closed loop characteristic equation as

$$s^4 + b_2 s^3 + (b_1 + \mathcal{K}\rho_d)\, s^2 + \left(b_0 + \mathcal{K}\rho_p\right) s + \mathcal{K}\rho_i = 0 \tag{6.15}$$

Step 3: Determine the control law by Linear Quadratic Regulator approach. The quadratic regulator approach is an optimal state feedback technique which is designed to minimize a specific quadratic cost function. The performance index can be designed for constraints like u, y, error(e) or unconstrained objectives of linear time invariant (LTI) system. The optimal control vector $u(t)$ is obtained from the control law given by $u(t)$ = -κ $x(t)$. Here, unconstrained optimal action is considered. Therefore, Performance Index (PI) of the system is defined as,

$$\psi = \int_0^\infty \left(x^T Q x + u^T R u\right) dt \tag{6.16}$$

where $Q \in \mathbb{R}^{m\times m}$ and $R \in \mathbb{R}^{l\times l}$ are symmetric positive semi definite and positive definite respectively. Here, for the LFC problem $m = 3$ and $l = 1$.

So, the closed loop system equation becomes,

$$\dot{x} = \tilde{A}x \tag{6.17}$$

where, $\tilde{A} = (A - B\kappa)$. Equation (6.16) can be re-written as,

$$\psi = \int_0^\infty \left(x^T \left(Q + \kappa^T R \kappa \right) x \right) dt \tag{6.18}$$

Also, $\frac{d}{dt}\left(x^T P x\right) = -\left(x^T \left(Q + \kappa^T R \kappa \right) x \right)$

$$\implies \left(x^T \left(Q + \kappa^T R \kappa \right) x \right) = -x^T P \dot{x} - \dot{x}^T P x \tag{6.19}$$

Using (6.17) in (6.19) and then substituting in (6.18), we obtain,

$$\psi = -\int_0^\infty x^T \left[P\tilde{A} + \tilde{A}^T P \right] x dt \tag{6.20}$$

It is necessary condition that P must be positive definite matrix. By comparing (6.19) with (6.20), we get,

$$P\tilde{A} + \tilde{A}^T P = -\left(Q + \kappa^T R \kappa \right) \tag{6.21}$$

As $(A - B\kappa)$ is a stable, its eigenvalues are on left side of s-plane. Therefore, solving for a positive definite matrix P which can satisfy (6.21), the cost function can be further simplified as,

$$\psi = \int_0^\infty \left(x^T \left(Q + \kappa^T R \kappa \right) x \right) dt \tag{6.22}$$

Equation (6.19) can be written as $\psi = -x^T P x \big|_0^\infty$, so we get

$$\psi = -x^T(\infty) P x(\infty) + x^T(0) P x(0) \tag{6.23}$$

Since (6.17) is asymptotically stable, and $x(\infty) \to 0$. Thus we get $\psi = x^T(0) P x(0)$. It is obtained in terms of initial condition.

Step 4: From (6.16), the minimization of ψ using Pontryagin's minimum principle gives the state feedback control law $u = -\kappa x$. The feedback gain κ is found as:

$$\kappa = R^{-1}B^T P \tag{6.24}$$

Using this control law and further simplifying (6.17), we get the Algebraic Riccati Equation(ARE) as,

$$A^T P + PA - PBR^{-1}B^T P + Q = 0 \tag{6.25}$$

In (6.25), Q and R can be selected in such a way that $Q = diag(q11, q22, q33)$, wherein $q11 > q22 > q33 > 0$ and $R = V^T V > 0$, where $V \in \mathbb{R}^m{}_{>0}$.

Step 5: Using ARE, (6.24), and (6.25), state feedback control gain κ is obtained as,

$$\kappa = [p_{13}\mathcal{K} \quad p_{23}\mathcal{K} \quad p_{33}\mathcal{K}] \tag{6.26}$$

Step 6: The closed-loop characteristic equation $(sI - \tilde{A}) = 0$ can thus be written as,

$$s^3 + \left(b_2 + p_{33}\mathcal{K}^2\right)s^2 + \left(b_1 + p_{23}\mathcal{K}^2\right)s + \left(b_1 + p_{13}\mathcal{K}^2\right) = 0 \tag{6.27}$$

Step 7: The closed-loop system in (6.15) is of fourth order and (6.27) is of third order. Therefore, in order to compare these two equations, we need to augment one pole to the latter. Thus, we obtain

$$\begin{aligned} s^4 + \left(\lambda_4 + \left(b_2 + p_{33}\mathcal{K}^2\right)\right)s^3 + \left(\left(b_1 + p_{23}\mathcal{K}^2\right) + \left(b_2 + p_{33}\mathcal{K}^2\right)\lambda_4\right)s^2 + \\ \left(\left(b_1 + p_{13}\mathcal{K}^2\right) + \left(b_1 + p_{23}\mathcal{K}^2\right)\lambda_4\right)s + \left(b_1 + p_{13}\mathcal{K}^2\right) = 0 \end{aligned} \tag{6.28}$$

Comparing (6.28) with (6.15), λ_4 can be computed as,

$$\lambda_4 = -p_{33}\mathcal{K}^2 \tag{6.29}$$

For the sake of comparison, equation (6.28) can be written in simplified form as,

$$s^4 + p_1 s^3 + p_2 s^2 + p_3 s + p_4 = 0 \tag{6.30}$$

Here,

$$\begin{aligned} p_1 &= p_{33}\mathcal{K}^2 + b_2 + p_{33}\mathcal{K}^2 \\ p_2 &= \left(b_1 + p_{23}\mathcal{K}^2\right) + \left(b_2 + p_{33}\mathcal{K}^2\right) p_{33}\mathcal{K}^2 \\ p_3 &= \left(b_1 + p_{13}\mathcal{K}^2\right) + \left(b_1 + p_{23}\mathcal{K}^2\right) p_{33}\mathcal{K}^2 \\ p_4 &= b_1 + p_{13}\mathcal{K}^2 \end{aligned} \tag{6.31}$$

Step 8: Finally, by comparing (6.15) and (6.30), we get the parameters of $C(s)$ as follows,

$$\begin{aligned} \rho_p &= \frac{1}{\mathcal{K}}\left(b_1 + p_{13}\mathcal{K}^2 + \left(b_1 + p_{23}\mathcal{K}^2\right) p_{33}\mathcal{K}^2 - b_0\right) \\ \rho_i &= \frac{1}{\mathcal{K}}\left(b_1 + p_{13}\mathcal{K}^2\right) \\ \rho_d &= \frac{1}{\mathcal{K}}\left(p_{23}\mathcal{K}^2 + \left(b_2 + p_{33}\mathcal{K}^2\right) p_{33}\mathcal{K}^2\right) \end{aligned} \tag{6.32}$$

The results will be obtained for two different conditions, initially we obtain the QRAWCP-PID without considering the worst-case polynomial and then with worst-case polynomial selection for designing the QRAWCP-PID for LFC problems.

6.4.1.1 For nominal plant

In this section, we take three different cases. In Case 1 and 2, we consider a single-area power system in the presence and absence of parametric uncertainties and non-linearities, while in case 3, a two-area scenario is discussed. Using QRAWCP approach, PID parameters are obtained as $\rho_p = 6.5208$, $\rho_i = 8.7649$ and $\rho_d = 3.1385$ and using the parameters of single area LFC from [59, 198, 208], we simulate the model and controller in MATLAB & Simulink environment.

Case studies and result analysis:

Case 1: Single area for N-R turbine: The nominal parameters for single-area power system with N-R turbine are considered from [208] as $K_P = 120$, $T_P = 20$, $K_T = 1$, $T_T = 0.3$, $K_G = 1$, $T_G = 0.08$, $R = 2.4$.

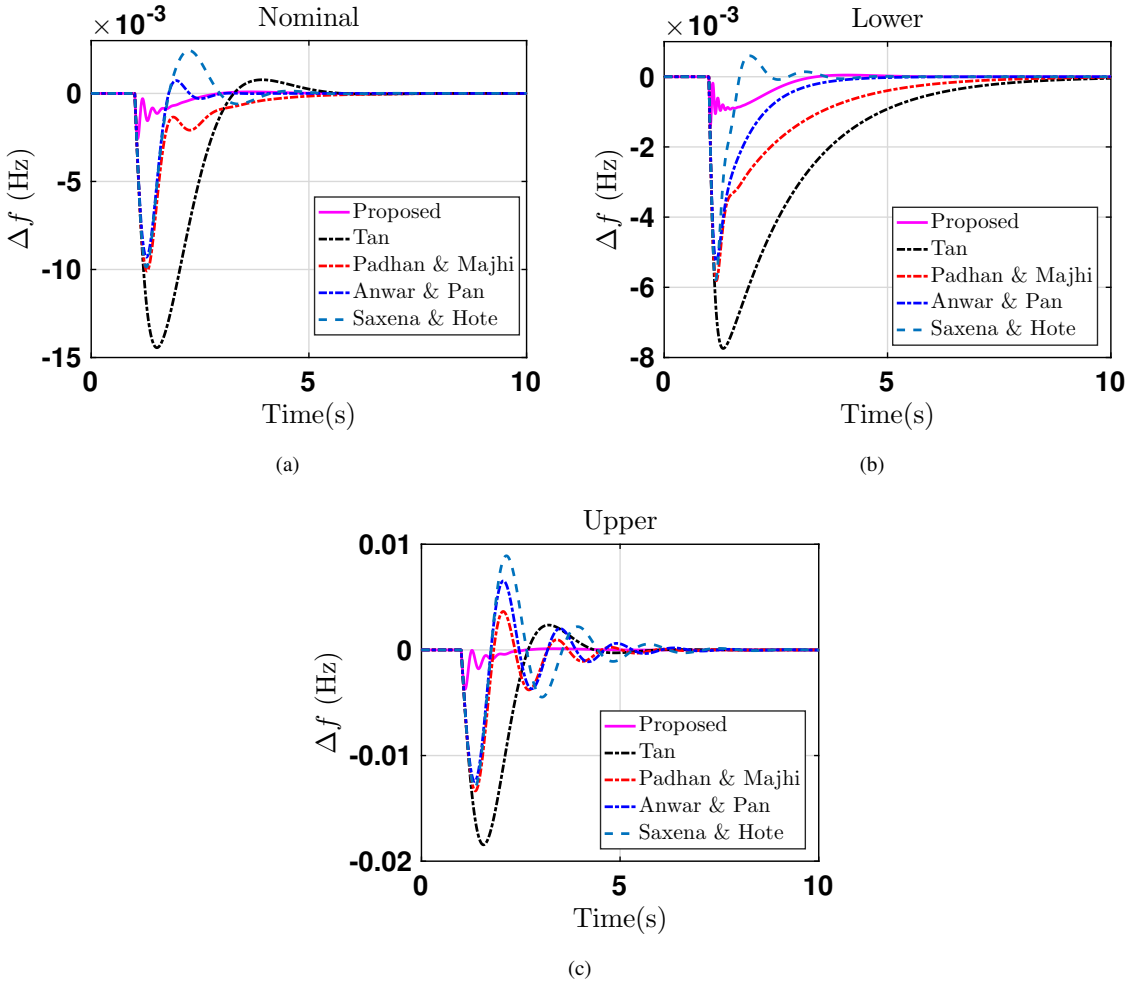

Figure 6.5: Time response for Case 1 (a)nominal,(b)−50%lower and (c)+50%upper parametric uncertainty of LFC

In this case, for the purpose of comparison with the proposed (QRAWCP-PID), we have considered the recently designed PID controller approaches, i.e., IMC-PID[58], direct synthesis approach[208], Laurent series based PID [59] and model order reduction based IMC-PID [190]. Fig. 6.5(a) shows the time evolution of frequency variation for a sudden load disturbance of 0.01 p.u. MW, which is applied at 1 s. It is seen that the QRAWCP scheme shows the least undershoot in comparison to other approaches. Further, we analyse the controllers in the presence of $\pm 50\%$ parametric variation from its nominal value, for lower and upper bound. It is shown in Fig. 6.5(b) and 6.5(c), that the frequency curve converges to zero with minimum undershoot and lesser time as compared to other considered approaches. The performance can also be measured quantitatively with the aid of integral performance indices such as Integral Square Error (ISE), Integral Absolute Error (IAE), Integral Times Squared Error (ITSE), Integral Time Absolute Error (ITAE). From Table 6.2, it is

evident that using the proposed scheme, minimum value of the integral error indices are obtained in both the cases.

Table 6.2: Performance indices for Non-reheated turbine($\times 10^{-4}$)

Methods	Nominal Plant				Lower -50% plant				Upper +50% plant			
	ISE	IAE	ITSE	ITAE	ISE	IAE	ITSE	ITAE	ISE	IAE	ITSE	ITAE
Proposed	0.013	13.79	0.018	25.24	0.0087	12.73	0.014	24.61	0.022	14.52	0.028	24.96
Tan	1.777	177.7	3.026	348.1	0.696	157.0	1.396	428.8	2.524	202.7	4.229	391.9
Padhan & Majhi	0.393	76.63	0.562	150.5	0.191	76.36	0.340	196.5	0.790	110.4	1.205	222.9
Anwar & Pan	0.289	44.35	0.378	61.97	0.110	39.99	0.155	70.23	0.786	124.6	1.291	275.6
Saxena & Hote	0.350	65.55	0.492	117.5	0.073	22.34	0.089	32.80	1.084	160.9	1.982	387.4

Case 2: LFC considering GRC and GDB constraints: For this case, we have considered real-time non-linearities of generation rate constraint (GRC), and governor dead band (GDB). Their specifications are GRC = 0.1 p.u./min. or 0.001667 p.u./sec. [58, 61] and GDB = 0.06% or 0.036 Hz/p.u. MW [211]. These are then applied to the LFC configuration given in case 1. Fig. 6.6(a) depict that QRAWCP performs better in comparison to other PID controller techniques given in [59, 190, 208, 212], Similar to case 1, $\pm$50% parametric variation has been considered, as shown in Fig. 6.6(b) and 6.6(c), which highlights robustness capability of proposed approach in comparison to others. The results obtained from the graphical analysis can be better understood using the integral performance indices values, given in Table 6.3, for respective control techniques including the proposed one. The values from this table clearly imply that the frequency of generated voltage suffers less variation, when controlled using QRAWCP approach.

Table 6.3: Performance indices in the presence of GRC and GDB ($\times 10^{-4}$)

Methods	Nominal Plant				Lower -50% plant				Upper +50% plant			
	ISE	IAE	ITSE	ITAE	ISE	IAE	ITSE	ITAE	ISE	IAE	ITSE	ITAE
Proposed	0.165	60.92	0.339	140.5	0.160	58.21	0.313	127.3	0.162	60.83	33.73	143.7
Tan	27.93	792.5	60.56	1864.4	13.55	719.8	31.24	2138.8	30.21	795.5	65.29	1828.6
Padhan & Majhi	5.129	352.5	9.423	815.8	3.551	351.0	7.296	969.2	5.738	352.5	10.33	806.4
Anwar & Pan	2.997	184.0	4.679	306.7	1.908	183.9	3.113	356.1	4.009	260.9	6.699	558.4
Saxena & Hote	3.412	231.8	5.612	456.3	0.953	92.53	1.332	147.5	6.062	426.1	12.85	1168.1

Case 3: LFC for two area control: In this case, we extend the application of the proposed technique to two-area power system model. The model assumed for this purpose consists of two

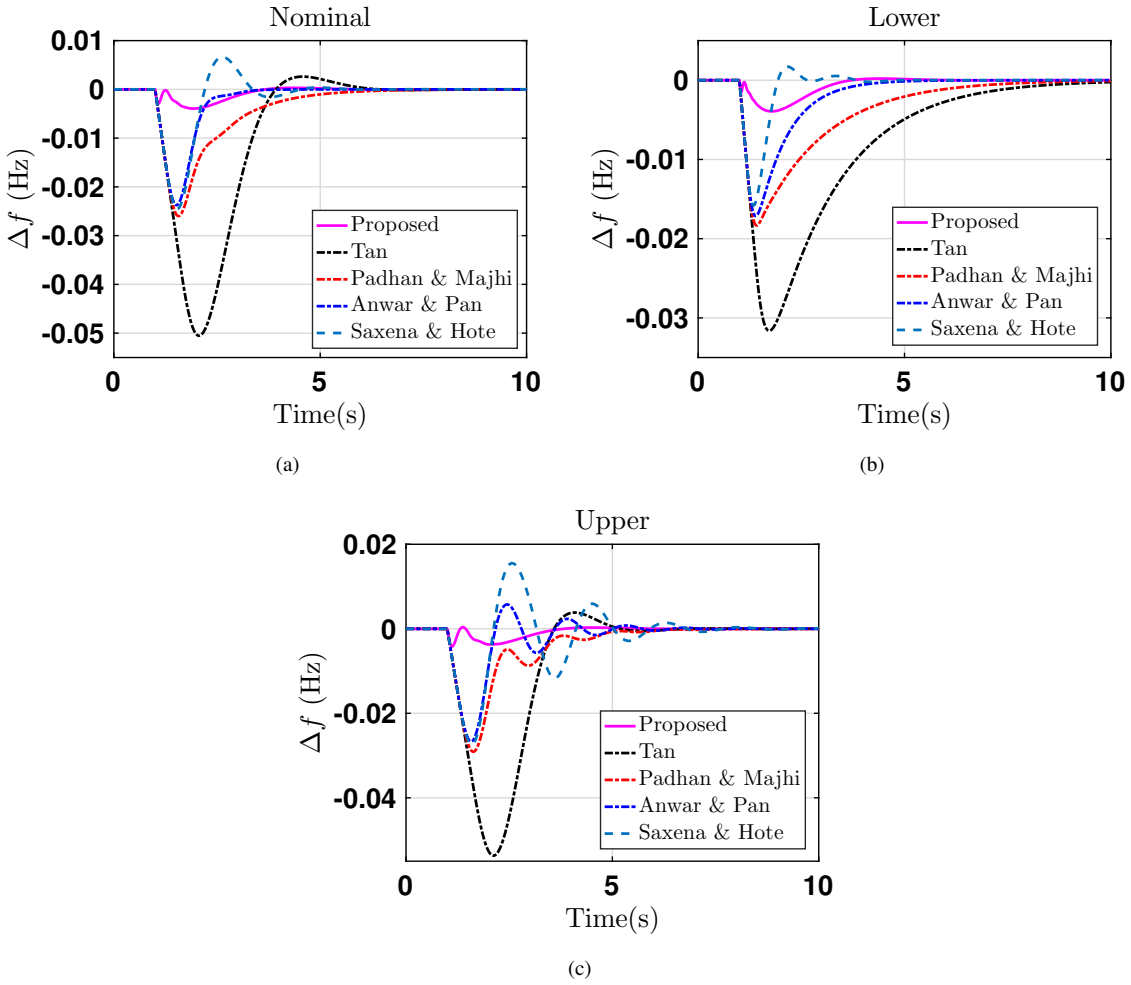

Figure 6.6: Time response for Case 2 (a)nominal,(b)−50%lower and (c)+50%upper parametric uncertainty with GRC and GDB of LFC

reheated generators, one in each area. The schematic of the individual areas and their interconnections is shown in Fig. 6.7, which is taken from [208] and [59]. The dynamics of each area are same as for the single area case, with the addition of the interconnected tie-line power of $T_{i1} = T_{i2} = 4.2$ and frequency bias is $B_1 = B_2 = 0.35$. The analysis of the two-area model is done by applying a load disturbance at 1 sec for ΔP_{d1}, and at 15 sec for ΔP_{d2}. The PID controller used for this analysis is identical to the one used for the single area situation, and the magnitude of the injected disturbance is: $|\Delta P_{d1}| = |\Delta P_{d2}| = 0.01$ p.u.MW. The results of this analysis are illustrated in Fig. 6.8, which shows that the load frequency curve exhibits lesser undershoot and quicker convergence to zero, as compared to using other techniques reported so far.

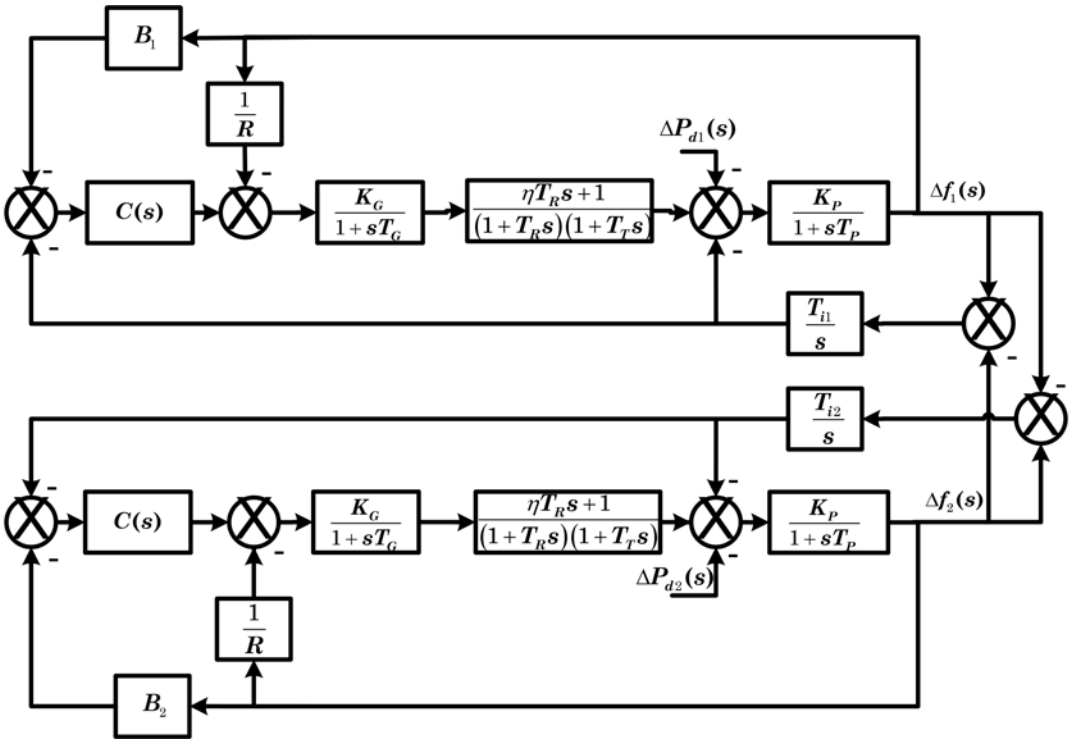

Figure 6.7: Block diagram of two area power system

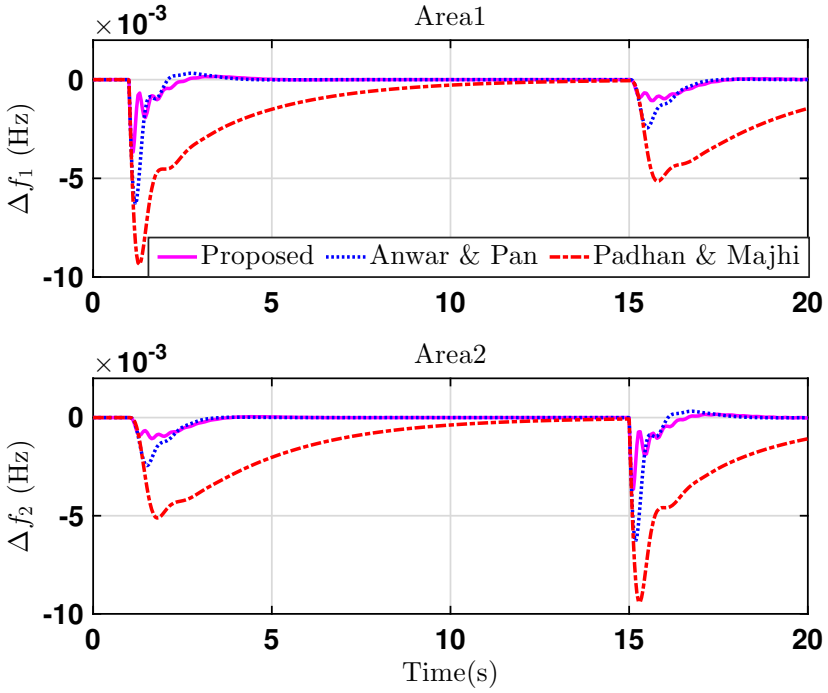

Figure 6.8: Comparison of responses of two area system for Case 3

6.4.1.2 Using worst-case polynomial selection

Case studies and result analysis:

1) Case 1: In this case, the efficacy of controller is evaluated for single area non-reheated turbine with droop characteristics based power system, in the presence of nominal parameters and parametric uncertainty (lower bound (-50%) and upper bound ($+50\%$)) where, 0.01 p.u. as step change is introduced in load disturbance at $t = 1$ sec.
The parametric uncertainties are considered as $K_P = [60, 180]$, $T_P = [10, 30]$, $T_G = [0.04, 0.12]$, $T_T = [0.15, 0.45]$, $R = [1.2, 3.6]$. Therefore, we get worst-case plant polynomial for considered system dynamics as $G_3(s) = 151 + 10.19s + 1.906s^2 + 1.62s^3$. Using QRAWCP approach and worst-case plant selection approach, we obtain the optimal PID gain values as $K_p = 6.5208$, $K_i = 8.7649$, and $K_d = 3.1385$.

For the ease of understanding, we subdivide Case 1 in two parts as follows, Case 1(a): Here, the effect of GRC and GDB is not taken into consideration. The resulting plots are shown in Fig. 6.13 (a-c). Case 1(b): Here, the effect of GRC and GDB are considered. The resulting plots are shown in Fig. 6.13 ((d)-(f)). It can be seen from Fig. 6.13((a)-(f)), that the proposed control schemes outperform the existing control schemes ([58, 59, 61, 208]).

2) Case 2: The single area Reheated turbine with droop characteristics-based power system is considered in this case. The parametric uncertainties are considered as $K_P = [60, 180]$, $T_P = [10, 30]$, $T_G = [0.04, 0.12]$, $T_T = [0.15, 0.45]$, $T_r = [2.1, 6.3]$, $c = [0.175, 0.525]$, $R = [1.2, 3.6]$ ([58, 198]). Therefore, we get worst-case plant polynomial for single area Reheated turbine with droop characteristics based power system $G_3(s) = 151 + 34.34s + 32.945s^2 + 109.6902s^3 + 10.2060s^4$. Using QRAWCP approach and worst-case plant polynomial, we obtain the optimal PID gain values: $K_p = 27.9082$, $K_i = 19.1910$, and $K_d = 14.3941$. We can demarcate Case 2 in two parts as follows, Case 2(a): Here, the effect of GRC and GDB is not taken into account. The corresponding plots are shown in Fig. 6.9 (a-c). Case 2(b): Here, the effect of GRC and GDB is considered. The corresponding plots are shown in Fig. 6.9 ((d)-(f)). It can be seen from Fig. 6.9((a)-(f)), that the proposed control schemes shows less frequency deviation as compared to the existing techniques. ([58, 59, 208]).

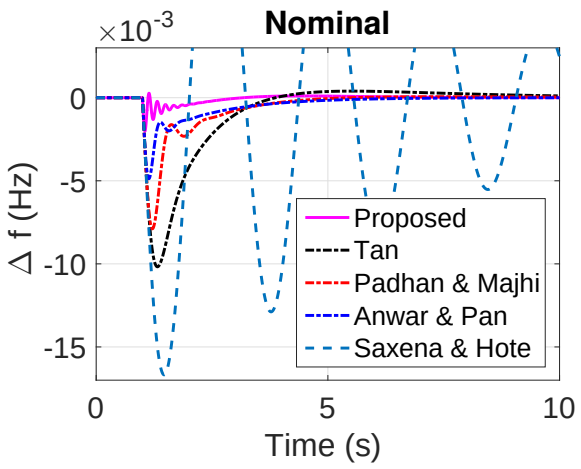

(a)

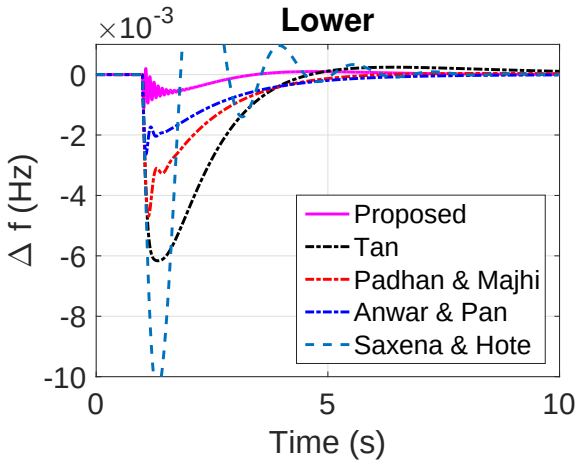

(b)

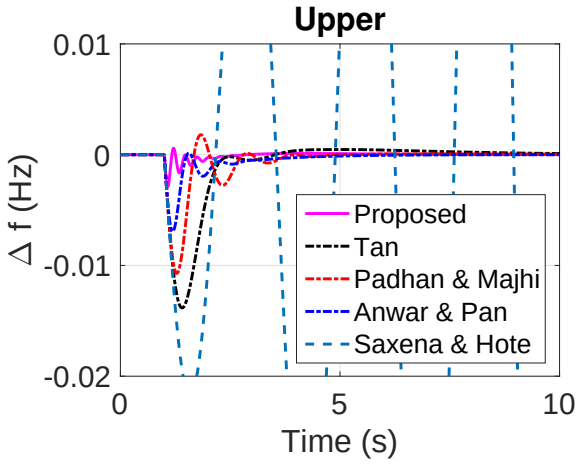

(c)

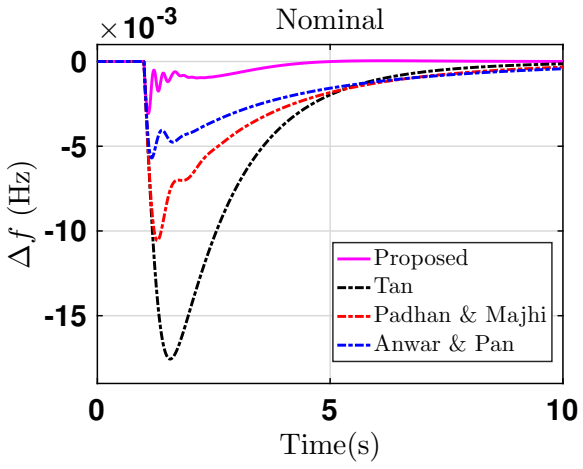

(d)

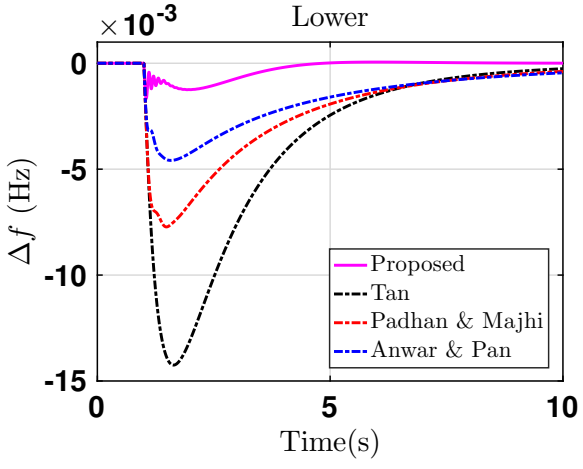

(e)

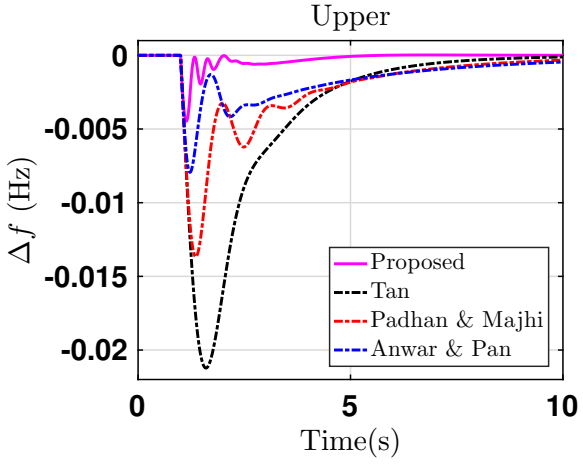

(f)

Figure 6.9: Time response of R-turbine based single area power system for case 2(a) without and (b) with GRC and GDB

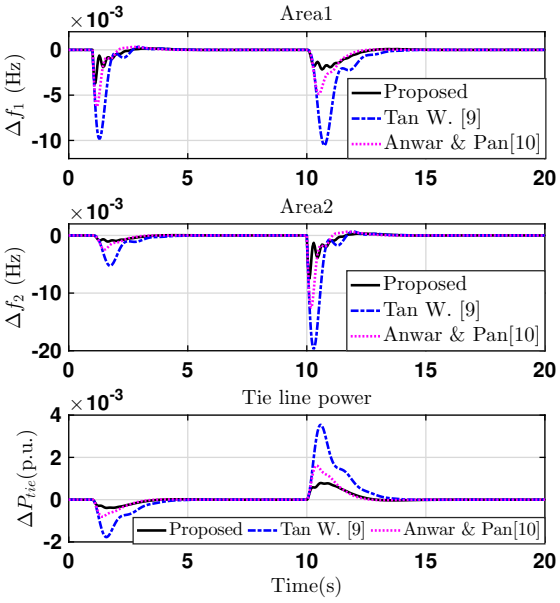
Area1
×10-3
Δf1 (Hz)
Proposed
Tan W. [9]
Anwar & Pan[10]
Area2
Δf2 (Hz)
Tie line power
ΔPtie(p.u.)
Time(s)

(a)

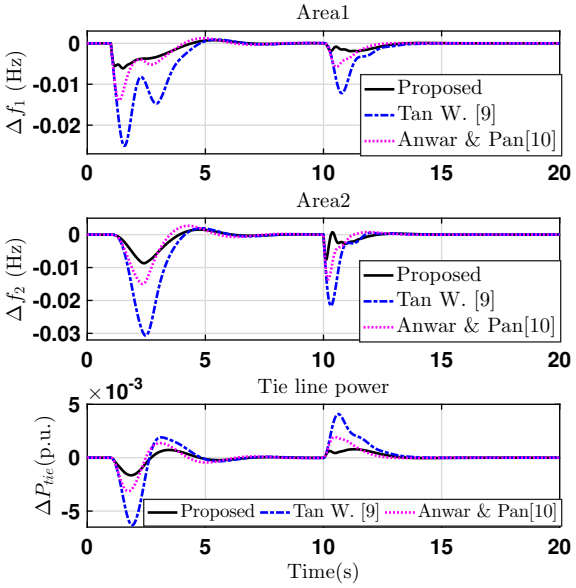
Area1
Δf1 (Hz)
Proposed
Tan W. [9]
Anwar & Pan[10]
Area2
Δf2 (Hz)
Tie line power
×10-3
ΔPtie(p.u.)
Time(s)

(d)

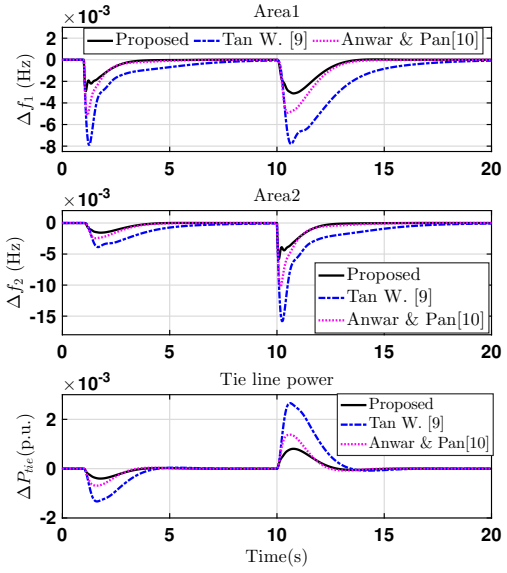
Area1
×10-3
Proposed
Tan W. [9]
Anwar & Pan[10]
Δf1 (Hz)
Area2
Δf2 (Hz)
Tie line power
ΔPtie(p.u.)
Time(s)

(b)

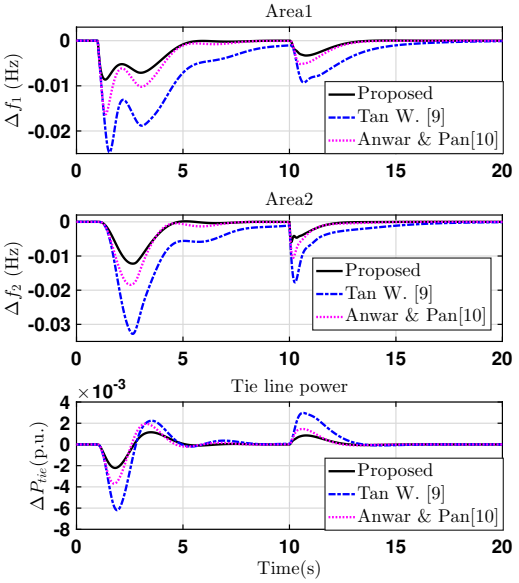
Area1
Δf1 (Hz)
Proposed
Tan W. [9]
Anwar & Pan[10]
Area2
Δf2 (Hz)
Tie line power
×10-3
ΔPtie(p.u.)
Time(s)

(e)

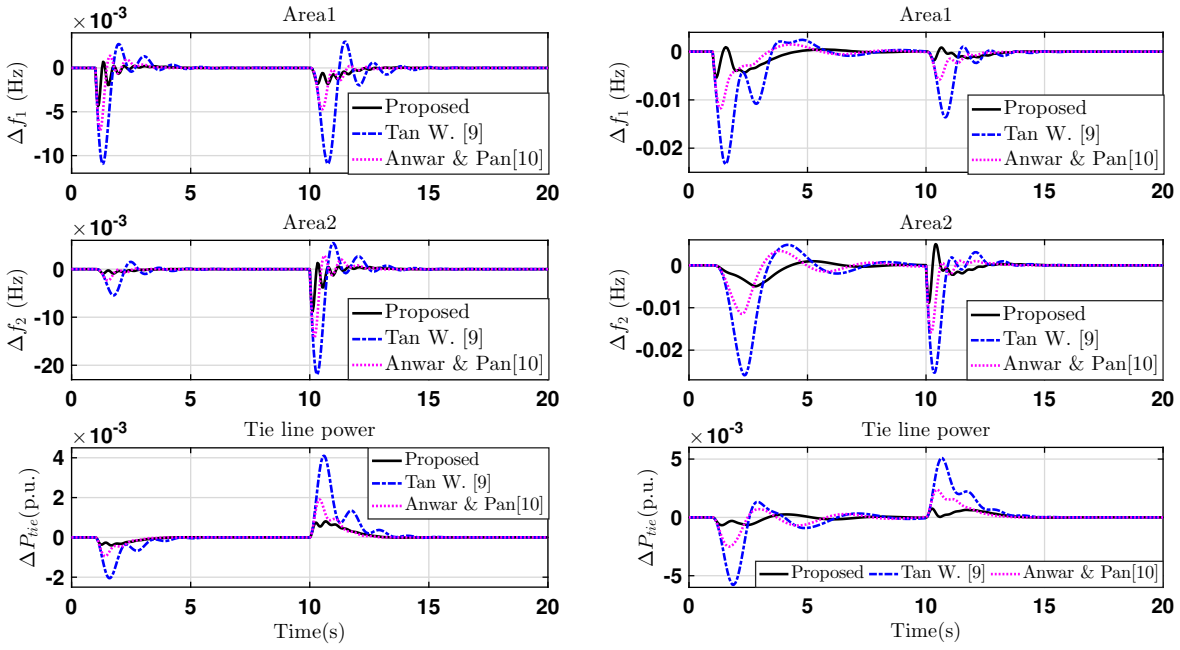

Figure 6.10: Time response of NR-turbine based two area power system for case 3(a) without, and case 3(b) with GRC and GDB.

3) Case 3: In this case, the proposed control scheme is extended for a two area power system based on NR turbine. The system parameters are taken from [59, 212]. Now, we apply the same procedure as discussed in case-1. Both areas in the given system are identical. Using QRAWCP approach and worst-case plant selection approach, we obtain the optimal PID gain values for each area as $K_p = 6.5208$, $K_i = 8.7649$, and $K_d = 3.1385$. The frequency deviation for area 1 (Δf_1) and area 2 (Δf_2), and tie-line power(Δp_{tie}) deviation of two area power system without GRC, GDB are given in Fig.6.10(a) and the robustness analysis for $\pm 50\%$ parametric uncertainty is shown in Fig. 6.10(b-c). Further, the simulation is carried out with GRC and GDB physical constraints in two area power system as shown in Fig. 6.10(d-f). From these results, it can be seen the proposed controller has the minimum frequency and tie-line power deviation compared to existing controller schemes [59, 212].

Table 6.4: Performance indices for NR-Turbine based single area power system without(case 1(a)) and with(case 1(b)) GRC and GDB

	Methods	Nominal Plant				Lower -50% plant				Upper +50% plant			
		ISE	IAE	ITSE	ITAE	ISE	IAE	ITSE	ITAE	ISE	IAE	ITSE	ITAE
Case 1(a)	Proposed	1.330	13.79	1.880	25.24	0.871	12.73	1.420	24.62	2.240	14.52	2.830	24.96
	Anwar & Pan	28.90	44.36	37.80	61.98	11.00	40.00	15.50	70.24	78.60	124.6	129.1	275.6
	Padhan & Majhi	39.30	76.63	56.20	150.6	19.10	76.36	34.00	196.5	79.00	110.4	120.5	223.0
	Saxena & Hote	35.00	65.55	49.20	117.5	7.300	22.34	8.890	32.80	108.5	160.9	198.2	387.4
	Tan	177.7	177.8	302.6	348.1	69.60	156.6	139.6	428.8	252.5	202.8	422.9	392.0
Case 1(b)	Proposed	16.54	60.92	33.9	140.6	16.04	58.22	31.33	127.4	16.17	60.84	33.73	143.8
	Anwar & Pan	299.7	184	467.9	306.7	190.8	184.0	311.3	356.0	400.9	260.9	669.9	558.4
	Padhan & Majhi	512.9	352.5	942.3	815.8	355.5	351.1	729.6	969.2	573.8	352.5	1033	806.4
	Saxena & Hote	341.2	231.8	561.2	456.3	95.33	92.53	133.2	147.5	606.2	426.1	1285	1168
	Tan	2793	792.5	6056	1864	1355	719.8	3125	2139	3021	795.6	6530	1829

*ISE=$\times 10^{-6}$, IAE=$\times 10^{-4}$, ITSE=$\times 10^{-6}$, and ITAE=$\times 10^{-4}$.

Table 6.5: Performance indices for R-Turbine based single area power system without(case 2(a)) and with(case 2(b)) GRC and GDB

	Methods	Nominal Plant				Lower -50% plant				Upper +50% plant			
		ISE	IAE	ITSE	ITAE	ISE	IAE	ITSE	ITAE	ISE	IAE	ITSE	ITAE
Case 2(a)	Proposed	0.643	11.81	0.981	31.60	0.429	11.39	0.782	32.68	1.160	12.68	1.550	31.28
	Anwar & Pan	7.100	40.04	10.90	92.65	4.930	39.98	9.150	105.7	12.20	40.33	16.50	84.93
	Padhan & Majhi	20.20	59.13	28.80	140.5	12.40	56.62	20.80	141.4	39.20	68.71	54.60	149.6
	Tan	62.00	116.0	97.90	309.6	39.30	103.9	69.40	289.7	99.60	121.7	149.4	304.3
Case 2(b)	Proposed	2.670	26.39	4.780	64.23	2.420	27.07	5.080	69.05	3.990	25.29	5.740	59.14
	Anwar & Pan	47.40	182.4	131.0	835.8	44.80	182.1	130.0	863.2	48.60	182.4	135.0	863.0
	Padhan & Majhi	112.0	237.8	254.0	880.4	99.60	237.6	246.0	936.8	127.0	237.9	268.0	869.2
	Tan	372.0	361.2	774.0	1029	306.0	361.1	695.0	1162	426.0	361.2	829.7	974.1

*ISE=$\times 10^{-6}$, IAE=$\times 10^{-4}$, ITSE=$\times 10^{-6}$, and ITAE=$\times 10^{-4}$.

6.4.1.3 New England (10 machine 39 bus) power system

This section describes a model of a New England (10 machine 39 bus) interconnected power system.

Here for study, we consider a realistic power system that is similar to network topology of the standard IEEE 39 bus test system ([213–215]). The single line diagram is depicted in Figure 6.11. In this test system, we consider GDB and GRC nonlinearities in the westing-house electro

Table 6.6: Performance indices of NR-Turbine based Two area power system with(case 3(a)) and without(case 3(b)) GRC and GDB

		Nominal plant				Lower -50% plant				Upper +50% plant			
	Methods	ISE	IAE	ITSE	ITAE	ISE	IAE	ITSE	ITAE	ISE	IAE	ITSE	ITAE
Area1 Case 3(a)	Proposed	6.859	47.21	48.28	359.0	16.35	81.46	141.2	665.5	5.190	34.82	25.40	233.4
	Tan	96.83	153.2	713.8	1176	122.7	292.9	1103	2675	103.7	163.6	696.8	1163
	Anwar & Pan	21.53	67.94	139.8	482.5	36.80	118.6	306.6	967.2	19.84	58.39	97.20	348.2
Area2 Case 3(a)	Proposed	88.83	190.0	335.5	943.0	205.7	275.9	695.4	1246	45.80	149.9	267.2	906.5
	Tan	1029	562.1	4085	2645	1559	999.4	6002	5693	797.3	533.1	4075	2933
	Anwar & Pan	247.9	291.1	1045	1420	439.0	403.4	1486	1848	175.5	255.8	964.7	1389
Area1 Case 3(b)	Proposed	51.45	161.7	155.6	766.1	141.5	274.9	469.8	1259	27.96	113.4	86.02	551.9
	Tan	658.8	523.8	2184	2404	1182	999.4	4598	5731	476.7	426.3	1758	2072
	Anwar & Pan	143.6	236.9	448.7	1076	308.1	403.4	989.6	1864	87.53	181.2	282.5	876.6
Area2 Case 3(b)	Proposed	88.83	190.0	335.5	943.0	205.7	275.9	695.4	1246	45.80	149.9	267.2	906.5
	Tan	1029	562.1	4085	2645	1559	999.4	6002	5693	797.3	533.1	4075	2933
	Anwar & Pan	247.9	291.1	1045	1420	439.0	403.4	1486	1848	175.5	255.8	964.7	1389

*ISE=$\times 10^{-6}$, IAE=$\times 10^{-4}$, ITSE=$\times 10^{-6}$, and ITAE=$\times 10^{-4}$.

hydraulic speed governor system without steam feedback ((IEEE Report, 1973). This test system is divided into three control areas. Only one generator in each area participates in the LFC task. These generation units are G3, G7 and G9 in area 1, area 2 and area 3 respectively. The test system specifications for generators, loads and lines parameters have been listed in [[214], [215]]. With the droop characteristics, the transfer function of plant model is given as follows [61].

$$G(s) = \frac{R}{\left\{ \begin{array}{l} (2HT_GT_Ts^3 + (2HT_G + DT_GT_T + 2HT_T)s^2 \\ +(2H + DT_G + DT_T)s)R + RD + 1 \end{array} \right\}} \tag{6.33}$$

Here, two tie-lines (the transmission lines between bus 1 and 39, bus 3 and 4), that exist between area 1 and area 3 are considered equivalent to one tie-line. The steam speed governing system is depicted in Figure 6.12.

Simulation and Result analysis: This section demonstrates the simulation results obtained in MATLAB/Simulink environment for evaluation of the performance of proposed control scheme

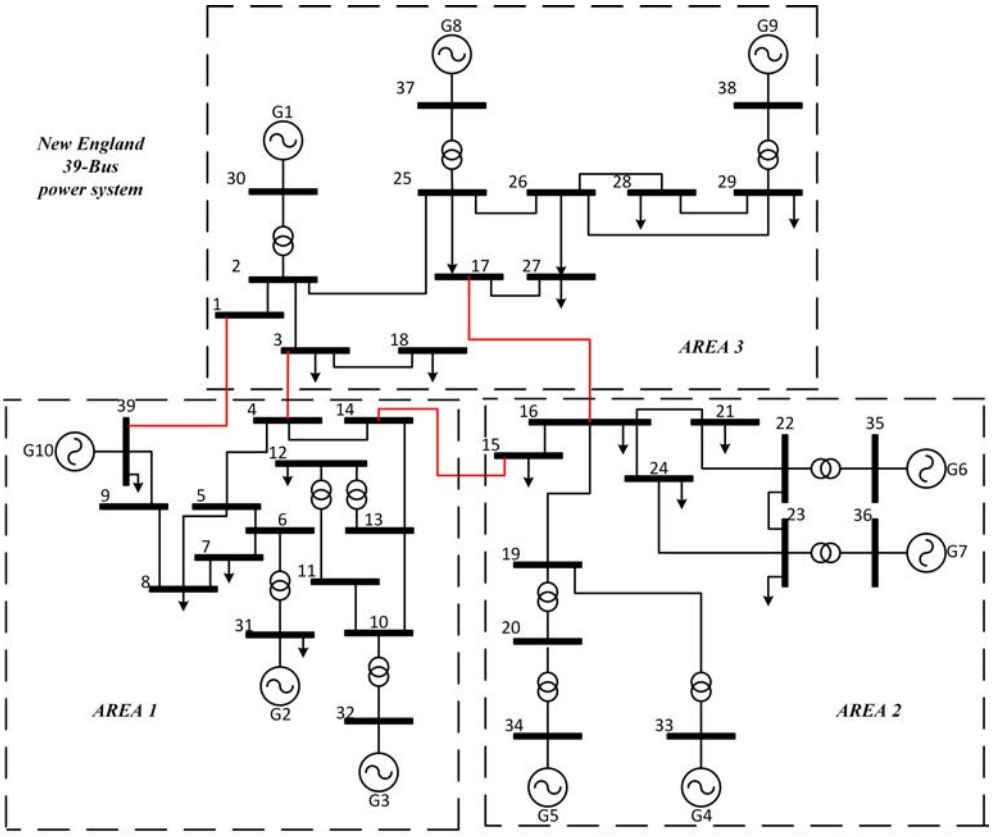

Figure 6.11: Single line diagram of New England 10 machine 39 bus power system.

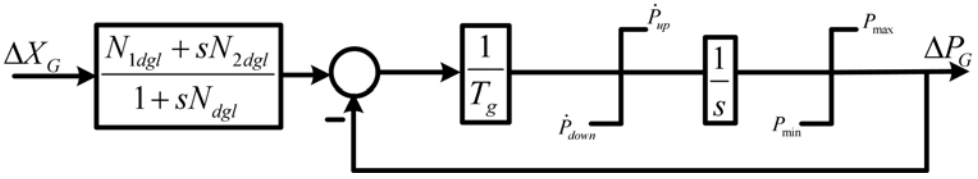

Figure 6.12: Steam speed governing system with GDB and GRC.

Table 6.7: System parameters

Parameters	H	D	T_G	T_T	P_{op}
G_3	35.8	10	0.15	0.3	6.50
G_7	26.4	8	0.1	0.3	5.60
G_9	34.5	14	0.1	0.3	8.30

for various case studies. The effectiveness of proposed control scheme is assessed and compared with existing control schemes.

Note 1: The specifications on non-linearities are given as GRC as 0.1 p.u./min. or 0.001667 p.u./sec. [216], [61] and GDB is 0.06% or 0.036 Hz/p.u. MW according to IEEE standard [211] for case 1 to 3.

Note 2: The nominal, lower bound (-50%) and upper bound (+50%) values of system parameters for single area non-reheated and reheated turbine based isolated power systems are given for case 1-3 as follows, ([58], [208]), [38], [39]) $B_i = 0.425$, $R_i = 2.4$, $T_{gi} = 0.08$, $T_{ti} = 0.3$, $T_{pi} = 20$, $K_{pi} = 120$, $T_{ri} = 4.2$, $T_{12} = 0.545$, and $i = 1,2$. The lower and upper bound values can be written as follows, $1/T_t \in [2.564, 4.762]$,, $1/T_g \in [9.615, 17.857]$,, $1/RT_g \in [3.081, 10.639]$,, $K_p/T_p \in [4, 12]$,, and $1/T_p \in [0.033, 0.1]$.

Note 3: Each area has a rating of 2 GW with a nominal load of 1 GW operating at frequency $f = 60$ Hz for case 1-3.

4) Case 4: From the practical point of view, the proposed controller is evaluated for New England (10 generator and 39 bus) power system. The different parameters are $R = 0.05$, $\dot{P}_{up} = 0.1$, $\dot{P}_{down} = -0.1$, $P_{max} = 2P_{op}$, $P_{min} = -P_{op}$, $N_{1dgl} = 0.8$, $N_{2dgl} = -0.2$, $T_{dgl} = 0.1$ and $B_i = D_i + \frac{1}{R}$ where $i = 1,2,3$[214], [61]. Then, considering interval parameters, $H \in [26,34]$, $D \in [8,14]$, $T_G \in [0.1,0.15]$, we get worst-case plant polynomial $G_3(s) = 34 + 55.2s + 21.04s^2 + 3.24s^3$. Using QRAWCP approach and worst-case plant selection approach, optimal value of PID gain are: $K_p = 4.3644$, $K_i = 1.1676$, and $K_d = 1.6518$.

During the simulation, a step change in load with magnitude of 0.038 p.u. MW, 0.064 p.u. MW and 0.043 p.u. MW for area 1, area 2 and area 3 is applied to bus 8 at $t = 1$sec, bus 16 at $t = 50$ sec and bus 3 at $t = 80$ sec, respectively. The response of frequency deviation Δf_1, Δf_2, Δf_3 for area 1, 2 and 3, and net tie-line power deviation ΔP_{tie1}, ΔP_{tie2}, ΔP_{tie3} of three area power system are given in Fig. 6.14, respectively. The simulation results show that the QRAWCP-PID scheme gives better results than [61].

Performance indices: Moreover, to measure the robustness and optimality of the proposed QRAWCP-PID scheme and existing control method, Integral Square Error ($ISE = \int_0^\infty \Delta f(t)^2 dt$), Integral Absolute Error($IAE = \int_0^\infty |\Delta f(t)| dt$), Integral Time Squared Error($ITSE = \int_0^\infty \Delta t f(t)^2 dt$) and Integral Time Absolute Error($ITAE = \int_0^\infty t|\Delta f(t)| dt$) are evaluated for all the cases in Table 6.4 for case 1, in Table 6.5 for case 2, in Table 6.6 for case 3, and in Table 6.8 for case 4. The value of performance indices for all the cases are minimum for the proposed scheme as compared to existing control schemes. Thus, the proposed control scheme in all the above cases is almost optimal and robust in nature.

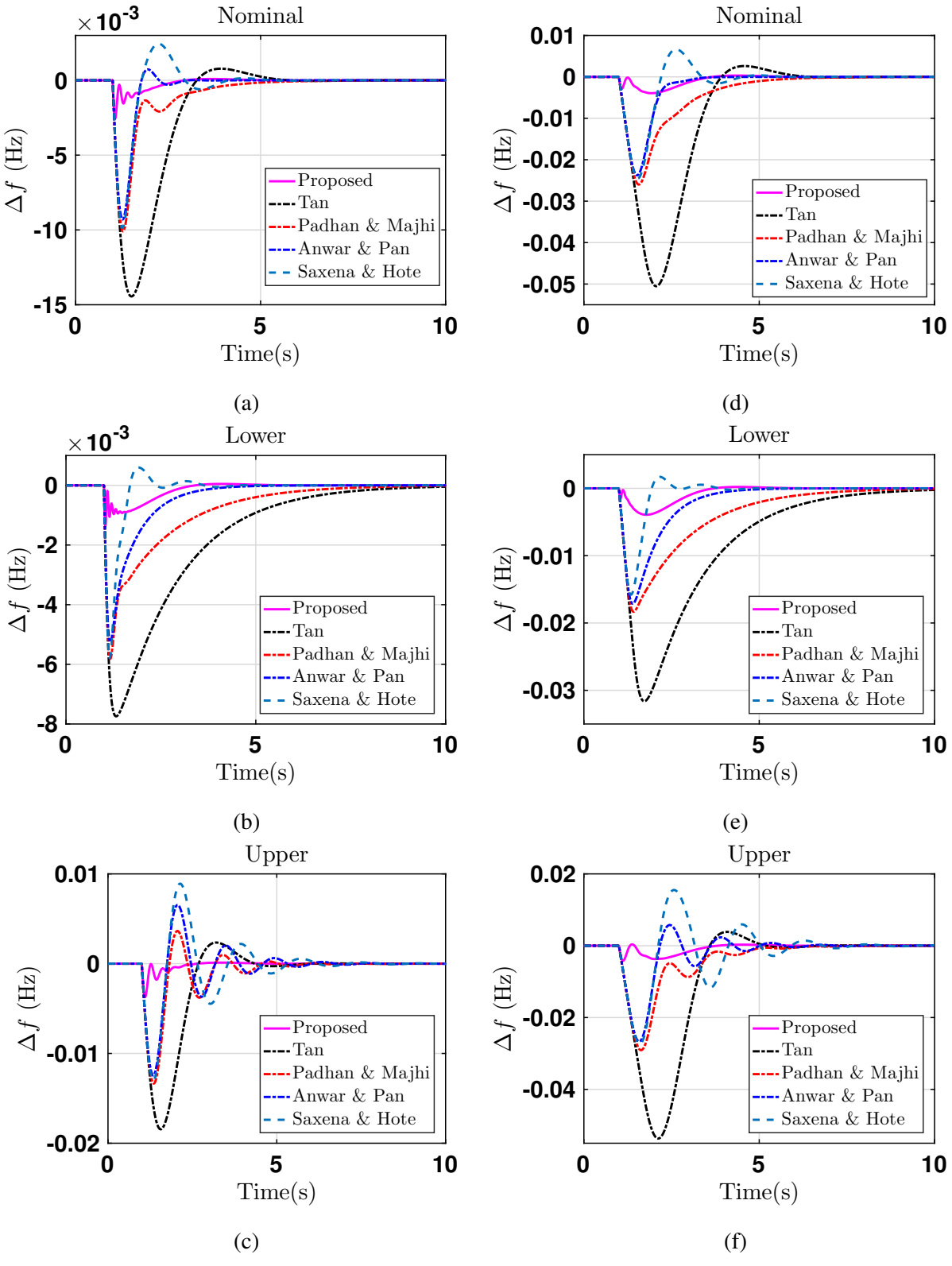

Figure 6.13: Time response of NR-turbine based single area power system for case 1(a) without and (b) with GRC and GDB

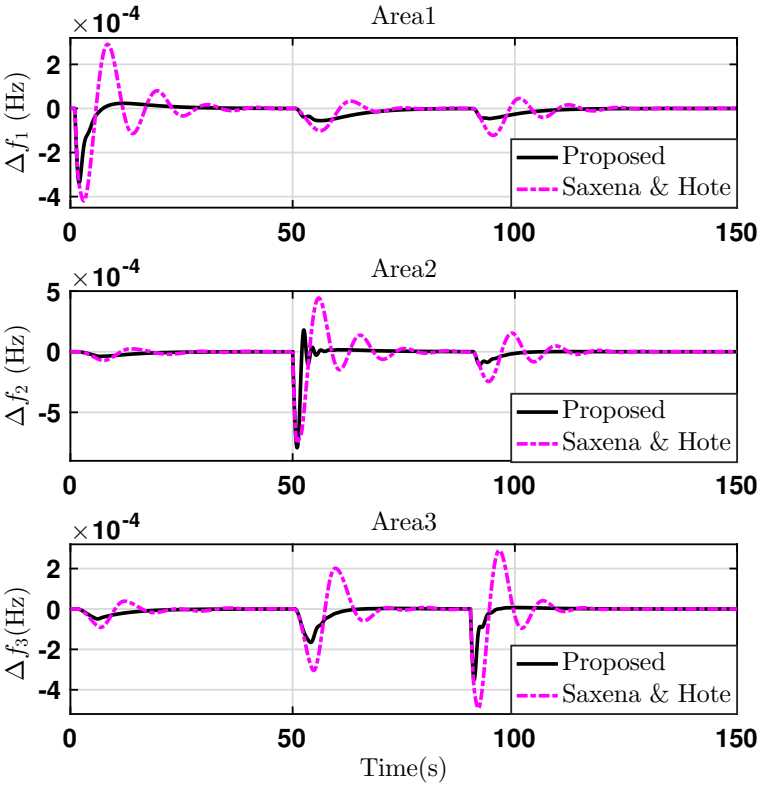

(a)

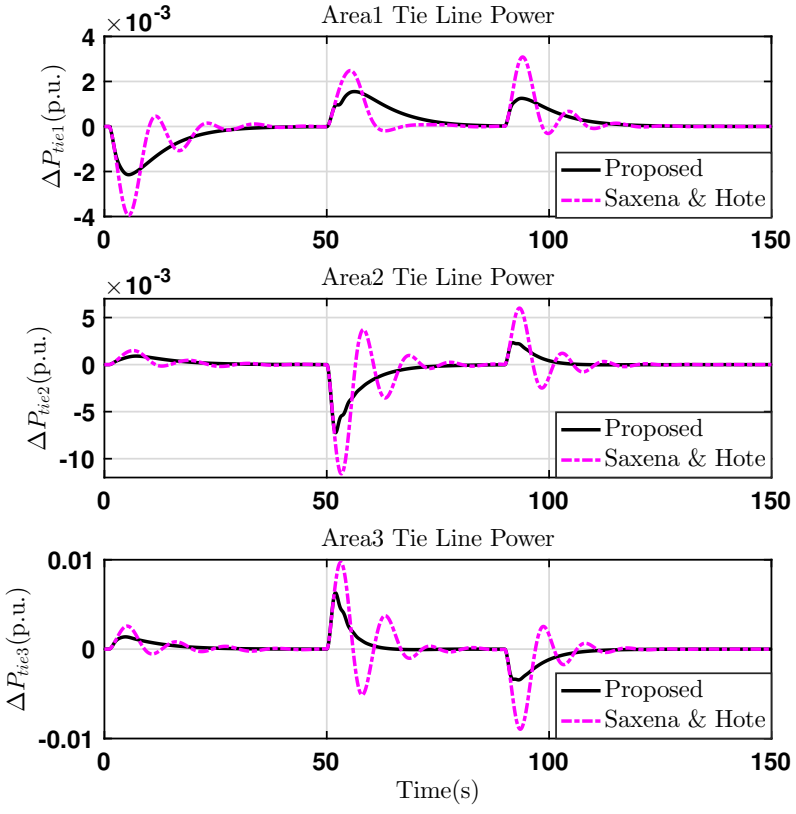

(b)

Figure 6.14: Time response of Case 4 New England 39 Bus system Δf and Tie line power ΔP_{tie}

Table 6.8: Performance indices for Case 4 New England 39 bus power system

	Methods	ISE	IAE	ITSE	ITAE
Area 1	Proposed	0.2100	23.19	3.480	1032
	IMC PID	0.8600	50.88	13.37	1782
Area 2	Proposed	0.7000	24.41	36.83	1353
	IMC PID	1.960	69.73	115.0	4535
Area 3	Proposed	0.220	19.34	15.83	1139
	IMC PID	1.190	56.65	94.1	4021

*ISE=$\times 10^{-6}$, IAE=$\times 10^{-4}$, ITSE=$\times 10^{-6}$, and ITAE=$\times 10^{-4}$.

6.4.2 Adaptive policy

Till date, various load frequency control (LFC) schemes have been reported and every scheme has its own way of disturbance rejection. Combining some of them together via switching mechanism may lead to an improved performance. Keeping this fact in mind, an adaptive control policy is proposed in this section. The policy incorporates the concept of enhancing and lowering the controller activity by assigning them weights at every instance throughout the operation. Thus, there is no need to go for a new control scheme until required; and a guaranteed improved performance would be achieved. Different case studies including single and multi-area power systems have been conducted to verify the accuracy and efficiency of the proposed method.

In power system studies, LFC is a subject of research for more than four decades and numerous control strategies have been developed. We believe that if some of the existing control strategies are included in LFC operation in a manner that their best features are extracted then a highly improved performance can be achieved. In this regard, an adaptive control policy is proposed which encapsulates two controllers and their activity is enhanced or decreased as per their performance throughout the control operation.

To simplify the analysis, but without loss of generality, a single/two-area system consisting of non-reheated thermal turbine is considered (see [58] for list of nomenclature and data). Figure 6.15 illustrates the schematic of the proposed closed-loop power system model G with two controllers C_1 and C_2 whose best features are to be extracted. One can select the controller on the basis of their performance merits (robustness, optimality, etc), wide area applicability and recent development.

The multiplying factors w_1 and w_2 are weights that emphasis the comparative role of C_1 and C_2, respectively. The control signal is:

$$U = w_1 u_1 + w_2 u_2 \tag{6.34}$$

Since, $\Delta f = G \times U$ and for single-area, the output is:

$$\Delta f(s) = \frac{\mathcal{K}}{s^3 + b_2 s^2 + b_1 s + b_0} U(s) \tag{6.35}$$

where, $\mathcal{K} = \frac{K_p}{T_G T_T T_P}$, $b_0 = \frac{K_p}{R T_G T_T T_P}$, $b_1 = T_G + T_T + T_P$, $b_2 = T_G T_T + T_G T_P + T_T T_P$. Note that for multi-area system, the system model for i^{th} control area becomes $B_i G_i$. Now, for the proposed

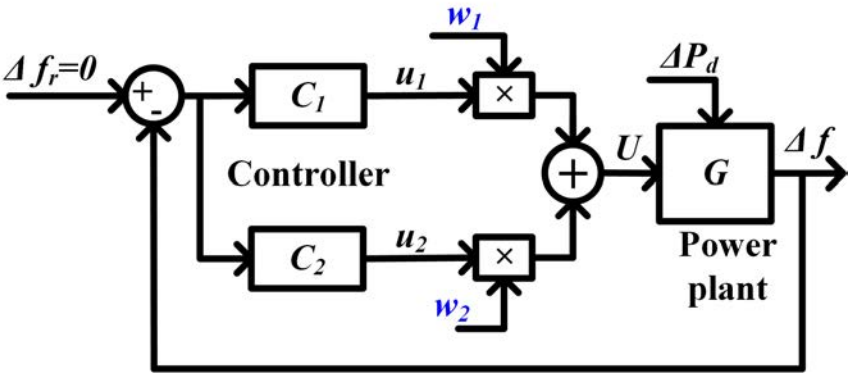

Figure 6.15: Schematic of the proposed control system

control structure, the control signal can be expressed using (6.35) as:

$$U(t) = \frac{1}{\mathcal{K}} \left[\Delta f^{(3)}(t) + b_2 \Delta f^{(2)}(t) + b_1 \Delta f^{(1)}(t) + b_0 \Delta f(t) \right] \tag{6.36}$$

We choose performance index (integral of a squared error):

$$I_s = \frac{1}{2} \int e^2(t) dt \tag{6.37}$$

as an objective function, where, $e(t) \equiv f_r(t) - f(t) = -f(t)$ (As $f_r = 0$ for disturbance rejection). To update the weights, we apply gradient descent algorithm [139]:

$$w_n(t+1) \leftarrow \left(w_n(t) - \alpha \frac{dI_s(t)}{dw_n(t)} \right); \quad n = 1, 2 \tag{6.38}$$

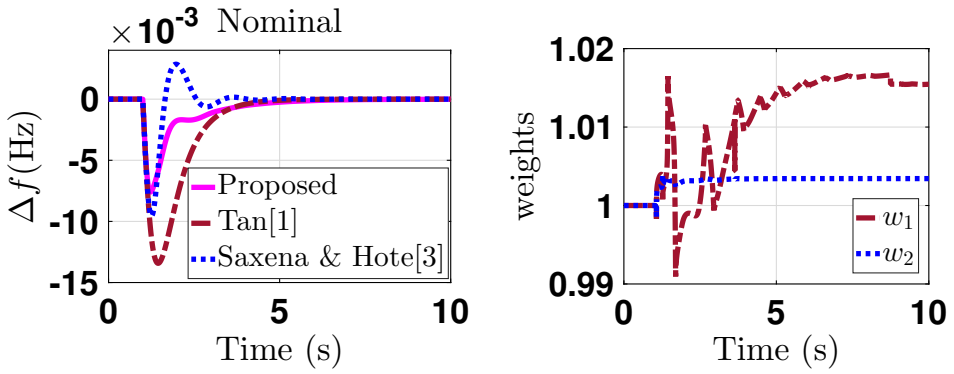

Figure 6.16: Time response and weight update pattern for Case 1

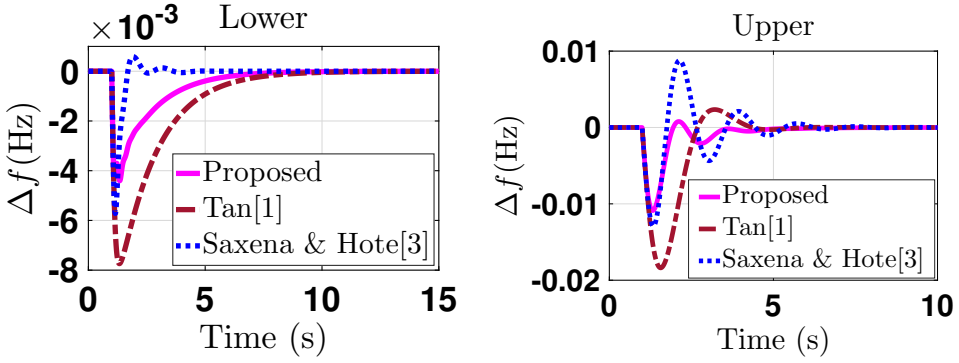

Figure 6.17: Response under parametric uncertainty in Case 1

Here, α is a learning rate. To obtain $\frac{dI_s(t)}{dw_n(t)}$, we apply chain rule: $\frac{dI_s(t)}{dw_n(t)} = \frac{dI_s(t)}{d\Delta f(t)}\frac{d\Delta f(t)}{dU(t)}\frac{dU(t)}{dw_n(t)}$. On performing differentiation of (6.34), (6.36) and (6.37), we get $\frac{dI_s(t)}{dw_n(t)} = \frac{u_n \Delta f}{\mathcal{D}(t)}$; $n = 1,2$ where $\mathcal{D}(t) = \frac{\Delta f^{(4)}(t) + b_2 \Delta f^{(3)}(t) + b_1 \Delta f^{(2)}(t) + b_0 \Delta f^{(1)}(t)}{\mathcal{K}\frac{d\Delta f(t)}{dt}}$. Therefore, weights in (6.38) follows the rule as:

$$w_n(t+1) \leftarrow \left(w_n(t) - \frac{\alpha u_n \Delta f}{\mathcal{D}(t)} \right); \quad n = 1,2 \tag{6.39}$$

With this update rule (6.39), the intensity of the individual controller C_1 and C_2 can be altered to achieve desired performance. Note that the control algorithm starts with initial weights as $w_1 = w_2 = 1$. A fair selection occurs when both the controllers are given equal priority.

Case Studies:

This section elaborates different case studies where cases 1 and 2 are the scenario of single-area, while case 3 illustrates the two-area scenario.

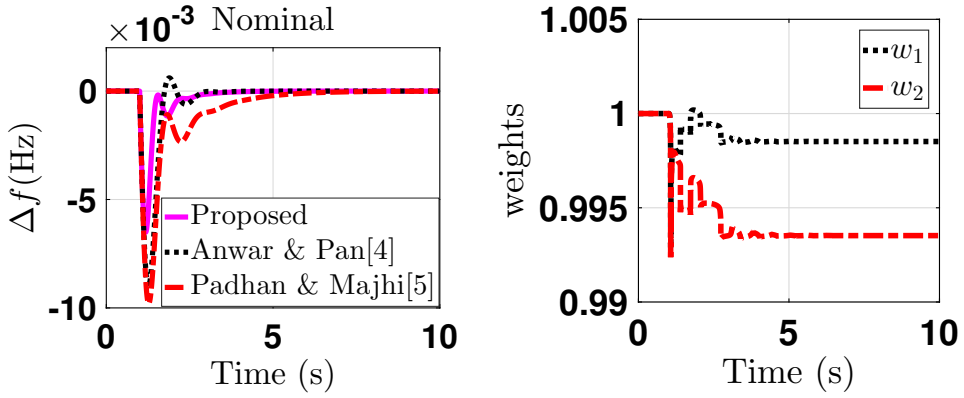

Figure 6.18: Time response and weight update pattern for Case 2

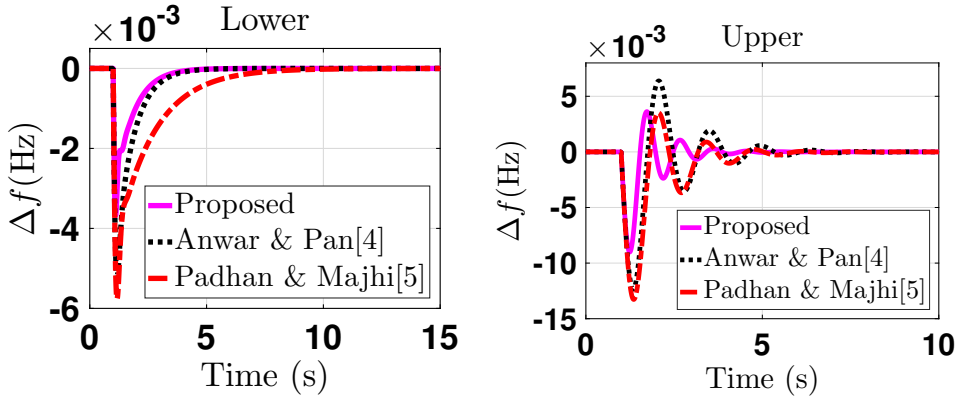

Figure 6.19: Response under parametric uncertainty in Case 2

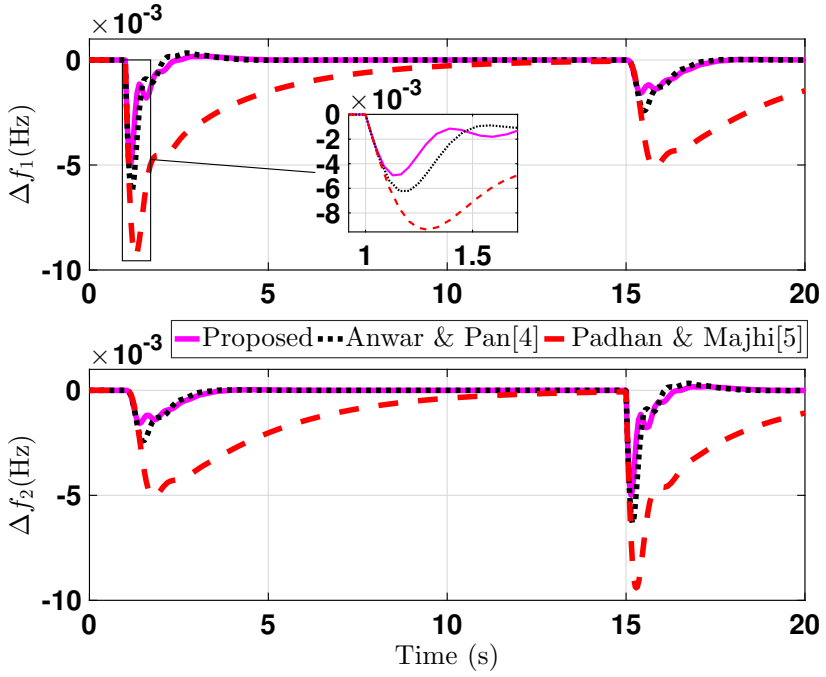

Figure 6.20: Time response for Case 3

Table 6.9: Performance indices ($\times 10^{-6}$)

	Method	Nominal		Lower		Upper	
		ISE	ITSE	ISE	ITSE	ISE	ITSE
Case 1	Proposed	27.9	42.4	16.7	31.0	52.1	75.4
	Tan[58]	138.1	229.3	69.6	139.6	251.6	421.8
	Saxena & Hote[190]	30.6	42.0	7.2	8.8	106.1	192.9
Case 2	Proposed	9.44	11.7	4.3	6.0	25.6	35.4
	Anwar & Pan[59]	26.3	34.2	11.0	15.5	76.7	125.2
	Padhan & Majhi[208]	36.1	52.3	19.1	34.0	77.7	118.0

Case 1: This case study considers two different type of control structure. The first controller C_1 acquires PID controller using W. Tan's technique [58] and the second one C_2 is obtained through internal model control technique using Saxena and Hote's method [190]. Fig. 6.16 illustrates the time evolution of frequency excursion for a sudden load disturbance of 0.01 p.u. MW. It can be observed that the proposed scheme initially follows the response of [190] due to low overshoot and then follows [58] because of its smooth response behavior while giving less importance to [190]. This can be easily understood by observing the weight update in Fig. 6.16. The response is also improved when $\pm 50\%$ parametric variations are present in the system (see Fig. 6.17).

Case 2: In this case study, two PID controllers for LFC are considered using Anwar and Pan [59] and Padhan and Majhi scheme [208]; and the weights are updated as per the proposed scheme. Fig. 6.18 depicts that the proposed scheme enhances the weights of [59] and decreases the weight of [208] to counteract the sudden disturbance. The proposed scheme also works well when uncertainty are present (see Fig. 6.19).

The error indices are also measured to analyze the optimal performance of proposed scheme; and from Table 6.9, it is evident that the scheme attains minimum value in both cases.

Case 3: For the two-area power system, again the PID schemes from [59] and [208] are taken into account. The proposed control scheme follows the control scheme in [59] and less weightage is given to scheme in [208] (see Fig. 6.20).

6.5 Concluding remarks

In this chapter, QRAWCP approach is applied to a single area and two area system. A keen observation of the results obtained from these analyses clearly indicate that the proposed approach is characterised by better disturbance rejection capability, minimal overshoots and undershoots as well as least steady state error. Further, it also shows better robustness towards parametric uncertainty and gives improved results, even when it is implemented on a 39 bus New England 10 machine system, which is susceptible to non-linearities like Governor dead band and generation rate constraint. Finally, an adaptive control scheme is also applied to design a controller for the LFC problem and it is observed that it is able to emulate the good properties of each candidate controller. A comprehensive comparison of the proposed techniques with the existing ones via integral performance indices is done and, in each case, it is observed that the proposed approach gives the least value of different indices. The simulation results are a testimony to the effectiveness of the proposed schemes. Finally, we are left with the last chapter, where we give the final remarks about the work done in this thesis and suggest further improvements, which can be undertaken by control practitioners to obtain better and improved results.

Chapter 7

Conclusion and Future Scope

The work presented in this thesis is primarily focused on the novel design methodologies for tuning of PID controllers via QRAWCP approach and adaptive control scheme. The authors have made an honest attempt in this thesis to enlist the past contributions as well as suggest some new design approaches that are computationally simple and easy to understand. To address any apprehensions regarding the practical implementation of the proposed work in the presence of uncertainties, non-linearities, an extensive experimental validation of the proposed techniques has been conducted on QUBE servo2 system, cart inverted pendulum and rotary inverted pendulum.

7.1 Conclusion

The following conclusions are drawn based on the accomplishments of this thesis:

- It is possible to bring the optimal control theory based LQR approach in actual practice via the use of PID controllers. Addition of a compensating pole to the optimal control theory is done in a well-structured manner. Simplicity, robustness and computational efficiency are the key features of this scheme. The efficient use of this approach has led to an optimal design of conventional PID controller. The hardware results further validate the effectiveness of the proposed scheme.

- Numerous techniques of PID tuning are available in literature, but a single control scheme combining the advantages of multiple PID controllers designed by various methods has never been formulated till date. This very deficiency is addressed in this thesis via the development of an adaptive control scheme in which the output response is shaped in such a way that it follows the best portions of the individual response curves when controlled by individual PIDs. This very technique is applied to the control of CIPS and LFC, under various constraints. The results obtained via the proposed approach are compared with the design approaches of the individual controllers.

  It is observed that the proposed adaptive strategy outperforms the individual control techniques, thus satisfying the proposed objective and motivation. Not only simulation-based verification, the hardware setup of CIPS system is also employed to carry out the validation, whereby it is found that the experimental results match closely with the ones obtained via simulation. This scheme thus opens up exciting avenues of further research.

- From the design and application of simpler control techniques like QRAWCP scheme, it can be concluded that, although mathematically complicated and computationally intensive control techniques promise superior performance than linear controllers, it is not always necessary to apply these methods. This has been observed from the stabilization of CIPS and performance improvement of DC servo system using the proposed QRAWCP scheme.

- In reality, the parametric variations of a system with respect to the nominal values leads to uncertainty. At this stage, robust stabilization is a primary issue. To handle this, one could use Kharitonov's theorem and design a robust PID controller using stability boundary locus (SBL). The adaptive control scheme proposed in this thesis employed one candidate controller designed by SBL, thus taking into consideration the problem of parametric uncertainty.

- The problem of load frequency control is one of the crucial issues in power system theory and one needs to maintain a constant system frequency and fixed tie-line power to maintain the faithful transmission and distribution of electric power. Both the QRAWCP and adaptive control scheme have demonstrated their applicability to this problem, which resulted in a robust control for single as well as multiple area power systems.

7.2 Future Scope

Research and development is a never ending process and there is always a possibility of improvement. Though the literature is voluminous, yet there is a scope for further exploration on the work presented in this thesis. As a result of investigation carried out in implementing QRAWCP and adaptive control strategies, following aspects are identified that leave rooms for future research:

- The schemes proposed in this thesis can be a benchmark for other real time applications particularly, power electronics, electrical drives, robotics, process control, aerospace engineering, chemical engineering, etc.
- The proposed schemes can be further applied to a class of nonlinear systems known as separable systems and a little more effort is needed for the treatment of highly nonlinear systems so called as non separable systems
- Fractional control theory is a recent development in the area of control engineering, and it is well known that the best fractional order control outperforms the best integer order controller. Thus, one could extend the proposed scheme to the fractional domain and strive to obtain better control along with the use of less control energy.
- As far as the interval systems are concerned, the future direction in this research is to make more efforts on developing the robust controller design of higher order interval plants.

Appendix A

Modelling of Cart inverted pendulum system

A.1 Proof for equations (5.3) and (5.4)

From Fig. 5.1, motions of pendulum around the center of gravity, $x_G = x + lcos\theta$ and $y_G = lcos\theta$ are given below.

The rotational and horizontal motions of pendulum are shown in (A.1) and (A.2).

$$\gamma l \sin\theta - \lambda l \cos\theta - \zeta \frac{d\theta}{dt} = J \frac{d^2\theta}{dt^2} \tag{A.1}$$

$$\begin{aligned} \lambda &= m \frac{d^2}{dt^2}(x + l\sin\theta) \\ &= m\ddot{x} + ml\ddot{\theta}\cos\theta - ml\dot{\theta}^2 \sin\theta \end{aligned} \tag{A.2}$$

Dynamic equation of the pendulum's center of gravity in the vertical direction can be written as:

$$\gamma = -ml\ddot{\theta}\sin\theta - ml\dot{\theta}^2\cos\theta + mg \tag{A.3}$$

Similarly, dynamic equation for horizontal motion of the cart can be written as:

$$M_c \frac{d^2x}{dt^2} = F - \lambda - b\frac{dx}{dt} \tag{A.4}$$

Substituting (A.2) in (A.4), we get,

$$(M_c + m)\ddot{x} + b\dot{x} + ml\ddot{\theta}\cos\theta - ml\dot{\theta}^2\sin\theta = F \tag{A.5}$$

Similarly, for pendulum using (A.2) and (A.3) in (A.1), we get:

$$(J + ml^2)\ddot{\theta} - mgl\sin\theta + ml\ddot{x}\cos\theta + \zeta\dot{\theta} = 0 \tag{A.6}$$

Using (A.5) and (A.6), the expression for $\ddot{x}$ can be written as:

$$\ddot{x} = \left(\frac{F - b\dot{x} - ml\ddot{\theta}\cos\theta + ml\dot{\theta}^2\sin\theta}{(M_c + m)} \right) \tag{A.7}$$

Replacing (A.7) in (A.6) and solving for $\ddot{\theta}$, we get:

$$\begin{aligned} &(J + ml^2)\ddot{\theta} - mgl\sin\theta \\ &+ ml\left(\frac{F - b\dot{x} - ml\ddot{\theta}\cos\theta + ml\dot{\theta}^2\sin\theta}{(M_c + m)} \right)\cos\theta \\ &+ \zeta\dot{\theta} = 0 \end{aligned} \tag{A.8}$$

Rewriting (A.8), we get (A.9),

$$\begin{aligned} &\{J(M_c + m) + ml^2M_c + m^2l^2 - m^2l^2\cos^2\theta\}\ddot{\theta} \\ &+ (\zeta\dot{\theta} - mgl\sin\theta)(M_c + m) \\ &+ ml(F - b\dot{x})\cos\theta + m^2l^2\dot{\theta}^2\cos\theta\sin\theta = 0 \end{aligned} \tag{A.9}$$

Further, rearranging (65), we get (66),

$$\ddot{\theta} = ml\left\{ \frac{\begin{pmatrix} (F - b\dot{x})\cos\theta + ml\dot{\theta}^2\cos\theta\sin\theta \\ -(\zeta\dot{\theta}/ml - g\sin\theta)(M + m) \end{pmatrix}}{(J(M_c + m) + ml^2M_c + m^2l^2\sin^2\theta)} \right\} \tag{A.10}$$

Substituting (A.10) in (A.7) and rewriting the expression for $\ddot{x}$, we get the following equation:

$$\ddot{x} = \left\{ \frac{\left(\begin{array}{c} (J+ml^2)\left(F - b\dot{x} + ml\dot{\theta}^2 \sin\theta\right) \\ +(ml\cos\theta)(\zeta\dot{\theta} - mgl\sin\theta) \end{array} \right)}{(J(M_c+m) + M_c ml^2 + m^2 l^2 \sin^2\theta)} \right\} \tag{A.11}$$

Appendix B

Mathematical modelling of RIPS

The rotary pendulum system, also known as a Furuta Pendulum [79, 217, 218], is a classic benchmark system often used to teach modelling and control in educational institutes. The free-body diagram of a basic RIPS is depicted in Fig. B.1. The rotary arm, which is attached to the motor pivot, makes an angle θ with X-axis in X-Y plane. Pendulum , which is attached to the end of the rotary arm, makes an angles α with Z-axis in plane that is perpendicular to rotary arm. θ denotes rotatory arm position and α denotes pendulum angle. The RIPS parameters are rotary arm mass (m_r), pendulum mass (m_p), rotary arm length (L_r), length of pendulum (L_p), rotary

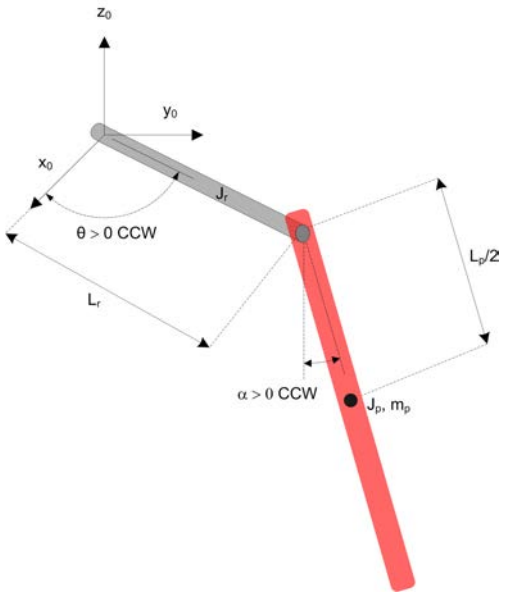

Figure B.1: Model of rotary inverted pendulum

Table B.1: Quanser Qube servo2 setup parameters

Symbol	Description	value	units
DC motor			
R_m	Terminal resistance	8.4	Ω
k_t	Torque constant	0.042	N.m/A
k_m	Motor back-emf constant	0.042	V/(rad/s)
J_m	Rotor inertia	4×10^{-6}	kg.m^2
L_m	Rotor inductance	1.16	mH
m_h	Load hub mass	0.0106	kg
r_h	Load hub radius	0.0111	m
J_h	Load hub inertia	0.6×10^{-6}	kg.m^2
Load Disk			
m_d	Mass of disk load	0.053	kg
r_d	Radius of disk load	0.024	m
Rotary pendulum			
M_r	Mass of rotary arm	0.095	kg
L_r	Length of rotary arm	0.085	m
J_r	Moment of inertia at pivot	$M_r L_r^2/12$	kg.m^2
M_p	Mass of pendulum	0.024	kg
L_p	Length of pendulum	0.129	m
J_p	Moment of inertia at pivot	$M_p L_p^2/12$	kg.m^2

arm movement of inertia (J_r), pendulum movement of inertia (J_p), viscous damping coefficient of rotary arm (D_p) and pendulum (D_r), gravitational constant (g) and applied torque (τ).

The equations of motion (EOM) for the pendulum system were developed using the Euler-Lagrange method. The complete derivation of the EOM has been considered from [79], The resultant non-linear EOM are:

$$\begin{aligned}
&\left(m_p L_r^2 + \frac{1}{4} m_p L_p^2 - \frac{1}{4} m_p L_p^2 \cos(\alpha)^2 + J_r\right) \ddot{\theta} \\
&- \left(\frac{1}{2} m_p L_p L_r \cos(\alpha)\right) \ddot{\alpha} + \left(\frac{1}{2} m_p L_p^2 \sin(\alpha)\cos(\alpha)\right) \dot{\theta}\dot{\alpha} \\
&+ \left(\frac{1}{2} m_p L_p L_r \sin(\alpha)\right) \dot{\alpha}^2 = \tau - D_r \dot{\theta}
\end{aligned} \tag{B.1}$$

$$\begin{aligned}
&\frac{1}{2} m_p L_p L_r \cos(\alpha) \ddot{\theta} + \left(J_p + \frac{1}{4} m_p L_p^2\right) \ddot{\alpha} \\
&- \frac{1}{4} m_p L_p^2 \cos(\alpha)\sin(\alpha)\dot{\theta}^2 + \frac{1}{2} m_p L_p g \sin(\alpha) = -D_p \dot{\alpha}.
\end{aligned} \tag{B.2}$$

A servo motor applies torque to rotary arm with equation:

$$\tau = \frac{k_m \left(V_m - k_m \dot{\theta} \right)}{R_m} \tag{B.3}$$

When the non-linear EOM are linearised about the operating point, the resultant linear EOM for the inverted pendulum are defined as:

$$\left(m_p L_r^2 + J_r \right) \ddot{\theta} - \frac{1}{2} m_p L_p L_r \ddot{\alpha} = \tau - D_r \dot{\theta}. \tag{B.4}$$

and

$$\frac{1}{2} m_p L_p L_r \ddot{\theta} + \left(J_p + \frac{1}{4} m_p L_p^2 \right) \ddot{\alpha} + \frac{1}{2} m_p L_p g \alpha = -D_p \dot{\alpha}. \tag{B.5}$$

Solving for the acceleration terms yields:

$$\begin{aligned} \ddot{\theta} = \frac{1}{J_T} \Bigg(& - \left(J_p + \frac{1}{4} m_p L_p^2 \right) D_r \dot{\theta} + \frac{1}{2} m_p L_p L_r D_p \dot{\alpha} \\ & + \frac{1}{4} m_p^2 L_p^2 L_r g \alpha + \left(J_p + \frac{1}{4} m_p L_p^2 \right) \tau \Bigg) \end{aligned} \tag{B.6}$$

and

$$\begin{aligned} \ddot{\alpha} = \frac{1}{J_T} \Bigg(& \frac{1}{2} m_p L_p L_r D_r \dot{\theta} - \left(J_r + m_p L_r^2 \right) D_p \dot{\alpha} \\ & - \frac{1}{2} m_p L_p g \left(J_r + m_p L_r^2 \right) \alpha - \frac{1}{2} m_p L_p L_r \tau \Bigg) \end{aligned} \tag{B.7}$$

where

$$J_T = J_p m_p L_r^2 + J_r J_p + \frac{1}{4} J_r m_p L_p^2. \tag{B.8}$$

Appendix C

Data for the 39-bus New England Power System

The 39-bus New England Power System [213, 214] , as shown in Fig. C.1, is used in the thesis for different simulations as given in the respective chapters. It is simplified representation of the 345 KV transmission system in the New England having 10 generators, 29 load buses and 46 transmission lines. The bus data and transmission line data are given at 100 MVA in Table C.1 and Table C.2 respectively

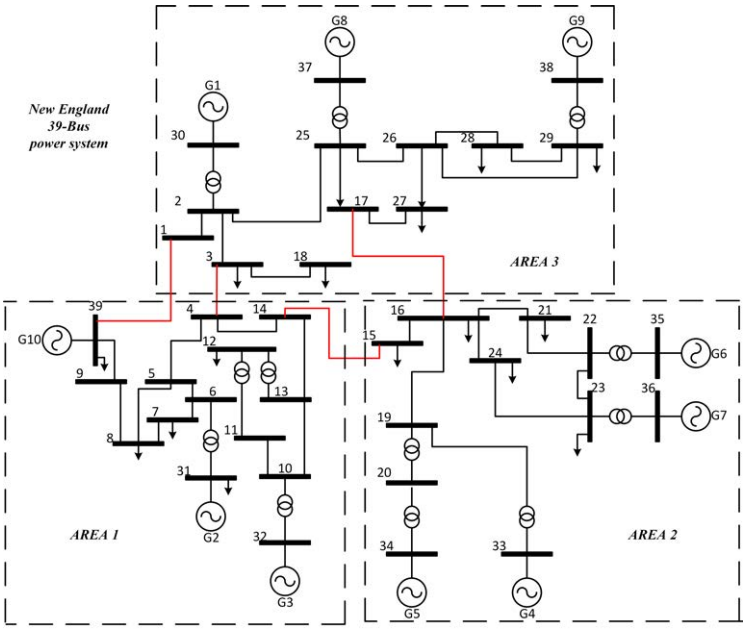

Figure C.1: Single line diagram of New England 10 machine 39 bus power system.

Table C.1: Bus data for the 39-bus New England Power System (in p.u.)

Bus No.	$P_{G,i}$	$P_{D,i}$	$Q_{G,i}$	$Q_{D,i}$	$Q_{G,i}^{max}$	$Q_{G,i}^{min}$	V_i	V_i^{max}	V_i^{min}	**Base kV**
1	5.5270	0.9200	1.6870	0.0460	2.0000	-1.5000	0.9800	1.06	0.94	345
2	10.0000	11.0400	2.4250	2.5000	4.0000	-2.0000	1.0300	1.06	0.94	345
3	6.5000	0.0000	1.7050	0.0000	2.7000	-1.3000	0.9800	1.06	0.94	345
4	5.0800	0.0000	1.6730	0.0000	2.3000	-1.0000	1.0100	1.06	0.94	345
5	6.3200	0.0000	0.7600	0.0000	2.5000	-1.2000	0.9900	1.06	0.94	345
6	6.5000	0.0000	2.6690	0.0000	2.5000	-1.3000	1.0400	1.06	0.94	345
7	5.6000	0.0000	2.4150	0.0000	2.5000	-1.1000	1.0600	1.06	0.94	345
8	5.4000	0.0000	0.2390	0.0000	2.2000	-1.1000	1.0200	1.06	0.94	345
9	8.3000	0.0000	0.6310	0.0000	3.2000	-1.7000	1.0200	1.06	0.94	345
10	2.5000	0.0000	1.7670	0.0000	1.8000	-0.5000	1.0400	1.06	0.94	345
11	0.0000	0.0000	0.0000	0.0000	0.0000	0.0000	1.0300	1.06	0.94	345
12	0.0000	0.0000	0.0000	0.0000	0.0000	0.0000	1.0200	1.06	0.94	345
13	0.0000	3.2200	0.0000	0.0240	0.0000	0.0000	0.9790	1.06	0.94	345
14	0.0000	5.0000	0.0000	1.8400	0.0000	0.0000	0.9450	1.06	0.94	345
15	0.0000	0.0000	0.0000	0.0000	0.0000	0.0000	0.9470	1.06	0.94	345
16	0.0000	0.0000	0.0000	0.0000	0.0000	0.0000	0.9480	1.06	0.94	345
17	0.0000	2.3380	0.0000	0.8400	0.0000	0.0000	0.9400	1.06	0.94	345
18	0.0000	5.2200	0.0000	1.7600	0.0000	0.0000	0.9410	1.06	0.94	345
19	0.0000	0.0000	0.0000	0.0000	0.0000	0.0000	1.0060	1.06	0.94	345
20	0.0000	0.0000	0.0000	0.0000	0.0000	0.0000	0.9540	1.06	0.94	345
21	0.0000	2.7400	0.0000	1.1500	0.0000	0.0000	0.9780	1.06	0.94	345
22	0.0000	0.0000	0.0000	0.0000	0.0000	0.0000	1.0070	1.06	0.94	345
23	0.0000	2.7450	0.0000	0.8400	0.0000	0.0000	1.0060	1.06	0.94	345
24	0.0000	3.0860	0.0000	0.9220	0.0000	0.0000	0.9670	1.06	0.94	345
25	0.0000	2.2400	0.0000	0.4720	0.0000	0.0000	1.0190	1.06	0.94	345
26	0.0000	1.3900	0.0000	0.1700	0.0000	0.0000	1.0050	1.06	0.94	345
27	0.0000	2.8100	0.0000	0.7550	0.0000	0.0000	0.9850	1.06	0.94	345
28	0.0000	2.0600	0.0000	0.2760	0.0000	0.0000	1.0090	1.06	0.94	345
29	0.0000	2.8350	0.0000	0.2690	0.0000	0.0000	1.0120	1.06	0.94	345
30	0.0000	6.2800	0.0000	1.0300	0.0000	0.0000	0.9800	1.06	0.94	345
31	0.0000	0.0000	0.0000	0.0000	0.0000	0.0000	0.9510	1.06	0.94	345
32	0.0000	0.0750	0.0000	0.8800	0.0000	0.0000	0.9310	1.06	0.94	345
33	0.0000	0.0000	0.0000	0.0000	0.0000	0.0000	0.9520	1.06	0.94	345
34	0.0000	0.0000	0.0000	0.0000	0.0000	0.0000	0.9500	1.06	0.94	345
35	0.0000	3.2000	0.0000	1.5300	0.0000	0.0000	0.9510	1.06	0.94	345
36	0.0000	3.2940	0.0000	0.3230	0.0000	0.0000	0.9670	1.06	0.94	345
37	0.0000	0.0000	0.0000	0.0000	0.0000	0.0000	0.9750	1.06	0.94	345
38	0.0000	1.5800	0.0000	0.3000	0.0000	0.0000	0.9750	1.06	0.94	345
39	0.0000	0.0000	0.0000	0.0000	0.0000	0.0000	0.9790	1.06	0.94	345

Table C.2: Transmission line data for the 39-bus New England Power System (in p.u.)

Line No.	**From Bus No.**	**To Bus No.**	R	X	B_{ch}**(full)**	**Transformer Tap-setting**	**Max.Line Rating**
1	39	30	0.0007	0.0138	0.0000	1	5.0000
2	39	5	0.0007	0.0142	0.0000	1	6.5000
3	32	33	0.0016	0.0435	0.0000	1	3.0000
4	32	31	0.0016	0.0435	0.0000	1	3.0000
5	30	4	0.0009	0.0180	0.0000	1	6.5000
6	29	9	0.0008	0.0156	0.0000	1	9.0000
7	25	8	0.0006	0.0232	0.0000	1	6.0000
8	23	7	0.0005	0.0272	0.0000	1	6.0000
9	22	6	0.0000	0.0143	0.0000	1	7.0000
10	20	3	0.0000	0.0200	0.0000	1	7.0000
11	16	1	0.0000	0.0250	0.0000	1	6.0000
12	12	10	0.0000	0.0181	0.0000	1	4.0000
13	37	27	0.0013	0.0173	0.3216	0	4.0000
14	37	38	0.0007	0.0082	0.1319	0	4.0000
15	36	24	0.0003	0.0059	0.0680	0	4.0000
16	36	21	0.0008	0.0135	0.2548	0	4.0000
17	39	36	0.0016	0.0195	0.3040	0	6.0000
18	36	37	0.0007	0.0089	0.1342	0	4.0000
19	35	36	0.0009	0.0094	0.1710	0	4.0000
20	34	35	0.0018	0.0217	0.3660	0	3.0000
21	33	34	0.0009	0.0101	0.1723	0	4.0000
22	28	29	0.0014	0.0151	0.2490	0	4.0000
23	26	29	0.0057	0.0625	1.0290	0	3.0000
24	26	28	0.0043	0.0474	0.7802	0	4.0000
25	26	27	0.0014	0.0147	0.2396	0	4.0000
26	25	26	0.0032	0.0323	0.5130	0	4.0000
27	23	24	0.0022	0.0350	0.3610	0	4.0000
28	22	23	0.0006	0.0096	0.1846	0	4.0000
29	21	22	0.0008	0.0135	0.2548	0	6.5000
30	20	33	0.0004	0.0043	0.0729	0	4.0000
31	20	31	0.0004	0.0043	0.0729	0	4.0000
32	19	2	0.0010	0.0250	1.2000	0	4.0000
33	18	19	0.0023	0.0363	0.3804	0	4.0000
34	17	18	0.0004	0.0046	0.0780	0	4.0000
35	16	31	0.0007	0.0082	0.1389	0	4.0000
36	16	17	0.0006	0.0092	0.1130	0	5.0000
37	15	18	0.0008	0.0112	0.1476	0	4.0000
38	15	16	0.0002	0.0026	0.0434	0	5.0000
39	34	14	0.0008	0.0129	0.1382	0	2.5000

List of Publication

SCI/SCIE Journals:

1. **S. D. Hanwate** and Y. V. Hote, “Design of PID controller for sun tracker system using QRAWCP approach,” *Int. J. Comput. Intell. Syst.*, Atlantis press, vol. 11, no. 1, pp. 133–145, 2018.[Impact factor=1.89].

2. **S. Hanwate** and Y. V. Hote, “Relative Stability Analysis of Perturbed Cart Inverted Pendulum: An Experimental Approach,” *IETE Tech. Rev.*, Taylor & francis, vol. 35, no. 6, pp. 1–16, 2018. [Impact factor=1.330].

3. **S. Hanwate**, Y. V. Hote, and S. Saxena, “Adaptive Policy for Load Frequency Control,” *IEEE Trans. Power Syst.*, vol. 33, no. 1, pp. 1142–1144, 2018.[Impact factor=5.680]

4. **S. D. Hanwate**, Y. V. Hote, and A. Budharaja, “Design and implementation of adaptive policy for cart inverted pendulum system,” *Proc. Inst. Mech. Eng. Part I J. Syst. Control Eng.*, Sage, pp. 1–16,2018. [Impact factor=0.988]

5. **S. D. Hanwate**, S. Bose, and Y. V. Hote, “Design and implementation of modified adaptive policy for cart inverted pendulum system,” *IEEE/ASME Transaction on Mechatronics*, pp. 1–5, (under review).

6. **S. Hanwate** and Y. V. Hote, "Design of Robust PID Controller for Perturbed Cart Inverted Pendulum System using Kharitonov’s Theorem," *System & Control letters, Elsevier* (Submitted).

7. **S. Hanwate** and Y. V. Hote, "A modified Adaptive Control Policy for Solar tracker system," *IEEE/CAA, Journal of Automatica Sinica* (Submitted).

8. **S. Hanwate**, Y. V. Hote, M. Kumar, and S. Jain, "Optimal QRAWCP-PID Controller Design Approach based on Worst Case Selection for Perturbed Load Frequency Control," *IEEE Trans. Power Syst.* (Submitted).

International/National Conference:

1. **S. Hanwate** and Y. V. Hote,"Optimal PID Design for Load Frequency Control Using QRAWCP Approach," in *3rd IFAC Conference on Advances in Proportional-Integral-Derivative Control*, Ghent, vol. 51, no. 4, pp. 651–656, 2018. [Scopus indexed]

2. **S. D. Hanwate**, A. Paharia, and Y. V. Hote, "Interactive and Animated GUI of Cart and Rotary Inverted Pendulum for Validation of Controllers," in *International Conference on Innovative Technologies in Engineering(ICITE)*, Hydrabad, 2018, pp. 1–6.[**Best paper award**].

3. **S. D. Hanwate** and Y. V. Hote, "Design of PID controller for inverted pendulum using stability boundary locus," in *2014 Annual IEEE India Conference (INDICON)*, Pune, 2014, pp. 1–6.

4. **S. D. Hanwate**, A. Budhraja, and Y. V. Hote, "Improved performance of cart inverted pendulum system using LQR based PID controller and ANN," in *2015 IEEE UP Section Conference on Electrical Computer and Electronics (UPCON)*, Allahabad, 2015, pp. 1–6.

Bibliography

[1] A. Ghosh, T. R. Krishnan, and B. Subudhi, "Robust proportional-integral-derivative compensation of an inverted cart-pendulum system: an experimental study," *Control Theory & Applications, IET*, vol. 6, no. 8, pp. 1145–1152, 2012.

[2] S. Hanwate and Y. V. Hote, "Relative Stability Analysis of Perturbed Cart Inverted Pendulum: An Experimental Approach," *IETE Technical Review*, pp. 1–16, Sep 2017.

[3] K. Ogata, *Modern Control Engineering*. Prentice Hall, 2010.

[4] R. C. Dorf and R. H. Bishop, *Modern Control Systems*, 12th ed. Pearson, 2011.

[5] K. J. Astrom' and T. Hagglund, *PID Controllers: Theory, Design and Tuning*, 2nd ed. ISA; 2nd Revised edition, 1995.

[6] K. H. Ang, G. Chong, Y. Li, Kiam Heong Ang, G. Chong, and Yun Li, "PID control system analysis, design, and technology," *IEEE Transactions on Control Systems Technology*, vol. 13, no. 4, pp. 559–576, Jul 2005.

[7] J. Guzman, K. Astrom, S. Dormido, T. Hagglund, M. Berenguel, and Y. Piguet, "Interactive learning modules for PID control [Lecture Notes]," *IEEE Control Systems Magazine*, vol. 28, no. 5, pp. 118–134, Oct 2008.

[8] C. Hang and K. Sin, "A comparative performance study of PID auto-tuners," vol. 11, no. 5, 1991.

[9] K. Åström and T. Hägglund, "The future of PID control," *Control Engineering Practice*, vol. 9, no. 11, pp. 1163–1175, Nov 2001.

[10] S. Majhi and L. Litz, "On-line tuning of PID controllers," in *Proceedings of the American Control Conference,*, vol. 6. IEEE, 2003, pp. 5003–5004.

[11] Yun Li, Kiam Heong Ang, and G. Chong, "PID control system analysis and design," *IEEE Control Systems Magazine*, vol. 26, no. 1, pp. 32–41, Feb 2006.

[12] I. Kaya, N. Tan, and D. P. Atherton, "A refinement procedure for PID controllers," *Electrical Engineering*, vol. 88, pp. 215–221, 2006.

[13] D. Atherton and S. Majhi, "Limitations of PID controllers," in *Proceedings of the 1999 American Control Conference (Cat. No. 99CH36251)*, vol. 6. IEEE, 1999, pp. 3843–3847.

[14] N. Tan, "Computation of stabilizing PI-PD controllers," *International Journal of Control, Automation and Systems*, vol. 7, pp. 175–184, 2009.

[15] N. Tan and D. P. Atherton, "Design of stabilizing PI and PID controllers," *International Journal of Systems Science*, 2006.

[16] T. Radhakrishnan, *Non-linear self-tuning control of chemical reactors with input and process constraints*. Elsevier Science Pub. Co, 1997, vol. 1-3, no. 9.

[17] M. A. Joordens and M. Jamshidi, "Consensus Control for a System of Underwater Swarm Robots," *IEEE Systems Journal*, vol. 4, no. 1, pp. 65–73, Mar 2010.

[18] J. K. Rai, R. P. Tewari, and D. Chandra, "An Optimal Control of Biped Robot for Human-Like Walking," *International Journal of Robotics and Automation*, vol. 28, no. 2, Jan 2013.

[19] S. Faroque, B. Horan, H. Adam, M. Pangestu, and M. Joordens, "Haptic Technology for Micro-robotic Cell Injection Training Systems–A Review," *Intelligent Automation & Soft Computing*, vol. 22, no. 3, pp. 509–523, Jul 2016.

[20] F. Yanfie, R. Fengyuan, and L. Chuang, "Design a pid controller for active queue management," in *Proceedings of the Eighth IEEE Symposium on Computers and Communications. ISCC 2003*, June 2003, pp. 985–990 vol.2.

[21] P. Albertos and E. Barbera, "Control structures in motivational psychology," *IFAC Proceedings Volumes*, vol. 29, no. 1, pp. 4527 – 4532, 1996, 13th World Congress of IFAC, 1996, San Francisco USA, 30 June - 5 July.

[22] A. Datta, M. T. Ho, and S. P. Bhattacharyya, *Structure and synthesis of PID controllers*. Springer, 2000.

[23] D. Kim, D. Lee, and K. C. Veluvolu, "Accommodation of actuator fault using local diagnosis and IMC-PID," *International Journal of Control, Automation and Systems*, vol. 12, no. 6, pp. 1139–1149, Dec 2014.

[24] S. Yadav, S. Verma, and S. Nagar, "Optimized PID Controller for Magnetic Levitation System," *IFAC-PapersOnLine*, vol. 49, no. 1, pp. 778–782, Jan 2016.

[25] H. Zhang, Y. Shi, and A. S. Mehr, "Robust H∞ PID control for multivariable networked control systems with disturbance/noise attenuation," *International Journal of Robust and Nonlinear Control*, vol. 22, no. 2, pp. 183–204, Jan 2012.

[26] J. G. Ziegler and N. Nichols, "Optimum Settings for Automatic Controllers," *Transacction of the A.S.M.E*, vol. 64, pp. 759–768, 1942.

[27] H. Wu, W. Su, and Z. Liu, "PID controllers: Design and tuning methods," in *2014 9th IEEE Conference on Industrial Electronics and Applications*. IEEE, Jun 2014, pp. 808–813.

[28] B. Champion, M. Jamshidi, and M. Joordens, "Increased functionality of an underwater robotic manipulator," in *2016 11th System of Systems Engineering Conference (SoSE)*. IEEE, Jun 2016, pp. 1–6.

[29] J. A. V. Selvi, T. Radhakrishnan, and S. Sundaram, "Performance assessment of PID and IMC tuning methods for a mixing process with time delay," *ISA Transactions*, vol. 46, no. 3, pp. 391–397, Jun 2007.

[30] X. S. Yang, *Nature-Inspired Optimization Algorithms*. Elsevier Science, 2014.

[31] A. Ali and S. Majhi, "Integral criteria for optimal tuning of PI/PID controllers for integrating processes," *Asian Journal of Control*, vol. 13, no. 2, pp. 328–337, Mar 2011.

[32] J. J. Wang, "Simulation studies of inverted pendulum based on PID controllers," *Simulation Modelling Practice and Theory*, vol. 19, no. 1, pp. 440–449, 2011.

[33] P. Kumar Padhy and S. Majhi, "Improved automatic tuning of PID controller for stable processes," *ISA Transactions*, vol. 48, no. 4, pp. 423–427, 2009.

[34] D. Choudhury, *Modern Control Engineering*. PHI Learning, 2005.

[35] M. M. Sabir and T. Ali, "Optimal PID controller design through swarm intelligence algorithms for sun tracking system," *Applied Mathematics and Computation*, vol. 274, pp. 690–699, Feb 2016.

[36] M. T. Ho, A. Datta, and S. P. Bhattacharyya, "An elementary derivation of the Routh-Hurwitz criterion," *IEEE Transactions on Automatic Control*, vol. 43, no. 3, pp. 405–409, 1998.

[37] G. J. Silva, A. Datta, and S. P. S. P. Bhattacharyya, *PID controllers for time-delay systems*. Birkhauser, 2005.

[38] M. N. Anwar and S. Pan, "Synthesis of the PID controller using desired closed-loop response," *IFAC Proceedings Volumes*, vol. 46, no. 32, pp. 385–390, Dec 2013.

[39] S. Saxena and Y. V. Hote, "Internal model control based pid tuning using first-order filter," *International Journal of Control, Automation and Systems*, vol. 15, no. 1, pp. 149–159, Feb 2017.

[40] Q.-b. Jin, Q. Liu, Q. Wang, S.-n. Li, and Z. Wang, "IMC-PID Design: Analytical Optimization for Performance/Robustness Tradeoff Tuning for Servo/Regulation Mode," *Asian Journal of Control*, vol. 16, no. 4, pp. 1252–1261, Jul 2014.

[41] I. J. Nagrath and M. Gopal, *Control systems engineering*, 5th ed. NEW AGE, 2009.

[42] R. E. Kalman, "Design of a Self-Optimizing Control Systems," *Transactions of ASME*, vol. 80, no. 01, pp. 468–478, 1958.

[43] E. Vinodh Kumar and J. Jerome, "Robust LQR Controller Design for Stabilizing and Trajectory Tracking of Inverted Pendulum," *Procedia Engineering*, vol. 64, pp. 169–178, 2013.

[44] R. T. O'Brien and J. M. Howe, "Optimal PID controller design using standard optimal control techniques," in *2008 American Control Conference*. IEEE, Jun 2008, pp. 4733–4738.

[45] W. Tan, J. Liu, T. Chen, and H. J. Marquez, "Comparison of some well-known PID tuning formulas," *Computers & Chemical Engineering*, vol. 30, no. 9, pp. 1416–1423, Jul 2006.

[46] Jing Zhou, Meng Joo Er, and K. Veluvolu, "Adaptive output control of nonlinear time-delayed systems with uncertain dead-zone input," in *2006 American Control Conference*. IEEE, 2006, p. 6 pp.

[47] E. Vinodh Kumar and J. Jerome, "LQR based optimal tuning of PID controller for trajectory tracking of magnetic levitation system," in *Procedia Engineering*, vol. 64. Elsevier, 2013, pp. 254–264.

[48] The Mathworks Inc., "MATLAB Documentation." [Online]. Available: https://in.mathworks.com/help/

[49] S. K. Verma, S. Yadav, and S. K. Nagar, "Optimization of Fractional Order PID Controller Using Grey Wolf Optimizer," *Journal of Control, Automation and Electrical Systems*, vol. 28, no. 3, pp. 314–322, Jun 2017.

[50] S. D. Hanwate and Y. V. Hote, "Design of PID controller for sun tracker system using QRAWCP approach," *International Journal of Computational Intelligence Systems*, vol. 11, no. 1, pp. 133–145, 2018.

[51] J. J. Rath, K. C. Veluvolu, and M. Defoort, "Active Control of Nonlinear Suspension System Using Modified Adaptive Supertwisting Controller," *Discrete Dynamics in Nature and Society*, vol. 2015, pp. 1–10, Jul 2015.

[52] N. Tan, I. Kaya, and D. P. Atherton, "Design of stabilizing PI and PID controllers," in *IEEE conference*, no. 2, 2003, pp. 876–881.

[53] O. Boubaker, "The Inverted Pendulum Benchmark in Nonlinear Control Theory: A Survey," *International Journal of Advanced Robotic Systems*, vol. 10, no. 5, p. 1, May 2013.

[54] H. Mehdi and O. Boubaker, "Position/force control optimized by particle swarm intelligence for constrained robotic manipulators," in *11th International Conference on Intelligent Systems Design and Applications*. IEEE, Nov 2011, pp. 190–195.

[55] S. K. Mishra and D. Chandra, "Stabilization of Inverted Cart-Pendulum System Using PID Controller : A Frequency-Domain Approach," *Chinese Journal of Engineering*, vol. 2013, no. 962401, 2013.

[56] V. L. Kharitonov, "Asymptotic stability of an equilibrium position of a family of systems fo linear differential equations," *Differential Equations*, vol. 14, pp. 1483–1485, 1979.

[57] N. Tan, I. Kaya, C. Yeroglu, and D. P. Atherton, "Computation of stabilizing PI and PID controllers using the stability boundary locus," *Energy Conversion and Management*, vol. 47, no. 18–19, pp. 3045–3058, Nov 2006.

[58] Tan W., "Unified tuning of PID load frequency controller for power systems via IMC," *IEEE Trans. Power Syst.*, vol. 25, no. 1, pp. 341–350, Feb. 2010.

[59] M. N. Anwar and S. Pan, "A new PID load frequency controller design method in frequency domain through direct synthesis approach," *Int. J. Electr. Power Energy Syst.*, vol. 67, pp. 560–569, May 2015.

[60] W. Tan, S. Chang, and R. Zhou, "Load frequency control of power systems with nonlinearities," *IET Generation, Transmission & Distribution*, vol. 11, no. 17, pp. 4307–4313, Nov 2017.

[61] S. Saxena and Y. V. Hote, "Stabilization of perturbed system via IMC: An application to load frequency control," *Control Engineering Practice*, vol. 64, pp. 61–73, Jul 2017.

[62] M. F. Golnaraghi and B. C. Kuo, *Automatic control systems*. Wiley, 2010.

[63] S. Mukhopadhyay, A. Patra, and G. P. RaO, "Irreducible model estimation for MIMO systems," *International Journal of Control*, vol. 53, no. 1, pp. 223–253, Jan 1991.

[64] E. Grassi and K. Tsakalis, "Pid controller tuning by frequency loop-shaping: application to diffusion furnace temperature control," *IEEE Transactions on Control Systems Technology*, vol. 8, no. 5, pp. 842–847, Sep 2000.

[65] M. E. Hmidi, I. B. Salem, and L. E. Amraoui, "Design and modeling of pid controller with 2dof: Application to thermal phase of an hybrid vehicle," in *2017 14th International Multi-Conference on Systems, Signals Devices (SSD)*, March 2017, pp. 419–424.

[66] J. H. Aylor, R. L. Ramey, and G. Cook, "Design and application of a microprocessor pid predictor controller," *IEEE Transactions on Industrial Electronics and Control Instrumentation*, vol. IECI-27, no. 3, pp. 133–137, Aug 1980.

[67] Y. Zhang, Y. Jia, T. Chai, D. Wang, W. Dai, and J. Fu, "Data-driven pid controller and its application to pulp neutralization process," *IEEE Transactions on Control Systems Technology*, vol. 26, no. 3, pp. 828–841, May 2018.

[68] W. Zhenbin, W. Zhenlei, C. Guangyi, and Z. Xinjian, "Digital implementation of fractional order pid controller and its application," *Journal of Systems Engineering and Electronics*, vol. 16, no. 1, pp. 116–122, March 2005.

[69] G. Silva, A. Datta, and S. Bhattacharyya, "Stabilization of first-order systems with time delay using the PID controller," in *Proceedings of the 2001 American Control Conference. (Cat. No.01CH37148)*, vol. 6. IEEE, 2001, pp. 4650–4655 vol.6.

[70] G. Cohen and G. Coon, "Theoretical consideration of retarded control," *Transactions of ASME*, vol. 75, pp. 827–834, 1953.

[71] C. Hang, W. Ho, and L. Cao, "A comparison of two design methods for PID controllers," *ISA Transactions*, vol. 33, no. 2, pp. 147–151, Jul 1994.

[72] "Chien-Hrones-Reswick Autotuning Method (PID and Fuzzy Logic Toolkit) - LabVIEW 2012 PID and Fuzzy Logic Toolkit Help - National Instruments." [Online]. Available: http://zone.ni.com/reference/en-XX/help/370401J-01/lvpidmain/chienforms/

[73] P. Cominos and N. Munro, "PID controllers: recent tuning methods and design to specification," *IEE Proceedings - Control Theory and Applications*, vol. 149, no. 1, pp. 46–53, Jan 2002.

[74] S. Pan and M. N. Anwar, "A Frequency Response Matching Method for PID Controller Design for Industrial Processes with Time Delay." Springer, Berlin, Heidelberg, 2013, pp. 636–646.

[75] S. Saxena and Y. V. Hote, "Advances in internal model control technique: A review and future prospects," *IETE Technical Review*, vol. 29, no. 6, pp. 461–472, 2012.

[76] C.-h. Lee, "A survey of PID controller design based on gain and phase margins," *International Journal of Computational Cognition*, vol. 2, no. 3, pp. 63–100, 2004.

[77] N. Tan, I. Kaya, and D. Atherton, "Computation of stabilizing PI and PID controllers," in *Proceedings of 2003 IEEE Conference on Control Applications, 2003. CCA 2003.*, vol. 2. IEEE, 2003, pp. 876–881.

[78] S. Das, I. Pan, K. Halder, S. Das, and A. Gupta, "LQR based improved discrete PID controller design via optimum selection of weighting matrices using fractional order integral performance index," *Applied Mathematical Modelling*, vol. 37, no. 6, pp. 4253–4268, Mar 2013.

[79] "Qube Servo 2 user manual," 2016. [Online]. Available: https://www.quanser.com/products/qube-servo-2/

[80] J. Kennedy and R. Eberhart, "Particle swarm optimization," in *Proceedings of ICNN'95 - International Conference on Neural Networks*, vol. 4. IEEE, 1995, pp. 1942–1948.

[81] X.-S. Yang, *Nature-inspired metaheuristic algorithms*. Luniver Press, 2008.

[82] X.-S. Yang and Suash Deb, "Cuckoo Search via Lévy flights," in *2009 World Congress on Nature & Biologically Inspired Computing (NaBIC)*. IEEE, 2009, pp. 210–214.

[83] D. S. Naidu, *Optimal control systems*. CRC Press, 2002.

[84] D. E. Kirk, *Optimal control theory: an introduction*. Dover Courier Corporation, 2004.

[85] N. Wiener *et al.*, "Cybernetics. j," *Wiley and Sons, New York, USA. 194p. Wilson JA (1968). Entropy not negentropy. Nature*, vol. 219, pp. 535–536, 1948.

[86] N. Wiener, *Extrapolation, interpolation, and smoothing of stationary time series with engineering applications*. Technology Press of the Massachusetts Institute of Technology, 1964.

[87] R. E. Bellman and S. E. Dreyfus, *Applied dynamic programming*. Princeton university press, 2015.

[88] R. Bellman and R. Kalaba, "Dynamic programming andmodem control theory," 1965.

[89] B. RE and S. Dreyfus, "Applied dynamic programming," 1962.

[90] H. J. Pesch, M. Plail, and D. Munich, "The maximum principle of optimal control: a history of ingenious ideas and missed opportunities," *Control and Cybernetics*, vol. 38, no. 4A, pp. 973–995, 2009.

[91] G. R. P. L. Boltyanskii, VG, "On the theory of optimal processes," *Dokl. Akad. Nauk SSSR*, 1956, (In Russian).

[92] L. S. Pontryagin, V. Boltyanskii, and R. Gamkrelidze, "Ef mishchenko the mathematical theory of optimal processes," *New York: Interscience*, 1962.

[93] R. V. Gamkrelidze, "Discovery of the maximum principle," *Journal of dynamical and control systems*, vol. 5, no. 4, pp. 437–451, 1999.

[94] R. E. Kalman *et al.*, "Contributions to the theory of optimal control," *Bol. Soc. Mat. Mexicana*, vol. 5, no. 2, pp. 102–119, 1960.

[95] R. E. Kalman, "A new approach to linear filtering and prediction problems," *Journal of basic Engineering*, vol. 82, no. 1, pp. 35–45, 1960.

[96] R. E. Kalman and R. S. Bucy, "New results in linear filtering and prediction theory," *Journal of basic engineering*, vol. 83, no. 1, pp. 95–108, 1961.

[97] J. Riccati, "Animadversiones in aequationes differentiales secundi gradus," *Actorum Eruditorum Supplementa*, vol. 8, no. 1724, pp. 66–73, 1724.

[98] S. Bittanti, A. J. Laub, and J. C. Willems, *The Riccati Equation*. Springer Science & Business Media, 2012.

[99] W. Chen and L. Qiu, "Linear quadratic optimal control of continuous-time lti systems with random input gains," *IEEE Transactions on Automatic Control*, vol. 61, no. 7, pp. 2008–2013, July 2016.

[100] R. Galván-Guerra and L. Fridman, "Robustification of time varying linear quadratic optimal control based on output integral sliding modes," *IET Control Theory Applications*, vol. 9, no. 4, pp. 563–572, 2015.

[101] B. Gao, J. Hong, S. Yu, and H. Chen, "Linear-quadratic output regulator with disturbance rejection: Application to vehicle launch control," in *2017 American Control Conference (ACC)*, May 2017, pp. 1960–1965.

[102] J. A. Queiroz, J. V. d. F. Neto, and A. K. Barros, "Solution of algebraic riccati equation for optimal control using non-square estimator," in *2015 IEEE 24th International Symposium on Industrial Electronics (ISIE)*, June 2015, pp. 125–130.

[103] Jian-Bo He, Qing-Guo Wang, and Tong-Heng Lee, "PI/PID controller tuning via LQR approach," in *Proceedings of the 37th IEEE Conference on Decision and Control (Cat. No.98CH36171)*, vol. 1. IEEE, 1998, pp. 1177–1182.

[104] J.-B. He, Q.-G. Wang, and T.-H. Lee, "Pi/pid controller tuning via lqr approach," *Chemical Engineering Science*, vol. 55, no. 13, pp. 2429–2439, 2000.

[105] R. M. Stefanescu, C. L. Prioroc, and A. M. Stoica, "Weighting matrices determination using pole placement for tracking maneuvers," *UPB Sci. Bull., Series D*, vol. 75, no. 2, pp. 31–41, 2013.

[106] A. Aydogan and O. Hasturk, "Adaptive lqr stabilization control of reaction wheel for satellite systems," in *2016 14th International Conference on Control, Automation, Robotics and Vision (ICARCV)*, Nov 2016, pp. 1–6.

[107] P. S and V. D. P, "Stabilization of an inverted pendulum using robust controller," in *2015 IEEE 9th International Conference on Intelligent Systems and Control (ISCO)*, Jan 2015, pp. 1–4.

[108] Y. Xin, J. Xu, B. Xu, and H. Xin, "The inverted-pendulum model with consideration of pendulum resistance and its lqr controller," in *Proceedings of 2011 International Conference on Electronic Mechanical Engineering and Information Technology*, vol. 7, Aug 2011, pp. 3438–3441.

[109] P. Hespanha and J. Hespanha, "Lecture notes on LQR/LQG Controller Design." Knowledge Creation Diffusion Utilization, 2005, vol. 90, ch. Notes on L, pp. 1–52.

[110] S. K. Choudhary, "LQR Based PID Controller Design for 3-DOF Helicopter System," *International Journal of Electrical and Information Engineering*, vol. 8, no. 8, pp. 1498–1503, 2014.

[111] S. Skogestad, "Simple analytic rules for model reduction and pid controller tuning," *Journal of Process Control*, vol. 13, no. 4, pp. 291 – 309, 2003.

[112] W. A. Wolovich, *Automatic control systems : basic analysis and design*. Saunders College Pub, 1994.

[113] G. B. K, S. R. A, and R. T.K., "Performance assessment of control loops involving unstable systems for set point tracking and disturbance rejection," *Journal of the Taiwan Institute of Chemical Engineers*, vol. 85, pp. 1–17, Apr 2018.

[114] R. T. Stefani, *Design of feedback control systems*. Oxford University Press, Inc., 1993.

[115] R. T. Stefani, B. Shahian, C. J. Savant, G. H. Hostetter, and G. Hostetter, *Design of Feedback Control Systems*, ser. Oxford Series in Electrical an. Oxford University Press, 2002.

[116] K. C. Veluvolu, Y. C. Soh, and W. Cao, "Robust discrete-time nonlinear sliding mode state estimation of uncertain nonlinear systems," *International Journal of Robust and Nonlinear Control*, vol. 17, no. 9, pp. 803–828, Jun 2007.

[117] J. Rai, R. Tewari, S. Pandey, and D. Chandra, "Optimised torque trajectory for humanoid robot based on human gait data," *International Journal of Mechatronics and Manufacturing Systems*, vol. 4, no. 2, p. 171, 2011.

[118] J.-J. Wang, "Stabilization and tracking control of X-Z inverted pendulum with sliding-mode control." *ISA transactions*, vol. 51, no. 6, pp. 763–70, Nov 2012.

[119] J. Aseltine, A. Mancini, and C. Sarture, "A survey of adaptive control systems," *IRE Transactions on Automatic Control*, vol. 6, no. 1, pp. 102–108, Dec 1958.

[120] Belaef Nikolai, "Self-stabilizing control mechanism," 1936.

[121] W. I. Caldwell, "Control system with automatic response adjustment," pp. 1–9, Aug 1950, uS Patent 743862.

[122] David W. Pessen, "Self adjusting control apparatus," 1954.

[123] H. P. Whitaker, J. Yamron, and A. Kezer, "Design of model-reference adaptive control systems for aircraft," M.I.T. Instrumentation Laboratory, Cambridge Mass., Tech. Rep., 1958.

[124] R. H. Middleton, G. C. Goodwin, D. J. Hill, and D. Q. Mayne, "Design issues in adaptive control," *IEEE Transactions on Automatic Control*, vol. 33, no. 1, pp. 50–58, 1988.

[125] X. D. Koutsoukos, P. J. Antsaklis, J. A. Stiver, and M. D. Lemmon, "Supervisory control of hybrid systems," *Proceedings of the IEEE*, vol. 88, no. 7, pp. 1026–1049, 2000.

[126] P. A. Ioannou and B. Fidan, *Adaptive control tutorial*. Society for Industrial and Applied Mathematics (SIAM), 2006.

[127] G. N. Saridis, J. M. Mendel, and Z. Z. Nikolic, "Report on definitions of self-organizing control processes and learning systems," *IEEE Control Systems Society Newsletter*, 1973.

[128] W. J. Rugh and J. S. Shamma, "Research on gain scheduling," *Automatica*, vol. 36, no. 10, pp. 1401–1425, Oct 2000.

[129] J. Shamma and M. Athans, "Analysis of gain scheduled control for nonlinear plants," *IEEE Transactions on Automatic Control*, vol. 35, no. 8, pp. 898–907, 1990.

[130] L. Yu, S. Fei, and W. Qian, "Robust adaptive control for single input/single output discrete systems via multi-model switching," *Proceedings of the Institution of Mechanical Engineers, Part I: Journal of Systems and Control Engineering*, vol. 228, no. 1, pp. 42–48, Jan 2014.

[131] D. Angeli and E. Mosca, "Adaptive switching supervisory control of nonlinear systems with no prior knowledge of noise bounds," *Automatica*, vol. 40, no. December, pp. 449–457, 2004.

[132] G. Battistelli, J. P. Hespanha, E. Mosca, and P. Tesi, "Model-free adaptive switching control of time-varying plants," *IEEE Transactions on Automatic Control*, vol. 58, no. 5, pp. 1208–1220, 2013.

[133] Z. R. Xiang, R. H. Wang, and Q. W. Chen, "Robust stabilization of uncertain stochastic switched non-linear systems under asynchronous switching," *Proceedings of the Institution of Mechanical Engineers, Part I: Journal of Systems and Control Engineering*, vol. 225, no. 1, pp. 8–20, Feb 2011.

[134] M. Dousti, S. C. Baslamısli, E. T. Onder, and S. Solmaz, "Design of a multiple-model switching controller for ABS braking dynamics," *Transactions of the Institute of Measurement and Control*, vol. 37, no. 5, pp. 582–595, May 2015.

[135] V. Veselý and A. Ilka, "Robust Switched Controller Design for Nonlinear Continuous Systems," *IFAC-PapersOnLine*, vol. 48, no. 11, pp. 1068–1073, Jan 2015.

[136] A. J. Koshkouei and L. Nowak, "Stabilisation of ship roll motion via switched controllers," *Ocean Engineering*, vol. 49, pp. 66–75, Aug 2012.

[137] I-Chun Chao, Kun-Yuan Tu, Shinn-Yan Lin, and Fan-Ren Chang, "Design and Implementation of a Switching Controller for Transient Improvement in a Time Synchronization System," *IEEE Transactions on Instrumentation and Measurement*, vol. 60, no. 7, pp. 2184–2190, Jul 2011.

[138] P. S. Saikrishna and R. Pasumarthy, "Multi-objective switching controller for cloud computing systems," *Control Engineering Practice*, vol. 57, pp. 72–83, Dec 2016.

[139] C.H. Chiu, "The Design and Implementation of a Wheeled Inverted Pendulum Using an Adaptive Output Recurrent Cerebellar Model Articulation Controller," *IEEE Transactions on Industrial Electronics*, vol. 57, no. 5, pp. 1814–1822, May 2010.

[140] S. Hanwate, Y. V. Hote, and S. Saxena, "Adaptive Policy for Load Frequency Control," *IEEE Transactions on Power Systems*, vol. 33, no. 1, pp. 1142–1144, 2018.

[141] W. Xie, "H ∞ performance realisation and switching controller design for linear time-invariant plant," *IET Control Theory & Applications*, vol. 10, no. 4, pp. 424–430, Feb 2016.

[142] S. K. Valluru and M. Singh, "Stabilization of nonlinear inverted pendulum system using MOGA and APSO tuned nonlinear PID controller," *Cogent Engineering*, vol. 4, no. 1, p. 1357314, Jul 2017.

[143] S. K. Verma, S. Yadav, and S. K. Nagar, "Optimized fractional order PID controller for non-minimum phase system with time delay," in *2016 International Conference on Emerging Trends in Electrical Electronics & Sustainable Energy Systems (ICETEESES)*. IEEE, Mar 2016, pp. 169–173.

[144] M. Zinkevich, "Online convex programming and generalized infinitesimal gradient ascent," *Machine Learning*, vol. 20, no. February, pp. 421–422, 2003.

[145] R. Dorf and R. Bishop, *Modern Control Systems*. Pearson Prentice Hall, 2014.

[146] "Precision modular servo control experiments-33-927S, User manual," Park Road, Crowborough, East Sussex, TN6 2QR, UK, pp. 1–43, 2002.

[147] G. Liu, Z. Zhou, H. Zhong, and S. Xie, "Gradient descent with adaptive momentum for active contour models," *IET Computer Vision*, vol. 8, no. 4, pp. 287–298, August 2014.

[148] J.-J. Wang, "Stabilization and tracking control of X-Z inverted pendulum based on PID controllers," in *2015 34th Chinese Control Conference (CCC)*. IEEE, Jul 2015, pp. 4202–4207.

[149] O. Boubaker, "The inverted pendulum: A fundamental benchmark in control theory and robotics," in *International Conference on Education and e-Learning Innovations*. IEEE, Jul 2012, pp. 1–6.

[150] J.-J. Wang, D.-L. LIU, and B.-J. WANG, "Research on One Type of Saturated Nonlinear Stabilization Control Method of X-Z Inverted Pendulum," *Acta Automatica Sinica*, vol. 39, no. 1, pp. 92–96, Jan 2013.

[151] M. A. Joordens, "Design of a low cost underwater robotic research platform," in *2008 IEEE International Conference on System of Systems Engineering*. IEEE, Jun 2008, pp. 1–6.

[152] "Digital pendulum control experiments manual (Feedback Instruments Ltd. UK)," 2002.

[153] J. Rai, R. Tewari, and D. Chandra, "Trajectory planning for all sub phases of gait cycle for human-like walking," *International Journal of Engineering Systems Modelling and Simulation*, vol. 1, no. 4, p. 206, 2009.

[154] Y. Hote, J. R. P. Gupta, and D. Choudhury, "Kharitonov's theorem and routh criterion for stability margin of interval systems," *International Journal of Control, Automation and Systems*, vol. 8, no. 3, pp. 647–654, 2010.

[155] A. A. Khandekar, G. M. Malwatkar, and B. M. Patre, "Discrete sliding mode control for robust tracking of higher order delay time systems with experimental application," *ISA Transactions*, vol. 52, no. 1, pp. 36–44, 2013.

[156] R. B. Fernandez, "Robust Feedback Linearization through Sliding Mode Control," in *Conference on Decision and Control*, no. December, 1990, pp. 3398–3399.

[157] C. Aguilar-Ibáñez, M. S. Suarez-Castanon, and N. Cruz-Cortés, "Output feedback stabilization of the inverted pendulum system: a Lyapunov approach," *Nonlinear Dynamics*, vol. 70, no. 1, pp. 767–777, Oct 2012.

[158] O. Boubaker and R. Iriarte, *The Inverted Pendulum in Control Theory and Robotics: From Theory to New Innovations - The IET*, 2017.

[159] S. Parvathy and V. Daniel P, "Stabilization of an Inverted Pendulum using robust controller," in *2015 IEEE 9th International Conference on Intelligent Systems and Control (ISCO)*. IEEE, Jan 2015, pp. 1–4.

[160] V. Kumar and K. Rana, "Nonlinear adaptive fractional order fuzzy PID control of a 2-link planar rigid manipulator with payload," *Journal of the Franklin Institute*, 2016.

[161] V. Krishnamurthi, "Correlation between Routh's stability criterion and relative stability of linear systems," *IEEE Transactions on Automatic Control*, vol. 17, no. 1, pp. 144–145, Feb 1972.

[162] A. K. Choudhary and S. K. Nagar, "Novel arrangement of Routh array for order reduction of z -domain uncertain system," *Systems Science & Control Engineering*, vol. 5, no. 1, pp. 232–242, Jan 2017.

[163] O. Boubaker, "The inverted pendulum: history and survey of open and current problems in control theory and robotics," in *The Inverted Pendulum in Control Theory and Robotics: From theory to new innovations*. Institution of Engineering and Technology, pp. 1–39.

[164] J.-J. Wang, "Position and speed tracking control of inverted pendulum based on double PID controllers," in *2015 34th Chinese Control Conference (CCC)*. IEEE, Jul 2015, pp. 4197–4201.

[165] M. Gopal, *Modern control system theory*. New Age International, 1993.

[166] S. D. Hanwate and Y. V. Hote, "Design of PID controller for inverted pendulum using stability boundary locus," in *India Conference*, Pune, 2014, pp. 1–6.

[167] N. Tan, "Robust analysis and design of control systems with parametric uncertainty." Ph.D. dissertation, University of Sussex, 1999.

[168] N. Tan and D. P. Atherton, "Robustness analysis of control systems with mixed perturbations," *Transactions of the Institute of Measurement and Control*, vol. 25, no. 2, pp. 163–184, 2003.

[169] B. Barmish, "A generalization of Kharitonov's four-polynomial concept for robust stability problems with linearly dependent coefficient perturbations," *IEEE Transactions on Automatic Control*, vol. 34, no. 2, pp. 157–165, 1989.

[170] S. P. Bhattacharyya, H. Chapellat, and L. H. Keel, *Robust control : the parametric approach*. Prentice Hall PTR, 1995.

[171] K. Furuta, M. Yamakita, and S. Kobayashi, "Swing-up Control of Inverted Pendulum Using Pseudo-State Feedback," *Proceedings of the Institution of Mechanical Engineers, Part I: Journal of Systems and Control Engineering*, vol. 206, no. 4, pp. 263–269, Nov 1992.

[172] J. Rajput and Z. Weiguo, "Fundamental methodologies for control of non-linear non-minimum-phase systems: An overview," *Proceedings of the Institution of Mechanical Engineers, Part I: Journal of Systems and Control Engineering*, vol. 228, no. 8, pp. 553–564, Sep 2014.

[173] K. G. Begum, A. S. Rao, and T. Radhakrishnan, "Optimal controller synthesis for second order time delay systems with at least one RHP pole," *ISA Transactions*, vol. 73, pp. 181–188, Feb 2018.

[174] H. Yu, Y. Liu, and T. Yang, "Closed-loop tracking control of a pendulum-driven cart-pole underactuated system," *Proceedings of the Institution of Mechanical Engineers, Part I: Journal of Systems and Control Engineering*, vol. 222, no. 2, pp. 109–125, Mar 2008.

[175] M. Ishitobi, Y. Ohta, Y. Nishioka, and H. Kinoshita, "Swing-up of a cart pendulum system with friction by energy control," *Proceedings of the Institution of Mechanical Engineers, Part I: Journal of Systems and Control Engineering*, vol. 218, no. 5, pp. 411–415, Aug 2004.

[176] Scilab, "Scilab 5.5.2 Open Source software." [Online]. Available: https://www.scilab.org/

[177] S. foundation, "SageMath - Open-Source Mathematical Software System." [Online]. Available: http://www.sagemath.org/

[178] Maplesoft, "Maple - The Essential Tool for Mathematics." [Online]. Available: https://www.maplesoft.com/products/Maple/

[179] Wolfram Mathematica, "Wolfram Mathematica: Modern Technical Computing." [Online]. Available: https://www.wolfram.com/mathematica/

[180] N. Aliane, "A Matlab/Simulink-Based Interactive Module for Servo Systems Learning," *IEEE Transactions on Education*, vol. 53, no. 2, pp. 265–271, May 2010.

[181] B. Wittenmark, H. Haglund, and M. Johansson, "Dynamic pictures and interactive learning," *IEEE Control Systems*, vol. 18, no. 3, pp. 26–32, Jun 1998.

[182] R. Garcia and B. Heck, "Enhancing classical controls education via interactive GUI design," *IEEE Control Systems Magazine*, vol. 19, no. 3, pp. 77–82, Jun 1999.

[183] M. Johansson, M. Gafvert, and K. Astrom, "Interactive tools for education in automatic control," *IEEE Control Systems*, vol. 18, no. 3, pp. 33–40, Jun 1998.

[184] M. Joordens, "The Tablet PC: A Complete Teaching Studio," pp. 149–163.

[185] L.-Y. Lu and Yao Jin-li, "Design and implementation of linear control system teaching software using MATLAB," in *2013 8th International Conference on Computer Science & Education*. IEEE, Apr 2013, pp. 1393–1396.

[186] J. Díaz and S. Dormido, "ITADLS: An Interactive Tool for Analysis and Design of Linear Systems," *IFAC-PapersOnLine*, vol. 48, no. 29, pp. 253–258, Jan 2015.

[187] S. Khan, M. H. Jaffery, A. Hanif, and M. R. Asif, "Teaching Tool for a Control Systems Laboratory Using a Quadrotor as a Plant in MATLAB," *IEEE Transactions on Education*, vol. 60, no. 4, pp. 249–256, Nov 2017.

[188] Control Tutorials for MATLAB and Simulink, "Animation for the Inverted Pendulum Example." [Online]. Available: http://ctms.engin.umich.edu/CTMS/index.php?aux=Animations_Invgui

[189] P. Kundur, *Power system stability and control*. McGraw-Hill, 1994.

[190] S. Saxena and Y. V. Hote, "Load frequency control in power systems via internal model control scheme and model-order reduction," *IEEE Trans. Power Syst.*, vol. 28, no. 3, pp. 2749–2757, Aug. 2013.

[191] N. V. Ramana, *Power system operation and control*. Pearson, 2010.

[192] B. Tyagi and S. Srivastava, "A LQG Based Load Frequency Controller in a Competitive Electricity Environment," *International Journal of Emerging Electric Power Systems*, vol. 2, no. 2, pp. 1–13, Jan 2005.

[193] L. B. Prasad, B. Tyagi, and H. O. Gupta, "Optimal Control of Nonlinear Inverted Pendulum System Using PID Controller and LQR : Performance Analysis Without and With Disturbance Input," *International Journal of Automation and Computing*, vol. 11, no. 6, pp. 661–670, 2014.

[194] H. A. Dryer, "Frequency Regulation- The Fundamental Problem," *Electrical World*, p. 342, 1932.

[195] C. Concordia, S. B. Crary, and E. E. Parker, "Effect of Prime-Mover Speed Governor Characteristics on Power-System Frequency Variations and Tie-Line Power Swings," *Transactions of the American Institute of Electrical Engineers*, vol. 60, no. 6, pp. 559–567, Jun 1941.

[196] H. Estrada, "Regulation of System Load and Frequency," *Transaction of the A.S.M.E.*, vol. 62, no. 3, pp. 221–232, 1940.

[197] S. Masuda, "PID controller tuning based on disturbance attenuation FRIT using one-shot experimental data due to a load change disturbance," *IFAC Proceedings Volumes*, vol. 45, no. 3, pp. 92–97, 2012.

[198] S. Saxena and Y. V. Hote, "Decentralized PID load frequency control for perturbed multi-area power systems," *International Journal of Electrical Power & Energy Systems*, vol. 81, pp. 405–415, Oct 2016.

[199] T. L. Blevins, "PID Advances in Industrial Control," *IFAC Proceedings Volumes*, vol. 45, no. 3, pp. 23–28, 2012.

[200] A. S. Bazanella, L. F. A. Pereira, and A. Parraga, "A New Method for PID Tuning Including Plants Without Ultimate Frequency," *IEEE Transactions on Control Systems Technology*, pp. 1–8, 2016.

[201] A. P. Nair, N. Selvaganesan, and V. Lalithambika, "Lyapunov based PD/PID in model reference adaptive control for satellite launch vehicle systems," *Aerospace Science and Technology*, vol. 51, pp. 70–77, 2016.

[202] Z.-L. Gaing, "A Particle Swarm Optimization Approach for Optimum Design of PID Controller in AVR System," *IEEE Transactions on Energy Conversion*, vol. 19, no. 2, pp. 384–391, Jun 2004.

[203] M. W. Iruthayarajan and S. Baskar, "Evolutionary algorithms based design of multivariable PID controller," *Expert Systems with Applications*, vol. 36, no. 5, pp. 9159–9167, 2009.

[204] F. Padula, R. Sandrini, and G. Cominardi, "Adaptive PI Control of an Organic Rankine Cycle Power Plant," *IFAC Proceedings Volumes*, vol. 45, no. 3, pp. 459–464, 2012.

[205] N. Kumar, B. Tyagi, and V. Kumar, "Multiarea Deregulated Automatic Generation Control Scheme of Power System Using Imperialist Competitive Algorithm Based Robust Controller," *IETE Journal of Research*, pp. 1–10, Sep 2017.

[206] S. Sondhi and Y. V. Hote, "Fractional order PID controller for load frequency control," *Energy Conversion and Management*, vol. 85, pp. 343–353, 2014.

[207] S. D. Hanwate and Y. V. Hote, "Optimal PID design for Load frequency control using QRAWCP approach," in *3rd IFAC Conference on Advances in Proportional-Integral-Derivative Control*, vol. 51, no. 4. Ghent: IFAC-PapersOnLine, 2018, pp. 651–656.

[208] D. G. Padhan and S. Majhi, "A new control scheme for PID load frequency controller of single-area and multi-area power systems," *ISA Trans.*, vol. 52, no. 2, pp. 242–251, Mar. 2013.

[209] B. Anderson, E. Jury, and M. Mansour, "On robust Hurwitz polynomials," *IEEE Transactions on Automatic Control*, vol. 32, no. 10, pp. 909–913, Oct 1987.

[210] Y. V. Hote, "A new approach to time domain analysis of perturbed PWM push-pull DC-DC converter," *Journal of Control Theory and Applications*, vol. 10, no. 4, pp. 465–469, 2012.

[211] . IEEE Standard-112, *112-1991 IEEE Standard Test Procedure for Polyphase Induction Motors and Generators.*, 1991.

[212] W. Tan, "Tuning of PID load frequency controller for power systems," *Energy Conversion and Management*, vol. 50, no. 6, pp. 1465–1472, Jun 2009.

[213] C. Canizares, T. Fernandes, E. Geraldi, L. Gerin-Lajoie, M. Gibbard, I. H. T. P. Chair), J. Kersulis, R. Kuiava, L. Lima, F. DeMarco, N. Martins, B. C. Pal, A. Piardi, R. R. T. Chair), J. dos Santos, D. Silva, A. K. Singh, B. Tamimi, and D. Vowles, "Benchmark models for the analysis and control of small-signal oscillatory dynamics in power systems," *IEEE Transactions on Power Systems*, vol. 32, no. 1, pp. 715–722, Jan 2017.

[214] H. Bevrani, *Robust Power System Frequency Control*. Boston, MA: Springer US, 2009.

[215] H. Bevrani and T. Hiyama, "Robust load-frequency control design for time-delay power systems," *Faculty of Built Environment and Engineering*, 2005.

[216] W. Tan and Z. Xu, "Robust analysis and design of load frequency controller for power systems," *Electric Power Systems Research*, vol. 79, no. 5, pp. 846–853, May 2009.

[217] F. Katsuhisa, Å. Karl J., K. Åström, and K. Furuta, "Swinging up a pendulum by energy control," *Automatica*, vol. 36, no. 2, pp. 287–295, Feb 2000.

[218] A. Kathpal and A. Singla, "SimMechanics based modeling, simulation and real-time control of Rotary Inverted Pendulum," in *2017 11th International Conference on Intelligent Systems and Control (ISCO)*. IEEE, Jan 2017, pp. 166–172.